UCC

University College Cork, Ireland
Coláiste na hOllscoile Corcaigh

Innovative Hull Design for Servicing Offshore Wind Turbines

Matthew Shanley

A Thesis Submitted for the Degree of Doctor of Philosophy

In the School of Engineering

Department of Civil and Environmental Engineering

National University of Ireland, Cork

March, 2018

Supervisors:

Dr. Jimmy Murphy & Prof. Tony Lewis

Head of School: Prof. Liam Marnane

Contents

Declaration vii

Abstract viii

Acknowledgements ix

List of Figures xviii

List of Tables xxi

List of Acronyms xxii

Nomenclature xxiv

1 Introduction **1**

1.1 Offshore Wind Energy 1

1.2 Offshore Wind O&M 4

1.3 Vessels for Servicing Offshore Wind Farms 5

1.4 Research Outline 7

1.5 Publications 9

2 Literature Review **10**

2.1 Introduction 10

2.2 O&M Vessels Utilised in Industry 11

2.2.1 Overview 11

2.2.2 Catamaran 12

2.2.3 Monohull 13

2.2.4 SWATH 14

2.2.5 Trimarans and TriSWACH Craft 15

2.2.6 Surface Effect Ships 16

2.2.7 Semi-SWATH 17
2.2.8 Floatel 18
2.2.9 Service Operation Vessels 19
2.2.10 Small Jack-Up Barges 20
2.3 Motion Compensating Gangway 20
2.3.1 Overview 20
2.3.2 Zbridge 21
2.3.3 Ampelmann 22
2.3.4 UPTIME 22
2.3.5 MaXccess 23
2.3.6 Autobrow 23
2.3.7 Turbine Access System (TAS) 23
2.3.8 Momac 24
2.4 New Maintenance Vessel Concepts 24
2.4.1 Overview 24
2.4.2 OffshoreShipDesigners, Sea-Wind Wind-Farm Maintenance Vessel (WMV) 25
2.4.3 Extreme Ocean, TranSPAR 26
2.4.4 Nauti-Craft 26
2.4.5 North Sea Logistics Pivoting Deck Vessel 27
2.4.6 Aerodynamically Alleviated Marine Vehicle 28
2.5 Rules, Regulations and Standards Applicable to WFSVs 28
2.6 WFSV Accidents 31
2.7 Industry Limits for Accessing Wind Turbines 31
2.8 Wave Climate 34
2.9 Weather Windows 34
2.10 Quantitative Motion Limits for Working on Ships 37
2.10.1 Overview 37
2.10.2 RMS Limit Measurements 37
2.10.3 Motion Induced Interruption 38

2.10.4 Task Effectiveness and Recovery Time 42
2.11 Motions of Floating Offshore Structures 43
2.11.1 Overview 43
2.11.2 Ship Motions 43
2.11.3 Response Amplitude Operators (RAO) 45
2.11.4 Natural Period 45
2.11.5 Minimisation of Response 46
2.12 Simulation of Floating Offshore Structures 48
2.13 State of the Art in Modelling WFSV Interaction with Offshore Wind Turbines at the Time of Transfer 50

3 Novel WFSV Designs **56**
3.1 Introduction 56
3.2 WFSV Concepts Analysed 58
3.2.1 Tubular Multihull Designs 58
3.2.2 Simple Catamarans Designs 62
3.2.3 Curved Hulled Catamaran with Single Heaveplates 63
3.2.4 Curved Hulled Catamaran with Dual Heaveplates 65
3.2.5 Grand Draught Catamaran 67
3.3 Discussion of Linear Wave Motion Effects 68
3.4 Summary 73

4 Numerical Modelling of Novel WFSV Designs **74**
4.1 Introduction 74
4.2 CFD Numerical Modelling 75
4.3 BEM Numerical Modelling 76
4.3.1 Overview 76
4.3.2 Standard Catamaran 78
4.3.3 Catamarans with Single Heaveplates 78
4.3.4 Heaveplate Depth and Area Comparison 79
4.3.5 Curved Hulled Catamaran with Dual Heaveplates 80

4.3.6 Catamarans with a Raised Heaveplate 83
4.4 Pressures from Numerical Modelling 83
4.5 Numerical Damping 84
4.6 Discussion 86

5 WFSV Motion at Zero Forward Speed 88
5.1 Introduction 88
5.2 Physical Modelling Overview 89
5.3 Wave Tank Calibration 90
5.4 Data Analysis 96
5.5 Natural Periods 97
5.6 RAO at Zero Forward Speed 100
5.6.1 Overview 100
5.6.2 Standard Catamaran 101
5.6.3 Tubular Multihull Designs 101
5.6.4 Catamarans with Single Heaveplates 103
5.6.5 Heaveplate Depth and Area Comparison 105
5.6.6 Curved Hulled Catamaran with Dual Heaveplates 106
5.6.7 Catamarans with a Raised Heaveplate 108
5.7 MII, and RMS of Accelerations and Pitch Angle at Zero Forward Speed 109
5.7.1 Overview 109
5.7.2 Standard Catamaran 111
5.7.3 Catamarans with Single Heaveplates 112
5.7.4 Curved Hulled Catamaran with Dual Heaveplates 120
5.7.5 Catamarans with a Raised Heaveplate 126
5.8 Comparison with Published Data 128
5.9 Discussion 129

6 Numerical and Physical Modelling Comparison 134
6.1 Introduction 134

6.2 Standard Catamaran 135
6.3 Tubular Multihull 136
6.4 Catamarans with Single Heaveplates 136
6.5 Heaveplate Depth and Area Comparison 139
6.6 Curved Hulled Catamaran with Dual Heaveplates 141
6.7 Catamarans with a Raised Heaveplate 144
6.8 Discussion 145

7 WFSV Interaction with a Monopile 146
7.1 Introduction 146
7.2 Modelling Overview 147
7.3 Limits for Carrying out a Transfer 150
7.4 Vessel Response in the Wake of a Monopile 152
7.5 WFSV Interacting with a Monopile in Head Seas 153
7.5.1 Overview 153
7.5.2 Standard Catamaran 154
7.5.3 Depth of Heaveplate 155
7.5.4 Narrow Hulled Catamaran with a Heaveplate 158
7.5.5 Bollard Pull 159
7.5.6 Curved Hulled Catamaran with Dual Heaveplates 163
7.6 Motions of a Catamaran WFSV Interacting with a Monopile at Varying Wave Headings 167
7.6.1 Introduction 167
7.6.2 RMS and Maximum Motions Recorded 167
7.6.3 Pass/Fail Graphs for a Standard Wide Hulled Catamaran WFSV with Varying Limits 177
7.7 Development of Polar Performance Plots 183
7.8 Estimation of Operational Limits from RAO Data 191
7.9 Discussion 193

8 Conclusions and Suggestions for Further Research 196

8.1 Introduction 196

8.2 Interaction of a WFSV with a Monopile 197

8.3 WFSV Operational Limits 197

8.4 Innovative Hull Design 198

8.5 Concluding Remarks 199

8.6 Further Research 200

References 202

Appendices 222

A Example WFSVs 223

B ANSYS AQWA and CFX 227

B.1 ANSYS AQWA 228

B.2 ANSYS CFX 229

C Model Properties 232

D CFD Numerical Modelling 237

D.1 Setup of a NWT 238

D.2 Simulation of Regular Waves in a NWT 242

D.3 Tubular Multihull Numerical Modelling 243

D.4 Results of the Tubular Multihull Numerical Modelling 247

E Experimental Test Outline 252

Declaration

I the author declare that this thesis, submitted for the degree of Doctor of Philosophy in the School of Engineering, is the author's own work and has not been submitted for another degree, either at University College Cork or elsewhere.

Matthew Shanley

Abstract

Accessing turbines for maintenance is a key operational issue for an offshore wind farm. Currently there is a 1.5m significant wave height (Hs) limit for the standard “step over” method of transferring personnel to an offshore wind turbine, though this varies with, vessel type, wave period and direction, as well as wind, and current conditions. The thesis aims to quantify limiting conditions for access, and increase the Hs at which offshore wind turbines can be accessed.

This thesis investigated the motion of novel ship hull designs, and quantified parameters that influence the transfer of personnel from a wind farm service vessel (WFSV) to a wind turbine. To complete the work for this thesis numerical, and physical techniques were utilised to model WFSV designs at zero forward speed in open water, and when docked with an offshore wind farm monopile. When designs were being investigated particular attention was paid to novel hull geometry, and the addition of heaveplates to catamaran hulls. A directional study on WFSV interaction with a monopile was carried out, and polar plots of performance were calculated. The limits of motion that a safe transfer can take place from the literature were compared with those of a basic standard catamaran design, and were then used to assess novel designs.

Critical issues at the monopile are, heave, surge, pitch, fender friction and bollard pull, for quartering and beam seas sway and roll are important. Heaveplates provide benefits, however increasing heave damping changes the principal fail condition from vertical slips to horizontal disconnects. Some of these failure cases could be predicted by vessel motion, which may be useful for a warning system. A vessel that can carry out transfers up to a 3.5m Hs was developed.

Acknowledgements

I acknowledge the Graduate Research Education Program in Engineering, and the MaREI research centre for the financial support of the project, as well as the Lir National Ocean Test Facility for the outstanding wave testing facilities and personnel. In addition, I wish to recognise the Irish Centre for High end Computing (ICHEC) for access to computing resources.

I wish to thank Dr Jimmy Murphy for his guidance, support, and encouragement over the past number of years. In addition, I wish to express thanks all the colleagues, past and present, who helped me understand this field.

Finally, I would like to show gratitude to my family; my wife, and our children for their patience and love, for keeping me motivated and lighting up my world every evening, as well as my friends, parents, and siblings for their support.

List of Figures

1.1 WindEurope, Cumulative and Annual Offshore Wind Installations 1993-2015 by MW [5] 3
1.2 WindEurope, Average Water Depth and Distance to Shore of Online, Under Construction and Consented Wind Farms [5] 3
1.3 Wind Turbine Evolution (reproduced from [5], source Principle Power) 4
1.4 Sample Service Operation Vessel: Esvagt Faraday [17] 6

2.1 Sample Catamaran: Windcat [27] 12
2.2 A2Sea Wind Supporter [28] 13
2.3 Sample SWATH; Natalia Bekker [29] 14
2.4 Austal TriSWACH [32] 15
2.5 Fjellstrand WindServer [34] 16
2.6 Surface Effect Vessel; Umoe Mandal's Wave Craft [35] 16
2.7 BMT Nigel Gee XSS [37] 17
2.8 Wind Power Support WindPerfection [39] 18
2.9 Sample Service Operation Vessel: Esvagt Faraday [17] 19
2.10 J/U WIND [40] 20
2.11 Zbridge Access Concept [44] 21
2.12 Ampelmann [42] 22
2.13 Uptime [46] 22
2.14 MaXccess [47] 23
2.15 Autobrow [48] 23

2.16 TAS [49] 23
2.17 Momac MOTS [50] 24
2.18 Offshore Ship Designers [51] 25
2.19 Extreme Ocean TranSPAR [54, 55] 26
2.20 Nauti-Craft [56] 27
2.21 North Sea Logistics Pivoting Deck Vessel [58] 27
2.22 Concept AAMV WFSV [59] 28
2.23 Example Performance Plot Comparing Three Vessels [20] 33
2.24 Scatter diagram. Typical North Sea conditions [91] 34
2.25 Irish Weather Buoy Network [96]. M1, M2, & M3 Highlighted . . 36
2.26 Weather Window Analysis [95] 36
2.27 Ship Axis Convention [109] 44
2.28 Wave Particle Force Direction in Relation to a Ship Length of Double the Wavelength 47
2.29 Wave Particle Force Direction in Relation to a Ship Length Equal to the Wavelength 47
2.30 Wave Particle Force Direction in Relation to a Ship Length Equal to the Wavelength Showing Small Showing Large Pitch Moment . 47
2.31 Principle Power's WindFloat [118, 119] 49

3.1 Ship Design Spiral [141] 57
3.2 Tubular Multihull Concept 58
3.3 Model Configurations of the Tubular Multihull 59
3.4 The Tubular Multihull in Regular Waves 59
3.5 Beam View Showing the Different Variables Analysed 60
3.6 Wide Hulled Catamaran with a Heaveplate, Slack Moored 62
3.7 Narrow Hulled Catamaran with a Heaveplate at a 12m Draught . 63
3.8 Wide Hulled Catamaran with a Heaveplate at a 12m Draught . . 63
3.9 Curved Hulled Catamaran with Varying Heaveplate Depths with a Constant Area of 178.5m^2 64

3.10 Curved Hulled Catamaran with Varying Heaveplate Areas at a Constant Draught of 12m 64
3.11 Curved Hulled Catamaran with a 178.5m^2 Heaveplate at a 12m Draught 64
3.12 Curved Hulled Catamaran with the Heaveplate Raised to Simulate the Transit Mode 64
3.13 Curved Hulled Catamaran with Dual Heaveplates Varying Heaveplate Angle at a Constant Draught of 12m, Each with an Area of 28m^2 for a Total Area of 56m^2 65
3.14 Curved Hulled Catamaran with Dual Heaveplates Varying Heaveplate Angle at a Constant Draught of 12m, Each with an Area of 56m^2 for a Total Area of 112m^2 66
3.15 28m^2 Dual Heaveplates Positioned at an Angle of 45° 66
3.16 56m^2 Dual Heaveplates Positioned at an Angle of 45° 66
3.17 GDC Isometric Drawing 67
3.18 Testing of the GDC in Irregular Waves 68
3.19 Water Particle Motion for a 3m Wave Height, 4s Period, 24.97m Wavelength in 25m water depth 70
3.20 Water Particle Motion for a 3m Wave Height, 8s Period, 93.27m Wavelength in 25m water depth 71
3.21 Water Particle Motion for a 3m Wave Hheight, 12s Period, 165.96m Wavelength in 25m water depth 72

4.1 Mesh Setup in AQWA 77
4.2 Numerical Modelling RAO Curves for a Standard Catamaran . . . 78
4.3 Numerical Modelling RAO Curves for Catamaran Hulls with a Heaveplate at a 12m Draught 79
4.4 Numerical Modelling RAO Curves Comparing Heaveplate Depth with the Curved Hulled Catamaran using a Heaveplate Area of 178.5m^2 80

4.5 Numerical Modelling RAO Curves Comparing Heaveplate Area Change at a 12m Draught on the Curved Hulled Catamaran . . . 80
4.6 Numerical Modelling RAO Curves Comparing Angle of Dual Heaveplates each 28m^2 at a 12m Draught 81
4.7 Numerical Modelling RAO Curves Comparing Angle of Dual Heaveplates each 56m^2 at a 12m Draught 82
4.8 Numerical Modelling RAO Curves Comparing Dual and Single Heaveplates of Similar Areas 82
4.9 Numerical Modelling RAO Curves for Catamarans with a Raised Heaveplate 83
4.10 Pressure Force Estimation on the Narrow Hulled Catamaran Model 84
4.11 Numerically Damping of the Narrow Hulled Catamaran 85
4.12 Numerically Damping of the GDC 86

5.1 Lir NOTF Ocean Basin 89
5.2 Regular Wave Timeseries H = 0.06 m, T = 0.8 s, Reflection Coefficient = 0.11 91
5.3 Regular Wave Timeseries H = 0.06 m, T = 1.6 s, Reflection Coefficient = 0.16 91
5.4 Regular Wave Timeseries H = 0.06 m, T = 2.4 s, Reflection Coefficient = 0.08 92
5.5 Regular Wave Timeseries Showing Effect of Radiated Waves H = 0.06 m, T = 0.8 s 92
5.6 Regular Wave Timeseries Showing Effect of Radiated Waves H = 0.06 m, T = 1.6 s 93
5.7 Regular Wave Timeseries Showing Effect of Radiated Waves H = 0.06 m, T = 2.4 s 93
5.8 GDC Wave Calibration 94
5.9 Comparison Between Theoretical and Actual Recorded Wave Spectra in the Wavetank: All JONSWAP with a 1.5m Hs 95

5.10 Comparison Between Theoretical and Actual Recorded JONSWAP and Bretschneider Wave Spectra in the Wavetank at a 3m Hs . . . 95
5.11 Comparison Between Theoretical and Actual Recorded Wave Spectra in the Wavetank: All Bretschneider with a 1.5m Hs 96
5.12 Sample Decay Tests for the GDC 98
5.13 Physical Modelling RAO Curves for a Standard Catamaran 101
5.14 Physical Model Testing RAO Curves of the Tubular Multihull . . . 102
5.15 Physical Modelling RAO Curves for the Narrow and Wide Hulled Catamarans with a Heaveplate at a 12m Draught 104
5.16 Physical Modelling RAO Curves Comparing the GDC with the Narrow Hulled Catamaran with a heaveplate at a 12m Draught . . . 104
5.17 Physical Modelling RAO Curves Comparing Heaveplate Depth Variation on a Heaveplate of 178.5m^2 Area 105
5.18 Physical Modelling RAO Curves Comparing Heaveplate Area Variation at a 12m Draught 106
5.19 Physical Model Testing Comparing Dual Heaveplates with a Combined Area of 56m^2, by Angle of Inclination 106
5.20 Physical Model Testing Comparing Dual Heaveplates with a Combined Area of 112m^2, by Angle of Inclination 107
5.21 Physical Modelling RAO Curves Comparing Catamarans with a Raised Heaveplate 108
5.22 MII and RMS Analysis of a Standard Catamaran 111
5.23 MII and RMS Analysis of a Wide Hulled Catamaran with a Heaveplate at 12m Draught 112
5.24 MII and RMS Analysis of the Narrow Hulled Catamaran with a Heaveplate at 12m Draught 113
5.25 MII and RMS Analysis of the Curved Hulled Catamaran with a 115.5m^2 Heaveplate at 12m Draught 114
5.26 MII and RMS Analysis of the Curved Hulled Catamaran with a 154m^2 Heaveplate at 12m Draught 115

5.27 MII and RMS Analysis of the Curved Hulled Catamaran with a 178.5m^2 Heaveplate at 12m Draught 116
5.28 MII and RMS Analysis of the Curved Hulled Catamaran with a 178.5m^2 Heaveplate at 9m Draught 117
5.29 MII and RMS Analysis of the Curved Hulled Catamaran with a 178.5m^2 Heaveplate at 6m Draught 118
5.30 MII and RMS of the GDC 119
5.31 MII and RMS Analysis of the Curved Hulled Catamaran with 0° Dual 28m^2 Heaveplates at 12m Draught 120
5.32 MII and RMS Analysis of the Curved Hulled Catamaran with 22.5° Dual 28m^2 Heaveplates at 12m Draught 121
5.33 MII and RMS Analysis of the Curved Hulled Catamaran with 45° Dual 28m^2 Heaveplates at 12m Draught 122
5.34 MII and RMS Analysis of the Curved Hulled Catamaran with 0° Dual 56m^2 Heaveplates at 12m Draught 123
5.35 MII and RMS Analysis of the Curved Hulled Catamaran with 22.5° Dual 56m^2 Heaveplates at 12m Draught 124
5.36 MII and RMS Analysis of the Curved Hulled Catamaran with 45° Dual 56m^2 Heaveplates at 12m Draught 125
5.37 MII and RMS Analysis of the Standard Wide Hulled Catamaran with a Raised Heaveplate 126
5.38 MII and RMS Analysis of the Curved Hulled Catamaran with a Raised Heaveplate 127
5.39 Heave and Pitch Nondimensional Amplitudes of the GDC and Standard Catamaran Compared with Published Data [162, 163, 164, 165] 128

6.1 Numerical and Physical Modelling RAO for a Standard Catamaran 135
6.2 Numerical and Physical Modelling RAO for the Tubular Multihull, T1000 136

6.3 Numerical and Physical Modelling RAO Curves for the Narrow Hulled Catamarans with a Heaveplate at 12m Draught 137
6.4 Numerical and Physical Modelling RAO Curves of the Wide Hulled Catamarans with a Heaveplate at 12m Draught 137
6.5 Numerical and Physical Modelling RAO for the Curved Hulled Catamaran with a Heaveplate at 12m Draught 138
6.6 Numerical and Physical Modelling RAO for the GDC with a Heaveplate at 12m Draught 138
6.7 Numerical and Physical Modelling of the 178.5m^2 Heaveplate on the Curved Hulled Catamaran at Varying Depths 139
6.8 Numerical and Physical Modelling RAO Curves Comparing Variation of Heaveplate Areas at 12m Depth on the Curved Hulled Catamaran 140
6.9 RAOs for Dual Heaveplates of an Area of 56m^2 at a 12m Draught 142
6.10 Numerical and Physical Modelling RAO Curves for the Dual Heaveplates of an Area of 112m^2 at a 12m Draught 143
6.11 Numerical and Physical Modelling RAO Curves for the Wide Hulled Catamaran and the Curved Hulled Catamaran with Heaveplates Raised 144

7.1 Model Setup for the Narrow Hulled Catamaran Experimental Testing of the Vessel with the Monopile 148
7.2 Experimental Testing of the Narrow Hulled Catamaran with the Monopile Interacting with Waves 148
7.3 Instrumentation at the Bow 149
7.4 Model in the Wake of the Monopile 152
7.5 Comparison of Performance in the Wake of the Monopile to the RAO Without a Monopile Present 153
7.6 Curved Hulled Catamaran with a Heaveplate Interacting with the Monopile in Head Seas 154

7.7 Heaveplate Depth Performance while Interacting with the Monopile for the 178.5m^2 Heaveplate, at a Constant Bollard Pull of 35t . . 158
7.8 X, Y, and Z Motion of the Curved Hulled Catamaran with a 178.5m^2 Heaveplate at a 3m Hs and 7s Tp at 0° Heading 160
7.9 X, Y, and Z Motion of the Curved Hulled Catamaran with a 178.5m^2 Heaveplate at a 3m Hs and 8s Tp at 0° Heading 161
7.10 Curved Hulled Catamaran with Dual Heaveplates 112m^2 0° at 12m Draught 164
7.11 Curved Hulled Catamaran with Dual Heaveplates of 112m^2 Performance while Interacting with the Monopile 166
7.12 Catamaran XYZ Motion at the Monopile: X Directional Motion . . 170
7.13 Catamaran XYZ Motion at the Monopile: Y Directional Motion . . 171
7.14 Catamaran XYZ Motion at the Monopile: Z Directional Motion . . 172
7.15 Catamaran Motion at the Monopile: RMS Angular Motion 173
7.16 Catamaran XYZ Motion at the Monopile: Maximum Angular Motion174
7.17 Catamaran XYZ Motion at the Monopile: RMS Acceleration . . . 175
7.18 Catamaran XYZ Motion at the Monopile: Maximum Acceleration 176
7.19 GDC Model Docked with the Monopile, Still Water 178
7.20 Bollard Pull Influence on a Standard Catamaran Performance while Interacting with the Monopile (Median Limits) 179
7.21 Standard Catamaran Performance while Interacting with the Monopile with a 45t Bollard Pull with Median Limits 180
7.22 Standard Catamaran Performance while Interacting with the Monopile with a 45t Bollard Pull with Strict Limits 181
7.23 Standard Catamaran Performance while Interacting with the Monopile with a 45t Bollard Pull with Relaxed Limits 182
7.24 Performance Plot, Showing Hs (m) Plotted Against Heading angle, (°) 183
7.25 GDC Model Docked with the Monopile 184

7.26 GDC Performance while Interacting with the Monopile 35t Bollard Pull with Median Limits 185
7.27 GDC Performance while Interacting with the Monopile 45t Bollard Pull with Median Limits 186
7.28 GDC Performance while Interacting with the Monopile 35t Bollard Pull with Strict Limits 187
7.29 GDC Performance while Interacting with the Monopile 35t Bollard Pull with Relaxed Limits 188
7.30 GDC Performance while Interacting with the Monopile 45t Bollard Pull with Strict Limits 189
7.31 GDC Performance while Interacting with the Monopile 45t Bollard Pull with Relaxed Limits 190

C.1 Curved Hulled Catamaran Lines Plan 236

D.1 CFD Layout 238
D.2 Wave Height Approaching and Leaving the Simulation Zone without a Model in Place 243
D.3 CFD Layout with the Rigid Body Geometry Inserted 245
D.4 Mesh Density of the CFX Domain 245
D.5 Detailed View of Mesh Around Tubes 246
D.6 Vessel Motion Throughout a Wave, H 3.67m, T 6.1s 247
D.7 Numerical Heave Time Series CFX 248
D.8 Numerical Pitch Time Series CFX 249
D.9 Model T1000 Regular RAO from Numerical Model Testing with ANSYS CFX Compared with a 25.9m Monohull from the Literature [162] 250
D.10 Wave Height Difference in Simulation 250
D.11 Velocity Vector of Flow 251
D.12 Velocity Curl Contour Map around Submerged Tubes 251

List of Tables

2.1 Beaufort Sea States 35
2.2 Criteria with Regard to Accelerations and Roll [RMS] [97] 38
2.3 General Operability Limiting Criteria for Ships and Fishing Vessels [97, 36, 99] 39
2.4 Empirically Derived MII Tipping Coefficients [104] 40
2.5 Threshold Levels for MII Detection; Threshold levels for Sliding and Tipping estimations [105] 41

3.1 Design Parameters 61
3.2 Naming Scheme for the Tubular Multihull Configurations 61

5.1 Natural Periods for the Tubular Multihull from Decay Tests 99
5.2 Natural Periods for the Curved Hulled Catamaran Models from Decay Tests 99
5.3 Natural Periods for Catamaran Model Properties (All designs 24m long at waterline) 100
5.4 Vessel Motion Limits 110
5.5 RMS Responses of a 25.9m (85-foot) Hardchine Monohull [162] 129

7.1 WFSV Monopile Access Limits 151
7.2 Properties of the Standard Catamaran when Docked at the Monopile with a 45t Bollard Pull 155
7.3 Vertical Slips Related to Depth of Heaveplate 156
7.4 Maximum Vertical Movement (m) Related to Depth of Heaveplate 157

7.5 X Direction Disconnects, where the Bow is Moved away from the Monopile in the X direction, Related to Depth of Heaveplate . . . 157
7.6 Properties of the Narrow Hulled Catamaran when Docked at the Monopile with a 25t Bollard Pull 159
7.7 Vertical Slips Related to Bollard Pull 162
7.8 Maximum Vertical Movement (m) Related to Change of Bollard Pull162
7.9 X Direction Disconnects Related to Bollard Pull for the Curved Hulled Catamaran with a 178.5m^2 Heaveplate at 12m Draught . 163
7.10 Vertical Slips Related to Angle of Heaveplate 165
7.11 Maximum Vertical Movement Related to Angle of Heaveplate . . 165
7.12 X Direction Disconnects Related to Angle of Heaveplate 166
7.13 WFSV Monopile Access Limits Sensitivity Analysis 177

A.1 Catamaran WFSV Examples 224
A.2 Monohull WFSV Examples 225
A.3 SWATH WFSV Examples 225
A.4 TriSWACH and SemiSWATH WFSV Examples 226

C.1 Main Particulars of the Tubular Multihull Models (All designs 24m long at waterline) 233
C.2 Catamaran Model Properties (All designs 24m long at waterline) 234
C.3 Curved Hulled Catamaran Model Properties (All designs 30m long at waterline) 235

D.1 CFX Input Physics 240
D.2 CFX Domain Configuration 241
D.3 Regular Waves Analysed in CFX 244
D.4 Rigid Body Numerical Model Properties 246

E.1 Test Schedule for the Tubular Multihull: Regular Waves 253
E.2 Test Schedule for the Tubular Multihull: Irregular Sea States . . . 254

E.3 Test Schedule for the Narrow and Wide Hulled Catamarans: Regular Waves 254
E.4 Test Schedule for the Narrow and Wide Hulled Catamarans: Irregular Sea States 255
E.5 Test Schedule for the Curved Hulled Catamaran 255
E.6 Test Schedule for the GDC: JONSWAP Sea States 256

List of Acronyms

[Acronym]	[Description]
AAMV	Aerodynamically Alleviated Marine Vehicle
ASA	Access System Accessibility
BEM	Boundary Element Method
CFD	Computational Fluid Dynamics
CTV	Crew Transfer Vessel
COG	Centre of Gravity
DNS	Direct Numerical Simulation
DNV-GL	Det Norske Veritas Germanischer Lloyd
DP	Dynamic Positioning
EWEA	WindEurope (formerly European Wind Energy Association)
FAROFF	Far Offshore Operation and Maintenance Vessel Concept Development and Optimisation Project
FVM	Finite Volume Method
G+	Global Offshore Wind Health and Safety Organisation
GDC	Grand Draught Catamaran
LCOE	Levelised Cost of Energy
LES	Large Eddy Simulations
MCA	Maritime & Coastguard Agency
MCG	Motion Compensating Gangway
MII	Motion Induced Interruption
NOTF	National Ocean Test Facility
NPL	National Physics Laboratory

[Acronym]	[Description]
NWT	Numerical Wave Tank
O&M	Operations and Maintenance
OREI	Offshore Renewable Energy Installation
P-Plot	Performance Plot
RANS	Reynolds-Averaged Navier-Stokes equations
RAO	Response Amplitude Operator
RMS	Root Mean Squared
RORO	Roll-On/Roll-Off
SES	Surface Effect Ship
SOV	Service Operations Vessel
SPH	Smooth Particle Hydrodynamics
SWATH	Small Waterplane Area Twin Hull
TriSWACH	Trimaran Small Waterplane Area Centre Hull
VOF	Volume of Fraction
WFSV	Wind Farm Service Vessel

Nomenclature

[Symbol]	[Definition]	[unit]
a_T	Traverse acceleration	(m s^{-2})
a_V	Vertical acceleration	(m s^{-2})
A_1	Area under the GZ curve	(m °)
A_f	Wavemaker stroke length at top of domain	(m)
A_{wl}	Area at waterline	(m^2)
b	Damping constant	
c	Damping coefficient	
C_T	Tipping coefficient	
D	CFX domain height	(m)
$\ddot{D}_2$	Horizontal acceleration	(m s^{-2})
$\ddot{D}_3$	Vertical acceleration	(m s^{-2})
E_{Task}	Task effectiveness	
F	Force component	(N)
F_0	Encountering wave force amplitude	(N)
g	Acceleration due to gravity	(m s^{-2})
$\overline{GM}$	Metacentric height	(m)
h	Still water height	(m)
h_e	Specific enthalpy	(m^2 s^{-2})
h_{tot}	Total enthalpy	(m^2 s^{-2})
h_p	a person's VCG	(m)
H	Wave height	(m)
$Hmax$	Maximum wave height	(m)

[Symbol]	[Definition]	[unit]
Hs	Significant wave height	(m)
I	Moment of inertia	(kg m^2)
I_a	Moment of added inertia	(kg m^2)
k	Wavenumber	(m^{-1})
K	Thermal conductivity	(kg m s^{-3} $^\circ$K^{-1})
l	Half-width of a person's stance	(m)
L	Length of Ship	(m)
M	Mass	(kg)
M_a	Added mass	(kg)
p	Pressure	(N m^{-2})
R_T	Tipping ratio	
S_0	Stroke length	(m)
S_E	Energy source	(kg m^{-1} s^{-3})
S_h	Horizontal spacing	(m)
S_M	Momentum source	(kg m^{-2} s^{-2})
S_v	Vertical spacing	(m)
t	Time	(s)
$t_{S_{f/a}}$	Tips per minute sliding to forward/aft	
$t_{S_{p/s}}$	Tips per minute sliding to port/starboard	
$t_{T_{f/a}}$	Tips per minute tipping to forward/aft	
$t_{T_{p/s}}$	Tips per minute tipping to port/starboard	
T	Wave Period	(s)
T_{Calm}	Completion time in calm sea conditions	(s)
T_{Heave}	Natural period of heave	(s)
Tp	Peak period	(s)
T_{Pitch}	Natural period of pitch	(s)
T_{Roll}	Natural period of roll	(s)
T_{Waves}	Completion time while underway	(s)
Tz	Zero Crossing period	(s)

[Symbol]	[Definition]	[unit]
u	Velocity component	(m s^{-1})
U	Vector of velocity $U_(x, y, z)$	(m s^{-1})
$\overline{V}$	Displaced volume	(m^3)
VCG	Vertical centre of gravity	(m)
x	Surge	(m)
X	Horizontal longitudinal ship axis	
X_{disp}	Wavemaker displacement	(m)
y	Sway	(m)
Y	Horizontal lateral ship axis	
z	Heave	(m)
z_{swl}	Distance from still water level	(m)
Z	Vertical ship axis	
α_q	Fluid properties of the q^{th} cell	
γ	Dynamic viscosity	(kg m^{-1} s^{-1})
η_4	Roll or pitch motion	
θ	Pitch	(°)
λ	Wavelength	(m)
μ	Molecular viscosity	(kg m^{-1} s^{-1})
μ_s	Coefficient of friction	
ϕ	Roll	(°)
Φ	Wave potential	
Φ_D	Diffracted wave potential	
Φ_I	Incident wave potential	
Φ_R	Radiated wave potential	
ρ	Density	(kg m^{-3})
ψ	Yaw	(°)
τ	Stress tensor	
ω_e	Encountering circular frequency	(rad s^{-1})

Chapter 1

Introduction

> Civil Engineering is a vital art, working with the great sources of power in nature for the wealth and well-being of the whole of society
>
> Institution of Civil Engineers

1.1 Offshore Wind Energy

Growth of the offshore wind industry has created an increased requirement for offshore wind turbine maintenance. To achieve the target of 95% availability, accessing a wind turbine during high sea states is a key operational issue. To reduce the lifetime, levelised cost of energy, offshore wind turbines need to be serviced regularly, and repaired promptly when they breakdown [1]. In addition to the large cost savings with adequate Operations and Maintenance (O&M), safety is a high motivating factor in increasing the significant wave height (Hs) range for personnel transfers between a wind turbine and a wind farm service vessel (WFSV). Currently there is a 1.5m Hs limit for the standard "step over" method of transferring personnel to an offshore wind turbine, though this varies with vessel type, wave height, period and direction as well as wind and current

factors. Furthermore, there is the skipper's, judgement on whether the transfer is safe to be carried out. The goal of this thesis is to develop methods and investigate design criteria that would allow access in sea states up to 3m Hs, in typical North Sea conditions with a Tp range of 5.5 - 12.5s, similar to Carbon Trust's Offshore Wind Accelerator programme.

Wind mills were historically used to mill grains, towards the end of the industrial revolution (1891) Poul LaCour from Denmark became the first person in Europe to generate electricity from wind [2]. USA built the world's first wind farm in 1980. In the 1990s, wind energy became a commercial reality in Europe. The first offshore wind turbine was in Sweden at Nogersund in 1991, where a 0.22MW turbine was installed in 7m of water, 250m offshore [3]. Denmark also ventured offshore in 1991 constructing the world's first offshore wind farm, with 11 0.45MW turbines 1.8km from shore in 2–4m of water at Vindeby [4].

Offshore wind energy is in a period of considerable growth in Europe, as is highlighted by WindEurope's graph in Figure 1.1, by the end of 2015 there were 3,230 offshore wind turbines grid connected in Europe with a combined capacity of 11,027.3MW in 84 wind farms from 11 countries [5]. In the first half of 2016 the increase in installed capacity is lower than that in the same period in 2016, however the number of foundations and turbines installed were greater [6]. Predictions of future growth are optimistic with the Sustainable Energy Authority of Ireland (SEAI) claiming that with favourable developments in policy and infrastructure, Ireland can achieve deployment of 30GW of offshore wind by 2050 [7].

Due to the growth of the offshore wind industry as the number of sites close to shore sites are exploited, sites further from shore in deeper water are pursued as is illustrated in Figure 1.2. Figure 1.3 shows how the design of wind turbines changes with water depth, it is worth noting that access to floating designs will pose different challenges to fixed wind turbines [8].

It is discernible that on the basis that offshore wind is in a period of expansion, requiring greater access in higher sea states, that vessels that can trans-

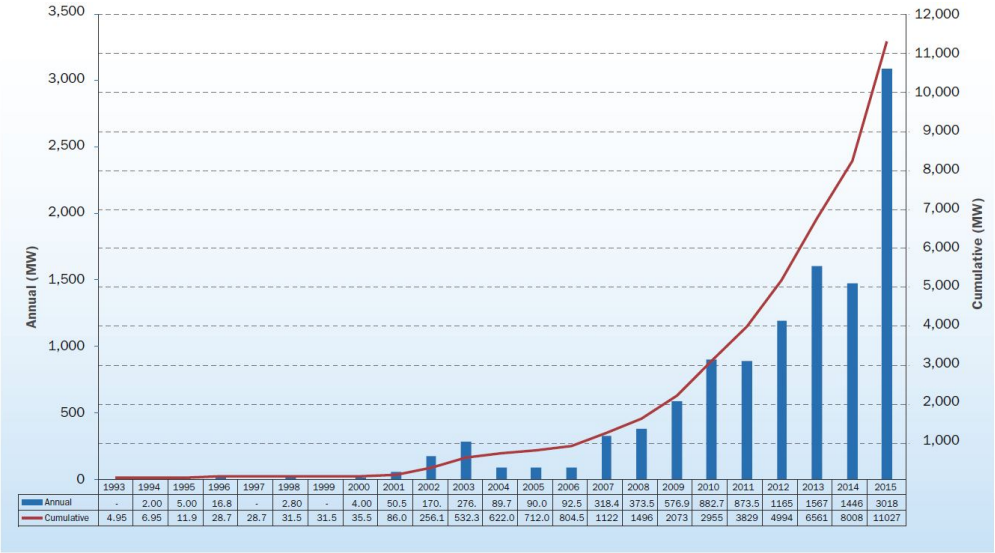

	1993	1994	1995	1996	1997	1998	1999	2000	2001	2002	2003	2004	2005	2006	2007	2008	2009	2010	2011	2012	2013	2014	2015
Annual	-	2.00	5.00	16.8	-	2.80	-	4.00	50.5	170.	276.	89.7	90.0	92.5	318.4	373.5	576.9	882.7	873.5	1165	1567	1446	3018
Cumulative	4.95	6.95	11.9	28.7	28.7	31.5	31.5	35.5	86.0	256.1	532.3	622.0	712.0	804.5	1122	1496	2073	2955	3829	4994	6561	8008	11027

Figure 1.1: WindEurope, Cumulative and Annual Offshore Wind Installations 1993-2015 by MW [5]

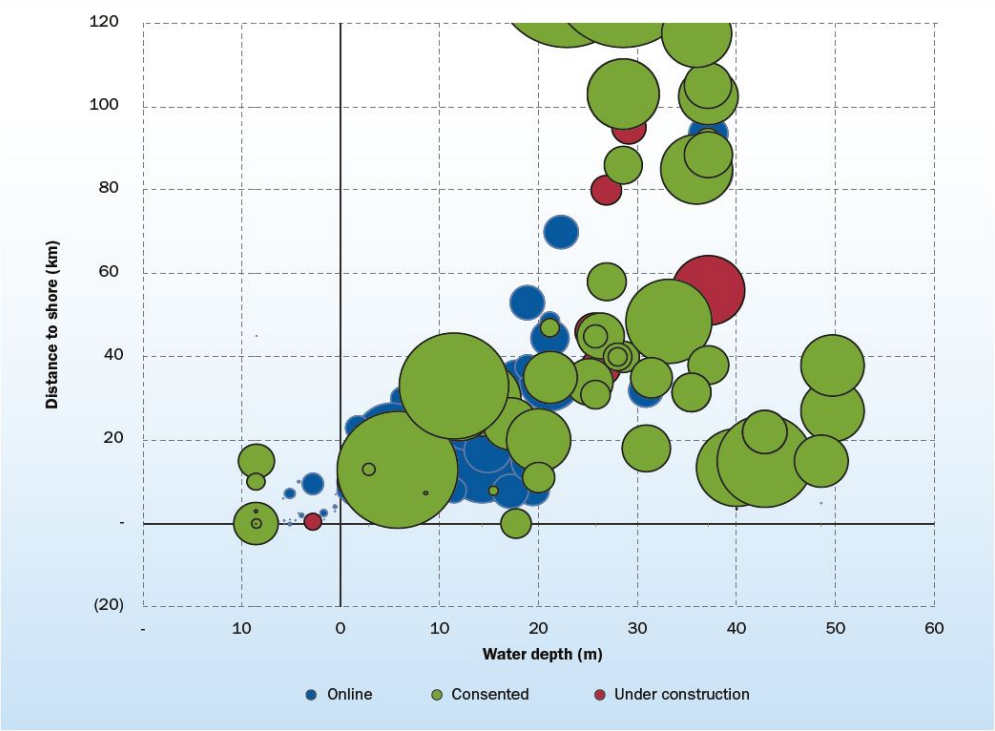

Figure 1.2: WindEurope, Average Water Depth and Distance to Shore of Online, Under Construction and Consented Wind Farms [5]

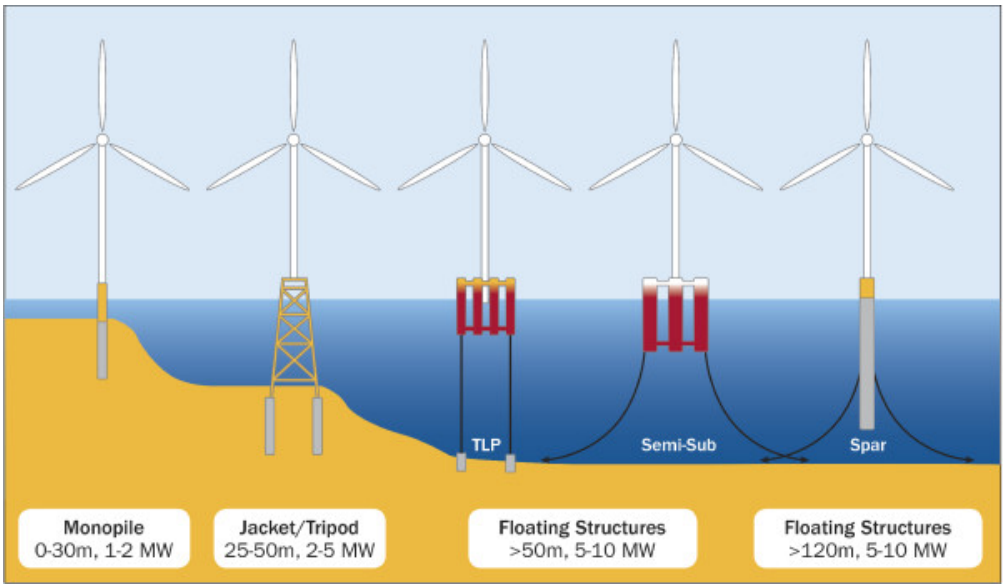

Figure 1.3: Wind Turbine Evolution (reproduced from [5], source Principle Power)

fer personnel safely in these conditions are required. Increasing the weather window that a vessel can operate in safely, decreases the amount of downtime offshore wind turbines have, and thus increase potential profits.

1.2 Offshore Wind O&M

Weather conditions limit maintenance, predominantly by wave height, period, and direction, as well as current, and wind speed. As the industry moves further offshore and into areas with increased wave heights, the cost implications of this impacts significantly on project works. For example, Dogger Bank; "The Crown Estate included an area from Dogger Bank within its third licence round for offshore wind. The Dogger Bank Zone, located between 125 and 290km off the east coast of Yorkshire, extended over approximately 8660km^2" [9]. Dogger Bank thus exemplifies the challenges facing future O&M operations, being an exceptionally large wind farm far from shore.

One of the major issues affecting the operators of WFSVs is safety of access at the wind farm in challenging sea states. Maintenance access is part of the

Carbon Trust's Offshore Wind Accelerator's research project to cut the cost of offshore wind by 10%. New methods, designs and changes in regulations could help the offshore wind service industry. "O&M represents about a quarter of the cost of energy from offshore wind. This high share stems from the cost of accessing and maintaining the turbines, as well as the lost revenue when turbines are not operating" [1, 10].

Safety of the operation is covered through best practice, and legislation, with the International Marine Contractors Association, RenewableUK, UK Maritime & Coastguard Agency, and the National Workboat Association providing the most comprehensive, and up to date guidance [11, 12, 13, 14]. The principal items that affect the risk associated with offshore turbine access included; environmental conditions such as sea state, vessel motion heave, pitch, and roll. In addition, the action of the water up surging between vessels or structures in close proximity, station keeping ability of the vessel involved, crushing or entrapment between the vessel and the ladder, and being stranded on the wind turbine if the met-ocean conditions change and a transfer becomes unsafe are critical factors.

1.3 Vessels for Servicing Offshore Wind Farms

O&M for offshore wind farms relies on a number of processes, and methods to effectively keep blades turning. Generally, this is carried out by a large number of small vessels in the region of 16m–24m long, as well as a smaller number of 24m–30m long vessels. These vessels are described as WFSVs, or sometimes as Crew Transfer Vessels (CTVs). WFSVs are additionally widely used to support construction and O&M of offshore wind farms [15]. 4C Offshore Ltd, "a leading consultancy and market research organisation targeting the offshore energy markets" has over 498 WFSVs listed in its data base [16]. WFSVs are used from the inception to completion of a project, that is from initial surveys, to aiding construction, to the main role in O&M, and will furthermore be used for decommissioning, hence as the number of offshore wind turbines grow, so should the

number of WFSVs [15]. However, upcoming wind farms will come with new challenges related to increased wave heights and distance to shore. In addition, there are a few very large Service Operations Vessels (SOVs), mother ships, and small jackup barges that support offshore wind O&M. An example of a SOV is Siemen's new 84m; "Esvagt Faraday" [17] depicted in Figure 1.4.

A large amount of innovative engineering has occurred for vessels that transfer service personnel to offshore wind turbines to carry out maintenance. WFSVs have developed substantially as more wind farms were developed from monohulls, to TriSWATCH, and surface effect ships. As the offshore wind industry continues to grow, continued improvements and innovation must be employed by designers, and operators so that they are more competitive and meet the client's O&M requirements for future wind farms [18, 19].

Figure 1.4: Sample Service Operation Vessel: Esvagt Faraday [17]

There are specific vessels are being designed to meet offshore wind industry requirements for WFSVs. Therefore, some are becoming better at transit and at transfer, and some are becoming better at just the transfer in conjunction with mother ships/accommodation platforms, for example BMT Nigel Gee's XSS and SWATH vessels versus Extreme Ocean's TranSPAR. In addition, there are large Offshore O&M vessels that can remain at the wind farm for long periods and utilise walk to work motion reducing gangways, for example the SOV in Figure 1.4. These are elaborated on in further detail in § 2.2, 2.3, & 2.4.

By studying the WFSVs currently in operation and their effectiveness for the wind farms they service, based on metrics such as distance from shore, bathymetry, tides, wave height, wave periods, wave directions as well as wind speed and direction, it may be observable which methods can and cannot work,

thus enabling the industry to develop new WFSVs and methods to access offshore wind turbines [20]. In addition, in order to access offshore wind energy structures, it is important to note that the vessel's motion should be minimised to ensure safe operations. The accelerations induced on the vessel agitate personnel in the form of seasickness when in transit, and impose risk when standing and stepping off the bow at time of transfer.

1.4 Research Outline

This thesis studies the issue of access for O&M, it examines the technical considerations, methods, and parameters that are of interest for the transfer of personnel to and from wind turbines at the wind farm. It investigates principal considerations of WFSV designs for the offshore wind industry. A variety of designs that address key parameters in relation to personnel transfers at a wind farm are analysed. From a radical tubular multihull design to very small waterplane area catamaran designs with heaveplates at various depths, and angles to increase the Hs that the vessel can operate, transferring personnel safely and effectively. As has been previously outlined O&M is limited by access to offshore wind turbines. The research presented will not provide a complete insight to designing an O&M campaign covering transporting technicians to the wind farm, offshore accommodation if necessary, and management of vessels around the wind farm. This thesis will specifically address the personnel transfer from vessel to wind turbine, analysing the differing variables that affect safe transfers, and methods that can be employed to analyse these variables. Thus, the objectives of this thesis can be summarised as:

1. Determine the metrics that limit transfer to an offshore wind turbine.
2. Examine the nature of a WFSV interaction with a monopile.
3. Explore novel designs to increase the Hs that transfers can take place.

This is achieved first by carrying out a literature review, subsequently investigating the motions of WFSVs at zero forward speed, both with numerical simulation and scaled physical model experiments, and finally by conducting physical model tests of WFSVs interacting with a monopile foundation. Novel WFSV designs are developed, compared, and limit metrics of motion are discussed throughout the thesis. A brief overview of each chapter follows:

Chapter 2 reviews the relevant information relating to WFSVs. A review of the O&M industry is carried out examining both existing vessels and access methods, as well as concepts in development. This chapter also focuses on the current industry limits, and guidance for accessing wind turbines as well as general methods of quantifying motion limits for working on ships. In addition, the current state of the art in modelling WFSV interaction with the wind turbine at the time of transfer is reviewed.

Chapter 3 discusses the development of the novel WFSV designs discussed in this thesis. An overview of each design, explaining how the different methods of analysis progressed the design development of the models is presented.

Chapter 4 outlines the numerical modelling carried out in this study. Firstly, analysis using the computational fluid dynamic (CFD) code ANSYS CFX is discussed, and secondly analysis with the boundary element method (BEM) code ANSYS AQWA is presented. Numerical damping is implemented to aid model development based on the results from the physical model testing carried out in Chapter 5.

Chapter 5 presents the physical model testing of WFSV designs at zero forward speed, discussing their motions characteristics. Response amplitude operators (RAOs) are developed as well as an examination of motion induced interruption (MII), and root mean squared (RMS) values for accelerations and pitch angles.

Chapter 6 compares the outcomes of the numerical simulations with the scaled physical model testing carried out in Chapters 4 & 5.

Chapter 7 investigates the interaction of a WFSV with a monopile. Physical scale model tests were carried out with a vessel slack moored close to the monopile, with a vessel applying a constant force into the monopile to maintain contact, and finally the angle of the wave direction in relation to the ships heading considered.

Chapter 8 presents the principal conclusions from the work discussed in the thesis, and gives some suggestions for further study.

1.5 Publications

From the work carried out during this study the following articles were published;

- M. Shanley, J. Murphy, and P. Molloy. Offshore wind farm service vessel, hull design optimisation. In 4th International Conference on Ocean Energy (ICOE), Dublin, 2012.
- M. Shanley, and J. Murphy. Physical and numerical analysis of a concept offshore wind farm service vessel hull design. In Design and Operation of Wind Farm Support Vessels, pages 155–163, London, United Kingdom, 2014. University College Cork, The Royal Institution of Naval Architects.
- M. Shanley. Stable ships for smooth servicing of offshore wind farms. The Boolean, pages 179–183, 2014.
- M. Shanley, S. Balke, and J. Murphy. An innovative hull design for an offshore wind farm support vessel. In Design and Construction of Wind Farm Support Vessels, pages 59–65, London, United Kingdom, 2016. University College Cork, The Royal Institution of Naval Architects.
- M. Shanley, S. Balke, and J. Murphy. Stepping up to the plate. Ship & Boat International September/October 2016, pages 30–35.

Chapter 2

Literature Review

2.1 Introduction

In this chapter the principal elements of the offshore wind industry in relation to access requirements are discussed. Firstly, a review of current vessels used in industry is carried out, separating the differing types of vessels in operation and motion compensating gangways utilised, new maintenance vessel concepts in development are then presented.

The rules, regulations and standards relating to wind farm service vessels (WFSVs) are then examined for guidance as well as accident reports relating to personnel transfers. The current industry limits for accessing turbines are examined followed by the maintenance requirements alongside a review of weather windows. Quantitative limits for working on ships are then discussed, reviewing guidance for different types of ships carrying out differing tasks including WFSVs.

Following on from this the motion of offshore structures are described with relevance to WFSVs, and the minimisation of motions including an overview of heaveplates. Subsequently, the different methods of numerical modelling of floating offshore structures are investigated. Finally, current state of the art in modelling WFSV interaction with offshore wind turbines at the time of transfer is discussed.

2.2 O&M Vessels Utilised in Industry

2.2.1 Overview

O&M of an offshore wind farm is substantially more expensive than for an onshore wind farm, it is vital that suitable vessels carry out maintenance, so that they can access the wind farm as often as possible, and that access is not unreasonably restricted by wave height [21].

WFSVs are an integral part of the offshore wind industry, in providing transit and transfers for a wide range of activities, throughout the lifecycle of the wind farm from initial surveys to decommissioning. Wind turbines need to be accessed on an on-going basis, with a requirement for differing O&M vessels throughout the lifetime of the wind farm for tasks ranging from turbine maintenance to foundation repairs [15].

The daily charter rate has a large impact on the cost of operating a WFSV. This is reducing the chartering of better vessels that can handle larger wave conditions. There is an example of one operator who procured a cheap long vessel that they had to decommission due to lack of use [22]. However, counter to this, the Carbon Trust have invested heavily in methods to reduce the cost of offshore wind "energy by 10% in time for Round 3" [20]. A major one of these methods are Access Systems, including both vessels and transfer systems.

The majority of displacement multihull vessels in current service are designed using the National Physics Laboratory (NPL) hull form series developed by Baily in 1976 [23]. Offshore wind farm service providers have developed these designs to create vessels particularly suited for offshore wind farm maintenance, by manipulating the bow and stern hull form and even using deep-V hull forms. These modifications have provided substantial improvements, notwithstanding this access to wind turbines in sea states with a 3m Hs or more, require radically new designs to be considered [24, 25].

There are a large number of WFSVs in operation in the European waters of the North Sea and Baltic Sea [16, 26]. Most of these vessels are catamarans,

ranging from roughly 16-30m in length with the majority being 20-24m long. There are a number of SWATHs, semiSWATHS, trimarans, triSWACHs in operation as well. In addition, there are some monohulls in the industry, though most are being phased out as operations advance. Larger vessels are entering the market that use dynamic positioning (DP) systems and motion compensating gangways. For future construction and O&M operations a range of these vessels may be useful. A sample of vessels in operation is presented to give a snapshot of the diversity of vessels in current service.

2.2.2 Catamaran

Catamaran WFSVs are used where the aim is to get to the wind farm as quickly as possible whilst keeping seasickness and fatigue at a minimum, an example is shown in Figure 2.1. Catamarans use the industry standard method of bow transfers using a reinforced bow with a rubber fender. A relatively large bollard pull allows the connection to be maintained safely for most wave spectrums with a 1.5m Hs. Table A.1 shows a range of catamaran WFSV examples. 4C Offshore Ltd, "a leading consultancy and market research organisation targeting the offshore energy markets" has 498 WFSVs in their database [16]. The vast majority of these vessels are high speed catamarans with a cruising speed for 15-25 knots and are generally between 15-24 metres in length. They can usually carry a cargo in the range of 3-15t. Typically they are aluminium, though glass reinforced plastic and other composites are used.

Figure 2.1: Sample Catamaran: Windcat [27]

Particular motion characteristics that are useful to the crew transfer opera-

tion for a catamaran are that is a very rigid vessel which is useful for stability in short seas, as due to the twin hulls there is a high resistance to roll. The planing hull allows for fast transit speeds, hence the catamaran can be efficient at carrying out many transfers within a short timeframe. However, there is a high fuel consumption rate at higher speeds, and the bow is prone to slipping when in contact with the wind turbine in higher sea states. The limit sea states relate to vessel length as a longer vessel is influenced less in heave by the waves encountered. In addition, the buoyancy at the bow is critical as if the buoyancy force is too great it will cause the bow to slip on the monopile.

2.2.3 Monohull

Monohulls can provide a similar service to that of catamarans. They were mostly used prior to the uptake of specialised catamarans into the market. Monohulls are generally limited at a 1.5m Hs. Table A.2 shows a range of monohull WFSV examples. Dong Energy concluded from two years of operating Nysted offshore wind farm that they required more access. To carry this out they commissioned the "Wind Supporter" a monohulled vessel with the following requirements; LOA = 24M, Speed 18 knots, a front mounted crane and a capacity for 24 passengers. Figure 2.2 shows the vessel positioned for a personal transfer to the turbine [28].

Figure 2.2: A2Sea Wind Supporter [28]

For the monohull the hull characteristics of the vessel allow a greater rolling motion than a catamaran of the same length, though heave and pitch motion are similar. One advantage a monohull has is that it is more comfortable in a larger

number of sea states due to the longer roll periods. The main disadvantages of the monohull compared to a catamaran stem from the increased roll motion which can reduce access limits, and deck loading.

2.2.4 SWATH

SWATH stands for Small Water plane Area Twin Hull. Two submersible hulls with a slender connection to the deck structure allows it to achieve a small water plane area. An example of a SWATH can be seen in Figure 2.3, the "Natalia Bekker" is a 26 metre SWATH vessel that can operate in wave conditions of up to 2.5m Hs [29]. SWATHs offer significantly more stability during transit and transfer, the increase in stability is due to the small water plane area and deeper draft. However, due to the deep draft, and the increased wetted area overall, SWATHs suffer from being more expensive to run. Moreover, SWATHs are expensive to build due to structural, and motion control system requirements of the design, therefore, could be best suited to the far shore wind farm. Table A.3 shows a range of SWATH WFSV examples.

Figure 2.3: Sample SWATH; Natalia Bekker [29]

The beneficial motion characteristics of SWATH vessels are reduced heave and pitch, which come from the reduced water plane area, and hulls at depth, hence the wave particle motion impact is less than that of vessels with greater buoyancy closer to the water surface. This advantage enables the vessel to access the monopile in higher sea states due to the reduced motion response in particular heave motion. Reduced fatigue from motion effects on technicians result in an improved performance overall. Very small lateral and longitudinal

metacentric heights increase the natural period of roll and pitch considerably, this results in the requirement for ongoing ballast optimisation, and active ride control systems, hence SWATHs are unable to carry large loads, particularly on deck. Additional disadvantages of using a SWATH are; for maintenance of the vessel a dry dock is required, in general they are slower than other craft, and are expensive to build, and have poor fuel economy. Due to the high costs the decision to use a SWATH in a wind farm O&M campaign is an economic decision, based on accessibility and turbine down time [30, 31].

2.2.5 Trimarans and TriSWACH Craft

Trimarans and triSWACH craft are best suited for servicing wind farms that require fast daily transit, and transfers at a Hs above 1.5m because they have an advantage of being faster, more efficient and stable than catamarans whilst avoiding some of the expense that a SWATH incurs. Figure 2.4 shows one of Austal's TriSWACH in operation. Another WFSV company, Mobimar are using trimarans extensively in their fleet, claiming safe access up to 2.5m Hs [33].

Figure 2.4: Austal TriSWACH [32]

Figure 2.5 shows a maintenance vessel that was launched in 2013 by Fjellstrand. the Fjellstrand WindServer is a trimaran designed for fast transit, it has a horizontal hydrofoil on the centre SWATH shaped hull at the bow which in addition to aiding speed and fuel efficiency it also reduces the heave motion of the bow when docking with a wind turbine [34]. Table A.4 shows a range of trimarans and triSWACH WFSV examples.

The motion characteristics that define both trimarans and triSWACH craft are due to the fact they are generally built with a smaller bow thus reducing the bouyancy force experienced by the bow when docking with a wind turbine. The main advantage that a triSWATCH has is that the centre hull has a small waterplane area thus reduces the drag the vessel experiences. The centre hull can be used as a horizontal foil which can improve performance while in transit and at the wind farm may act as a damper to vertical motion at the bow. In addition, the vessels have a relativly large lateral metacentric height similar to a catamaran.

Figure 2.5: Fjellstrand WindServer [34]

2.2.6 Surface Effect Ships

Surface effect ships (SES) are lifted by an air cushion enclosed by hulls on either side and a flexible rubber sealing in the bow and stern. The heave motion of the vessel is reduced by the air-cushion that the surface effect vessel has created. This air cushion can carry up to 80% of the weight of the vessel. The motion characteristics of surface effect vessels are due to the air cushion reducing the effect of wave loads on the vessels motion [36]. The air cushion also enhances sea keeping and passenger comfort combined with a high service speed [35]. Figure 2.6 shows Umoe Mandal's Wave Craft a Surface Effect Vessel Interacting with an Offshore Wind Turbine.

Figure 2.6: Surface Effect Vessel; Umoe Mandal's Wave Craft [35]

A SES has a more significant involuntary speed loss in waves than a catamaran of similar size, thus there is reduced benefit in higher seastates. SES vessels have issues with maneuvering due to significant air cushion drag, resulting from high drift angles, and associated feeding problems of the waterjets. In addition, vehicle speed and turning radii are cropromised at high wind speeds, thus this may be an issue for docking at a wind farm, which often have larger wind speeds by design. As a result of resonant compressible flow effects in the air cushion during small sea states, vertical accelerations are induced (called the cobblestone effect). An automatic control system is generally used to negate this effect [36].

SES vessels use less power and maintains a higher speed than a catamaran due to the reduced resistance, even when the air cushion fans are accounted for. In general, due to the damping effect of the air cushion and the reduction in water elevation inside the cushion, the SES has less vertical motion than a catamaran [36].

2.2.7 Semi-SWATH

Similar to trimarans and triSWACH vessels, semi-SWATHs are suitable for servicing wind farms that require fast daily transit, and transfers at a Hs above 1.5m. Semi-SWATHs are a compromise between a SWATH and a catamaran, for example BMT Nigel Gee's XSS (Figure 2.7) this design substantially improved on the seakeeping characteristics of a catamaran whilst only modestly affecting the cost [37]. The semi-SWATHs favourable motion characteristics are achieved by having narrow sections at the waterline, and a lower centre of buoyancy reduc-

Figure 2.7: BMT Nigel Gee XSS [37]

ing wave load [37].

2.2.8 Floatel

Floatels are another type of vessel (they are generally converted cruise ships, ferries or roll-on/roll-off (RORO) ferries) that are currently being used in the offshore wind industry to provide accommodation to staff at the wind farm to reduce transport to and from the wind farm. Generally, floatels are used for installation and construction crew, these vessels are the precursor to the mother ship. Wind Power Support, see Figure 2.8 are an example of a company providing floatels for the offshore wind sector, providing ships in the region of 120–150m long with a capacity to accommodate 80–130 technicians [38].

Figure 2.8: Wind Power Support WindPerfection [39]

The motion characteristics that define a floatel are smooth long period motions associated with ferries, floatels are generally a long and large ship, therefore they have a minimal response to waves. Hence, for its purpose there is a good response suited to crew comfort. However, as a flotel is an accommodation vessel it still requires a small service vessel to transfer technicians from the floatel to the wind turbine.

2.2.9 Service Operation Vessels

A number of large dedicated service vessels are entering the market at present, these vessels are in the region of 100m long can accommodate around 80 technicians, utilise dynamic positioning (DP) and have a motion compensating gangway installed. These ships have been designed to suit the particular needs of O&M, for example Seimens and Damen have very efficient vessels, with Seimens boasting the ability to access turbines every 30 minutes with the Esvagt Farady as seen in Figure 2.9 [17].

Figure 2.9: Sample Service Operation Vessel: Esvagt Faraday [17]

Similar to a flotel a service operation vessels motion characteristics are dependent on the long large ship so motions are minimal in general due to its size. In addition, there is often a larger beam than usual to allow greater lateral stability so it can access turbines in a greater number of sea states. However, a service operation vessel is costly to build and run, as stated earlier it requires a motion compensating gangway to operate, dynamic positioning, and hence the time between transfers is quite large compared to a catamaran.

2.2.10 Small Jack-Up Barges

Jack-up barges carry out a substantial amount of work during the construction phase of an offshore wind farm project, due to their ability to lift heavy components from a fixed structure, for O&M jack-ups can carry out heavier lifts such as gearbox or blade replacement. DBB have designed a smaller jack-up barge Wind Server to carry out O&M tasks. As a jack-up barge it can operate above 2.5m Hs [40]. Figure 2.10 shows DBB's mini jack-up Barge "J/U WIND" carrying out a blade replacement.

Figure 2.10: J/U WIND [40]

A jack-up barge requires a small sea state to carry out the jacking operation so as to avoid any damage to the jacks and does not "punch through" the sea bed. This vessel has resticted use to carrying out large O&M lifts to make it an economical option.

2.3 Motion Compensating Gangway

2.3.1 Overview

Motion compensating gangway (MCG) also referred to as "walk to work" systems are a useful tool in increasing the operational window that a WFSV can carry out transfers. MCGs can increase the maximum transfer Hs from 1.5m for a catamaran under 18m long to 2m Hs and can allow Service Operations Vessels (SOVs) to carry out transfers up to 3.5m Hs [41].

A MCG is a valuable tool in connecting the WFSV to the turbine and minimising the relative accelerations and displacements. These can entail a full six degree of freedom motion stabilising device, or a heave compensating bridging mechanism. They can then attach to the wind turbine so that personnel

can safely walk onto the turbine as the bridge remains stationary relative to the turbine. Some of the larger MCGs have closed roofs to protect personnel from falling objects such as ice, and can enable easy transport of parts and equipment from the WFSV to the turbine with wheeled trolleys or pallet carriers. However, despite the benefits of MCGs there are drawbacks. MCGs require a large amount of deck area, they reduce the WFSVs cargo capacity, and the capital cost of the equipment and installation can be high. MCGs require their own power source, take up deck area and need to be fitted to the vessel, furthermore they are limited by their ability to react to conditions and travel of hydraulic rams, and as such are used cautiously as this may cause incidents. They must hence prove beyond doubt that the conditions with which they can operate in [42]. Vessel ability is not always the limit but a blanket safety limit. “Health and safety regulations in place are slow to adapt to improving vessel capabilities and hence, 1.5m Hs is still a cut-off point regardless of vessel size and capability” [43].

There are number of MCGs on the market such as Ampelmann, Damen shipyards Walk-to-work, MaXccess, Mobimar, Wind Servant and Houlder TAS and not only do they make it safer for personnel to transfer, the transfer can often take place in higher sea states. This is in part due to larger vessels incorporating the access systems.

2.3.2 Zbridge

Figure 2.11 shows the Zbridge access concept a design from Ztechnologies a company that focuses on innovations for access in the Offshore Wind sector. The Zbridge design comprises of a motion compensated mast & bridge assembly, allowing direct access to the turbine. It can provide safe access up to 3.5m Hs and a top wind speed of $18\,\mathrm{m\,s^{-1}}$.

Figure 2.11: Zbridge Access Concept [44]

2.3.3 Ampelmann

Ampelmann is a 6 degree for freedom MCG that operates up to 3m Hs. Ampelmann utilises a Stewart platform that is often used for flight simulators as illustrated in Figure 2.12. It can provide safe access up to 2.5m on vessels above 50m length and 3m Hs on vessels above 70m length [42, 45]. Ampelmann operates on a ship with dynamic positioning (DP), and provides a direct walkway to the wind turbine. It is being used for ship to ship transfers, and access to a wide variety of offshore structures.

Figure 2.12: Ampelmann [42]

2.3.4 UPTIME

UPTIME (Figure 2.13) have two motion compensating gangways depending on the size of the vessel that they would be installed on: A 6–12m one suitable for small WFSVs that would carry out step across bow transfers; and a 15–40m one suitable for larger support vessels. The maximum Hs that the gangways can carry out transfers is 2.5m and 3.5m for the small and large gangway respectively.

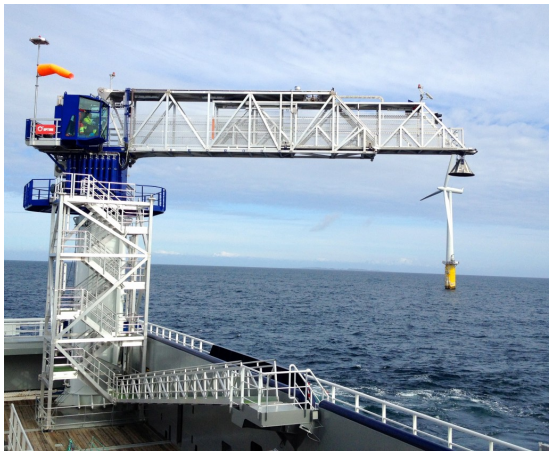

Figure 2.13: Uptime [46]

2.3.5 MaXccess

Figure 2.14 shows the MaXccess motion compensating gangway that has the ability to clamp to the wind turbine tower, this eliminates the risk of the MCG loosing contact with the tower and hence reducing the risk of a man overboard incident. On WFSVs under 18m it can operate up to 2m Hs and above on ships over 18m [47].

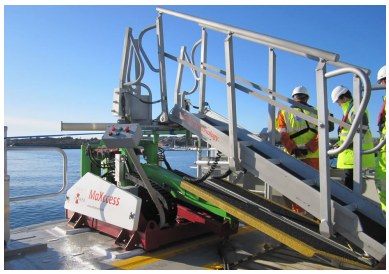

Figure 2.14: MaXccess [47]

2.3.6 Autobrow

Figure 2.15 shows Autobrow an automatically controlled gangway that minimises the vertical motion between the ship and the wind turbine tower. Autobrow is being developed by Ad Hoc Marine and aim to operate up to 2.5–3m Hs depending on the vessel [48].

Figure 2.15: Autobrow [48]

2.3.7 Turbine Access System (TAS)

Houlder and BMT Nigel Gee have developed Turbine Access System (TAS) illustrated in Figure 2.16 it is an automatically controlled gangway that minimises the motion between the WFSV and the turbine tower. The innovation has been tested up to a 1.8m Hs [49].

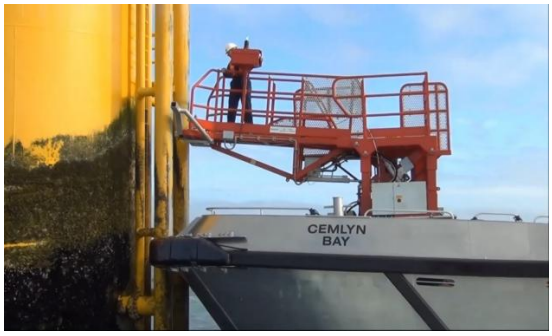

Figure 2.16: TAS [49]

2.3.8 Momac

Figure 2.17 shows an articulated crane type system developed by Momac that transfers personnel to the wind turbine in a custom designed man-basket. Momac have developed two offshore access systems MOTS 500 and MOTS G / 1000. MOTS 500 can accommodate up to 3.2m heave, 15° roll, 10° pitch and 10° yaw. MOTS G / 1000 can accommodate 4m in heave 1.5m is surge and sway and 10° in all rotations [50].

Figure 2.17: Momac MOTS [50]

2.4 New Maintenance Vessel Concepts

2.4.1 Overview

Future vessels for O&M are going to be very varied, as is perceptible from the current trends in the different vessels currently available, in addition to the designs being developed. Combining opposing design restraints such as good sea keeping and fuel efficiency is a challenge facing WFSV designers [37]. One method to design future WFSVs is to identify the parameters that affect the desired performance. Hs is the current metric from which designs are measured, but other factors play a large role in determining how a well a WFSV will perform its tasks. Factors such as wave direction and wave period, current, wind speed and direction, capacity, vessel speed, comfort, safety, fuel economy and charter costs are all useful metrics. Moreover, transit from port or mother ship to turbine, approach to turbine, transfer from vessel to turbine, maintained speed, safety,

capacity, and operating cost, must all be taken into account. Modelling these metrics will allow operators to determine which systems are most appropriate for a specific location.

Carbon Trust with their offshore wind accelerator program are promoting innovative designs in the industry, such as: TranSPAR, Fjellstrand WindServer, Nauti-Craft, and Pivoting Deck Vessel. In addition, there are many other designs that are at the concept stage of development in research centres from universities to large industry enterprises to small start-ups. Each of these designs have the potential to revolutionise wind farm access and the designs that are successful will have far reaching effects on the entire offshore industry. A sample of proposed designs are presented below to give a snapshot of the diversity of vessels in development.

2.4.2 OffshoreShipDesigners, Sea-Wind Wind-Farm Maintenance Vessel (WMV)

Figure 2.18 shows a new maintenance vessel concept by Offshore Ship Designers. The Sea-Wind Wind-Farm Maintenance Vessel (WMV) design is for a mother ship, which would remain on station in deep-water offshore wind farms providing a safe haven for multiple numbers of catamaran workboats to carry engineers to service the turbines [51]. The following mother ship options are also being developed [18, 19, 52, 53].

Figure 2.18: Offshore Ship Designers [51]

The motion characteristics that define this vessel are that it is a large ship with passive motion characteristics; its design principle relies on lifting vessels

out of the sea which is quite challenging.

2.4.3 Extreme Ocean, TranSPAR

Figure 2.19 shows a new maintenance vessel concept by ExtremeOcean, named TranSPAR. This concept relies on the principle that a small water plane area reduces wave load on the vessel and hence motions. The design also has a deep keel to provide stability [54, 55]. The motion characteristics of Extreme Ocean's unusual design TranSPAR are that it has a deep draught with a ballasted keel, small waterplane area, has a spar like response, it could have issues with heave at resonance, but that is easily mitigated. Hence, it has minimal wave load and response, however it has a low trust so needs to clamp on to the wind turbine tower, and must work in conjunction with a mothership.

Figure 2.19: Extreme Ocean TranSPAR [54, 55]

2.4.4 Nauti-Craft

Figure 2.20 shows the testing of an 8.5m Nauti-Craft prototype being tested in a sea trial. The Nauti-Craft separates the catamaran hull and deck of the vessel and implements a suspension system between them to reduce the motion experienced on the ship's deck [56, 57].

This vessel works with a suspension system that allows better ride control and minimises the movement on the deck part of the vessel, hence there is very small response to waves on deck. The reliability of suspension system is critical, and

Figure 2.20: Nauti-Craft [56]

once maximum travel of the suspension system is reached it must then default to a fixed hull system similar to that of a catamaran.

2.4.5 North Sea Logistics Pivoting Deck Vessel

North Sea Logistics' Pivoting Deck Vessel is a catamaran type WFSV in which the deck itself pivots about a point just in front of the cabin. A simulation of the design is shown in Figure 2.21. The concept is based on the central foredeck of the vessel that interacts with the monopile staying relatively still while the rest of the ship pivots about it [58].

Figure 2.21: North Sea Logistics Pivoting Deck Vessel [58]

The Pivoting Deck Vessel behaves similarly to a catamaran but with a pivot system in the foredeck which removes the perception of pitch from the bow of the vessel, and reduces the effect of large bow buoyancy forces. This reduces the vertical motion at the bow when docked onto the monopile. The vertical motion at the bow is a critical factor that is addressed by the system minimising the pitch motion but not the overall heave motion, thus there is limited potential. With additional moving parts it must be noted that the reliability of the pivot system is a critical factor in sustaining performance.

2.4.6 Aerodynamically Alleviated Marine Vehicle

Figure 2.22 shows a concept proposed for a WFSV based on an aerodynamically alleviated marine vehicle (AAMV) design [59]. AAMVs reduce their perceived weight by utilising aerodynamic lift whilst maintaining contact with the water surface thus allowing them to travel efficiently at high speed. Due to these unique high speed properties AAMVs could potentially offer a faster and more comfortable method of transit to a wind farm with greater efficiency. Speed is the only unique aspect of the design, when docked at the wind turbine it would behave similar to a catamaran [60, 61, 36].

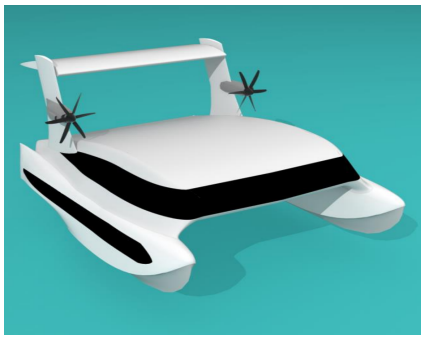

Figure 2.22: Concept AAMV WFSV [59]

2.5 Rules, Regulations and Standards Applicable to WFSVs

Currently there is no harmonised international code or regulation specifically for WFSVs, operators are classing vessels with either the UK Maritime & Coastguard

Agency (MCA) or Det Norske Veritas Germanischer Lloyd (DNV-GL). Most current sites can be serviced by MCA Cat 2 vessels, as a consequence most current WFSVs are generally less than 24m long, and are restricted to operate within 60mn from a safe haven. MCA Cat 1 regulations for ships greater than 24m are more onerous and stipulate additional safety features, however they can operate at a greater distance from a safe haven (up to 150nm), making these regulations more suited to upcoming offshore wind farms. Alternatively, the vessel could be specially coded by a classification society such as DNV-GL. The construction of wind farms further than 60nm is producing changes in the types of vessels and methods used for access. Up to date regulation will provide opportunities to class the WFSVs operating in this region. The regulations currently in place are not adequate for the work being carried out, the better developed the regulations are, and the more standardised access requirements are, the safer it will be to access offshore wind farms [62, 63].

The wellbeing and safety of the offshore wind turbine technicians who commute to the wind farm on a WFSV is increasingly significant as wind farm operators aggressively pursue increases in the limits for O&M access. As wind farms are constructed further offshore, WFSVs have to travel greater distances in difficult conditions. Larger vessels are more capable with larger Hs and wind speed, but the accelerations and stresses placed on the personnel must be taken into account. A challenge facing the industry is the time technicians can spend in transit each day. A 12h day for technicians are standard when the commute is factored into account, fatigue levels due to this are very high. The technicians that service offshore wind farms are not seafarers and hence suffer more severely from motion induced fatigue than other offshore workers. WFSV designers have mitigated these concerns by integrating features such as windows that enable passengers to see the horizon and vibration and suspension seating [52, 64, 65].

There are a number of design codes and guidance documents that are relevant to WFSVs. A selection of these documents are briefly outlined in relation to their impact on the design and operation of a WFSV, with a particular focus on

the access limits and safety of the transfer of personnel to offshore wind turbines.

Items that affect the risk associated with offshore turbine access includes; environmental conditions such as wind speed and direction, sea state including swell height and direction, current or tide speed and direction and vessel motion heave, pitch, and roll. In addition, the action of the water up surging between vessels or structures in close proximity and station keeping ability of the vessel involved are critical factors [11]. Some of the principal safety hazards associated with offshore turbine access include; falling, either onto the vessel, in the water of being suspended by the fall arrest system; crushing or entrapment between the vessel and the ladder; being stranded on the wind turbine if the met-ocean conditions change and a transfer becomes unsafe [12].

Additional information on the details of procedures for transfers between vessels and the general naval architecture requirements of WFSVs are available, yet quantitative assessment of motions or accelerations that affect a transfer are lacking. It had been recommended that the ships maximum thrust should be greater than the maximum wave force on the vessel [66], though with recent research better guidance may be possible [67, 68, 69]. An assessment by the ship's master should be carried to ensure that a transfer is safe to occur [13, 14]. Guidelines on the WFSV vessel naval architecture are available though they tend to focus on the general requirements of the vessel and not the specific task of transfer [63, 66, 70].

Maritime pilots regularly embark and disembark from other vessels and as such have a wide range of best practices to follow, in relation to the physical boat to boat transfer, there is strict guidance on ship design so that the ladders provided are safe for boarding [71]. A detailed procedure of pilot embarkation and disembarkation is provided in guidance notes [72]. The main hazards associated with boat transfers for pilots are: a fall from a height, drowning, impact or crushing injuries, impact with a vessel after a fall, sprains, twists and/or pulls, cold water immersion, hazardous weather and/or sea conditions [73].

2.6 WFSV Accidents

Accident and incident reports relating to the offshore wind O&M industry are poorly reported. The Global Offshore Wind Health and Safety Organisation (G+) provide annual statistics on offshore wind incident data within Europe with the first report appearing in 2013 [74, 75, 76], in addition to an annual report on UK offshore wind health and safety statistics [77, 78]. Quite a few near misses and minor accidents have been reported in relation to access to offshore wind turbines with no fatalities recorded to date [79, 80, 81, 82].

In the offshore wind industry, reported incidents and accidents inform the regulations [22], for example for the incidents in the previous paragraph there is a corresponding guideline in the RenewableUK: Offshore Wind and Marine Energy Health and Safety Guidelines volume 2 [12].

Although not transfers relating to a wind turbines the following highlights the risk associated with personnel transfers. A recent accident relating to transfer from one vessel to another was recorded, the crush incident occurred during transfer from a barge to a tug resulting in the loss of one life [83]. The oil and gas industry has carried out a large number of marine transfer of personnel offshore, and incurred a number of accidents and fatalities which serves to inform the offshore wind industry that transfers pose significant risk [84, 85]. Similar to a transfer between a WFSV and an offshore wind turbine is the boarding and disembarking of pilots from ships entering and exiting harbours, with which there are a large number of fatalities associated [71].

2.7 Industry Limits for Accessing Wind Turbines

Generally, catamarans can carry out transfers up to 1.5m Hs, though some operators may claim more [22]. The SWATH vessel Natilia Bekker can access wind farms up to 2.5m Hs [29]. An Ampelmann device attached to a 70m long vessel is proven to be able to access wind turbines up to 3m Hs. It is worth noting

that Ampelmann's limit on motion is determined by displacement, which is 0.5 meters at the top of the platform [42, 45].

The motion limits of a WFSV in operation depend on the access method. To typical methods of accessing a wind turbine are either for the bow of the vessel to maintain contact with the wind turbine tower using a high friction fender and large thrust force, or to maintain station close to the turbine and use an access system such as MaXccess or Ampelmann.

By examining the motions of a WFSV it can be seen that for bow transfers the two components of motion that restrict the personnel transfer operation are accelerations, and displacements at the bow of the vessel [69]. Excessive vertical displacements of the bow of the WFSV make it difficult to step across at a specific height, grabbing a specific rung of the ladder. Furthermore, excessive displacements caused by loss of frictional contact between the WFSV and the monopile could cause a serious incident if a transfer operation was being carried out. Additionally, as a consequence of high accelerations, personnel lose balance; this is referred to as tipping and sliding.

Operability diagrams are used in seakeeping analysis to present the variability of operability in seas of differing headings. These are often carried out using polar plots. Polar plots are also used to present various seakeeping parameters such as directional RAOs, incidence of slamming events, the limit speeds the vessel may travel, or the accuracy with which station keeping may be maintained for a vessel using dynamic positioning (DP). In this case polar plots are used to represent the limit sea states with which transfers may be made to a turbine. These are referred to as performance plots (P-Plots).

Performance plots as shown in Figure 2.23 are part of Carbon Trust's proposed method of rating WFSVs and quantifying their accessibility to turbines. Performance plots are being developed because "current methods for assessing access system performance are limited." Currently the industry typically uses Hs and wind speed and as such does not directly consider factors such as wave direction, period, or current. Carbon Trust's Offshore Wind Accelerator (OWA)

believes that more quantitative and robust measures are required. This is not just met-ocean quantities, but additionally speed, passenger capacity, comfort, safety, fuel economy, and charter costs. This would help improve vessel and transfer system development as well as vessel and transfer system selection, in addition to O&M modelling ability [20].

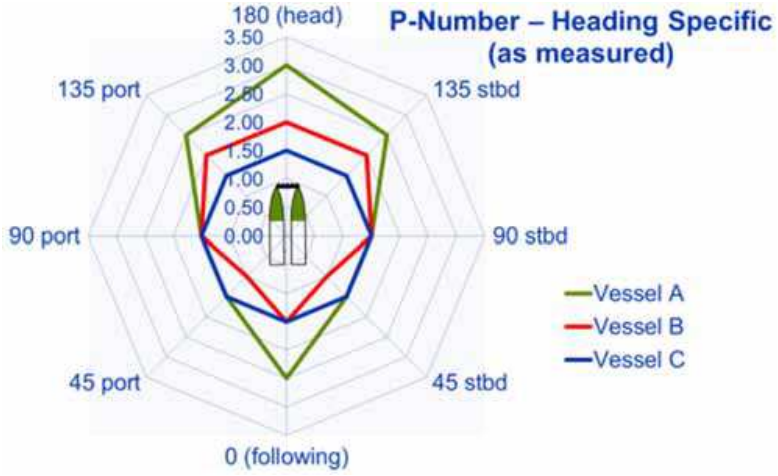

Figure 2.23: Example Performance Plot Comparing Three Vessels [20]

The Carbon Trust are also working on their Access System Accessibility (ASA) tool. The Access System Accessibility tool combines the specific met-ocean conditions at a wind farm with the Performance Plot. The Carbon Trust envision that this will help developers evaluate their vessel requirement and create optimal access strategies [86].

Seaspeed Marine Consulting Ltd. have carried out a substantial amount of experimentation in collaboration with the Carbon Trust on the evaluation of WFSVs, and have shown that safe access limits are often far below 1.5m Hs [87, 88, 89]. They suggested that the Root Mean Squared (RMS) acceleration limits in the technical saloon of a WFSV is approximately 0.05g for vertical motion and 0.04g for horizontal motion. Furthermore, it was suggested that for the "step across transfer that the relative motion between the point on the vessel and the turbine docking poles should be essentially zero." In regards to angular motions, the RMS of roll should not exceed 3° [88].

2.8 Wave Climate

The wave climate studied in this thesis was predominately described by the JONSWAP spectrum [90] for the North Sea. Consideration was also made for the longer period conditions found in the North Atlantic Ocean off the coast of Ireland, where a large array of floating wind turbines may be positioned in the far future. Practically, however, the shorter wave period conditions in the North Sea were examined as there is an upcoming requirement for better access vessels. The typical conditions in the North Sea [91] are shown in Figure 2.24 and show a range of 5.5–12.5s Tp for the most frequent conditions.

mean class Tp / HS	2.5	3.5	4.5	5.5	6.5	7.5	8.5	9.5	10.5	11.5	12.5	13.5	14.5	15.5	16.5	17.5	18.5	19.5	20.5
0.5	42	429	1172	1662	1634	1291	888	558	331	189	105	57	31	17	9				
1.5	2	109	964	3034	5260	6292	5902	4689	3317	2160	1325	778	443	246	135	73	39	21	11
2.5		2	76	578	1837	3373	4297	4248	3504	2532	1659	1009	581	320	171	89	46	23	11
3.5			2	47	320	1006	1881	2442	2436	2000	1419	900	523	285	147	73	35	16	7
4.5				2	33	206	635	1181	1519	1485	1179	797	475	257	128	60	27	12	5
5.5					1	22	133	395	715	888	829	619	388	212	103	46	19	7	3
6.5						1	16	85	242	414	485	420	287	163	79	34	13	5	2
7.5							1	11	55	144	228	244	191	117	58	25	9	3	1
8.5								1	8	35	83	117	112	77	41	18	6	2	1
9.5									1	6	22	45	55	45	27	12	4	1	
10.5										1	4	13	22	23	16	8	3	1	
11.5											1	3	7	10	9	5	2	1	
12.5													2	4	4	3	1		
13.5														1	2	1	1		
14.5																1			

Figure 2.24: Scatter diagram. Typical North Sea conditions [91]

2.9 Weather Windows

A weather window is the period of time that the weather conditions are equal or better than required for transit and transfers. Wind turbines need to be accessed on a regular basis, yet estimates as to how often wind turbines need to be accessed vary from 6 times per year to 10 [22, 92]. With regard to wind turbine maintenance the Hs, period and wind speed are the principal limiting factors. Table 2.1 shows sea states with their corresponding wave height range. The current operational limit of WFSVs is that of a sea state code 4, the goal of

this project is to examine which methods and variables could allow a WFSV to operate within sea state 5. A 1.5m Hs is seen as a general limit for bow transfers, there are, however vessels that can operate up to 2.5/3.5m Hs depending on whether or not a motion compensating gangway (MCG) is utilised. The current trend is to design vessels that operate within a sea state of 4–5. A Limit of Hs 2m was suggested by one report [21]. A slightly more conservative limit of 1.5m Hs is more commonly given for a catamaran [93]. Although it must be noted that these are not necessarily true limits, but a limit for a certain wave direction with favourable other met-ocean conditions. [88]. Note: wind speed was not taken into consideration in this thesis, nonetheless it can be noted that the general limit for wind speed is $12\text{m}\,\text{s}^{-1}$ [21, 43, 94].

Table 2.1: Beaufort Sea States

Sea State Codes	Hs	Description
0	0 [metres]	Calm (Glassy)
1	0 – 0.1	Calm (rippled)
2	0.1 – 0.5	Smooth (mini-waves)
3	0.5 – 1.25	Slight
4	1.25 – 2.5	Moderate
5	2.5 – 4.0	Rough
6	4.0 – 6.0	Very Rough
7	6.0 – 9.0	High
8	9.0 – 14.0	Very High
9	$>$ 14.0	Huge

Figure 2.25 shows the Irish weather buoy network. A weather window analysis was carried out on these sites and compared to two North Sea sites, see Figure 2.26. The comparison demonstrated the major improvements in operability that a 2.5m Hs would mean. In the North Sea access is possible above 80% of the time and sites in the Atlantic Ocean accessible 40–50% of the time [95].

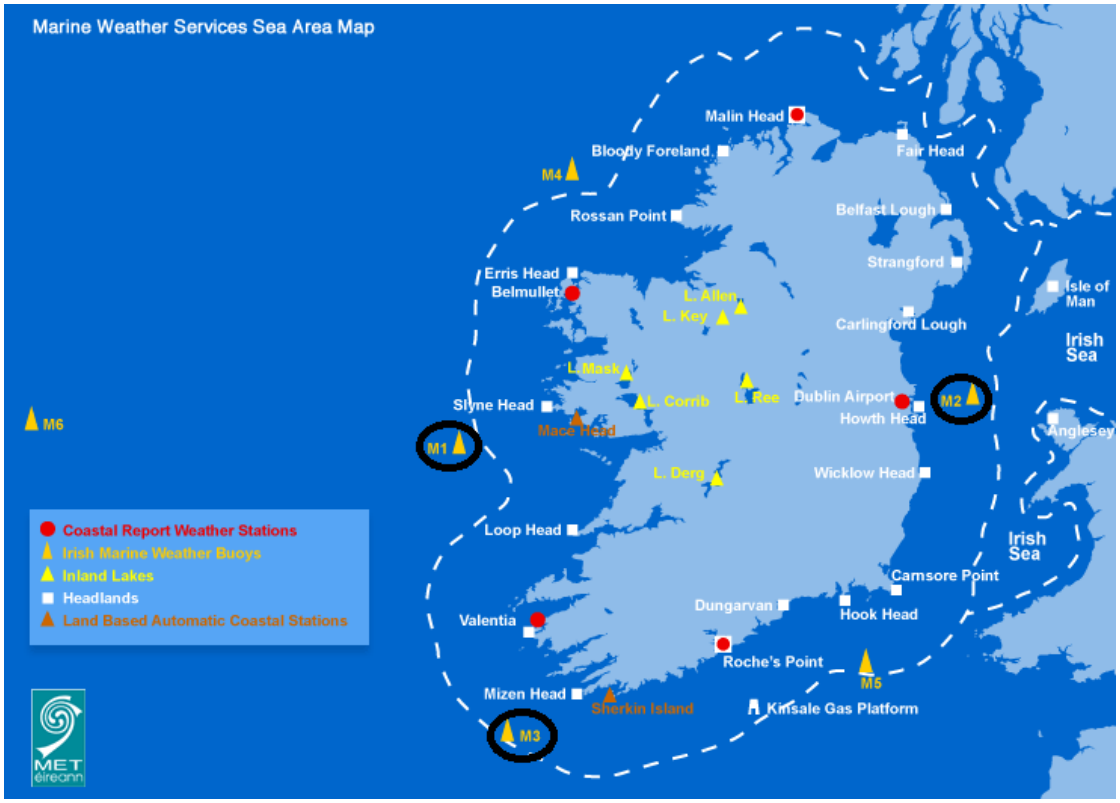

Figure 2.25: Irish Weather Buoy Network [96]. M1, M2, & M3 Highlighted

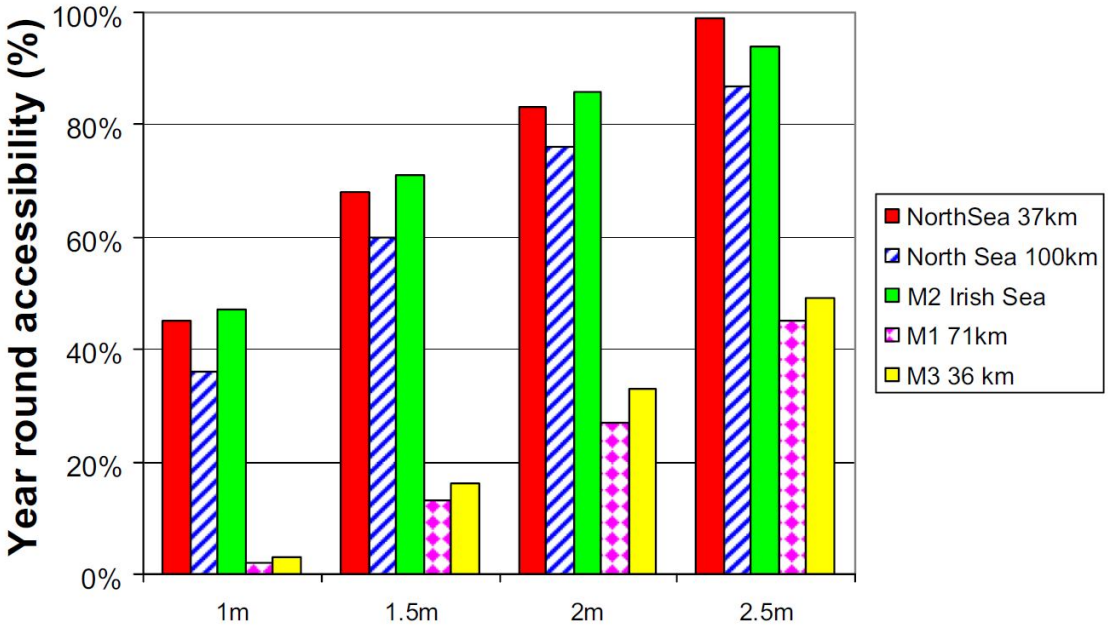

Figure 2.26: Weather Window Analysis [95]

Experimental testing of catamaran WFSVs carrying out transfers showed that the range of accessibility was dependent on wave direction, and in the range of 0.75–1.6m Hs with an average well below 1.5m Hs [69, 88]. When this is compared with a weather window study [95] which shows that for a 1.5m Hs limit % accessibility is low, it becomes clear just how much of an issue the current weather windows are and will become as wind farms expand to less favourable met-ocean sites.

2.10 Quantitative Motion Limits for Working on Ships

2.10.1 Overview

There are a number of different limits for working on a vessel depending on the method of measurement, type of work being performed, or the class of the vessel. Motion Induced Interruption (MII) is recorded as the total number of MII events in a given duration or by tips per minute. It is a useful time domain parameter that can be used to set safety limits on the transfer of personnel to offshore wind turbines, explained further in 2.10.3. RMS is a useful tool in averaging data to determine safety limits.

2.10.2 RMS Limit Measurements

Table 2.2 shows the limits based on the type of work being carried out. These limits would be more suited to moving around the deck whilst transfer operations are being conducted. Limits for transit passengers are provided; 0.05g for RMS of vertical acceleration, RMS of lateral accelerations is 0.04g, and RMS of roll is 2.5° [97]. A study on WFSVs found from experience that the RMS limits of vessel motion during step across transfer are; 0.05g for vertical acceleration in the saloon, 0.04g for the horizontal acceleration, and 3° for roll [88].

The limits on operability of a vessel applying to the journey between port and the wind farm are well developed. The operability criteria based on the type of

Table 2.2: Criteria with Regard to Accelerations and Roll [RMS] [97]

	Vertical Acceleration (RMS)	Lateral Acceleration (RMS)	Roll (RMS)
Light manual work	0.20g	0.10g	6.0°
Heavy manual work	0.15g	0.07g	4.0°
Intellectual work	0.10g	0.05g	3.0°
Transit Passengers	0.05g	0.04g	2.5°
Cruise Liner	0.02g	0.03g	2.0°

craft is shown in Table 2.3, a fast small craft could appropriate a WFSV. The general operability limiting criteria for fast small craft lists the vertical acceleration at the forward perpendicular RMS as 0.275g, the vertical acceleration at bridge RMS as 0.2g, the lateral acceleration at bridge as RMS 0.1g, the roll RMS as 4.0°, the slamming criteria estimated as probability as 0.03, and the deck wetness criteria estimated as probability as 0.05 [98, 97, 36, 99]. Lateral acceleration also limits operability and 0.1 g RMS is the recommended limit [98]. It has been reported that for transit journeys in a WFSV, the limits were 0.15g for RMS of vertical acceleration, 0.12g for RMS of horizontal acceleration, 6° for roll, 4° for pitch, and a slamming rate of 5–10 per hour [88].

2.10.3 Motion Induced Interruption

Motion induced interruption (MII) is defined as any motion that causes the operative to temporarily lose balance and stop the task that they were carrying out due to ship motions. MII generally results in extra holding of handrails, increased spinal loading and increases the difficulty of tasks. It has been suggested that more than 4° of roll oscillation had progressively deleterious effects on shipboard activities and concluded that work should halt when roll exceeds 10° [100]. MII could potentially be used to predict the possibility of a personnel transfer between a WFSV and a wind turbine.

Table 2.3: General Operability Limiting Criteria for Ships and Fishing Vessels [97, 36, 99]

Phenomena	Merchant Ships	Naval Vessels	Fast Small Craft	Fishing Vessels
Vertical acceleration at forward perpendicular (RMS)	0.274g (L$\leq$ 100m)* 0.05g (L$\geq$ 330m)*	0.275g	0.65g	0.35g
Vertical acceleration at Bridge (RMS)	0.15g	0.2g	0.275g	0.20g
Lateral acceleration at Bridge (RMS)	0.12g	0.1g	0.1g	0.15g
Roll (RMS)	6.0 deg	4.0 deg	4.0 deg	6.0 deg
Slamming criteria (probability)	0.03 (L$\leq$ 100m)* 0.01 (L$\geq$ 330m)*	0.03	0.03	0.06
Deck wetness criteria (probability)	0.05	0.05	0.05	0.05

* The limiting criterion for lengths between 100 and 330m varies almost linearly between the values L = 100 and 330m, where L is the length of the ship.

The Graham Method and/or the Applebee-Baitis Method can be used to quantify MII at a particular location on a ship once the ships motions are known. In addition, task effectiveness and recovery time are useful measurement parameters. Task effectiveness, defined as the ratio of time required to complete a task under calm sea conditions to the observed time to complete the same task while underway [101], is discussed further in 2.10.4. MII occur when the tipping ratio, R_T, exceeds the tipping coefficient, C_T, producing a tip inequality:

$$R_T > C_T \tag{2.1}$$

Where R_T is a ratio of the horizontal and vertical acceleration that a person is experiencing. This may be calculated in differing ways two are presented in § 2.10.3 & 2.10.3. C_T is derived from a person's vertical centre of gravity, VCG, and is given by:

$$C_T = \frac{l}{h_p} \tag{2.2}$$

Where l is the half-width of a person's stance and h_p is a person's VCG above the deck on which they are standing. C_T is generally estimated to be a value of 0.25 [102]. The tipping coefficient from a stance half-width of 0.23m and a VCG of 0.91m [103]. Empirically derived MII tipping coefficients depending on the task being carried out are detailed in Table 2.4 [104]. More general threshold levels for sliding and tipping are expressed as a fraction of acceleration due to gravity and are given in Table 2.5 [105].

Table 2.4: Empirically Derived MII Tipping Coefficients [104]

Task	C_T
Standing Facing Fwd/Aft (Task A)	0.270
Weapon Loading	0.200
Standing Facing Fwd/Aft with Arms Aloft	0.292
Walking on a Treadmill	0.273
Standing Facing Athwart Ships (Task B)	0.182
All Tasks (Task B)	0.243

Examining the risk levels for deck operations of naval vessels, a possible MII related accident could occur with 0.1 tips per minute and it is probable an accident could occur with 0.5 tips per minute [103]. As the tips per minute increase so does the risk; serious, severe and extreme risk levels are quantified by 1.5, 3.0, and 5.0 tips per minute respectively [103]. It has been recommended that rather than giving an exhaustive list of MII limits, that a particular task should be monitored and the limits be based on those measurements [106]. This is an

excellent method of continually evaluating safety on the deck of a vessel, though costly and time consuming to implement and requiring a large amount of co-operation. The following criteria gives some rules for determining seakeeping criteria; “criteria must be related to a particular task”; “the responses chosen for criteria assessment should be of actual concern to the task being considered”; “numerical values of criteria should be determined by monitoring the apparent performance of actual ships at sea” [106].

Table 2.5: Threshold Levels for MII Detection; Threshold levels for Sliding and Tipping estimations [105]

Sliding to Port/Starboard	Sliding to Forward/Aft	Tipping to Port/Starboard	Tipping to Forward/Aft
$t_{S_{p/s}} = \mu_s g$	$t_{S_{f/a}} = 0.886\mu_s g$	$t_{T_{p/s}} = (b/h_p)g$	$t_{T_{f/a}} = (d/h_p)g$

Where:

- $t_{S_{p/s}}$ is tips per minute sliding to Port/Starboard;
- $t_{S_{f/a}}$ is tips per minute sliding to Forward/Aft;
- $t_{T_{p/s}}$ is tips per minute tipping to Port/Starboard;
- $t_{T_{f/a}}$ is tips per minute tipping to Forward/Aft;
- μ_s is the friction coefficient;
- The quotient b/h is called the Lateral Tipping Coefficient, for which is assumed a representative equal to 0.25 [107].
- The quantity d/h is called the Longitudinal Tipping Coefficient and was estimated to be 0.17 [107]. Since a person can resist a larger force from the back than from the front, different values for the forward and aft tipping coefficients can be chosen.
- d is the distance between the subject’s ankle joint and toes;
- h_p is the height to a persons centre of gravity.
- and g is acceleration due to gravity.

Applebee-Baitis Method

The Applebee-Baitis method is based on the assumption that ship motions are inherent in acceleration measurements such that rotational motions or rates are not needed to calculate the tipping ratio. The tipping ratio for the AB method is defined as the ratio of the transverse acceleration of the vessel, a_t, to the vertical acceleration, a_v, of the vessel and is given by:

$$R_T = \frac{|a_t|}{a_v + g} \tag{2.3}$$

The tip inequality becomes:

$$\frac{|a_t|}{a_v + g} > \frac{l}{h} \tag{2.4}$$

The vertical and transverse accelerations are taken in the ship reference frame. To account for gravity, g, is added to the vertical acceleration term.

Graham Method

The Graham method assumes that a tip will occur form the inequality below:

$$\frac{|-1/3h\ddot{\eta}_4 + \ddot{D}_2 + g\eta_4|}{\ddot{D}_3 + g} > \frac{l}{h} \tag{2.5}$$

where: $\ddot{\eta}_4$ is roll or pitch acceleration, η_4 is roll or pitch motion, $\ddot{D}_2$ is the horizontal acceleration experienced by the person, $\ddot{D}_3$ is the vertical acceleration experienced by the person.

2.10.4 Task Effectiveness and Recovery Time

Task effectiveness, E_{Task}, was defined by Graham and Colwell as the ratio of the time required to complete a task under calm sea conditions, T_{Calm}, to the observed time to complete the same task while underway, T_{Waves} [101]:

$$E_{Task} = \frac{T_{Calm}}{T_{Waves}} \tag{2.6}$$

This can be expressed as MII_{CRIT}, which enables MII criteria to be used in the ship design assessment process [102, 104, 108].

$$MII_{CRIT} = \left(\frac{1 - E_{Task}}{D_{MII}}\right) 60 \tag{2.7}$$

2.11 Motions of Floating Offshore Structures

2.11.1 Overview

A critical aspect of WFSV operation is the vessels stability when approaching a wind turbine foundation and the ability for crew members and technicians to be able to work safely on the foredeck. In order to reduce the possibilities of rough contact with the monopile and if for any reason the WFSV must move suddenly then the crew and technicians are safe on the deck. This section explores the motions of a WFSV that affect its performance in allowing personnel to access wind turbines. Understanding, predicting and minimising these motions directly impacts the WFSVs ability to carry out transfers in higher sea states by allowing the vessel to manoeuver with low amplitude motions and small accelerations.

2.11.2 Ship Motions

The motions of a floating body are defined by six degrees of freedom heave, pitch, roll, yaw, surge and sway, these are illustrated in Figure 2.27 [109].

- Surge, x is the linear longitudinal motion in the X direction
- Sway, y is the linear lateral motion in the Y direction
- Heave, z is the linear vertical motion in the Z direction
- Roll, ϕ is the rotational motion about the X axis
- Pitch, θ is the rotational motion about the Y axis
- Yaw, ψ is the rotational motion about the Z axis

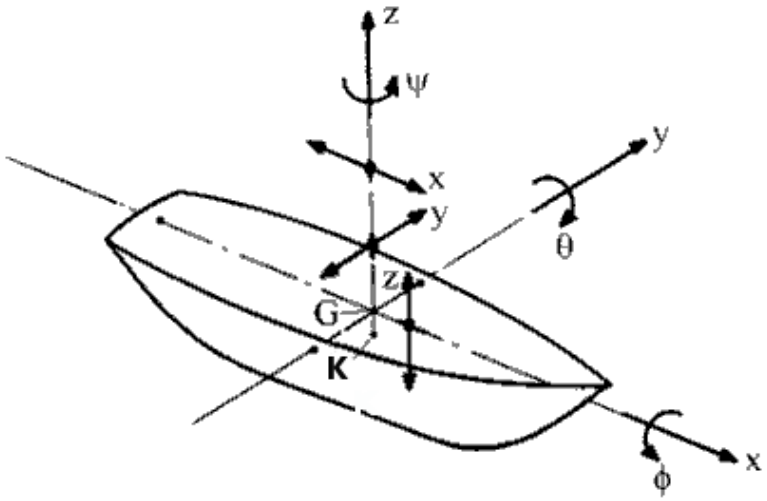

Figure 2.27: Ship Axis Convention [109]

As a WFSV is a free floating body it responds to incoming waves, wind and current, in addition to the ship's thrusters, and the interaction between the monopile and the WFSV results in motion in six degrees of freedom. Heave, pitch, and roll are oscillatory, a restoring moment acts on these motions when they a moved from equilibrium and can be described by simple harmonic motion. When a floating structure is surging, swaying, or yawing, it does not generally return to its original position unless it is restrained in some way, in the case of a WFSV docking with a turbine tower there are steering and thruster forces imparted by the vessel that create a balancing reaction with the wave induced loads in surge, sway and yaw. In this work, head seas will be defined as a 0° heading angle and following seas with a 180° heading angle [110]. The equilibrium condition of the equation of motion for a forced oscillating floating structure is:

$$(M + M_a)\,\ddot{z} + b\dot{z} + cz = F_0\, cos\, \omega_e t \tag{2.8}$$

Where z is a degree of freedom (heave in this case), M_a is the mass plus added mass, b is the damping constant, c is the restoring, or spring constant F_0 is the amplitude of the encountering force ω_e is the circular frequency of the encountering force and t is time [111, 112].

2.11.3 Response Amplitude Operators (RAO)

The RAO graphs the effect that any given sea state has on the motion of a ship. Generally, the RAO's relationship with wave height and steepness is not linear beyond linear wave theory, however the variables in equation 2.9 can be determined for any input condition:

$$\mathrm{RAO}\,(\omega) = \frac{z}{\zeta_a} \tag{2.9}$$

Where ω is the oscillation frequency, z is the degree of freedom of the floating body (heave in this case), and ζ_a is the wave height. Linear motion is non-dimensional, however angular motion is not. This is dealt with in two ways in the thesis where relevant, usually by using full scale measurements, and secondly by nondimensionalising the Pitch RAO by the wavenumber k when comparing differing vessels.

In the case of a linear system analysed using a wave spectra the following transfer function may be utilised [112].

$$S_R(\omega) = [RAO(\omega)]^2 S(\omega) \tag{2.10}$$

Where S_R is the response spectrum, S is the wave spectrum, and ω is the oscillation frequency.

2.11.4 Natural Period

The natural period of heave, roll, and pitch of a vessel are dependent on the geometry and mass variables of the vessel as well as the added mass component, Equations 2.12 & 2.11. A challenge of designing a floating offshore structure is that there are a number of interlinked properties such that if one is improved then another is hindered meaning that any design is a compromise. Designing a ship with a suitable natural period outside the operating range and a favourable GM and associated stability curve is one such compromise. The natural period formula for heave is:

$$T_{Heave} = 2\pi\sqrt{\frac{M + M_a}{\rho g A_{wl}}} \tag{2.11}$$

Where:

- T_{Heave} is the natural period in heave
- M is the mass
- M_a is the added mass
- ρ is the density of the liquid the model is in
- g is acceleration due to gravity
- A_{wl} is the water plane area

The natural period formula for Roll and Pitch is:

$$T_{Roll,Pitch} = 2\pi\sqrt{\frac{I + I_a}{\rho g \overline{V}.\overline{GM}}} \tag{2.12}$$

Where:

- $T_{Roll,Pitch}$ is the natural period in either roll or pitch
- I and I_a are the inertia and the added inertia of rotational motion
- ρ is the density of the liquid the model is in
- g is acceleration due to gravity
- $\overline{V}$ is the displaced volume
- $\overline{GM}$ is the metacentric height

2.11.5 Minimisation of Response

Minimisation of ship response in the oscillatory motions of heave, pitch, and roll is of particular importance to a WFSV. In the case of heave motion, it has been noted in the literature that for a floating offshore structure if the effective wavelength is less than half the length of the ship the heaving force is small. This is due to the wave acting in opposing directions on the ship over a fraction of the ships length. This is illustrated in Figure 2.28 where the sum of the vertical forces acting on the ship are substantially balanced.

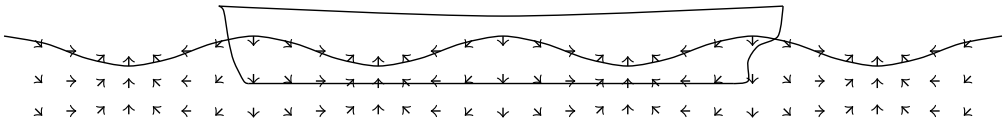

Figure 2.28: Wave Particle Force Direction in Relation to a Ship Length of Double the Wavelength

In addition, the heaving force is small or moderate when the effective wavelength is equal to the ship's length [111] as there is no net change in the buoyancy force as illustrated in Figure 2.29.

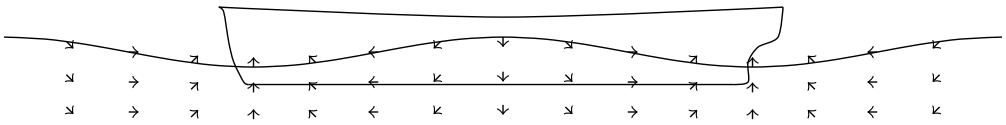

Figure 2.29: Wave Particle Force Direction in Relation to a Ship Length Equal to the Wavelength

In the case of pitch motion, damping is increased by increasing the beam, decreasing draught, or an increase in V-form. It is also noted that when the effective wavelength is less than half the ship's length, the pitching moment is small as can be seen in Figure 2.28 as the sum of the moments due to the wave partical acceleration is small, conversely when the effective wavelength equals the ship's length, the pitching moment is high [111] as can be seen in Figure 2.30.

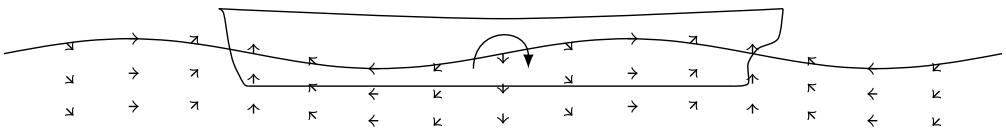

Figure 2.30: Wave Particle Force Direction in Relation to a Ship Length Equal to the Wavelength Showing Small Showing Large Pitch Moment

For roll motion reduction of a floating offshore structure the following methods for both passive and active motion stabilization are utilised in ships and offshore structures. Static hull features include skegs and bilge keels, and active mechanical devices include counterweights, antiroll tanks and stabilizers. The

damping force on a floating structure when it is rolling is predominantly from a combination of the waves generated, water friction on the ship surface or eddy making, bilge keels, and other appendages [111]. $\overline{GM}$ is directly proportional to the magnitude of roll damping for an offshore structure in still water.

Minimisation of surge is of importance to the effectiveness of bollard pull while maintaining contact with the monopile. Minimising the wave load on the vessel reduces its motions, semisubmersibles and SWATHS use this to their advantage. This also implemented by having a low resistance design and minimising wetted surface area. Tuned Liquid Column Dampers have been shown to reduce the surge motion of tension moored floating wind turbines [113, 114].

Offshore structures are often designed with large flat surfaces called heaveplates to increase heave damping thus reducing heave motion [115, 116] and are regularly used in floating offshore wind platforms [117], for example WindFloat as can be seen in Figure 2.31 [118, 119]. They increase added mass altering the natural period of the floating structure. Vortices generated at the edge of the heaveplates create a damping force [120, 121]. Heaveplates are useful at resonance where increased damping is of particular importance [122, 123]. The design of a heaveplate may be improved by changing porsosity [124]. Optimising flow separation improves heaveplate performance [125, 126].

2.12 Simulation of Floating Offshore Structures

The simulation of floating offshore structures is dictated by the forces acting on the bodies of interest. The forces acting on an offshore structure are: hydrostatic, Froude-Krylov [127], diffraction, radiation, drag (Morison's equation [128]), as well as second order wave drift forces and drag forces due to the current and wind. The hydrostatic restoring force is applicable to all floating bodies and dependent on the relationship between the centre of gravity and the centre of buoyancy. The Froude-Krylov force originates from the incident wave pressure on the surface of the structure.

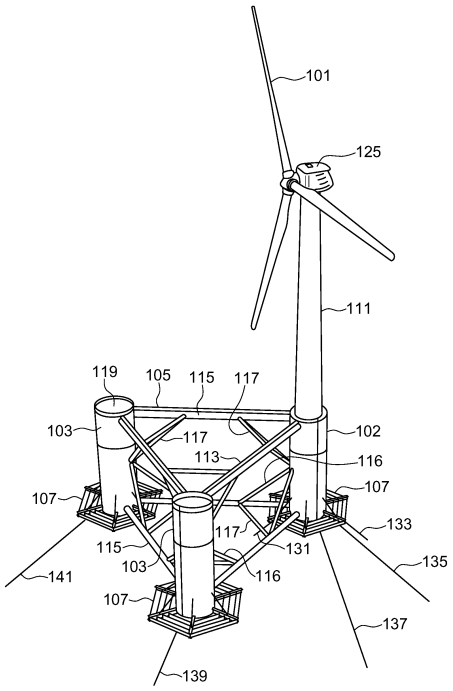

Figure 2.31: Principle Power's WindFloat [118, 119]

For structures that are large enough to alter the wave field then the diffracted waves and associated force are taken into account. As the structure moves as a reaction to the incident and diffracted waves it radiates waves and this produces a radiation force on the structure. Morison's equation is best utilised when the drag force on the structure is dominant, for example when the structure is small compared to the water wave length or very slender. The second order wave drift forces and drag forces due to the current and wind are generally small compared to the other forces.

Linear potential flow theory is used to describe the wave potential from the incident, diffracted, and radiated waves that influence the floating structure, through the Laplace equation with associated boundary conditions. This theory is based on the assumption that the flow is irrotional and non-viscous. This can be then solved by a boundary element method (BEM) code. Other forces may then be integrated into the BEM code. ANSYS AQWA described in Appendix B.1 is an example of a BEM solver.

To include viscous effects, the full Navier-Stokes equations must be solved. Including viscous effects in the numerical simulation accounts for the drag forces due to the water flow around the structures surfaces. These drag forces effect the resistance of ships and consequently fuel consumption and speed properties, in regards to offshore platforms these drag forces generally reduce the heave response to waves. The numerical modelling of viscous effects can be carried out using a wide range of methods depending on the application from, Reynolds-averaged Navier-Stokes (RANS) equations, to Smooth Particle Hydrodynamics (SPH), Large Eddy Simulations (LES), or even Direct Numerical Simulation (DNS) [112, 129, 130, 131]. These methods are collectively referred to as Computational Fluid Dynamics (CFD). ANSYS CFX is a finite volume method RANS solver and is described in Appendix B.2. RANS solvers generally simulate complex floating structures with a high level of accuracy and are quite useful for describing the flow around the structure, however it suffers from a high computational cost [132, 133].

2.13 State of the Art in Modelling WFSV Interaction with Offshore Wind Turbines at the Time of Transfer

The motions of a WFSV carrying out transfer operations are challenging to simulate. The two usual methods of accessing a wind turbine are either for the bow of the vessel to maintain contact with the wind turbine tower with a fender friction and applying a thrust force, or to maintain station close to the turbine and use a motion compensating gangway (MCG). Investigating the motions of a WFSV at full scale can produce data difficult to analyse [87], on the other hand physical and numerical models struggle from the issue of defining and implementing all the relevant motions and forces acting on the vessel.

The numerical and physical modelling of the interaction of a WFSV with an

offshore wind turbine both fixed and floating has been analysed using a range of methods. Numerical modelling studies have examined the problem using time and frequency domain modelling and used a variety of methods to account for the frictional contact between the WFSV and the wind turbine tower. In addition, a number of methods of combining the solutions to each part of the system defined by the wind turbine, MCG systems have been modelled.

In relation to physical modelling, studies have predominantly surrounded fixed turbines, with a focus on measuring the forces, accelerations, angular motion, and frictional characteristics of the fender in separate experiments. Directional studies have been carried out in addition to studies involving on board propulsion.

A numerical method of predicting whether not a slip will occur was developed by using a qusai-static and dynamic model to describe the system and the Coulomb frictional relationship at the contact point. The major forces of the system were accounted for and a static and dynamic analysis were carried out in the time domain focusing on whether or not a slip would occur. It was found that slips generally occur in the positive Z direction and that the coefficient of friction is of significant importance [134].

The relative motion between a WFSV and a monopile and the relative motion between a crane and the monopile, was calculated using statistical methods to analyse RAO, sea state, system geometry, and performance criteria. The local motions of the WFSV and whether the motions were below the permissible criteria were determined. Friction was not accounted for and as a result the vessels motions are quite large relative to the sea state, however the principle of statistically analysing the WFSVs interactions with the monopile are promising [135].

The numerically modelled statistical methods of analysis of the docking procedure was examined for the Far Offshore Operation and Maintenance Vessel Concept Development and Optimisation (FAROFF) project. Two methods of transfer were examined with a fixed turbine one using an MCG and another using a bow transfer. Based on the RAO for the WFSV and the active compensation

limits of the MCG a limiting Hs and Tp were computed for a range of headings in the frequency domain. The model for bow transfer is more complicated as it involves estimating the coefficient of friction and tolerance of the standard deviation of the slips. Nonetheless, when combined with the sea state, estimations of accessibility may be determined. It was found that upwards slips were more likely to occur than downwards slips. In addition, for the statistical method presented the peakedness of the spectrum was found to have a negligible effect on the performance assessment [69].

For the Carbon Trust's Offshore Wind Accelerator programme a series of experimental modelling was carried out with self-propelled generic catamaran models [87, 88, 89]. Scale model tests of a 24m WFSV with an active motion compensated brow were carried out and the vertical forces recorded [87]. It was noted that performance was limited more by stern swamping and propulsion ventilation in stern seas and severe roll in beam seas rather than exceedance of the thresholds of the access system [87].

Limits relating to the confidence of a slip not occurring, acceleration and roll motion were presented and used in demonstrating the formation of performance plots [88]. Performance plots are presented for a 16m catamaran WFSV, in head and stern seas slips reduced the acceptable Hs of transfer and in beam and quartering seas roll motion was the limiting factor for short and medium period waves. For long period waves accessing the monopile in beam seas was shown to be greater than that of head or stern seas [88]. A flexible fixed fender that allowed angular motion was used to record the longitudinal and vertical forces, and a free rubber fender was also used to study the slip mechanism, force data was also recorded for the free fender [89]. A static push-on longitudinal thrust was applied and the longitudinal and vertical forces were recorded, it was found that the coefficient of friction was constant but that the combination of horizontal and vertical forces to create a slip varied considerably. It was found that for head seas that slips were more common in the positive Z direction. In addition, it was noted that the efflux from the propellors caused an increase in

wave steepness, which in turn caused a greater variation in longitudinal force, and consequently slips [89].

Numerical and experimental investigation of WFSV at an offshore wind turbine were simulated in a comprehensive study [136]. The model was validated with experimental results showing that the numerical method is able to quantify the risk of a slip occurring. The fender was attached to the WFSV using load cells measuring axial and tangential force. Fender friction was also considered in a separate series of dry tests. The monopile did not have a traditional boat landing but one similar to the friction tests carried out. Displacement and forces at the bow of the vessel were recorded. A time domain simulation using BEM was created considering the Froude-Krylov forces and forces on the catamaran were considered in addition to the diffraction due to the monopile, and the friction contact was modelled as Coulomb friction. Good agreement was found between the numerical and physical simulation [136].

A structural model considering the ship hull as a rigid structure and the fender as a deformable body using a high order finite element solver has been created. The flow equations are described within the time domain using the Finite Volume Method (FVM) to solve the incompressible Navier-Stokes equations. A partitioned approach is then used to solve the coupled flow and structural problem. The author first examines the flow around the monopile, then the contact between the fender and the monopile, followed by the hydrodynamic behaviour of a catamaran WFSV with and without the monopile present, and finally contact between a generic monohull and a monopile were considered. Throughout this process the author describes the requirements of the numerical model to carry this out [137]. In a follow up paper by the same author the numerical model is further elaborated on with a hyperelastic material is used to describe the mechanical behaviour of the fender and is analysed using the finite element method (FEM). Again time domain solvers are employed using a partitioned approach to solve the fluid equations, the rigid body equations, and the deformable body equations describing the fender. Experimental and BEM results

were used to validate the numerical solver created, examining the sub-problems as well as the complete system. The fender was modelled with Neo-Hook and Moony-Rilvin models [138].

Although the work presented in this thesis is related to fixed offshore wind turbines it is interesting to examine how the docking operation is modelled with a floating turbine, as the docking operation is similar. The access problem with a floating turbine has been studied with a two body frequency domain BEM model, modelling the contact point as fixed and recording the forces at the point and by applying an equation to describe the frictional contact. The mooring forces of the floating wind turbine are linearised as the entire model is solved using linear systems in the frequency domain. Static friction is assumed to hold for a transfer to be safe, however a high coefficient of friction of 1.2 is used. It was found that the wake of the floating wind turbine and the relative motion between the two bodies had significant effects on transfer. For the simulation of the MCG the relative motion between the tip of the gangway and the floating wind turbine must be within the compensation limits of the MCG [8, 139, 140].

A wide range of methods have been utilised with regard to the modelling of WFSV interaction with offshore wind turbines at the time of transfer. In summary the following have been found using a range of methods from physical modelling to time and frequency domain numerical modelling:

- A reduction in zero forward speed RAO would produce a decrease in the relative motion and may increase the possibility of transfers [135].
- Numerical and physical modelling have both shown that slips are more common in the positive Z direction [69, 89, 134].
- A range of vertical and longitudinal force combinations cause slips [89]
- The propellors cause an increase in wave steepness for stern seas [89].
- Stern seas cause the propellors to leave the water and loose thrust [89].
- Probablistic based statistical methods in the frequency domain produce an estimation of accessibility over a broad range of conditions realitivly

quickly when combined with sea state data [8, 69, 135, 139, 140].

- Modelling of friction can be complex but simple models show good agreement with experimental results [136, 138].
- Time domain methods and physical testing are able to investigate specific phenomena in greater detail [87, 88, 89, 137, 138].
- For floating wind turbines only frequency domain linear models have been investigated due to the complexity of the problem. The relative motion of both bodies is particularly important for the transfer operation. Also the wake effects of the floating wind turbine significantly aid the transfer operation [8, 139, 140].

Chapter 3

Novel WFSV Designs

3.1 Introduction

Ship design is often carried out using the design spiral, illustrated in Figure 3.1, to constantly revisit the objectives, this can be referred to as point based design [141]. The design spiral can use concurrent design to aid its speed and chance of developing the most optimised solution. Multi-objective optimization, parametric analysis, and set-based design are other methods that can be utilised to find an optimised engineering solution to a problem [142]. Cross pollination is another method for finding a solution to an engineering problem where ideas or concepts are sought from other fields or non-specialists [143]. Continuous or evolutionary design involves continuously taking advantage of opportunities to improve a design. When a flaw is found it is fixed and when something works well it is improved upon [144, 145, 146].

The work presented in this thesis began with an idea of cross pollination of taking an ancient design based on traditional methods and applying them to a modern industrial application. The design did not perform as well as expected, however one aspect of the design performed very well. Coupling this with a more standard design using evolutionary optimisation a design coupling, both a heaveplate and catamaran hulls was developed. Within this design window a number of designs were brainstormed. Thus, a design evolved.

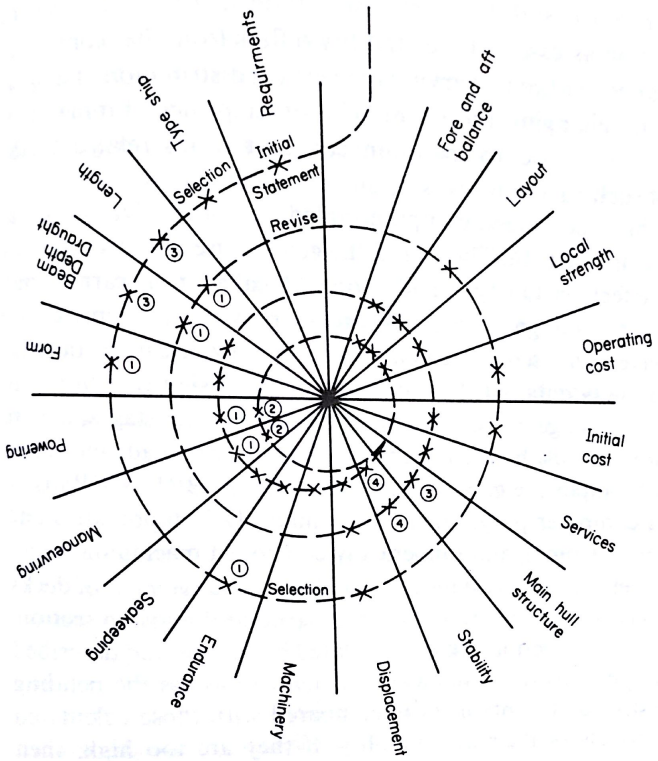

Figure 3.1: Ship Design Spiral [141]

There were a number of designs analysed in the course of this study, which evolved through different methods of analysis carried out, through numerical and physical model testing. The first 10 listed are based on a traditional bamboo boat from Vietnam and China [147], generally called a “Tubular Multihull” in the text due to the geometry of the craft. The second grouping is two basic catamaran models with heaveplates that was inspired from the tubular multihull tests that showed the advantages of a heaveplate. The third grouping is a series of designs that incorporated the advantages of each of the basic catamaran models. Finally, the last design tested is called “Grand Draught Catamaran” or GDC for short. This design took the most promising design to date and was reviewed and redesigned to take account of relevant Naval Architectural considerations.

The model properties of each design analysed in this thesis are outlined in Appendix C.

3.2 WFSV Concepts Analysed

3.2.1 Tubular Multihull Designs

The tubular multihull addresses access Hs limit issue by examining a concept hull design for an offshore wind farm service vessel (WFSV). The proposed design is intended to reduce the vessels overall motion in particular heave by damping its response to the wave action.

The design has a large number of buoyant tubes that comprise the ship hull utilising the resistance each tube creates cumulatively to dampen the ships overall motion as can illustrated in Figures 3.2–3.4. This idea was initially formulated by Dr Padraig Molloy of NUIG Galway based on a traditional bamboo craft described in "The China Voyage" by Tim Severin [147].

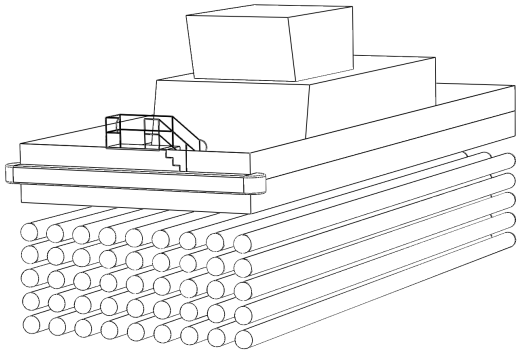

Figure 3.2: Tubular Multihull Concept

Excerpts from The China Voyage, demonstrate the dynamic stability that the bamboo raft (named the "Hsu Fu") had and the price it paid in terms of forward speed.

In response to the first gale they encountered Tim Severin stated; "there was one thing that was totally and completely different - the calm response Hsu Fu. In every other boat I had ever sailed, we would have been clinging to handholds or bracing ourselves against the lurch and heave of the vessel." However, the great stability came at a price; "Hsu Fu was advancing at a sedate one or two knots." This was the general speed of the vessel under sail in normal conditions without any favourable current. The raft being constructed of bamboo with open ends, with the vast majority of the raft underwater, had sacrificed speed for stability. In fact, the raft being tied together from spliced lengths of bamboo actually flexed with each passing wave.

There are two main principles by which the traditional bamboo ship is so dynamically stable; firstly, because the wave passes around the bamboo components unhindered, hence the vessel does not pass over the wave as much as a normal monohull or similar. Secondly, the vessel flexes over what little heave, pitch, and roll it experiences. It is unclear how much each part affects the overall performance. In addition, a flexible hull that bends with the waves similar to the one Tim Severin sailed would provide considerable challenges when incorporated to a rigid deck.

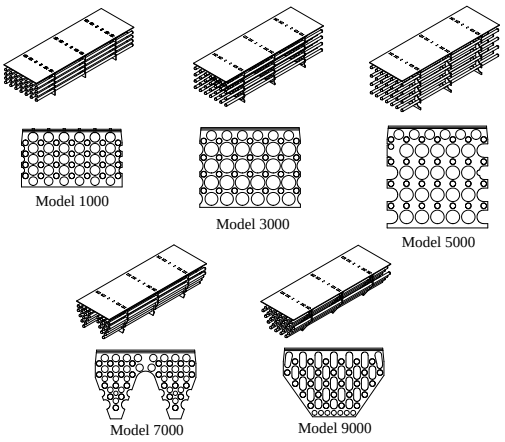

Figure 3.3: Model Configurations of the Tubular Multihull

The tubes were enclosed and spaced further apart to carry out a proof of concept analysis of the design. The flexibility of the tubes was not examined in this study, but could be added to the design in future research. The concept was a hull composed of a number of buoyant tubes. The buoyant tubes dampen the vessels motion due to the viscous action of the water around the tubes.

Ordinarily a WFSV has a beam close to 8m and a displacement of approximately 65t. Hence, the concept design was analysed with these parameters in mind. A design that was statically stable which met the above requirements and adhered to the fundamental design concept, resulted in a design with the following parameters as illustrated in Figure 3.5 this was then modelled at 1:25 scale. At this early design stage, the vessels mass was broken down into three components: Firstly, the buoyant tubes and associated supporting structure at 39t, secondly the deck

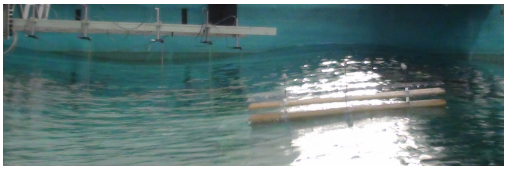

Figure 3.4: The Tubular Multihull in Regular Waves

structure at 15t and thirdly a cargo of 11t, additional details are provided in Table 3.1.

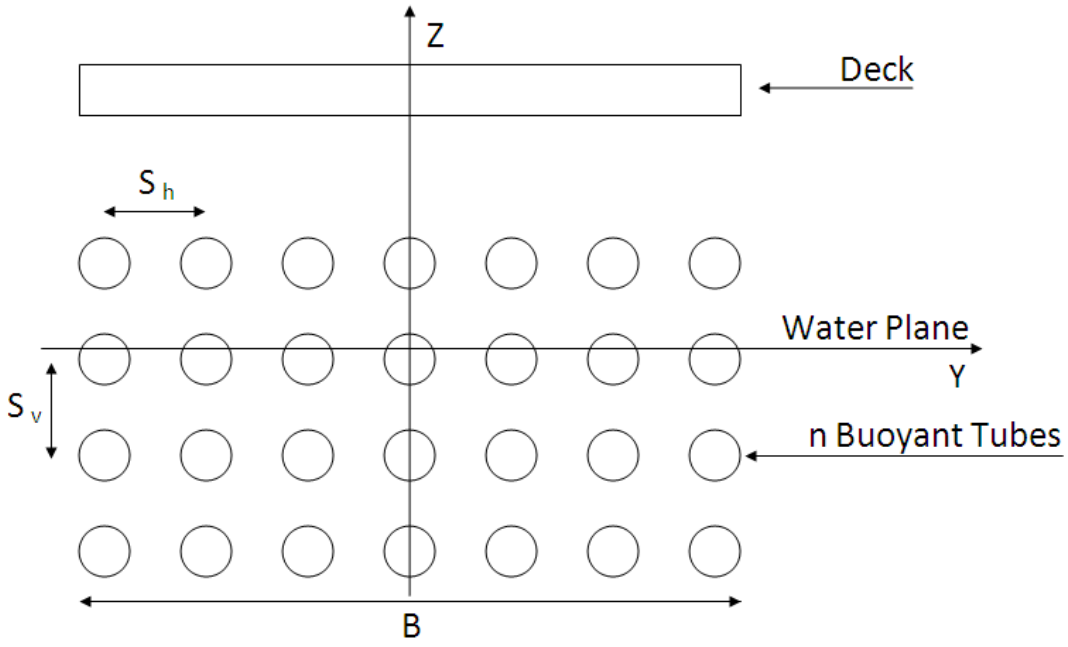

Figure 3.5: Beam View Showing the Different Variables Analysed

The vertical spacing of the model was varied, as is illustrated in Figure 3.3, additionally a heaveplate of 192m^2 was added. (The heaveplate was 24m x 8m and below the lowest bouyant tube at a distance equal to the vertical spacing between the tubes.) This culminated in ten configurations of the design to be tested, see Table 3.2. Due to the change in geometry of the model, the meta-centric height, draft and centre of gravity varied with each model configuration in order to maintain static stability. Table C.1 details the main particulars of each configuration which are visually represented in Figure 3.3. These designs were then tested in the Lir National Ocean Test Facility (Lir NOTF) wave basin. From the testing of the multihull the one of the principle promising parts of the tubular multihull was the attachment of a heaveplate. In the following sections catamarans with heaveplates attached are discussed.

Table 3.1: Design Parameters

Parameter	Value
Horizontal spacing (Sh)	1.259m
Vertical spacing (Sv)	0.9m–1.8m
Number of tubes vertically	4
Number of tubes horizontally	7
External radius of tubes	0.225m

Table 3.2: Naming Scheme for the Tubular Multihull Configurations

Test ID	Description
T1000	0.9m Spacing without a Heaveplate
T2000	0.9m Spacing with a Heaveplate
T3000	1.5m Spacing without a Heaveplate
T4000	1.5m Spacing with Heaveplate
T5000	1.8m Spacing without a Heaveplate
T6000	1.8m Spacing with a Heaveplate
T7000	Catamaran Style without a Heaveplate
T8000	Catamaran Style with a Heaveplate
T9000	Monohull Style without a Heaveplate
T10000	Monohull Style with a Heaveplate
T11000	Model 6000 Placed Behind a Monopile

3.2.2 Simple Catamarans Designs

In this section, simple catamaran designs with and without heaveplates are introduced, Figure 3.6 shows the wide hulled catamaran with a heaveplate lowered, in the wave basin. The first design was that of a standard basic catamaran design used a control model throughout the thesis. The mass and basic geometry of the catamaran was estimated from other similar sized WFSVs, principally the length was 24m, the beam was 8m, the demihull was 2.0m, and the displacement was 68.1t. This catamaran and another design with a narrower demihull (0.625m demihull) were then analysed with a large single heaveplate. Figures 3.7 & 3.8 provide a schematic of the catamaran designs, each with a heaveplate of 154m^2. A number of different variations on these designs were tested numerically and the best overall designs were tested physically. A preliminary structural design of the heaveplate and jacks was carried out using pressures from undamped numerical simulations and DNV-GL codes [148, 149], thus an estimation of the steel and aluminium required was formed.

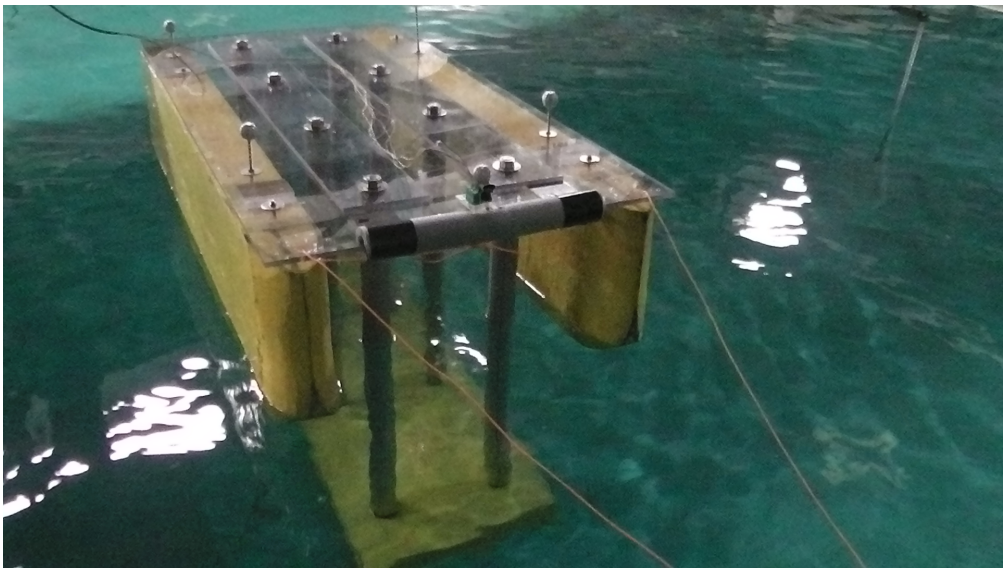

Figure 3.6: Wide Hulled Catamaran with a Heaveplate, Slack Moored

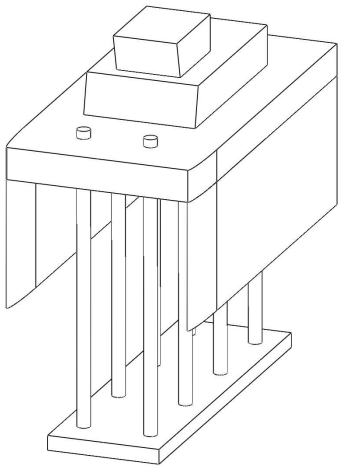

Figure 3.7: Narrow Hulled Catamaran with a Heaveplate at a 12m Draught

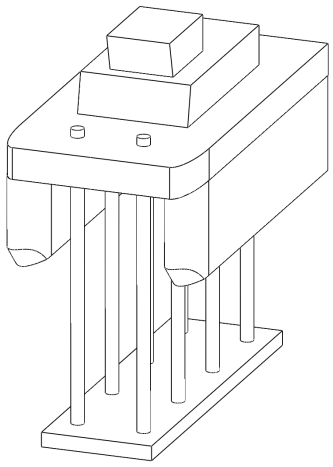

Figure 3.8: Wide Hulled Catamaran with a Heaveplate at a 12m Draught

3.2.3 Curved Hulled Catamaran with Single Heaveplates

A curved hulled catamaran design is depicted in this section. This hull design was inspired from the catamaran with a heaveplate series of analysis carried out on the designs in the previous section. It was found that to carry out personnel transfer the narrow hulled catamaran was best, yet if one wanted to also use the ship for transit then the heaveplate would need to be raised to reduce drag. To provide enough stability to support the mass of the heaveplate when raised in this mode, the catamaran hull would need to be wider. A hull section where it curved from narrow to wide was considered for this. A lines plan is provided in Figure C.1 to clarify the hull concept. Furthermore, this design was used to compare differing heaveplate, depths, areas and angles. The different heaveplate depths are illustrated in Figure 3.9, and the areas are shown in Figure 3.10. Photographs of the built model are provided in Figures 3.11 & 3.12.

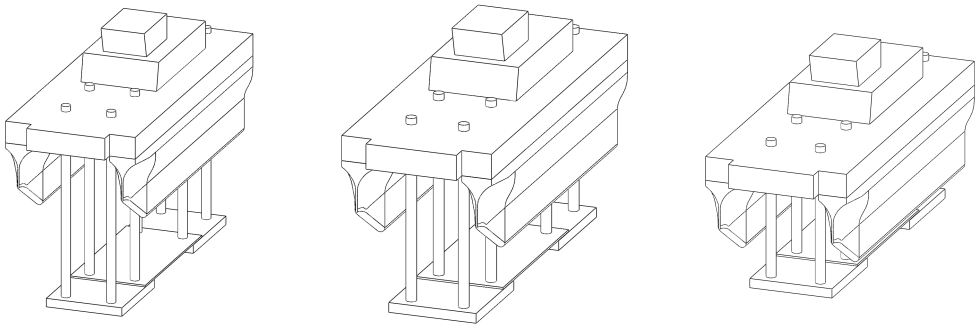

(a) 12m (b) 9m (c) 9m

Figure 3.9: Curved Hulled Catamaran with Varying Heaveplate Depths with a Constant Area of 178.5m^2

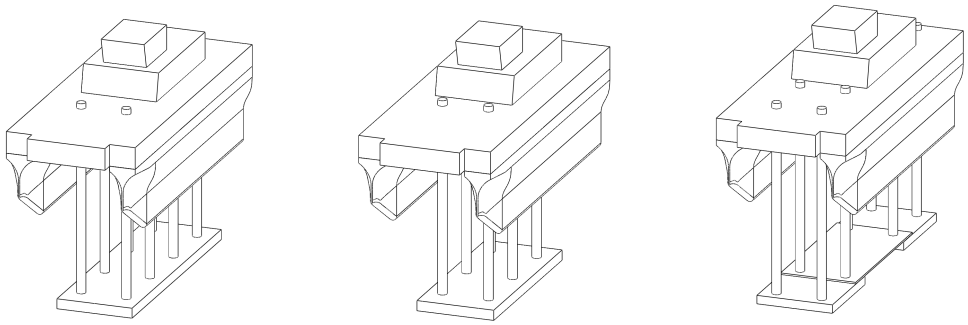

(a) 154m^2 (b) 115.5m^2 (c) 178.5m^2

Figure 3.10: Curved Hulled Catamaran with Varying Heaveplate Areas at a Constant Draught of 12m

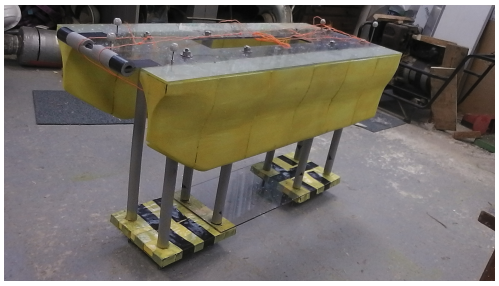

Figure 3.11: Curved Hulled Catamaran with a 178.5m^2 Heaveplate at a 12m Draught

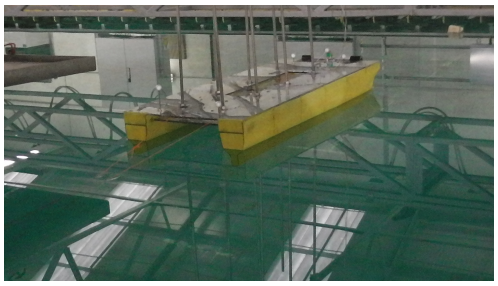

Figure 3.12: Curved Hulled Catamaran with the Heaveplate Raised to Simulate the Transit Mode

3.2.4 Curved Hulled Catamaran with Dual Heaveplates

To reduce the size of the heaveplate whilst maintaining the positive heave and pitch characteristics that the heaveplate demonstrates, dual heaveplates were considered with one located close to the bow of the vessel and the other close to the stern. Dual heaveplates could potentially create larger damping of motion than a singular heaveplate of the same area, from the extra pitch resistance. In addition, setting the heaveplate at an angle could possible increase motion reduction.

A number of dual heaveplate designs were investigated physically as shown in Figures 3.13 to 3.16. A constant draught of 12m was maintained with heaveplate area and angle being varied, specifically 28m^2 to 56m^2 per heaveplate at angles of 0°, 22.5° and 45°.

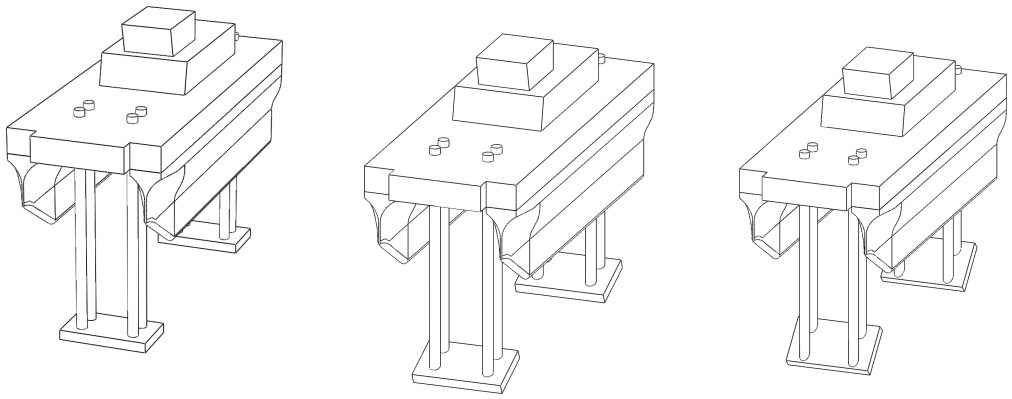

(a) 0° (b) 22.5° (c) 45°

Figure 3.13: Curved Hulled Catamaran with Dual Heaveplates Varying Heaveplate Angle at a Constant Draught of 12m, Each with an Area of 28m^2 for a Total Area of 56m^2

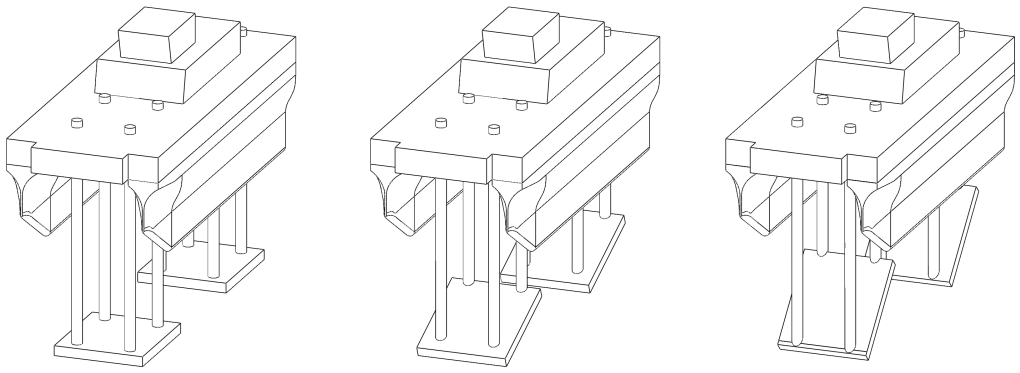

(a) 0° (b) 22.5° (c) 45°

Figure 3.14: Curved Hulled Catamaran with Dual Heaveplates Varying Heaveplate Angle at a Constant Draught of 12m, Each with an Area of 56m^2 for a Total Area of 112m^2

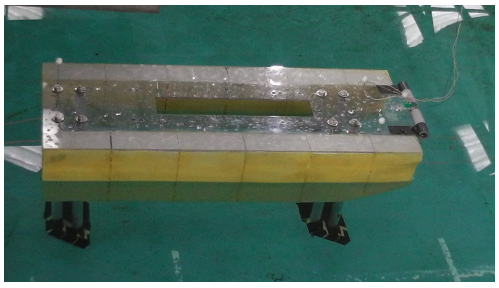

Figure 3.15: 28m^2 Dual Heaveplates Positioned at an Angle of 45°

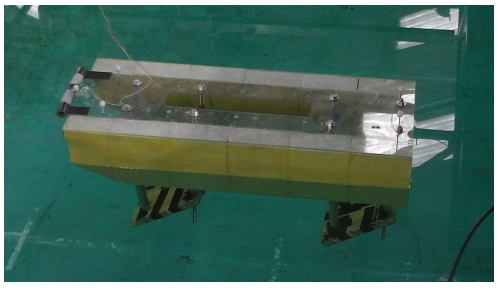

Figure 3.16: 56m^2 Dual Heaveplates Positioned at an Angle of 45°

3.2.5 Grand Draught Catamaran

The Grand Draught Catamaran (GDC) as shown in Figures 3.17 & 3.18 was an upgraded design of the narrow hulled catamaran with 625mm wide demihulls that included extra space for engines, and access. In addition, the bow was inclined at a greater angle and the fender projected further forward. The mass properties were more accurate than the narrow hulled catamaran with a heaveplate it was based on.

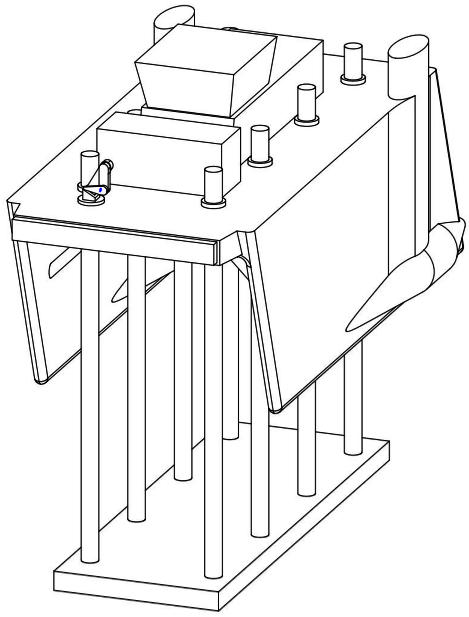

Figure 3.17: GDC Isometric Drawing

The GDC had a number of different geometrical and mass differences to the narrow hulled catamaran with a heaveplate. The hulls are enlarged horizontally at the stern to accommodate engines. In addition, the requirement for access to the engines results in an enlargement of the hulls locally in the vertical direction. These extra volumes move the centre of buoyancy and gravity towards the stern and produced an increased wave load on the vessel, particularly in head waves. Furthermore, to prevent any contact between the hulls and the monopile the bow tapers at a greater angle than the narrow hulled catamaran with a heaveplate, and the horizontal distance between the front of the heaveplate and the forward perpendicular is larger. The deck of the GDC is higher than the narrow hulled catamaran with a heaveplate to prevent slamming to the underside of the tunnel and minimise water on deck due to large waves and the model's reduced heave and pitch RAOs. Structurally the GDC included struts that braced the slender demihulls to the deck structure of the catamaran, though above the waterline

they add to the wave load on the GDC for larger waves. The physical model properties of the GDC are displayed in Table C.2.

3.3 Discussion of Linear Wave Motion Effects

The main drivers of bow movement are wave loads and the ratio of wave length to ship length. The movement at the bow is governed by heave and pitch motion in open water, however when docked at the monopile this is mostly from wave force on the bow of the vessel, both from the water particle acceleration and the additional buoyancy force caused. The heaveplate reduces the vessel's heave and pitch response, and the wave load is minimised by making the bow of the vessel very narrow. Factors other than Hs that drive vessel behaviour due to the physics of the wave and vessel interaction are: wave period, water particle trajectories and associated accelerations; as well as the vessels properties such as waterplane area, buoyancy and mass distribution, bow shape, length, draught, and breath of the vessel.

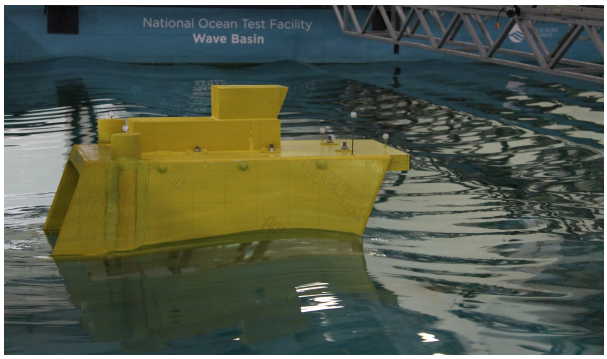

Figure 3.18: Testing of the GDC in Irregular Waves

As a damping mechanism the heaveplate increases the natural period as does reducing the waterplane area. Without the heaveplate in place the natural period is much smaller, however this is mostly due to the increase in waterplane area required to achieve the metacentric height (when the heaveplate is in place the centre of gravity is lowered relative to the centre of buoyancy thus a smaller waterplane area is possible). Thus the variation of the hull form has a significant effect as an excitation component.

From the following diagrams, Figures 3.19–3.21, it can be seen that the wave-

length to ship length ratio changes dramatically as different periods of the North Sea are considered. With the shorter waves shown in Figure 3.19 the effect of the reduction of wave motion with depth is more pronounced (for example a 4s wave which results in a 24.97m wavelength for the 25m depth considered). The 24m long vessel is close to the wavelength, thus the heaving force is small and the pitch force is large, as discussed in § 2.11.5. In Figure 3.20 the pitch force is small and the heave force is larger than at 4s, here the wavelength is 93.27m which is more than triple the length of the vessels considered in this thesis. In Figure 3.21 a 12s wave period is considered, and the pitch motion is minimal while the heave motion is very large.

The magnitude of the water particle displacement reduces substantially with depth particularly for the shorter waves which could be considered as deep water waves. At the surface there is an amplitude of displacement of 1.5m and at a depth of 12m the amplitude of motion for the 4s waves shown in Figure 3.19 is 0.07m. However, for the longer wave periods the motion becomes gradually more elliptical with Figure 3.20 having an x amplitude of 0.81m and z amplitude of 0.57m. In Figure 3.21 the x motion is 1.54m and the z motion is 0.70m. When the z motion at 12m depth increases the effectiveness of the heaveplate decreases.

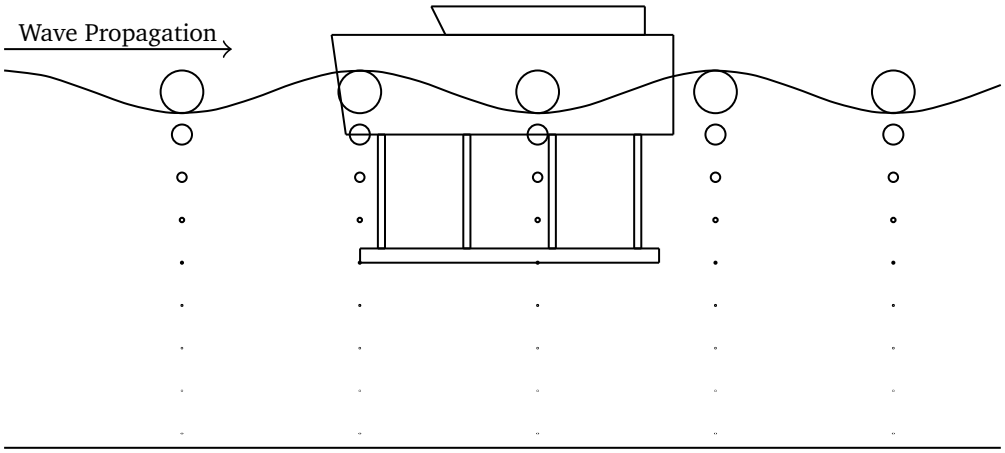

(a) Water Particle Displacement

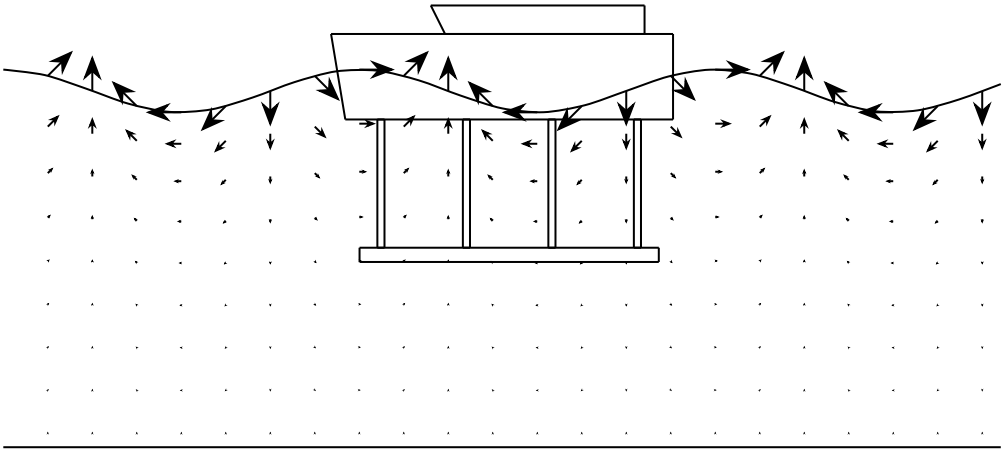

(b) Water Particle Velocity

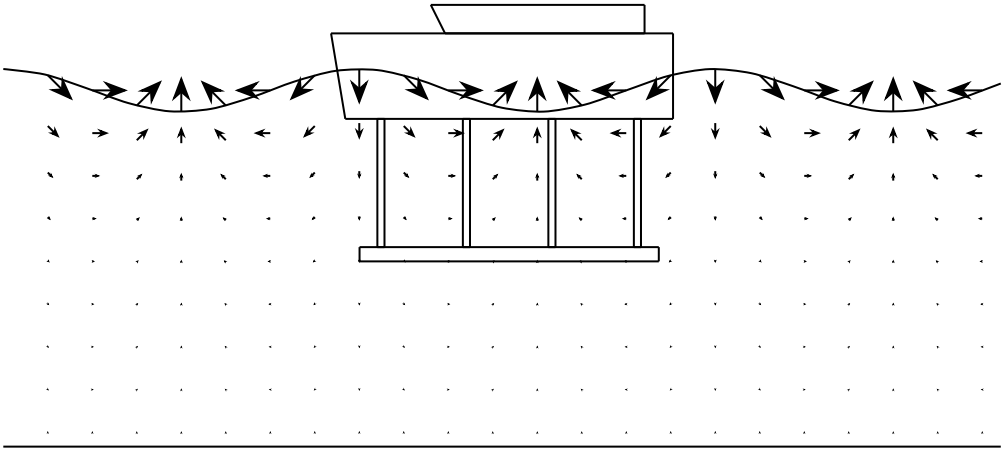

(c) Water Particle Acceleration

Figure 3.19: Water Particle Motion for a 3m Wave Height, 4s Period, 24.97m Wavelength in 25m water depth

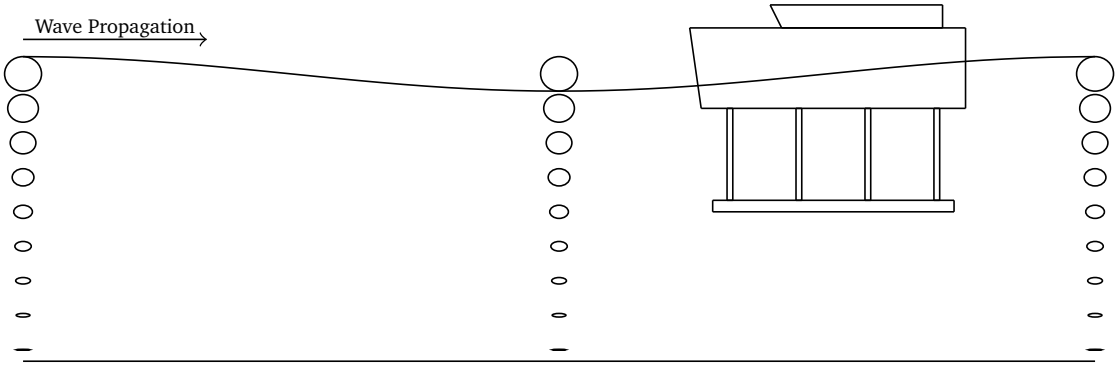

(a) Water Particle Displacement

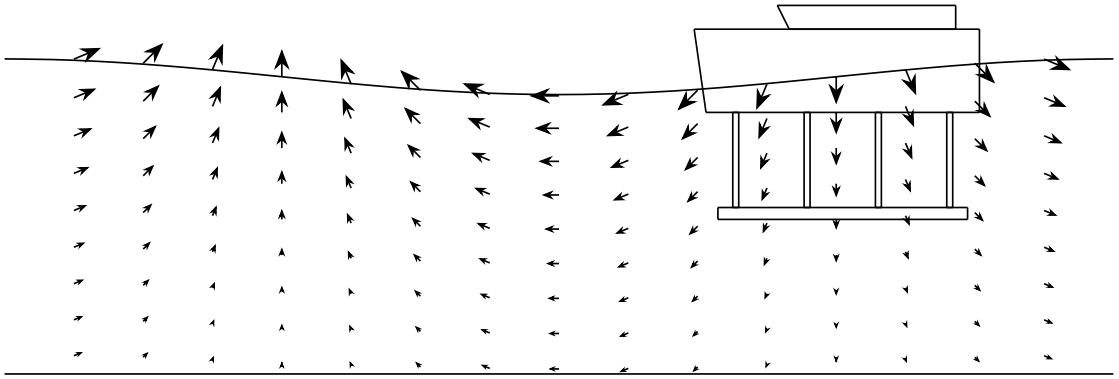

(b) Water Particle Velocity

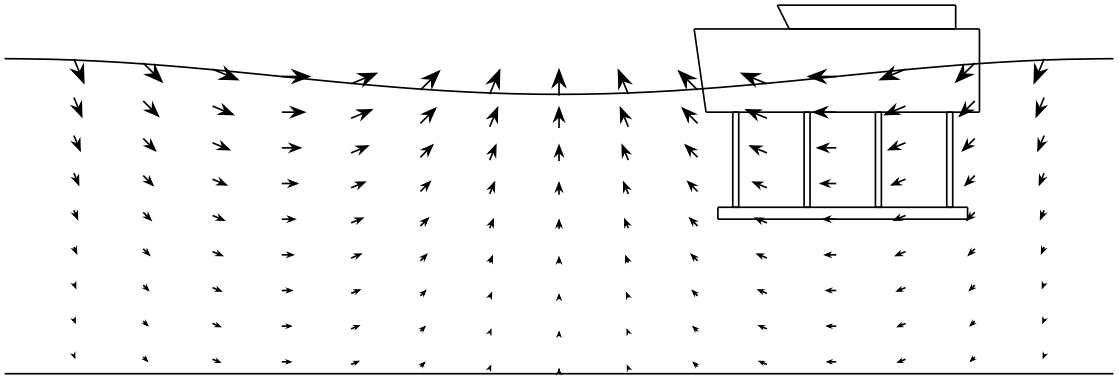

(c) Water Particle Acceleration

Figure 3.20: Water Particle Motion for a 3m Wave Height, 8s Period, 93.27m Wavelength in 25m water depth

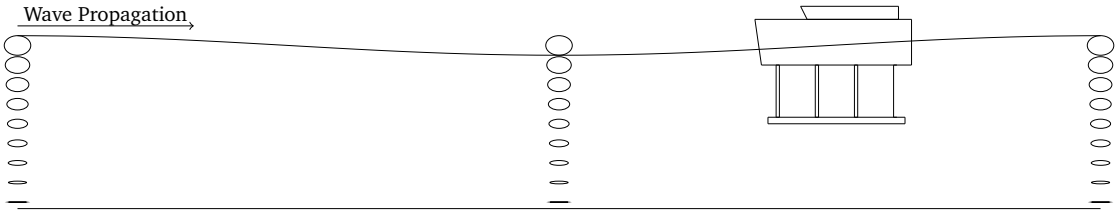

(a) Water Particle Displacement

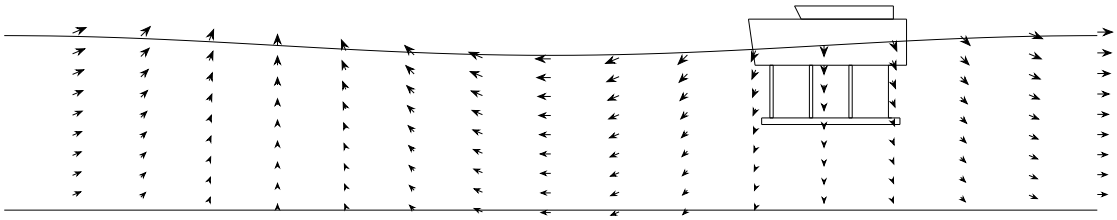

(b) Water Particle Velocity

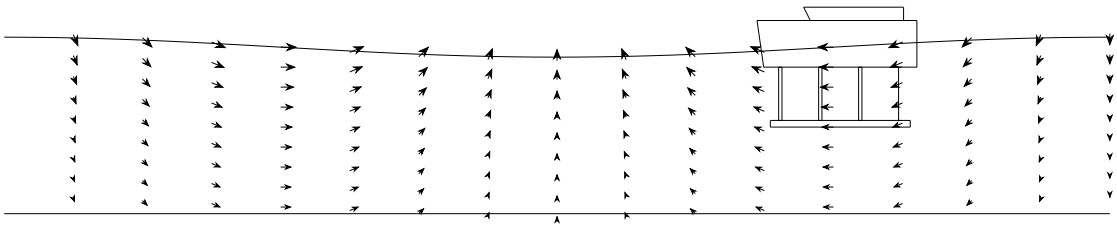

(c) Water Particle Acceleration

Figure 3.21: Water Particle Motion for a 3m Wave Hheight, 12s Period, 165.96m Wavelength in 25m water depth

3.4 Summary

In this chapter a number of concept designs for WFSVs were presented, the tubular multihull designs, followed by the narrow hulled and wide hulled catamarans, then the curved hulled catamaran with a variety of heaveplate combinations including dual heaveplates and finally the GDC. The effect of water particle motion on the vessel length and heaveplate depth was reviewed. The designs discussed in this chapter will be used throughout this thesis to discuss the different methods of analysis for investigating and comparing the motions of a WFSV when at zero forward speed at a wind farm and when docked at a monopile foundation. In the following chapter the numerical modelling of these designs is discussed.

Chapter 4

Numerical Modelling of Novel WFSV Designs

4.1 Introduction

This chapter details the numerical modelling carried out on wind farm service vessel (WFSV) hull designs to compare the consequence of altering different features. Numerical modelling is important in the design phase of new craft, as it is generally an inexpensive way to understand the effects of altering various parameters.

As described in Chapter 3 the designs to be analysed numerically are; the tubular multihull, the narrow hulled and wide hulled catamarans, the curved hulled catamaran with a variety of heaveplate combinations, and the Grand Draught Catamaran (GDC). Due to the nature of the different designs two modelling techniques were utilised, a computational fluid dynamics (CFD) RANS finite volume solver ANSYS CFX, and a potential flow theory boundary element method (BEM) ANSYS AQWA. The first is used where the viscous flow is of significant importance, and the latter where viscous flow is not a principal contributor to the vessels motion, as outlined in § 2.12, and described in further detail in Appendix B.1 & B.2.

The BEM model was used to get an estimation of the effects of alterations to

the geometry of a catamaran, to model the influence of a heaveplate, examining the hull form, and the heaveplate's; depth, size, area, and angle. Novel floating bodies such as the ones analysed in this research require the numerical model to be verified experimentally. In undamped numerical analysis the RAO tends to be large at resonance, damping is introduced into the system based on physical model test data.

Numerical modelling fits into the development process of hydrodynamic analysis as an initial analysis tool to determine the relevant parameters of a design at a stage where the cost of such a change is small, rather than altering a physically built model. Numerical modelling can then be used throughout the design process to continually optimise the design, using the physical modelling to inform the numerical model. This chapter will outline the results from the numerical modelling carried out to aid the physical model testing.

4.2 CFD Numerical Modelling

The CFD analysis undertaken is limited in detail and robustness. It was carried out to understand the model's behaviour in greater detail, from this understanding it was envisaged that an optimisation would occur, however due to the time and computational limitations it was not progressed as far current standards can achieve. Thus the physical modelling of this platform was carried out detailing a large number of design configurations in an attempt to understand its properties in greater detail.

Appendix D discusses the creation of a Numerical Wave Tank (NWT) using the finite volume CFD solver ANSYS CFX. CFD was required for this analysis as the main area of interest was the influence of the viscous forces on the horizontal tubes of the design. The research outlined in the appendix details the methodology of setting up and calibrating a NWT in CFD using ANSYS CFX. One of the tubular multihulls was then analysed in three degrees of motion (heave, pitch, and surge) using symmetry.

4.3 BEM Numerical Modelling

4.3.1 Overview

Following on from the modelling of the tubular multihull in CFX, modelling of catamarans are modelled with the potential flow BEM solver ANSYS AQWA (described in Appendix B.1) in this section. Catamarans being wall sided and not relying predominantly on viscous damping are generally well represented by BEM solvers. The heaveplate effects are partly modelled by AQWA through potential flow theory, the neglected effects being extra drag associated with vortices at the corners of the heaveplate, which are not calculated.

Adding a heaveplate is a proven method of damping an offshore structures movement and as catamarans are a favoured WFSV type it is envisioned to combine these two concepts to create a catamaran that can access wind turbines up to a 3m Hs. The modelling in this section aims to design suitably sized catamarans with heaveplates, and to compare the effects of changing critical parameters.

It is required to specify the numerical damping employed in AQWA, for more accurate results particularly at resonance. In addition, it has been noted that an understanding of the hydrodynamic properties of a floating offshore structure be fully understood before adding damping [150, 151, 152]. Therefore, the RAO amplitude at peak frequency tended to infinity and only served as a reference point for the natural period. Following on from the physical model testing some linear damping was applied to aid the progression of the GDC from the narrow hulled catamaran.

The distribution of volume and mass was estimated from standard catamarans and the mass of the heaveplate was then added. The mass of steel for the heaveplate and jacks was estimated from basic structural calculations based on the pressure force induced on the structure.

Each model considered in AQWA had the same the same setup. The structure was free to move in all directions. A point mass for the geometry of the model

in question was defined explicitly along with the mass moments of inertia. From the geometry file the draught was set, and the mass was dependent on the mesh generated. Figure 4.1 shows an example of a the AQWA setup, the mesh was created comprising of quadrilateral and triangular panels was utilised with a defeaturing tolerance of 0.3m and a maximum element size of 1m. In AQWA the defeaturing tolerance determines how the small details are meshed, any details smaller than the defeaturing tolerance may have a mesh element spanning across it. The hydrodynamic diffraction and radiation were then solved for the desired heading angles and frequencies.

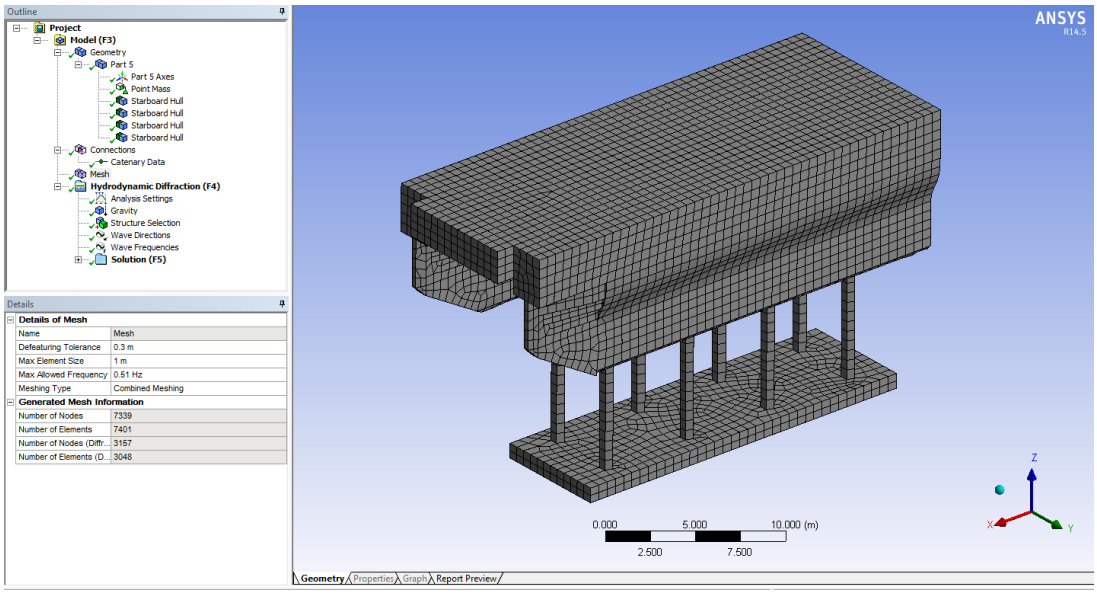

Figure 4.1: Mesh Setup in AQWA

In the subsequent sections the following are investigated:

§ 4.3.2 provides the numerical model RAO for a basic standard catamaran WFSV

§ 4.3.3 studies different catamaran hull designs with single heaveplates

§ 4.3.4 models the result of varying heaveplate depth and area

§ 4.3.5 examines the influence of using dual heaveplates

§ 4.3.6 discusses catamarans with a raised heaveplate

4.3.2 Standard Catamaran

The undamped RAO curves are presented for the standard catamaran model described in § 3.2.2 in Figure 4.2. This model represents a baseline from which subsequent models may be compared to.

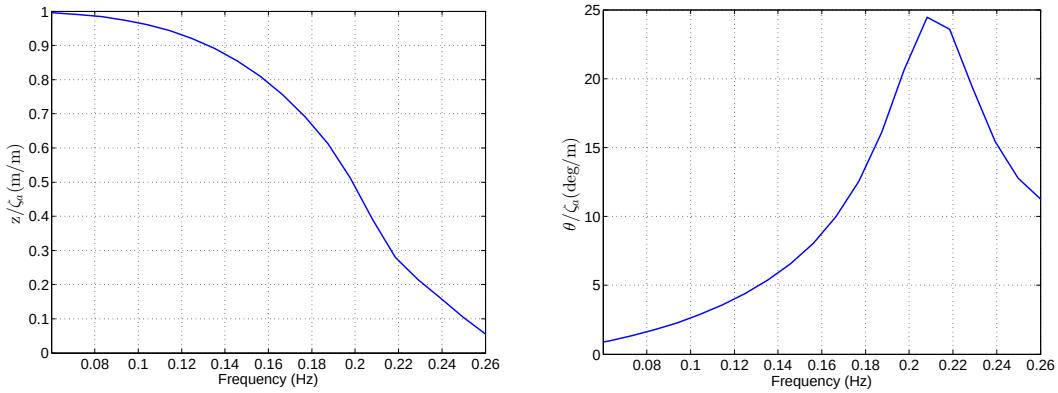

(a) Heave

(b) Pitch

Figure 4.2: Numerical Modelling RAO Curves for a Standard Catamaran

4.3.3 Catamarans with Single Heaveplates

In Figure 4.3 the heave and pitch for four catamaran hulls with a heaveplate at 12m draught is depicted. The size of the heaveplate varied for each hull. Both the narrow hulled catamaran and the wide hulled catamaran had a heaveplate of 22m x 7m, the curved hulled catamaran had a heaveplate of 25.5m x 7m and the GDC had a heaveplate of 22m x 8m.

Examining the difference between the wide hulled catamaran and the narrow hulled catamaran it is evident that the overall magnitude of the heave and pitch RAO is reduced as the draught increases for the same displacement, that is a reduction in waterplane area (WPA). Though the magnitude of the heave RAO for the narrow hulled catamaran is larger at the natural period, it is likely due to the specific frequency tested (with no damping) and is not representative as the other model could have been higher at other frequencies. Furthermore, the small WPA results in a reduction of the peak frequency of the model. The curved

hulled catamaran has a reduction in heave and pitch RAO compared to the wide hulled catamaran. The GDC (a design that incorporated additional buoyancy to accommodate motors and access to same motors that the narrow hulled catamaran model did not account for) shows a similar RAO curve as per the narrow hulled catamaran, with a similar natural period. The magnitude of the off peak pitch RAO is slightly larger than the narrow hulled catamaran though still much less than the other designs. All models show an improvement on the standard catamaran RAO in Figure 4.2 particularly when the natural frequency is low.

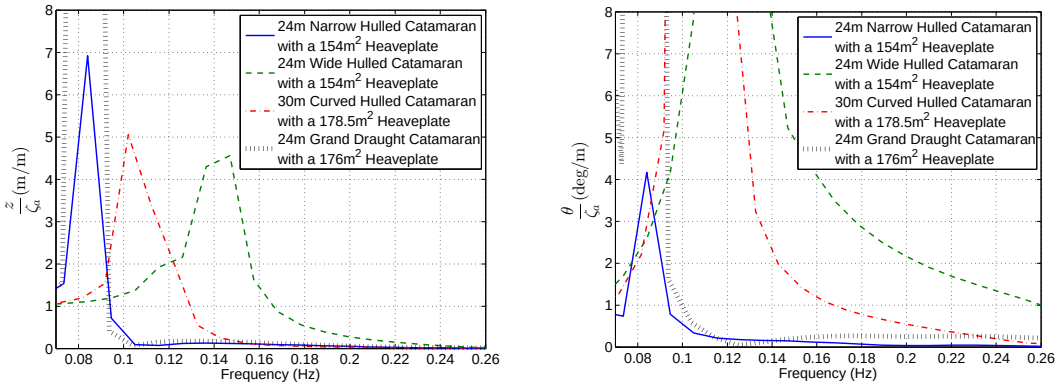

(a) Heave

(b) Pitch

Figure 4.3: Numerical Modelling RAO Curves for Catamaran Hulls with a Heaveplate at a 12m Draught

4.3.4 Heaveplate Depth and Area Comparison

Figure 4.4 shows the effects of heaveplate depth on the heave and pitch RAO for the 30m long curved hulled catamaran. Increasing the heaveplate depth had a marginal impact on the RAO curves.

Figure 4.5 shows the effects of heaveplate area on the heave and pitch RAO for a 30m long curved hulled catamaran. An increase in heaveplate area increases the natural period of both heave and pitch RAO. Increasing the heaveplate area also yielded a substantial decrease in heave and pitch motion. When comparing the decrease in motions from area increase with that of depth in-

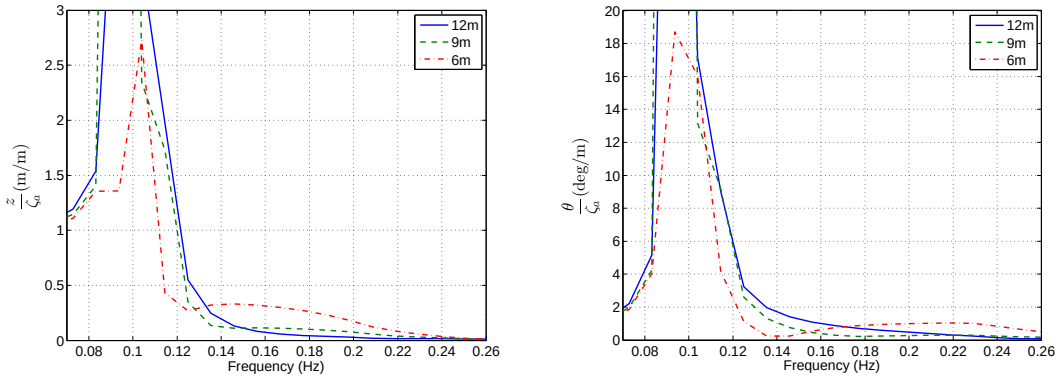

(a) Heave (b) Pitch

Figure 4.4: Numerical Modelling RAO Curves Comparing Heaveplate Depth with the Curved Hulled Catamaran using a Heaveplate Area of 178.5m^2

crease, it can be deducted that the area increase creates a larger effect on both RAO curves.

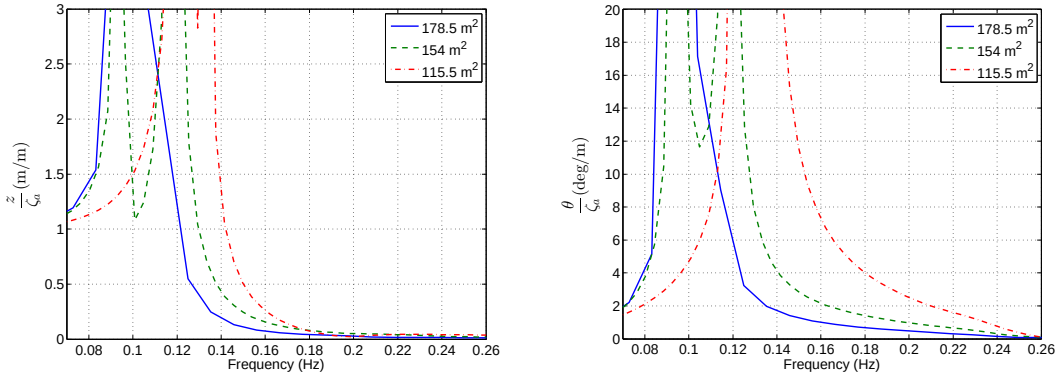

(a) Heave (b) Pitch

Figure 4.5: Numerical Modelling RAO Curves Comparing Heaveplate Area Change at a 12m Draught on the Curved Hulled Catamaran

4.3.5 Curved Hulled Catamaran with Dual Heaveplates

Figure 4.6 graphs the effects of two heaveplates, one at the bow and one at the stern of the ship at a depth of 12m each with an area of 28m^2 for a total area of 56m^2. The resultant RAO graph shows a small change between the angle of the

heaveplate and magnitude of RAO. In pitch, there is an anomaly at 0.16–0.18Hz that could be investigated further with a smaller frequency interval. In heave, the RAO tends to reduce as the angle of the heaveplate increases. In pitch, the natural period reduces with increased heaveplate angle and the RAO appears to marginally increase. These models do not show much improvement on the standard catamaran RAO in Figure 4.2.

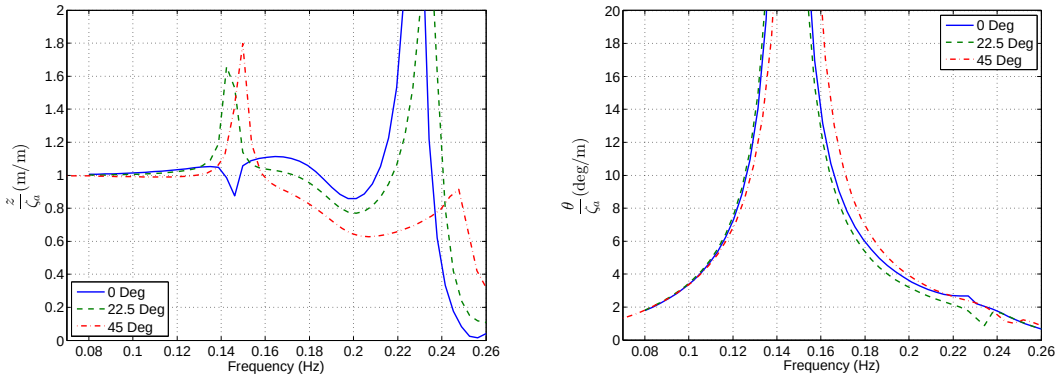

(a) Heave (b) Pitch

Figure 4.6: Numerical Modelling RAO Curves Comparing Angle of Dual Heaveplates each 28m^2 at a 12m Draught

Figure 4.7 shows the results for a similar setup with each heaveplate 56m^2 for a total heaveplate area of 112m^2. When compared to Figure 4.6 it can be observed that the heave and pitch natural periods increased and with that, the amplitude of the RAOs has reduced, particularly for the model set horizontally. This is probably due to the larger, heave resistance and pitch resistance the horizontal heaveplates yield. These models show some improvement on the standard catamaran RAO in Figure 4.2. However, they also show some issue with heave and pitch coupling. In addition, dual heaveplates showed their most promising results when placed horizontally (and consequently at a deeper average draught) and with a larger heaveplate, similar to the conclusion in § 4.3.4.

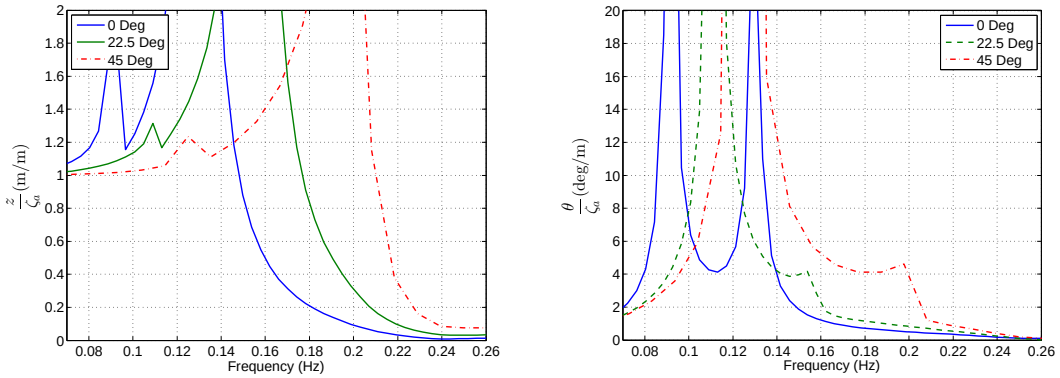

(a) Heave (b) Pitch

Figure 4.7: Numerical Modelling RAO Curves Comparing Angle of Dual Heaveplates each 56m^2 at a 12m Draught

Figure 4.8 compares the model with two heaveplates with a combined area of 112m^2 set horizontally, to the one with a 115.5m^2 heaveplate, both at a draught of 12m on the curved hulled catamaran graphed in Figure 4.5, it is evident that they perform similarly in heave but for pitch motion the model with dual heaveplates has a lower responce off peak, however the large amount of pitch and heave coupling is disconcerting.

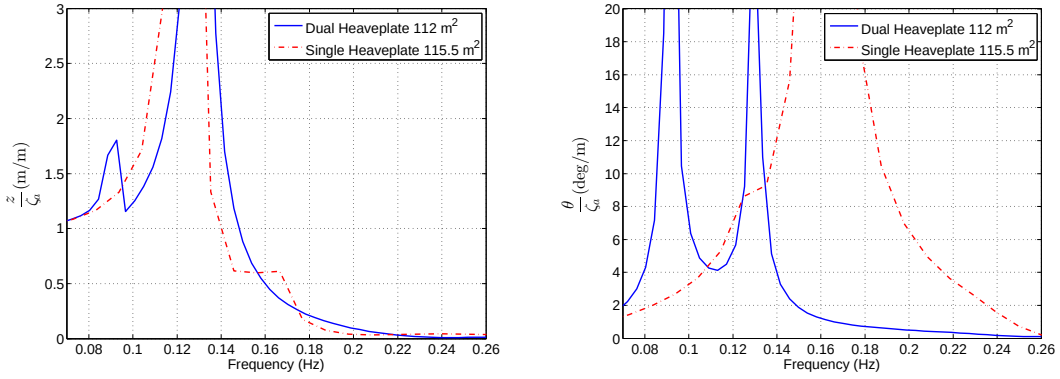

(a) Heave (b) Pitch

Figure 4.8: Numerical Modelling RAO Curves Comparing Dual and Single Heaveplates of Similar Areas

4.3.6 Catamarans with a Raised Heaveplate

Investigating the influence of hull shape on zero forward speed RAO for the catamarans suitable to manoeuvre with the heaveplate in the raised position yielded some interesting output, as is depicted in Figure 4.9. The catamarans that were designed for transit with the heaveplate raised were the wide hulled catamaran and the curved hulled catamaran. In both cases, the curved hulled catamaran performs marginally better in heave and pitch. There is a substantial increase in pitch RAO at the natural frequency, however this is an undamped case, in addition the curved hulled catamaran was longer than the wide hulled catamaran, 30m to 24m. It may also be noted that the RAO curves are similar to the ones for a standard catamaran RAO in Figure 4.2.

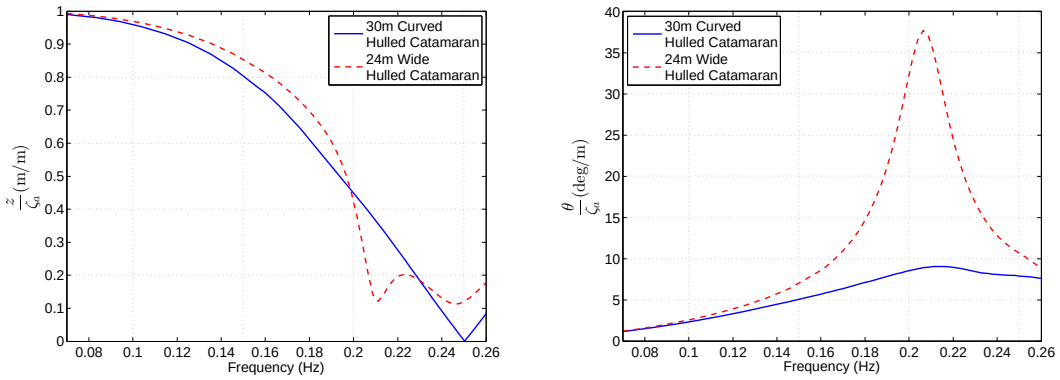

(a) Heave

(b) Pitch

Figure 4.9: Numerical Modelling RAO Curves for Catamarans with a Raised Heaveplate

4.4 Pressures from Numerical Modelling

The distribution of pressure force on the vessel through ANSYS AQWA was used to give an indication of the amount of steel and aluminium required to construct the vessel. By investigating the pressure force in the frequency domain a conservative design estimate for the pressure force may be determined. A wave height

of 6m was utilised as it is the Hmax of a 3m Hs where Hmax = 2 x Hs [153]. From the pressure force the loads on the heaveplate and columns could be estimated. The heaveplate was estimated as a simple beam with the maximum pressure applied to its entire area and the columns were designed to withstand that same force in compression.

Figure 4.10a shows the mesh setup along with the pressure force for a 6m regular wave at a period of 11.9s for the narrow hulled catamaran model. This output was used to produce Figure 4.10b which shows the pressure force exerted on the body for frequencies between 0.08–0.26Hz for a 6m regular wave. The maximum was taken as $4.5 \times 10^5 \mathrm{N\,m^{-2}}$ and used as a constant pressure on the model to design the heaveplate and jacks.

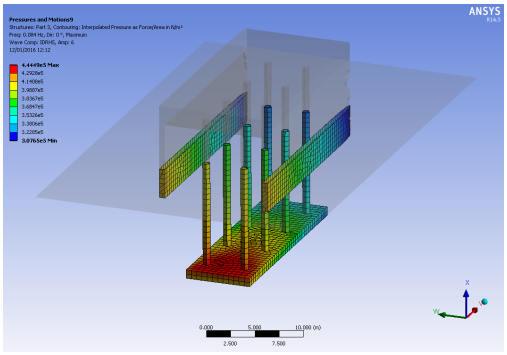

(a) Pressure Force; 6m H, 11.9s T

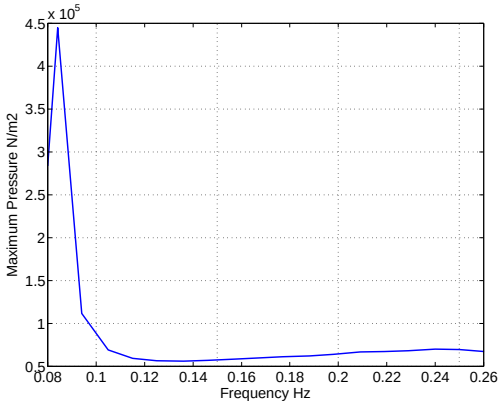

(b) ANSYS AQWA Pressure Force

Figure 4.10: Pressure Force Estimation on the Narrow Hulled Catamaran Model

4.5 Numerical Damping

As BEM codes are the fastest way to get useful results for floating bodies they are widely utilized, however unlike finite volume method RANS solvers and physical modelling they do not account for certain phenomena such as viscous damping which cause the model to both under and over predict motions and forces. To account for this various methods may be employed namely; the addition of

frequency dependent or independent viscous drag damping terms or the by the viscous damping term of the Morison equation which is determined by the coefficient C_d [154]. The dissipation force may be included with a BEM solver particularly in the resonance zone. These terms unfortunately are exceptionally difficult to predict for complex geometrical floating bodies. In this particular case of a catamaran with a heaveplate there is significant overestimation of the vessels motion at resonance, hence linear frequency independent damping was added to aid the estimation of forthcoming designs based on the previous experimental work.

Following the physical model testing of the narrow hulled catamaran, frequency independent damping was implemented on the numerical model as shown in Figure 4.11. Frequency independent damping of 5x10^{4}N/(m/s) in heave and 5x10^{4}Nm/(°/s) in pitch was found to be representative of the experimental RAO magnitude of the narrow hulled catamaran at resonance.

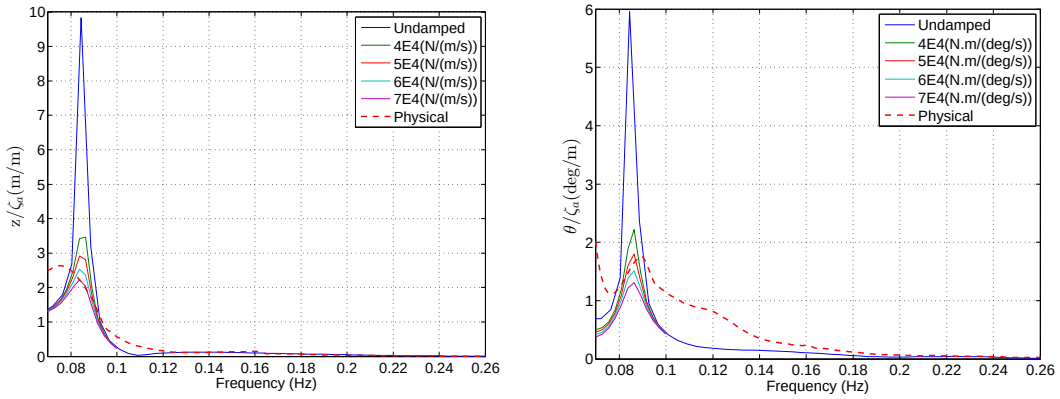

(a) Heave RAO

(b) Pitch RAO

Figure 4.11: Numerically Damping of the Narrow Hulled Catamaran

This damping was then used on the GDC in Figure 4.12 to predict its motions prior to physical testing, as the frequency independent damping for this model tended to reduce the off peak RAO when compared to the physical model it was only used to give a clearer estimation of the response at resonance. It can be seen in the RAO curves that heave is still over predicted and pitch is closer to the

experimental results.

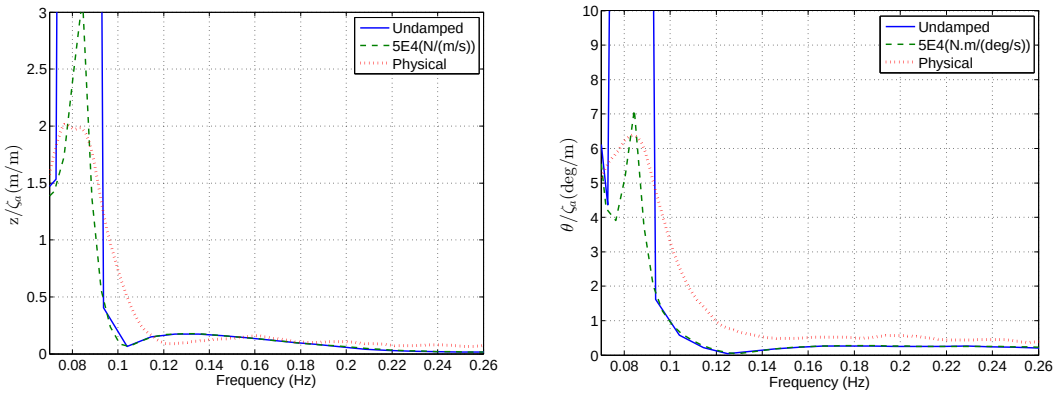

(a) Heave RAO

(b) Pitch RAO

Figure 4.12: Numerically Damping of the GDC

4.6 Discussion

The research outlined in this chapter includeds the methodology of setting up and calibrating a NWT in CFD using ANSYS CFX. One of the tubular multihulls was analysed in three degrees of motion (heave, pitch, and surge) using symmetry. CFD was shown to be time and computationally expensive. Numerical modelling in the BEM modelling software ANSYS AQWA investigated the RAO for a variety of catamarans with various heaveplates to examine the effect of changes to hull geometry, as well as the size, depth, and orientation of the heaveplate. The simulations showed that:

- Increasing heaveplate depth did not significantly improve performance.
- An increase in area provided a large reduction in RAO and change in natural period.
- A design with dual heaveplates, with one at the stern and one at the bow provided a large reduction for the area of heaveplate, when compared to a larger one piece heaveplate.

- When placed at an angle dual heaveplates did not provide greater reductions in RAO over horizontal heaveplates.

The pressure on the narrow hulled catamaran model was extracted from the undamped case for a conservative estimate of design pressure, this allowed for a preliminary structural design to be carried out.

The GDC design that adds buoyancy to allow a very small waterplane area design with the required features for a practical design show a similar RAO profile to that of the deep narrow hulled catamaran it was based on was modelled. Frequency independent damping was applied to the narrow hulled catamaran at resonance and was used to give a better approximation of the GDC's response.

ANSYS AQWA identified the natural period of the designs in question and aided the identification of designs that have minimal response to waves. Frequency independent numerical damping was implemented following physical model testing to aid future design development both from a structural and motion standpoint. Frequency dependent damping may perform better as by adding damping the model's motions are under predicted for off peak values.

By reviewing the confidence limits of the numerical modelling it can be seen that the accuracy of the work presented in this chapter is dependent on the model used and its input conditions. The CFD numerical modelling is limited in its methodology as outlined in § 4.2. In relation to the BEM modelling, ANSYS AQWA can solve either the first or second order equations. A first order solution was carried out as it is used in the current state of the art models [69, 137, 138]. The second order drift forces may be of concern but their magnitude should be negligible, particularly in comparison with numerical damping. Numerical damping has a large effect on the accuracy of the solution, either frequency dependent or independent damping may be utilised. In this research frequency independent damping was used, however it can be noted that in Figures 4.11 & 4.12 that this unrealistically increased damping at off peak frequencies.

Chapter 5

WFSV Motion at Zero Forward Speed

5.1 Introduction

Following on from the numerical modelling where the designs were sized and RAO curves were estimated, the physical modelling carried out focused on improving these estimates and validating the numerical modelling carried out. Each of the designs presented in Chapter 4 were modelled experimentally and in the case of the tubular multihull additional designs were investigated in the physical modelling carried out. In addition, the physical modelling fed back into the numerical modelling, providing estimates of numerical damping to be made and determining which models were performing well. The numerical and physical modelling though presented in different chapters were an iterative process.

Providing quantitative limits to the operability criteria of a wind farm service vessel (WFSV) is paramount to increasing the safety and consistency for offshore WFSV operations. A critical aspect of WFSV operation is the vessels stability when approaching a wind turbine foundation and the ability for crewmembers and technicians to be able to work safely on the foredeck. In order to reduce the possibilities of rough contact with the monopile and if for any reason the WFSV must move suddenly then the crew and technicians are safe on the deck. The

research presented focused on maximising the wave height for which transfer is possible. In particular, zero forward speed RAO, motion induced interruptions (MII), and RMS of accelerations and pitch angle are critical because if a vessel has a large amplitude of motion or large accelerations whilst preparing to make contact with the monopile, then the maximum wave conditions will be limited.

5.2 Physical Modelling Overview

To determine if the numerical models accurately approximated reality, physical model testing was carried out. All models were tested at 1:25 scale in the ocean basin which is 25m long 18m wide and had a depth of 1m. Figure 5.1 shows a picture of the ocean basin with a model, wave probes and instrument bridge in the foreground, and the flap type wavemaker paddles in the background. The waves were created with a flap-type wavemaker with active absorption, at the opposing end of the wave basin was a sloped beach followed by a horizontal section with triangular cages incorporating flexible geotextile material to minimize reflections. The motions of the model were recorded using a Qualisys ProReflex, non-contact 6 DOF, motion capture measurement system. Infrared cameras

Figure 5.1: Lir NOTF Ocean Basin

were used to measure the motion of each model using a set of reflective markers attached to the model. Wave heights were recorded with resistance based wave probes. Incident wave data was used in the analysis [155]. All data recorded concurrently at a frequency of 32Hz. The models were slack moored to maintain position and avoid additional forces being imparted on the model [150]. The wave conditions tested with each model are outlined in Appendix E.

5.3 Wave Tank Calibration

Wave calibration was carried out with current wave probes that measured the instantaneous water height at 32Hz with an accuracy of approximately +/-1mm. To set up a steady state system in the wave basin, waves were first allowed to propagate to the beach and any reflections return to the wavemaker before recording the data for analysis. The incident and reflected wave components were computed using the Funke & Mansard method [155]. The regular waves were run for 64s each and some sample time series are presented in Figures 5.2, 5.3 & 5.4, for the most part these waves are reasonably stable with some reflections present. The reflection coefficient is dependent on the wave height and period, for the examples given in Figures 5.2, 5.3 & 5.4 there was a range of 0.08–0.16s.

Figures 5.5, 5.6 , & 5.7 show a time series for a wave probe that was placed between the model location and the wave tank side wall to the paddles to show the impact of radiated waves fom the model on the wave climate in the tank.

The spectra generated were based on JONSWAP and Bretschnieder generated spectra from the Edinburgh Designs Ltd. wavemaker software. These were then evaluated for incident wave height and peak period. The input parameters were then changed in the wavemaker software to account for any differences between the intended and actual output at the test location, Figure 5.8 shows the actual Hs & Tp and error for the calibrated waves. However, this does not account for shape differences shown in Figures 5.9, 5.10, & 5.11.

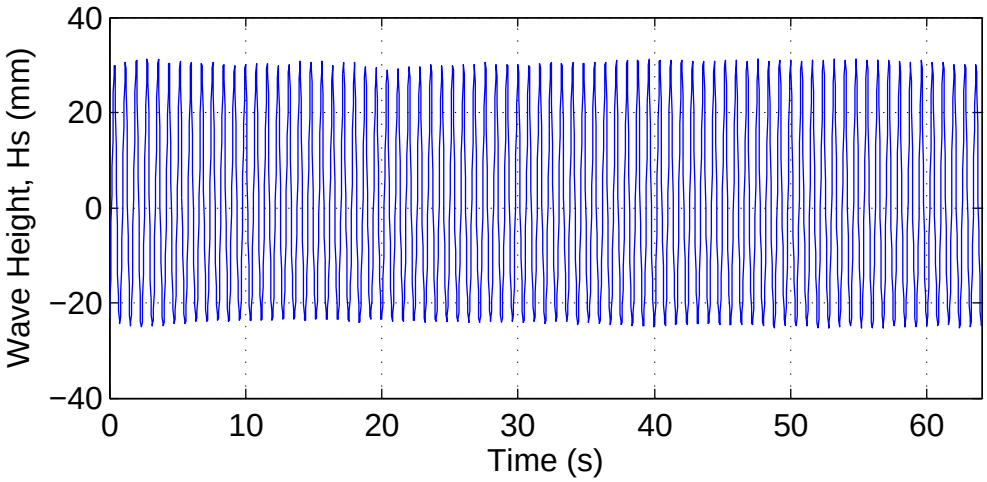

Figure 5.2: Regular Wave Timeseries H = 0.06 m, T = 0.8 s, Reflection Coefficient = 0.11

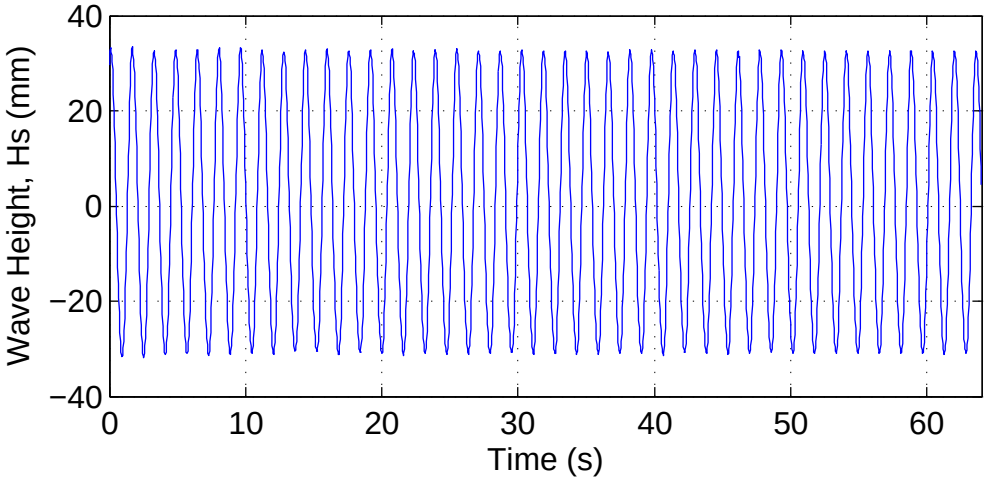

Figure 5.3: Regular Wave Timeseries H = 0.06 m, T = 1.6 s, Reflection Coefficient = 0.16

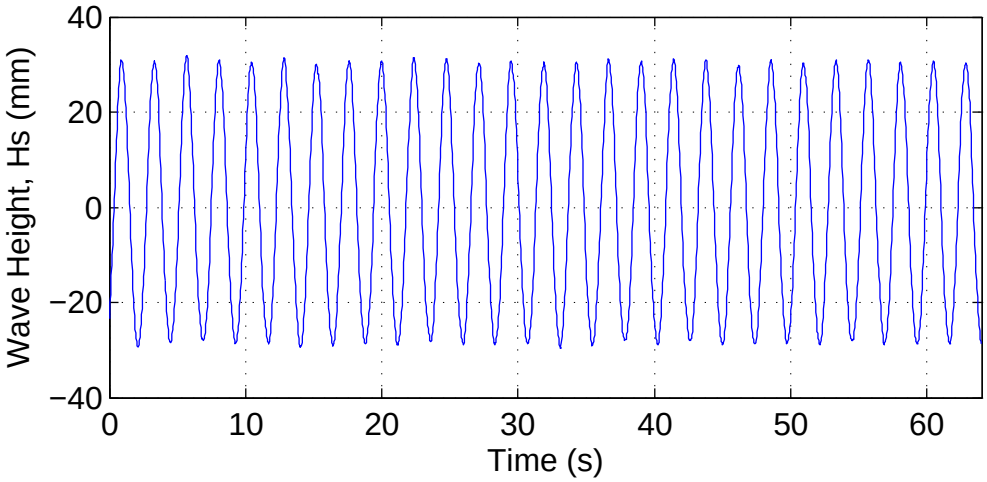

Figure 5.4: Regular Wave Timeseries H = 0.06 m, T = 2.4 s, Reflection Coefficient = 0.08

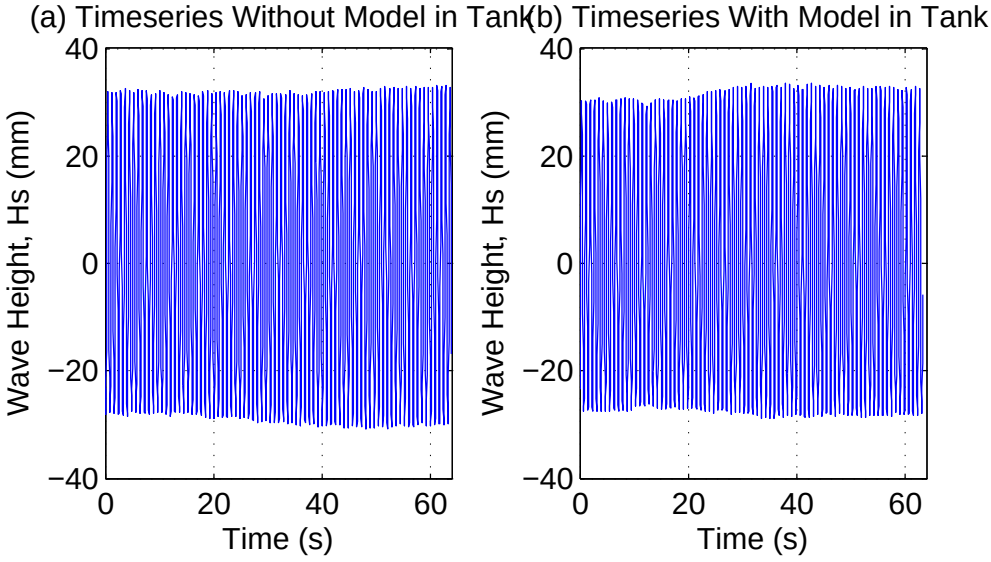

Figure 5.5: Regular Wave Timeseries Showing Effect of Radiated Waves H = 0.06 m, T = 0.8 s

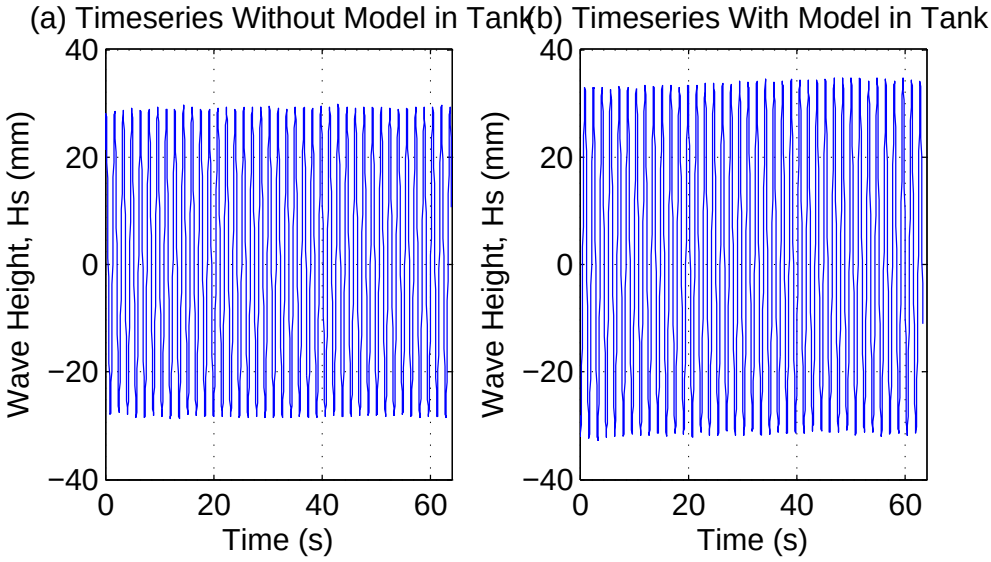

Figure 5.6: Regular Wave Timeseries Showing Effect of Radiated Waves H = 0.06 m, T = 1.6 s

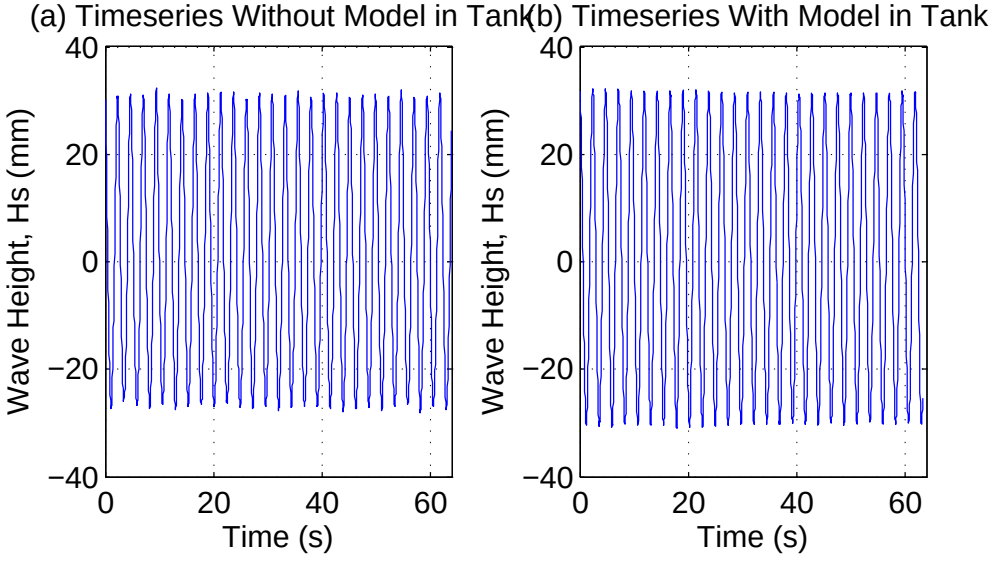

Figure 5.7: Regular Wave Timeseries Showing Effect of Radiated Waves H = 0.06 m, T = 2.4 s

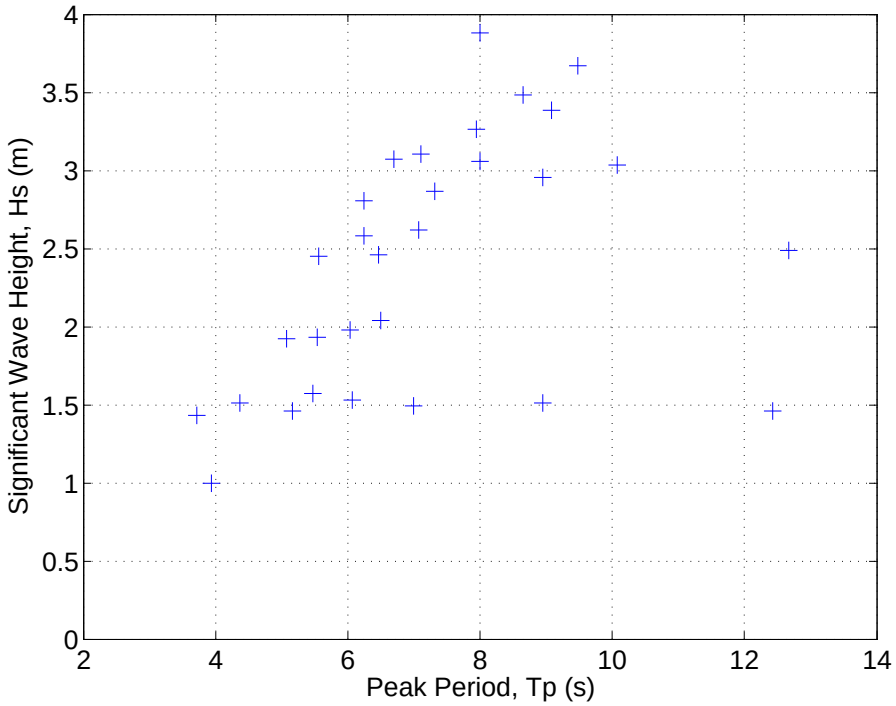

(a) Actual Hs & Tp

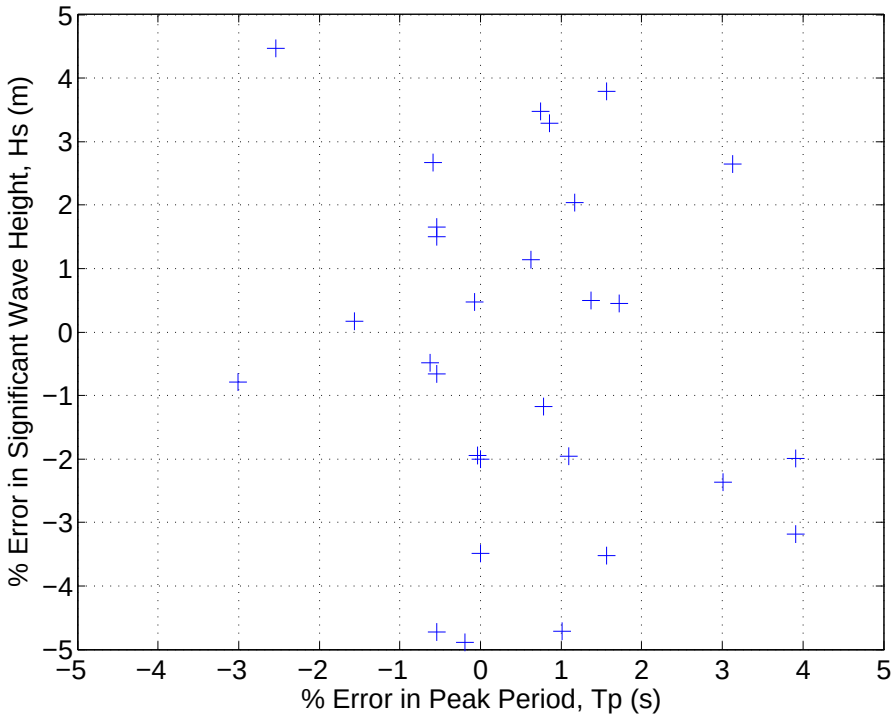

(b) Error

Figure 5.8: GDC Wave Calibration

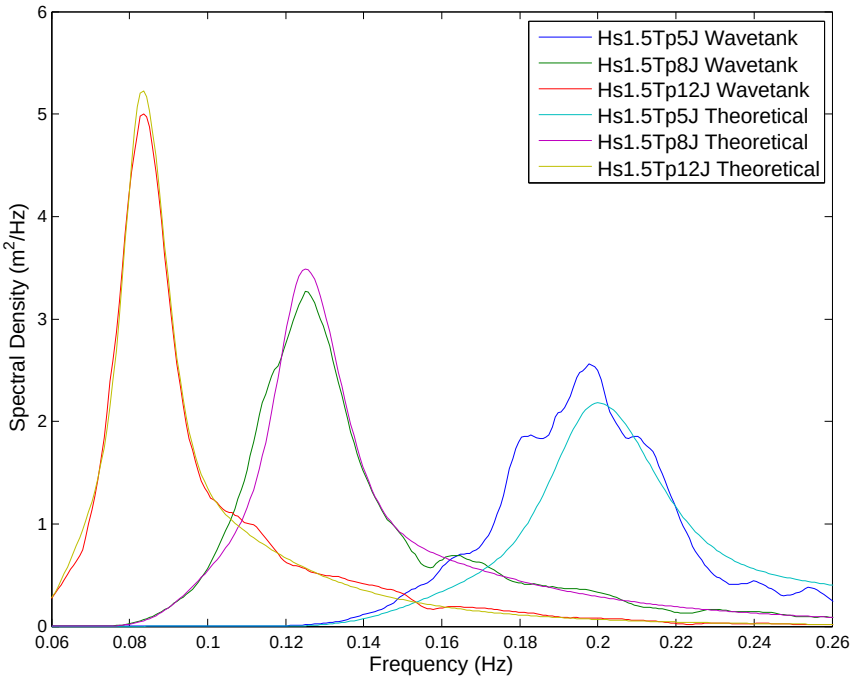

Figure 5.9: Comparison Between Theoretical and Actual Recorded Wave Spectra in the Wavetank: All JONSWAP with a 1.5m Hs

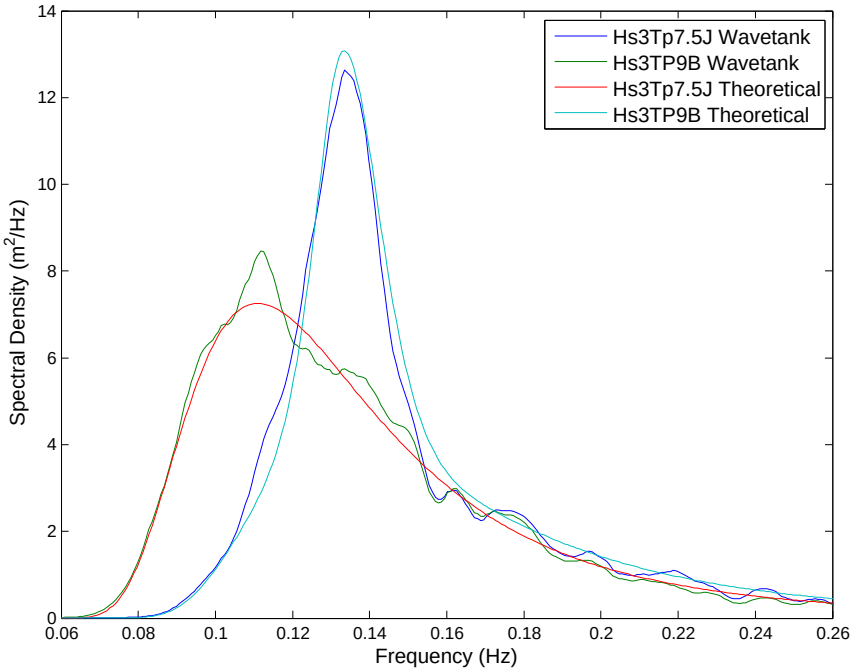

Figure 5.10: Comparison Between Theoretical and Actual Recorded JONSWAP and Bretschneider Wave Spectra in the Wavetank at a 3m Hs

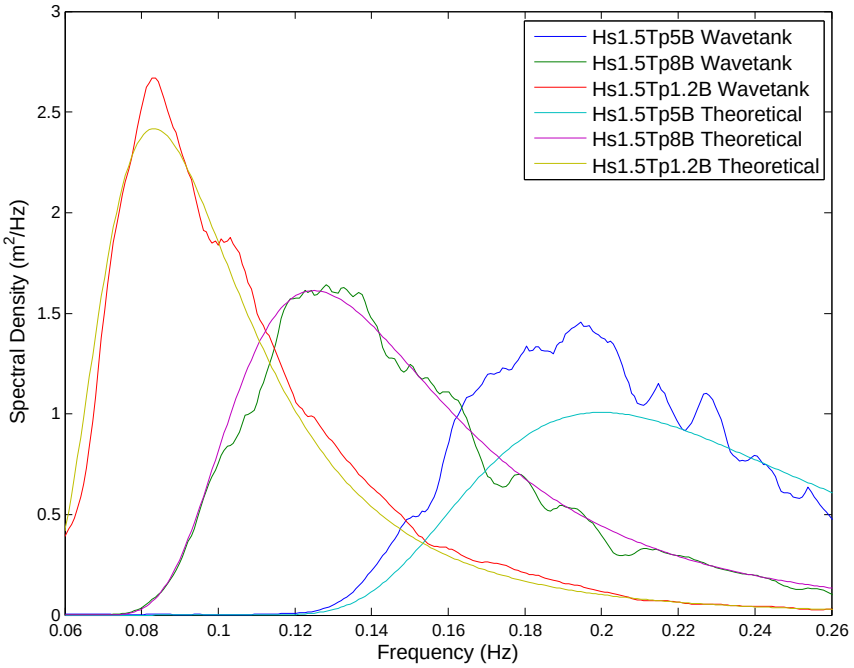

Figure 5.11: Comparison Between Theoretical and Actual Recorded Wave Spectra in the Wavetank: All Bretschneider with a 1.5m Hs

5.4 Data Analysis

Time series data of each model's motions was recorded using the Qualisys system. Analysing scale model data requires care to ensure that scale effects are not brought into the results. By recording at a suitable frequency and by smoothing the resultant data scale effects may be reduced.

The standard sampling frequency used in Lir NOTF is 32Hz which adequately exceeds the recommended resolution for recording the general motions and associated accelerations of a floating body [156, 157].

There are a number of different methods of filtering high frequency data from a time series. A least squares method of averaging or a polynomial could be fit to a specified section of the time series e.g. The SavitzkyGolay filter [158] or the low pass Butterworth filter [159]. These methods are best used to remove spikes in the data that may not be real. Filtering time series data to a specified frequency is difficult as it depends on the amplitude of the high frequency com-

ponents. Another method is to use a low pass filter by carrying out a fast Fourier transform of the time series to remove frequencies higher than the required cut off point [160], this method was applied to the recorded data.

To create the RAO curves the response to a number of incident spectra was utilised, averaging the output around the peak frequency of each spectrum. This was then pieced together to give the RAO curve between 0.08–0.26Hz and smoothed to remove any localised variations. Accelerations were calculated by double differentiating positional data for frequencies between 0.01–0.96Hz in order to omit any slamming and other high frequency effects that require a higher recording frequency to accurately record [161, 157]. The number of motion induced interruptions (MII) were then calculated for each spectrum using the Applebee-Baitis method.

5.5 Natural Periods

To experimentally determine the natural periods of heave, pitch and roll, the still water method of inducing a displacement, releasing and allowing the model to oscillate to estimate decay periods was carried out for all models tested. The model was inclined at an angle and then released or in the case of heave, it was submerged and then released. Figure 5.12 shows sample time series and frequency components of the decay tests for the Grand Draught Catamaran (GDC). The frequency components of the decay test can aid in the determination of the natural frequency, in addition the quality of the decay test may be examined.

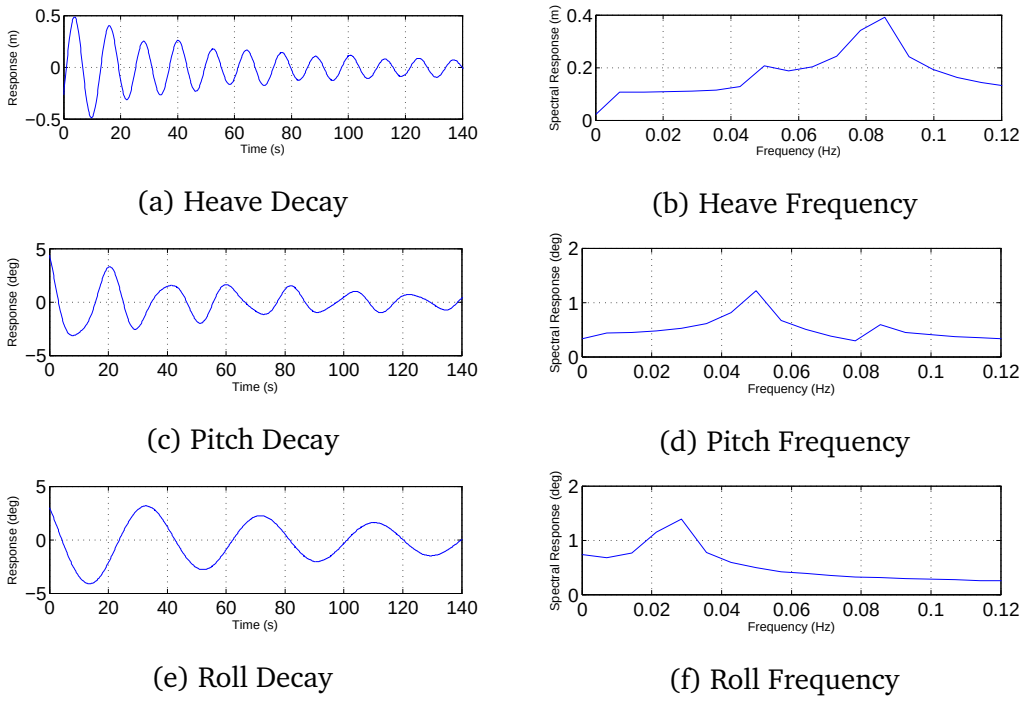

(a) Heave Decay

(b) Heave Frequency

(c) Pitch Decay

(d) Pitch Frequency

(e) Roll Decay

(f) Roll Frequency

Figure 5.12: Sample Decay Tests for the GDC

In Table 5.1 the natural periods without a heaveplate placed the model's natural frequencies outside the frequencies range, but when the heaveplate was added the natural frequencies were inside the range tested, however as this increased damping the RAO seems unaffected.

Comparing the models with the heaveplate raised and lowered in Tables 5.2 & 5.3 it can be seen that having the heaveplate interact with the water increased the natural periods of heave and pitch, and little effect on roll. This is due to the heaveplate reducing the acceleration experienced by the vessel, in addition to variations of mass, inertia, waterplane area, and metacentric height as a result of adding the heaveplate, this is discussed further in § 2.11.4. Without a heaveplate attached the standard catamaran hulls had shorter heavily damped natural periods, this was ascertained by bobbing the model in water, moving the model at its natural period.

Table 5.1: Natural Periods for the Tubular Multihull from Decay Tests

Model	Heave (s)	Pitch (s)	Roll (s)
1000	2.1	2.2	3.6
2000	7.9	3.7	6.4
3000	2.2	2.1	3.9
4000	7.2	6.7	5.9
5000	2.2	2.5	4.5
6000	7.2	6.7	6.6
7000	2.1	3.2	3.3
8000	6.4	6.0	4.9
90000	2.4	2.4	3.4
10000	7.0	6.6	6.1

Table 5.2: Natural Periods for the Curved Hulled Catamaran Models from Decay Tests

Model	Heave (s)	Pitch (s)	Roll (s)
178.5m^2 Heaveplate at 12m draught	8.5	10.9	9.8
178.5m^2 Heaveplate at 9m draught	9.4	8.9	9.8
178.5m^2 Heaveplate at 6m draught	9.1	7.6	7.9
154m^2 Heaveplate at 12m draught	8.5	10.9	9.8
115.5m^2 Heaveplate at 12m draught	9.1	10.8	10.4
28m^2 Dual Heaveplates at 0° inclination	4.7	7.2	6.8
28m^2 Dual Heaveplates at 22.5° inclination	4.5	7.8	7.0
28m^2 Dual Heaveplates at 45° inclination	4.4	7.5	7.0
56m^2 Dual Heaveplates at 0° inclination	6.8	11.18	11.0
56m^2 Dual Heaveplates at 22.5° inclination	6.4	11.4	8.9
56m^2 Dual Heaveplates at 45° inclination	5.5	9.4	8.4
Heaveplate Raised	3.1	8.5	3.9

Table 5.3: Natural Periods for Catamaran Model Properties (All designs 24m long at waterline)

Model	Heave (s)	Pitch (s)	Roll (s)
Standard Catamaran	3.0	2.9	3.5
Wide Hulled Catamaran With a heaveplate	7.0	8.1	8.1
Wide Hulled Catamaran With a heaveplate Raised	3.4	6.7	4.6
Narrow Hulled Catamaran	11.9	19.9	17.7
GDC	11.7	37.7	20.6

5.6 RAO at Zero Forward Speed

5.6.1 Overview

In this section, similar to the numerical analysis, RAO at zero forward speed is discussed. Zero forward speed RAO is representative of the ability of a WFSV to safely approach a wind turbine foundation with personnel on the deck, or when during a transfer the skipper must manoeuvre away from the monopile at short notice, for example in a man overboard incident. This section is broken down into the following subsections:

§ 5.6.2 provides the physical model RAO for a standard catamaran WFSV.
§ 5.6.3 discusses different tubular multihull designs
§ 5.6.4 presents the RAOs for catamarans with single heaveplates
§ 5.6.5 compares the effect of heaveplate area and depth
§ 5.6.6 examines the influence of using dual heaveplates
§ 5.6.7 discusses the RAOs of catamarans with a raised heaveplate

5.6.2 Standard Catamaran

Figure 5.13 shows the baseline RAO curves for the standard catamaran model described in § 3.2.2 and numerically modelled in § 4.3.2 for comparison.

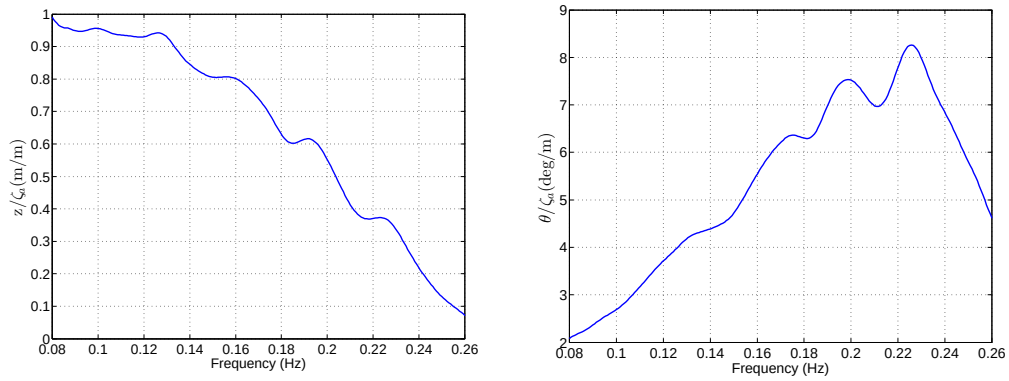

(a) Heave

(b) Pitch

Figure 5.13: Physical Modelling RAO Curves for a Standard Catamaran

5.6.3 Tubular Multihull Designs

Figures 5.14a & 5.14b show the heave and pitch RAO for different layouts of the tubular hull geometry. There is little benefit shown in changing the spacing of the tubes. Modest improvements are evident depending on wave period. For larger waves in heave T7000 performs best but in pitch T5000 performs best on average T9000 appears to be best but the difference in RAO between T1000 and T9000 is marginal at best, whereas the difference in build geometry and hence associated cost as well as the effect on the stability curve is large. Figure 5.14c & 5.14d show the effect of adding a heaveplate to these designs. The heaveplate was the entire length and breadth of the model and situated at a depth equal to the vertical spacing of the tubes of that model below the lowest tube. This produced a greater reduction in RAO and a greater variation between one model and another. Model T6000 with a largest spacing and the deepest heaveplate appears to perform best.

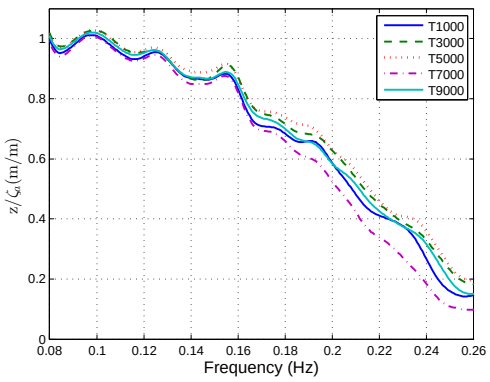

(a) Heave for Models without a Heaveplate

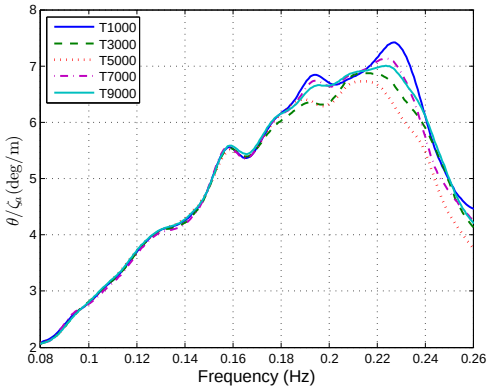

(b) Pitch for Models without a Heaveplate

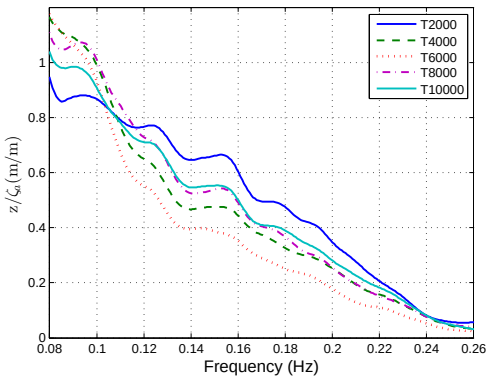

(c) Heave for Models with a Heaveplate

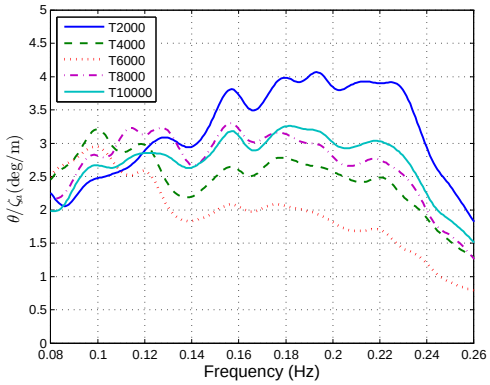

(d) Pitch for Models with a Heaveplate

Figure 5.14: Physical Model Testing RAO Curves of the Tubular Multihull

The forced oscillations due to various irregular waves produced different natural periods to the free decay tests as predicted in the literature [111]. Examining the tubular multihull models in particular, the natural periods differ between the decay tests carried out and the RAO plots, as is noticeable when comparing the results in Figure 5.14 and Table 5.1 the maximum difference in heave is 3.1s and 2.1s in pitch. The average difference is then 1.4s in heave and 0.6s in pitch. It is known that the excessive damping in heave makes it harder to estimate the heave damping period, particularly from still water decay tests. The roll decay test cannot be compared to an RAO as beam seas were not tested.

5.6.4 Catamarans with Single Heaveplates

Figure 5.15 shows the effect of adding a heaveplate to catamaran hulls, one with a 2m wide demihull and the other a 625mm wide demihull. The 2m catamaran performed poorly as is discernible from the heave and pitch RAOs. When the heaveplate was in the lowered position the 2m catamaran demihull had a very shallow draught. Having such a large area at the water surface taking wave load resulted in larger heave and pitch motions than the narrow hulled catamaran. In addition, the larger waves tended to slam on the underside of the model's demihull as it resisted heave motion, this is evident in the heave RAO curve. The narrow hulled catamaran with a heaveplate had a deeper draught and consequently, less volume close to the water surface, therefore much smaller RAOs, save for the natural frequency of heave at just below 0.08Hz or 12.5s.

Figure 5.16 shows the heave and pitch RAO for the GDC and the narrow hulled catamaran with a heaveplate. It is clear that the GDC's heave and pitch RAO is slightly larger at the natural period. The extra pitch is due to the vessels inclination to dip its stern following a long wave (this was due to the centre of gravity and buoyancy being significantly aft of midship) and the vessels greater waterplane area and volume near the water surface.

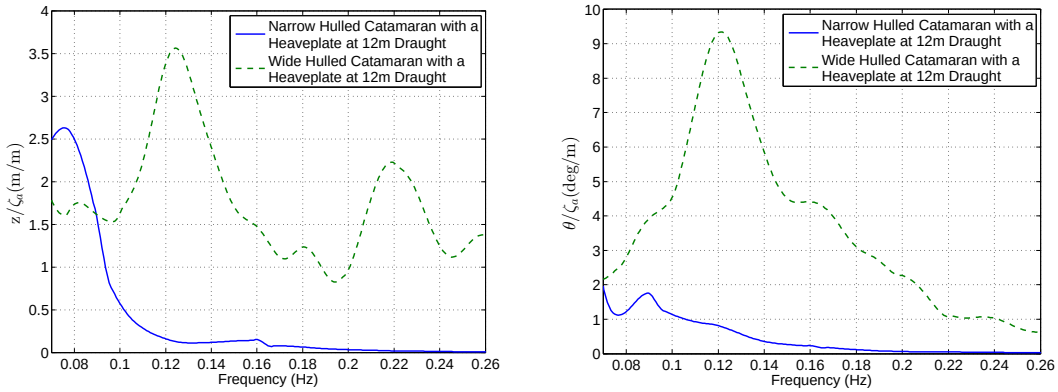

(a) Heave (b) Pitch

Figure 5.15: Physical Modelling RAO Curves for the Narrow and Wide Hulled Catamarans with a Heaveplate at a 12m Draught

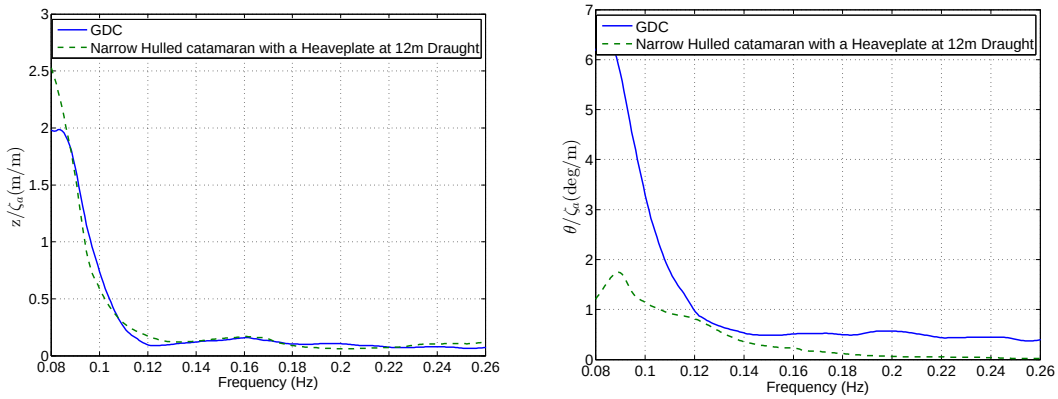

(a) Heave (b) Pitch

Figure 5.16: Physical Modelling RAO Curves Comparing the GDC with the Narrow Hulled Catamaran with a heaveplate at a 12m Draught

5.6.5 Heaveplate Depth and Area Comparison

Figure 5.17 compares the models with a heaveplate of 178m^2 at various draughts. The best performing model in these graphs is the one with the heaveplate set at a 12m draught, where raising the heaveplate increased the pitch and heave RAO, but they remain within an acceptable range. The model with a 178m^2 area was used in subsequent analysis, investigating depth variation in Figure 5.17 and the interaction with a monopile in Chapter 7 as it gave the best RAO curves for the three heaveplate areas chosen, 115.5m^2, 154m^2 and 178m^2 as can be viewed in Figure 5.18. It can be seen that there is a coupling between the heave and pitch motion for the 115.5m^2 heaveplate model.

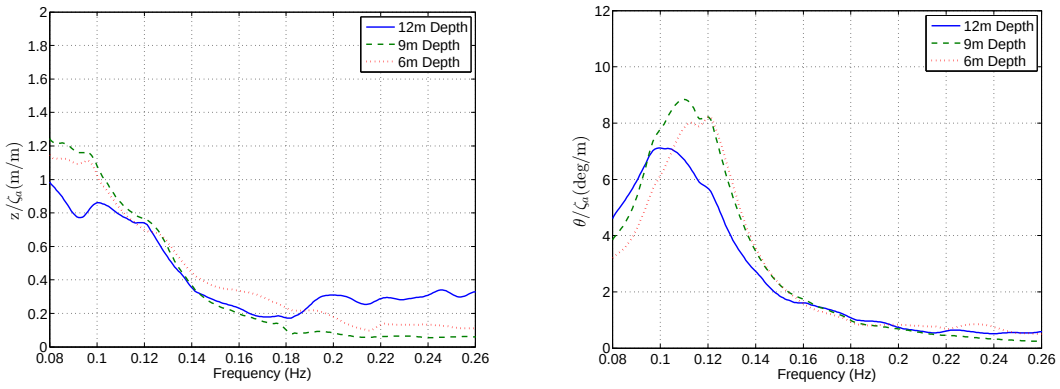

(a) Heave

(b) Pitch

Figure 5.17: Physical Modelling RAO Curves Comparing Heaveplate Depth Variation on a Heaveplate of 178.5m^2 Area

As the heaveplate area was reduced, the pitch increased. This was due to the heaveplate being at the centre hence reducing the lever arm that the heaveplate was using to damp pitch motion. In addition, heave increased and the motion became increasingly erratic with reductions in heaveplate area. In general, it was noted that there was a large effect from changes in area and less so from changes in depth.

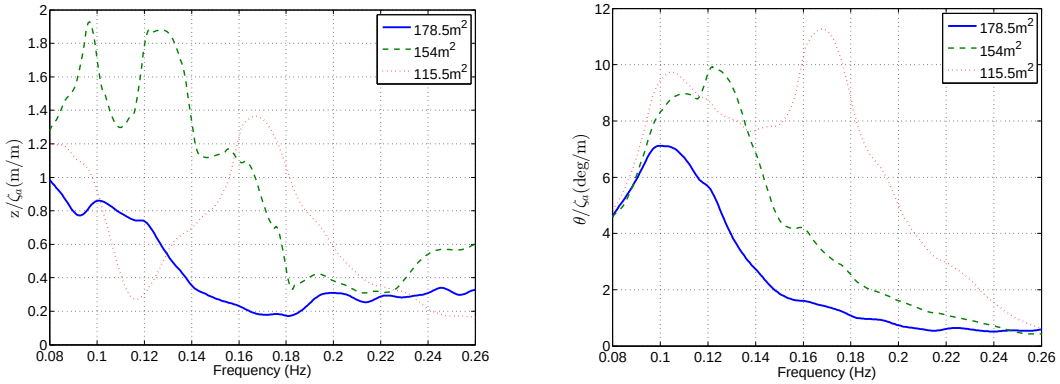

(a) Heave (b) Pitch

Figure 5.18: Physical Modelling RAO Curves Comparing Heaveplate Area Variation at a 12m Draught

5.6.6 Curved Hulled Catamaran with Dual Heaveplates

Examining the effect of separate bow and stern heaveplates of differing sizes and angles in Figures 5.19 & 5.20 it is apparent that the consequences of changing these parameters can be quite substantial. In heave any benefit from the larger heaveplates was negated by the change in natural period to an unfavourable frequency. For both heaveplate sizes the models with flat heaveplates performed better than the angled ones in heave.

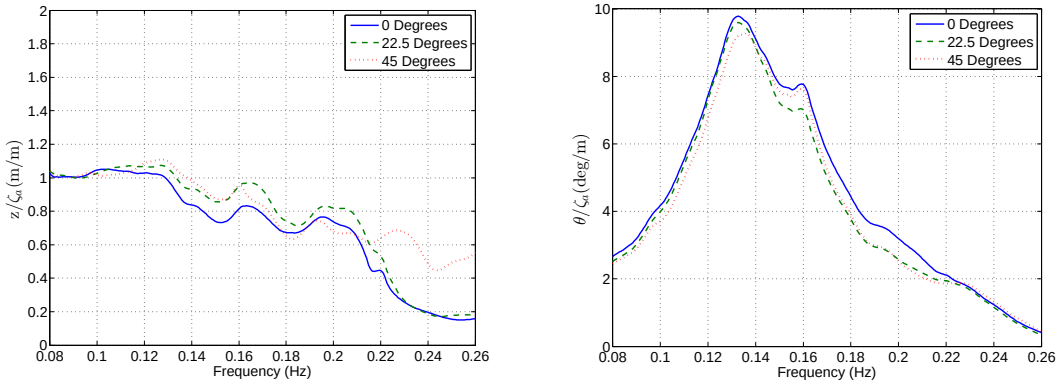

(a) Heave (b) Pitch

Figure 5.19: Physical Model Testing Comparing Dual Heaveplates with a Combined Area of 56m^2, by Angle of Inclination

In pitch the models with 56m^2 total heaveplate area perform the worst, with all angles of inclination producing very similar results. The models with 112m^2 total heaveplate area perform better on average with the angle of the heaveplate having a significant effect on the natural period. The model with a heaveplate set at 22.5° shows a substantial improvement over the others, implying that the angle of heaveplate can have a positive outcome on pitch damping.

Comparing the curved hulled catamaran with dual heaveplates totalling 112m^2 set horizontally in Figure 5.20 with the curved hulled catamaran with a singular 115.5m^2 heaveplate in Figure 5.18 it can be seen that the former performs much better in pitch, and heave. Thus it could be stated that if the area of the heaveplate is not sufficiently spread from the COG then the damping for pitch motion was found to be small and as the heave is damped the pitch response was found to be large. It can be inferred from the results presented that heaveplates should be sufficiently large and sufficiently spread from the COG in X and Z to produce optimal results.

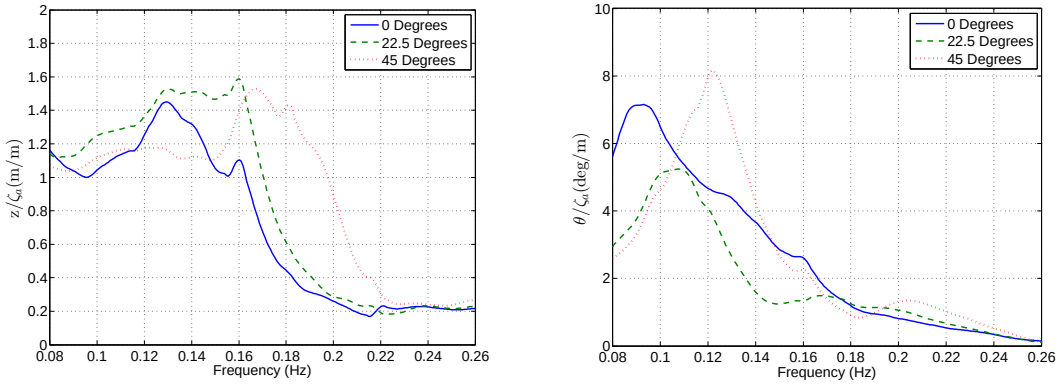

(a) Heave

(b) Pitch

Figure 5.20: Physical Model Testing Comparing Dual Heaveplates with a Combined Area of 112m^2, by Angle of Inclination

5.6.7 Catamarans with a Raised Heaveplate

Figure 5.21 shows the results for wide hulled catamaran with the heaveplate raised, as this was intended to be a transit condition. Figure 5.21 shows the heave and pitch RAO for two catamarans in transit mode to a wind farm; the 2m standard wide hulled catamaran with a heaveplate raised representing a generic WFSVs with a capability of using a heaveplate. It can be seen in Figure 5.21 that the curved hulled catamaran with the heaveplate in the raised position performs similarly to the catamaran for frequencies above 0.18Hz and better for frequencies below. In pitch the curved hulled shape reduces the RAO for frequencies below 0.22Hz and increase for frequencies above.

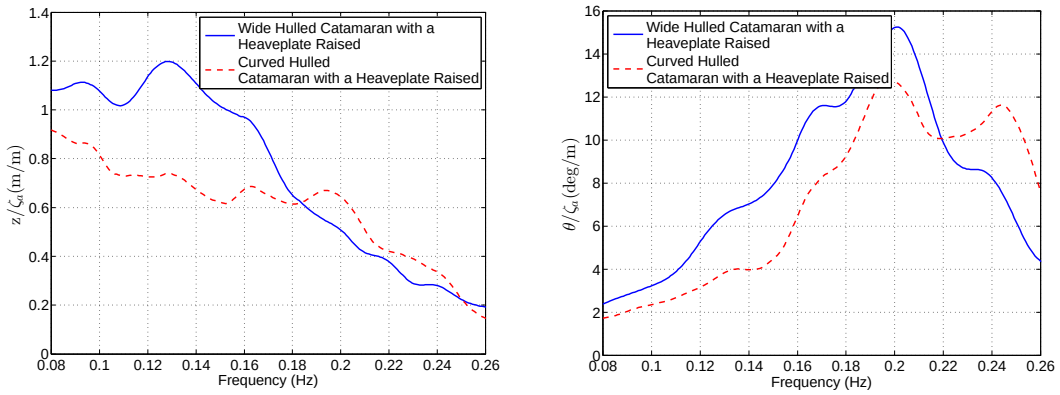

(a) Heave

(b) Pitch

Figure 5.21: Physical Modelling RAO Curves Comparing Catamarans with a Raised Heaveplate

5.7 MII, and RMS of Accelerations and Pitch Angle at Zero Forward Speed

5.7.1 Overview

In this section MII, RMS of vessel acceleration and pitch are discussed as similar to RAO in the previous section they are representative of the ability of a WFSV to safely approach a wind turbine foundation with personnel on the deck.

MII analysis was carried out on the wave simulations run for the RAO analysis, and the summary conclusions are considered in this section. The MII was carried out at the bow of the vessel using the accelerations derived from the Qualisys marker placed there. The results of the MII analysis show which models have the most suitable motions in general for personnel to stand freely towards the bow of the vessel while it is manoeuvring around the monopile in a wind farm.

The limit motions for working on ships were presented in the Section 2.10. The motions most related to having technicians in a cabin, moving around on the foredeck and carrying out transfers were outlined. MII is dependent on risk level, the risk level where a MII event was deemed possible was 0.1, and at 0.5 tips per minute for a probable occurrence [103]. The physical modelling tests were carried out for 21min 20s at full scale which equates to 2 MII events for conservative estimates and 10 MII events for less conservative estimates. 1.5, 3.0 and 5.0 tips per minute was classed as serious, severe and extreme respectively, which for the experimental study in question is 32, 64 and 106 total MII events.

RMS of vertical acceleration at the forward perpendicular vary depending on the type of ship in question; a fast small craft has a limit of 0.65g and fishing vessels have a limit of 0.35g see Table 2.3 [97]. RMS of heave acceleration is relevant, a fast small craft has a limit of 0.275g and fishing vessels have a limit of 0.2g [97]. WFSVs are generally fast small craft, though for a WFSV that is not fast the limits for fishing vessels might be more applicable. The limit of RMS of

Pitch during transit to a wind turbine has been suggested as 4° [88].

The limit motions for ships in transit are larger than that on approach to a monopile as there is no crew or technicians on the deck. For MII a limit of 0.1–0.5 tips per minute is acceptable [103]. RMS of vertical acceleration at the forward perpendicular is set at 0.15g the limit for heavy manual work [97]. The RMS vertical acceleration at the COG are set as 0.05g the limit for transit passengers [97], applying this limit to the RMS of acceleration in the passenger saloon has been found to predict whether or not a transfer will take place [88]. RMS of pitch are limited at 4° [88]. These vessel motion limits applied to the zero forward speed motion of a WFSV in this research are summarised in Table 5.4.

Table 5.4: Vessel Motion Limits

MII of Pitch and Heave Accelerations at the Forward Perpendicular	RMS of Vertical Acceleration at the Forward Perpendicular	RMS of Vertical Acceleration at the COG	RMS of Pitch Angle at the COG
2–10 [No. of events]	0.15g [1.47m s^{-2}]	0.05g [0.49m s^{-2}]	4 [°]

MII, RMS of vessel acceleration and pitch is discussed in the succeeding sub-sections characterised as follows:

§ 5.7.2 presents the standard catamaran used as a control model

§ 5.7.3 outlines catamarans with single heaveplates

§ 5.7.4 discusses the curved hulled catamaran with dual heaveplates

§ 5.7.5 examines catamarans with a raised heaveplate

5.7.2 Standard Catamaran

Examining Figure 5.22 the MII for the standard catamaran is 0 for all cases, this was expected as the catamaran at zero forward speed is wave following. The RMS of vertical acceleration at the forward perpendicular is relatively high for steep waves reducing as the wave length increases. In all cases the acceleration at the forward perpendicular is below the threshold of $1.47\,\mathrm{m\,s^{-2}}$. The RMS of vertical acceleration at the COG is largest for waves at a 3m Hs but does not exceed the limit of $0.49\,\mathrm{m\,s^{-2}}$. The RMS of pitch angle does not exceed 4°.

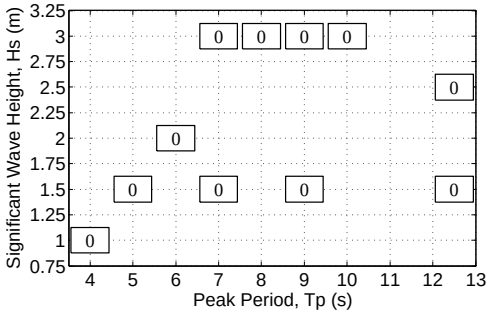

(a) MII of Pitch and Heave Accelerations at the Forward Perpendicular

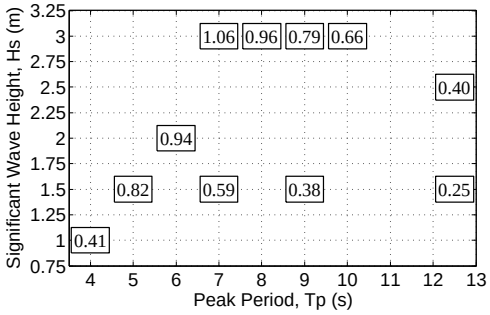

(b) RMS of Vertical Acceleration at the Forward Perpendicular

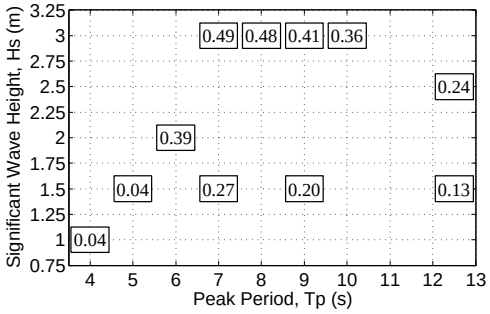

(c) RMS of Vertical Acceleration at the COG

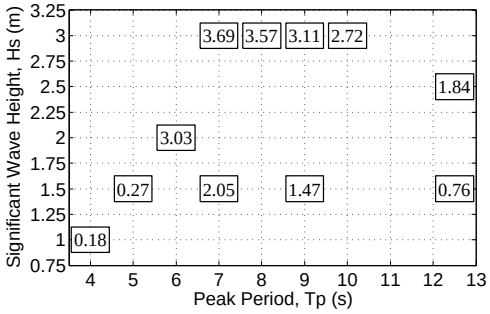

(d) RMS of Pitch Angle at the COG

Figure 5.22: MII and RMS Analysis of a Standard Catamaran

5.7.3 Catamarans with Single Heaveplates

In this subsection all the catamarans with a single lowered heaveplate are discussed so as to avoid repetition. In Figure 5.23 MII is shown for the wide hulled catamaran with a heaveplate, where the MII is 0 for all cases tested. The RMS of vertical acceleration at the forward perpendicular reaches 0.76m s^{-2} for a 3m Hs sea state, in addition the RMS of vertical acceleration at the COG exceeds the recommended limits for periods above 7s matching the large RAO for these periods shown in Figure 5.15. The pitch angle is below the limit of 4° for all cases. Overall this model performed poorly only passing all four criteria for the sea state 1.5m Hs and 5s Tp.

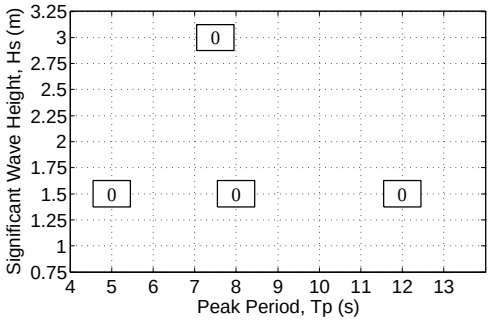

(a) MII of Pitch and Heave Accelerations at the Forward Perpendicular

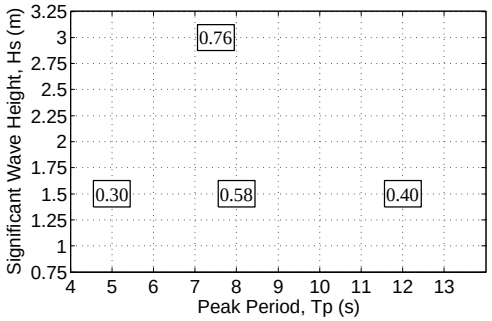

(b) RMS of Vertical Acceleration at the Forward Perpendicular

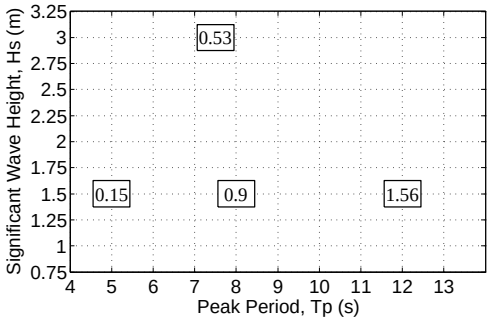

(c) RMS of Vertical Acceleration at the COG

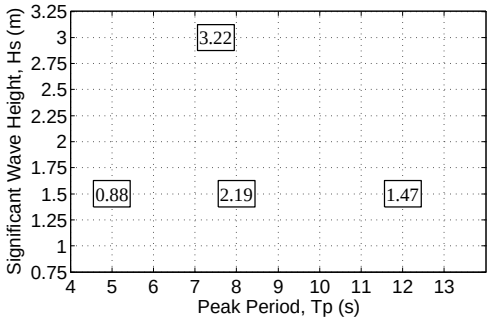

(d) RMS of Pitch Angle at the COG

Figure 5.23: MII and RMS Analysis of a Wide Hulled Catamaran with a Heaveplate at 12m Draught

MII, RMS of accelerations and pitch angle are shown for the narrow hulled catamaran with a heaveplate in Figure 5.24. The MII is 0 for all cases tested indicating a very steady working surface. The RMS of vertical acceleration at the forward perpendicular and COG is smaller than recommended limits for all cases. The RMS of pitch angle is less than a degree for each sea state tested, less than the limit of 4° recommended, hence although only four different sea states were described the design appears to perform very well.

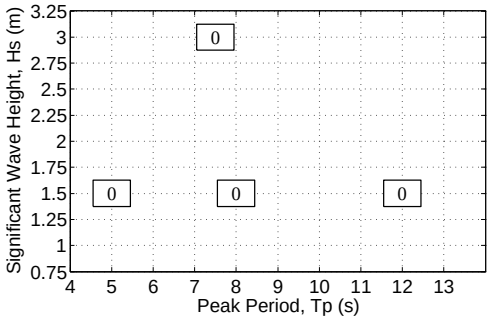

(a) MII of Pitch and Heave Accelerations at the Forward Perpendicular

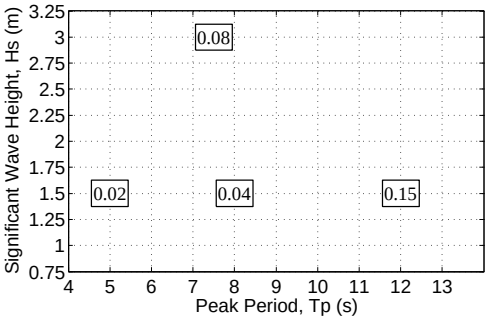

(b) RMS of Vertical Acceleration at the Forward Perpendicular

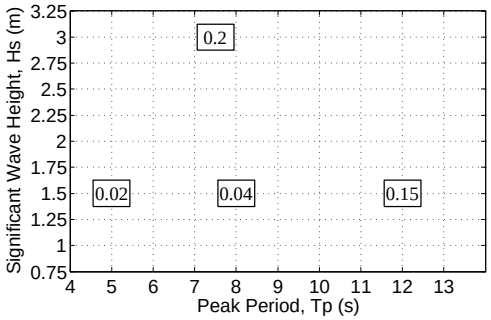

(c) RMS of Vertical Acceleration at the COG

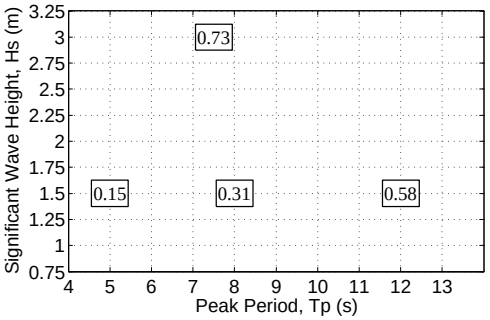

(d) RMS of Pitch Angle at the COG

Figure 5.24: MII and RMS Analysis of the Narrow Hulled Catamaran with a Heaveplate at 12m Draught

In Figure 5.25 the MII for the curved hulled catamaran with a 115.5m^2 heaveplate at 12m draught fails for the following sea states a 2m Hs and a 6s Tp, and a 3m Hs with 7, 8, and 9s Tp. The RMS of vertical acceleration at the forward perpendicular fails for the same sea states. The RMS of vertical acceleration at the COG passes for all sea states except 2m Hs with a 6s Tp and a 3m Hs with a 7s Tp. The RMS of pitch angle is large, failing for all cases above a 1.5m Hs. Overall this demonstrates that the sea states that curved hulled catamaran with a 115.5m^2 heaveplate at 12m draught does not improve on the standard wide hulled catamaran.

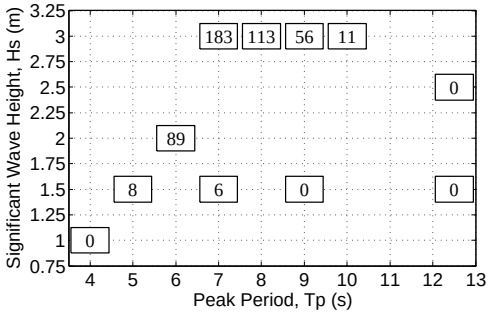

(a) MII of Pitch and Heave Accelerations at the Forward Perpendicular

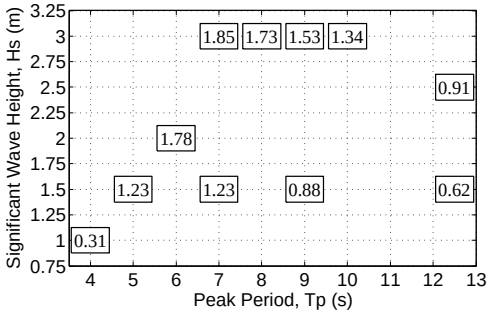

(b) RMS of Vertical Acceleration at the Forward Perpendicular

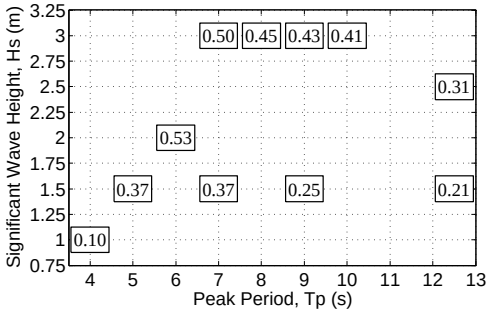

(c) RMS of Vertical Acceleration at the COG

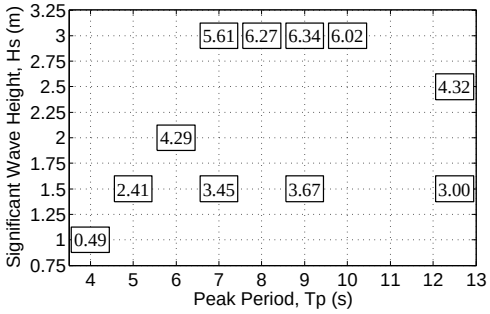

(d) RMS of Pitch Angle at the COG

Figure 5.25: MII and RMS Analysis of the Curved Hulled Catamaran with a 115.5m^2 Heaveplate at 12m Draught

Figure 5.26 shows the MII and RMS values for curved hulled catamaran with a 154m^2 heaveplate at 12m draught a similar vessel to the last one discussed but with a larger heaveplate. The MII for passes for most waves tested but fails for a 3m Hs with a 7s and 8s Tp. The RMS of vertical acceleration at the forward perpendicular passes for all cases. The RMS of vertical acceleration at the COG fails again for all sea states except for 1.5m Hs with a 5s Tp and a 1m Hs with a 4s Tp. The RMS of pitch angle is less than 4° for all cases where the Hs is at or below 2.0m. Overall this demonstrates that the curved hulled catamaran with a 154m^2 heaveplate at 12m draught does not improve on the standard wide hulled catamaran.

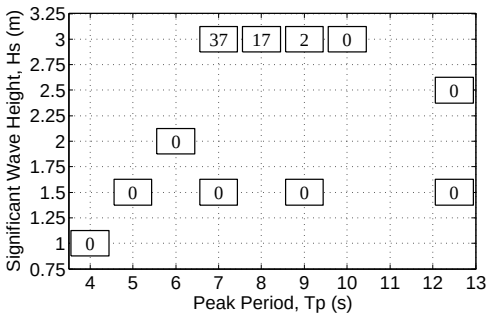

(a) MII of Pitch and Heave Accelerations at the Forward Perpendicular

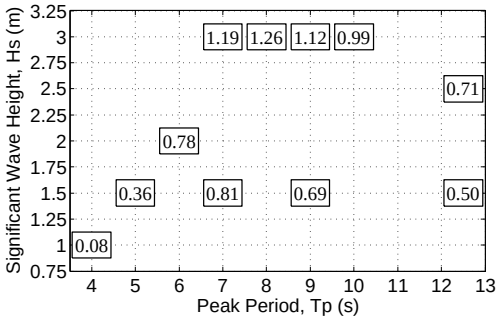

(b) RMS of Vertical Acceleration at the Forward Perpendicular

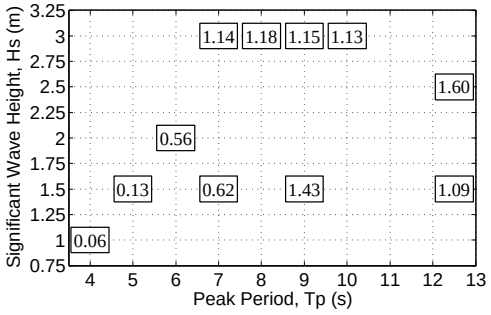

(c) RMS of Vertical Acceleration at the COG

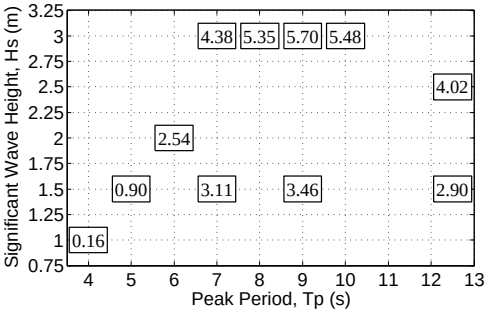

(d) RMS of Pitch Angle at the COG

Figure 5.26: MII and RMS Analysis of the Curved Hulled Catamaran with a 154m^2 Heaveplate at 12m Draught

Figure 5.27 illustrates the MII and RMS values for a similar vessel to the previous two, but with a larger heaveplate 178.5m^2 at the same draught. The MII was 0 for all cases tested. The RMS of vertical acceleration at the forward perpendicular and the RMS of vertical acceleration at the COG passes for all cases. The RMS of pitch angle is less than 4° for all cases except for the sea states 3m Hs with a 9s and 10s Tp.

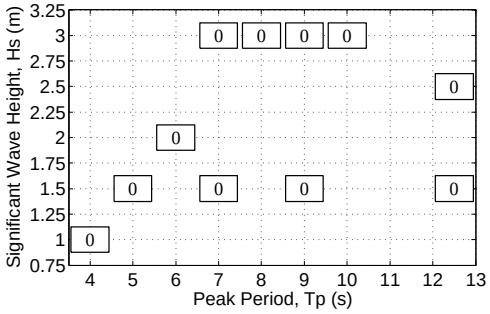

(a) MII of Pitch and Heave Accelerations at the Forward Perpendicular

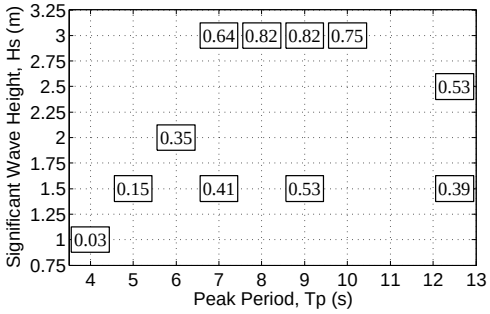

(b) RMS of Vertical Acceleration at the Forward Perpendicular

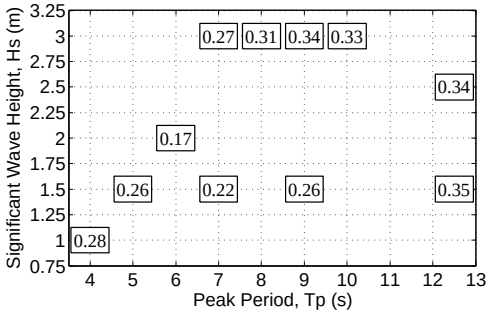

(c) RMS of Vertical Acceleration at the COG

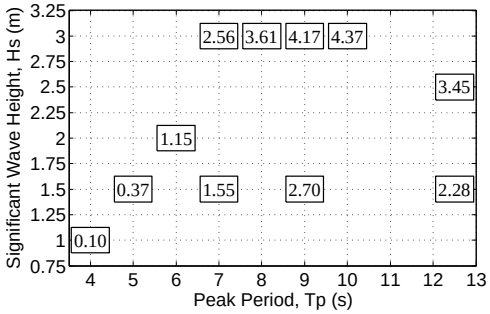

(d) RMS of Pitch Angle at the COG

Figure 5.27: MII and RMS Analysis of the Curved Hulled Catamaran with a 178.5m^2 Heaveplate at 12m Draught

The MII for the curved hulled catamaran with a 178.5m^2 at a 9m draught passes for all waves tested as is evident in Figure 5.28. The RMS of vertical acceleration at the forward perpendicular and the RMS of vertical acceleration at the COG passes for all sea states. The RMS of pitch angle is less than 4° for all cases except for 3m Hs sea states with an 8, 9, and 10s Tp. Compared to the previous model the curved hulled catamaran with a 178.5m^2 heaveplate at a 9m draught performs quite similarly.

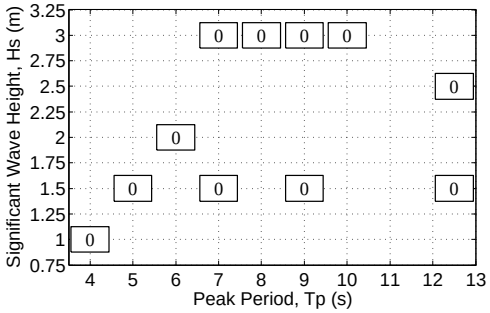

(a) MII of Pitch and Heave Accelerations at the Forward Perpendicular

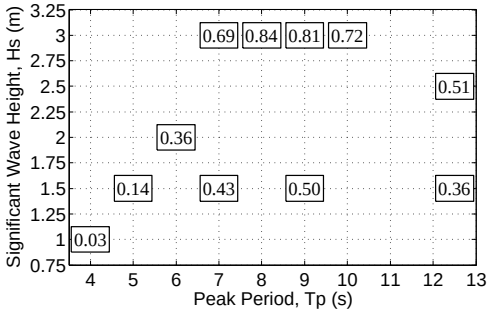

(b) RMS of Vertical Acceleration at the Forward Perpendicular

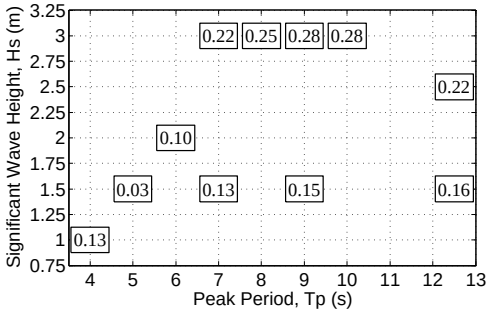

(c) RMS of Vertical Acceleration at the COG

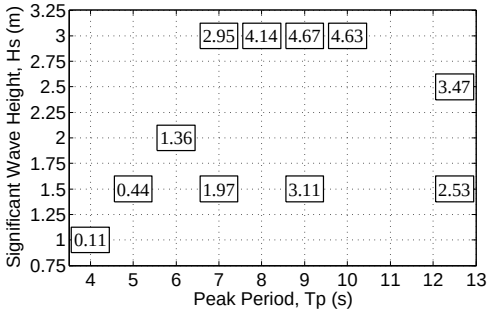

(d) RMS of Pitch Angle at the COG

Figure 5.28: MII and RMS Analysis of the Curved Hulled Catamaran with a 178.5m^2 Heaveplate at 9m Draught

The relevant MII and RMS values for the curved hulled catamaran with a 178.5m^2 heaveplate at a 6m draught are illustrated in Figure 5.29. MII passes for all waves tested. The RMS of vertical acceleration at the forward perpendicular passes for all waves as does the RMS of vertical acceleration at the COG. The RMS of pitch angle is less than 4° for all cases except for 3m Hs sea states with a 9, and 10s Tp, similar to the pitch RAO in Figure 5.17. The models with a 6 and 9m draught faired relatively well in these metrics, showing that the difference in heaveplate depth between 6, 9, and 12m may not be as significant as postulated.

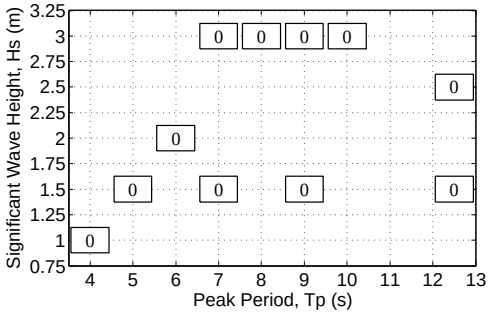

(a) MII of Pitch and Heave Accelerations at the Forward Perpendicular

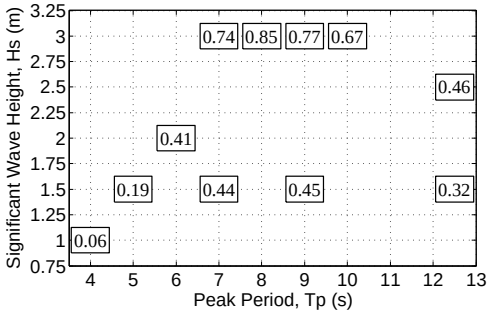

(b) RMS of Vertical Acceleration at the Forward Perpendicular

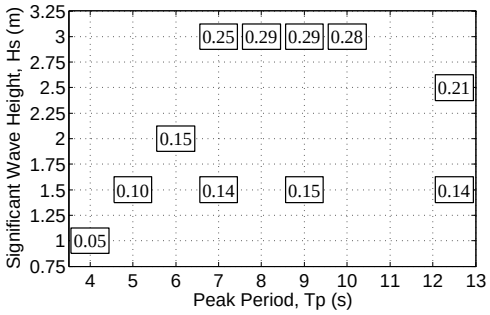

(c) RMS of Vertical Acceleration at the COG

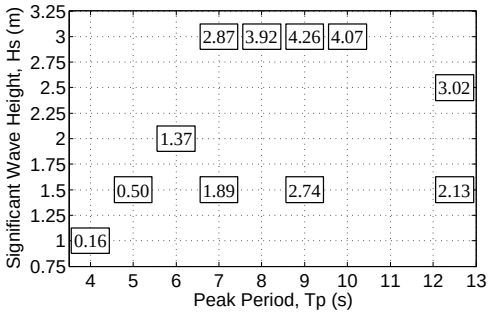

(d) RMS of Pitch Angle at the COG

Figure 5.29: MII and RMS Analysis of the Curved Hulled Catamaran with a 178.5m^2 Heaveplate at 6m Draught

Figure 5.30 Illustrates the MII and RMS values for the GDC. The GDC passes MII requirements up to a 3.75m Hs. The RMS of vertical acceleration at the forward perpendicular passes for all sea states, with a maximum of $0.15\mathrm{m\,s^{-2}}$. The RMS of vertical acceleration at the COG again passes for all sea states, with a maximum of $0.22\mathrm{m\,s^{-2}}$. The RMS of pitch angle is less than 4° for all cases. The GDC performs exceptionally well, passing the proposed limits for all sea states tested.

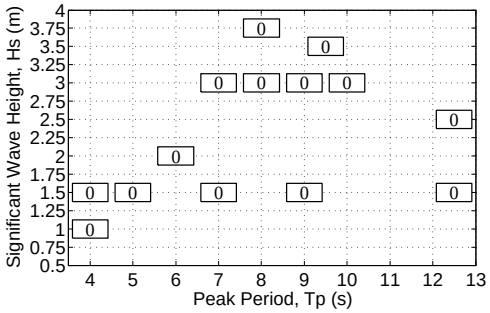

(a) MII of Pitch and Heave Accelerations at the Forward Perpendicular

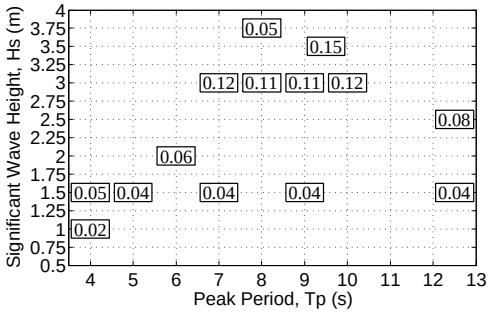

(b) RMS of Vertical Acceleration at the Forward Perpendicular

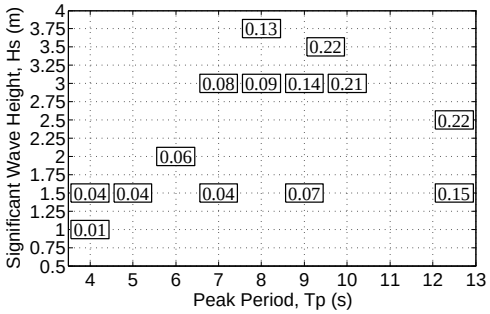

(c) RMS of Vertical Acceleration at the COG

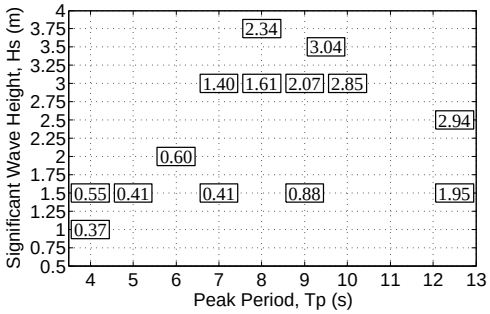

(d) RMS of Pitch Angle at the COG

Figure 5.30: MII and RMS of the GDC

5.7.4 Curved Hulled Catamaran with Dual Heaveplates

As was seen in § 5.6.6 effects of separate bow and stern heaveplates of differing sizes and angles can be quite substantial. Figure 5.31 illustrates the MII and RMS for curved hulled catamaran with a dual 28m^2 heaveplate set horizontally. The MII for this model passes for all sea states tested except a 3m Hs with a 7s Tp, where it fails outright. For the sea states of 3m Hs at 8 and 9s Tp the MII is between 2–10 MII events. The RMS of vertical acceleration at the forward perpendicular passes for all waves, but only just for the 3m Hs with a 7s Tp. The RMS of vertical acceleration at the COG passes for most sea states, failing for 3m Hs at 7 and 8s Tp. The RMS of pitch angle is above 4° for all sea states tested above 2.5m Hs.

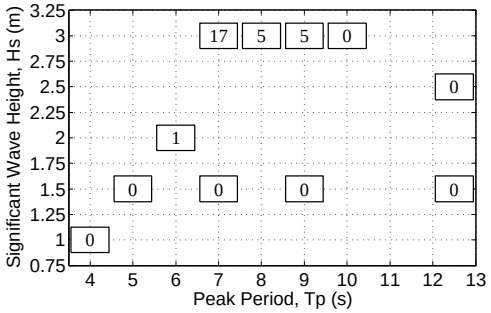

(a) MII of Pitch and Heave Accelerations at the Forward Perpendicular

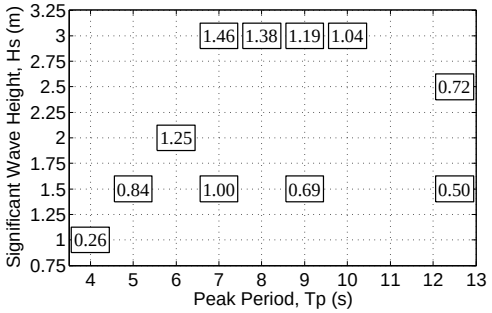

(b) RMS of Vertical Acceleration at the Forward Perpendicular

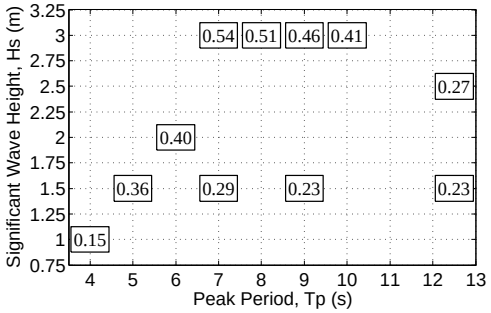

(c) RMS of Vertical Acceleration at the COG

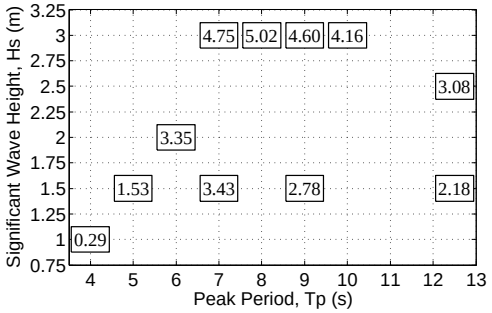

(d) RMS of Pitch Angle at the COG

Figure 5.31: MII and RMS Analysis of the Curved Hulled Catamaran with 0° Dual 28m^2 Heaveplates at 12m Draught

Figure 5.32 illustrates the MII and RMS for the curved hulled catamaran with dual 28m^2 heaveplates set at 22.5°. The MII for this model passes for all sea states tested except Hs 3m Tp 7s. The MII is between 2–10 for the sea states, 2m Hs 6s Tp and 3m Hs with 8 and 9s Tp. The RMS of vertical acceleration at the forward perpendicular passes for all sea states. The RMS of vertical acceleration at the COG performs poorly for the same sea states that the MII performs poorly on, failing for 3m Hs with a 7, 8 and 9s Tp and narrowly passing for a 2m Hs with a 6s Tp. The RMS of pitch angle is greater than 4° for all the 3m sea states.

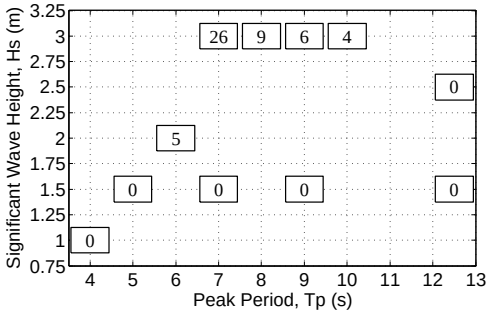

(a) MII of Pitch and Heave Accelerations at the Forward Perpendicular

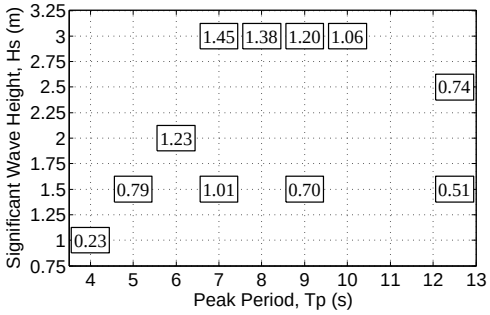

(b) RMS of Vertical Acceleration at the Forward Perpendicular

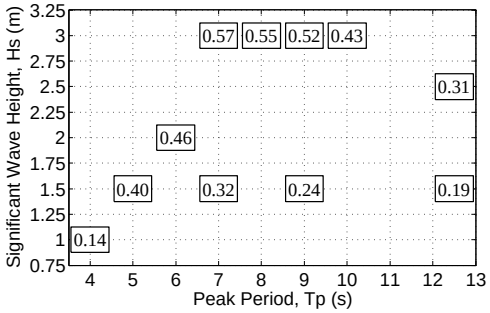

(c) RMS of Vertical Acceleration at the COG

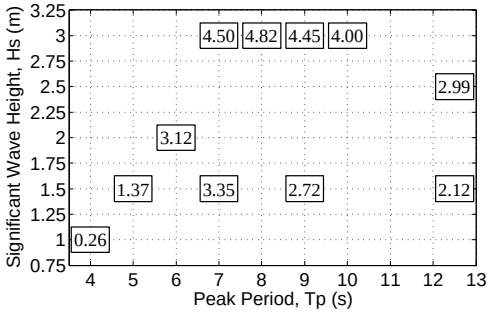

(d) RMS of Pitch Angle at the COG

Figure 5.32: MII and RMS Analysis of the Curved Hulled Catamaran with 22.5° Dual 28m^2 Heaveplates at 12m Draught

Figure 5.33 illustrates the MII and RMS for the curved hulled catamaran with dual 28m^2 heaveplates set at 45°. Similar to the previous model with the heaveplates set at 22.5°. The MII for this model passes for all sea states tested except for a 3m Hs at a 7, and 8s Tp. It is above the conservative limit of 2 for 1.5m Hs at 7s Tp and 2m Hs at 6s Tp and 3m Hs at 9, and 10s Tp. The RMS of vertical acceleration at the forward perpendicular passes for all sea states being right on the limit of 1.47m s^{-2}. The RMS of vertical acceleration at the COG fails all the 3m Hs sea states, and for the 2m Hs at a 6s Tp. The RMS of pitch angle is above 4° for all 3m Hs sea states except for the 3m Hs at a 10s Tp sea state. There is very little difference between the three models with dual 28m^2 heaveplates at different angles, each slightly increasing on one metric over the other.

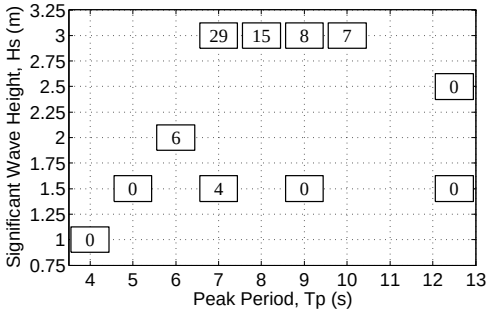

(a) MII of Pitch and Heave Accelerations at the Forward Perpendicular

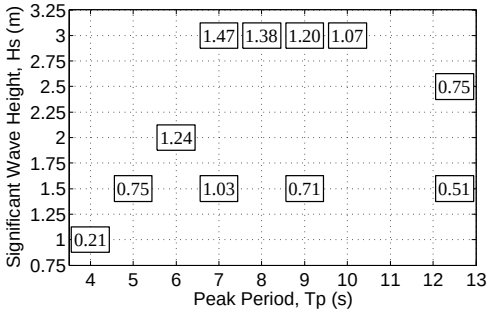

(b) RMS of Vertical Acceleration at the Forward Perpendicular

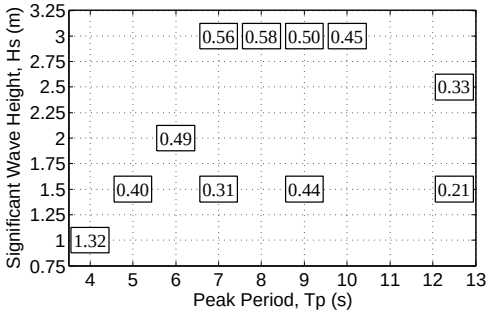

(c) RMS of Vertical Acceleration at the COG

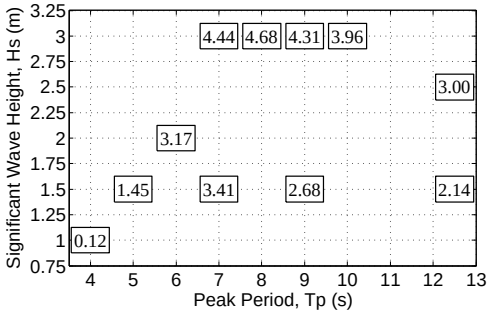

(d) RMS of Pitch Angle at the COG

Figure 5.33: MII and RMS Analysis of the Curved Hulled Catamaran with 45° Dual 28m^2 Heaveplates at 12m Draught

In Figure 5.34 it can be seen that the MII of the curved hulled catamaran with dual 56m^2 heaveplates set horizontally is 0 for all sea states tested. The RMS of vertical acceleration at the forward perpendicular passes for all sea states. The RMS of vertical acceleration at the COG passes for most sea states, failing for a 3.0m Hs with a 7, and 8s Tp. The RMS of pitch angle is above 4° for the for the 3m Hs at a 10s Tp sea state.

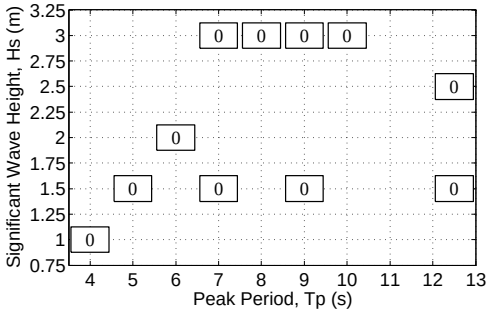

(a) MII of Pitch and Heave Accelerations at the Forward Perpendicular

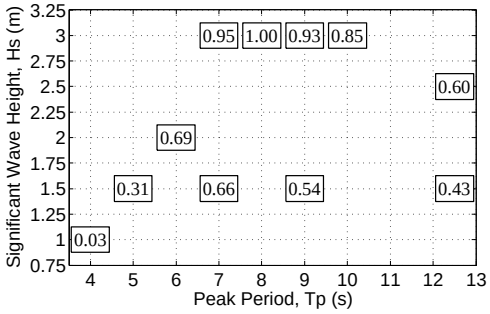

(b) RMS of Vertical Acceleration at the Forward Perpendicular

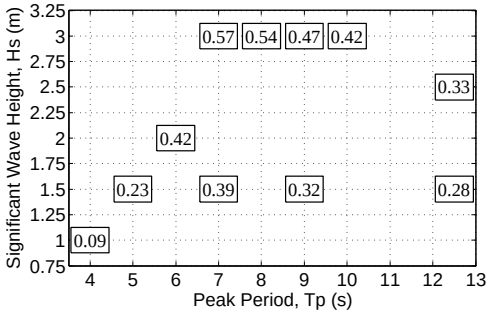

(c) RMS of Vertical Acceleration at the COG

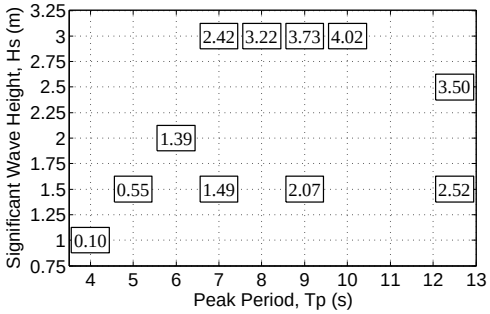

(d) RMS of Pitch Angle at the COG

Figure 5.34: MII and RMS Analysis of the Curved Hulled Catamaran with 0° Dual 56m^2 Heaveplates at 12m Draught

In Figure 5.35 it can observed that the MII for the curved hulled catamaran with dual 56m^2 heaveplates set at 22.5° passes for all sea states tested except for a 3m Hs at 7s Tp. The RMS of vertical acceleration at the forward perpendicular passes for all sea states. The RMS of vertical acceleration at the COG passes for 1.0m Hs at a 4s Tp and 1.5m Hs at 5, 7, and 9s Tp and for the 2.5m Hs 12.5s Tp. The RMS of pitch angle is less than 4° for all sea states.

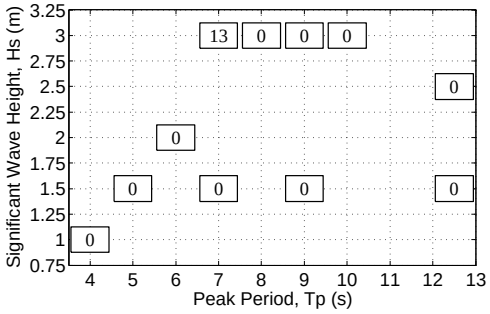

(a) MII of Pitch and Heave Accelerations at the Forward Perpendicular

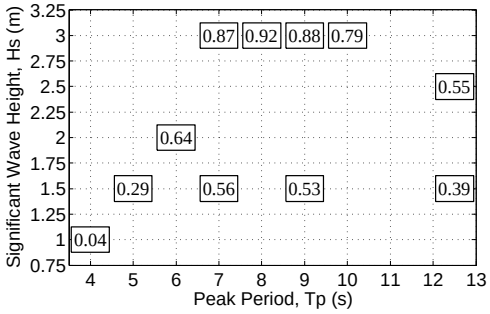

(b) RMS of Vertical Acceleration at the Forward Perpendicular

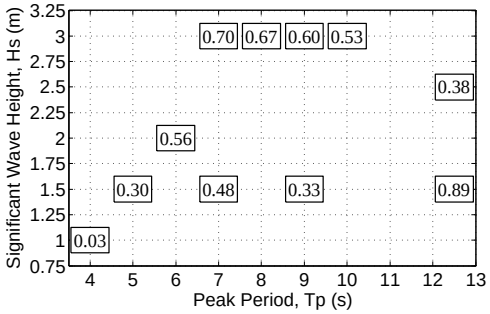

(c) RMS of Vertical Acceleration at the COG

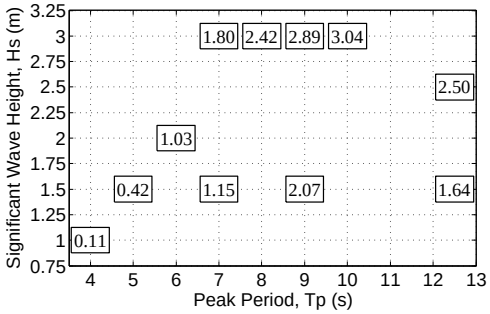

(d) RMS of Pitch Angle at the COG

Figure 5.35: MII and RMS Analysis of the Curved Hulled Catamaran with 22.5° Dual 56m^2 Heaveplates at 12m Draught

In Figure 5.36 it is evident that the MII for the curved hulled catamaran with dual 56m^2 heaveplates set at 45° passes for all sea states tested except for a 3m Hs with a 7s Tp and is above the conservative limit of 2 for 3m Hs at 8s Tp. The RMS of vertical acceleration at the forward perpendicular is below the limit in all cases. The RMS of vertical acceleration at the COG fails for all the 3m Hs sea states tested and the 6s Tp sea states at a 2m Hs. The RMS of pitch angle is less than 4° for all sea states.

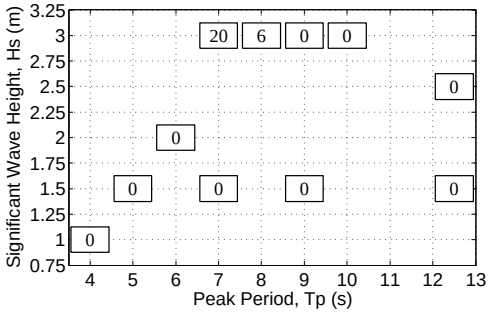

(a) MII of Pitch and Heave Accelerations at the Forward Perpendicular

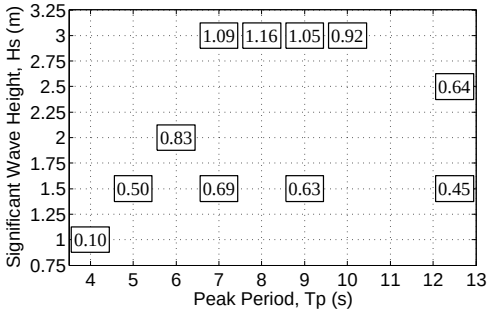

(b) RMS of Vertical Acceleration at the Forward Perpendicular

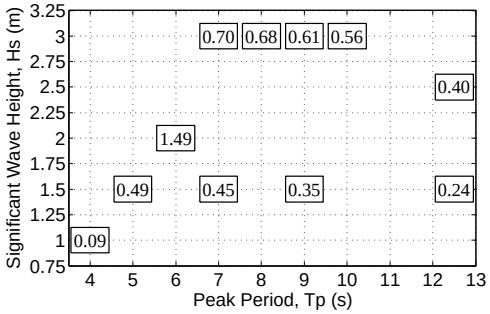

(c) RMS of Vertical Acceleration at the COG

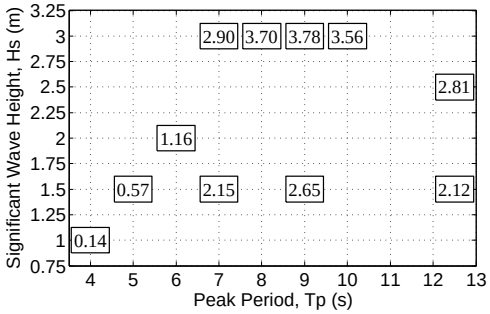

(d) RMS of Pitch Angle at the COG

Figure 5.36: MII and RMS Analysis of the Curved Hulled Catamaran with 45° Dual 56m^2 Heaveplates at 12m Draught

5.7.5 Catamarans with a Raised Heaveplate

Figure 5.37 shows the results for wide hulled catamaran with the heaveplate raised, as this was intended to be a transit condition. The MII was 0 for a 8 and 12s Tp at a 1.5m Hs, it then moved into the range of 2–10 for a 7.5s Tp and 3m Hs and failed for the short waves in the 5s Tp, 1.5m Hs sea state. The RMS of vertical acceleration at the forward perpendicular fails for the shorter waves similar to the MII results and passed for 8s and 12s Tp sea states, matching the pitch RAO. The RMS of vertical acceleration at the COG exceeds the recommended limits for a 3m Hs sea state and passes for all other cases, however as this is not a scenario where the WFSV is considering docking at the monopile higher limits apply [36] which are passed. The RMS of pitch angle at the COG fails for a 1.5m Hs and 5s Tp and a 3m Hs and 7.5s Tp, again following the RAO.

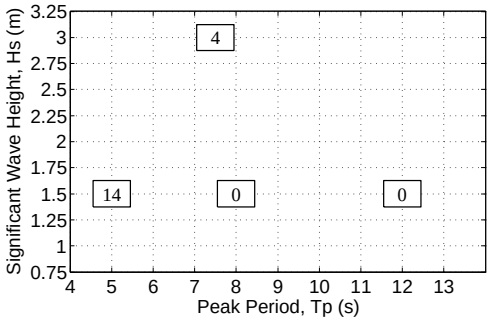

(a) MII of Pitch and Heave Accelerations at the Forward Perpendicular

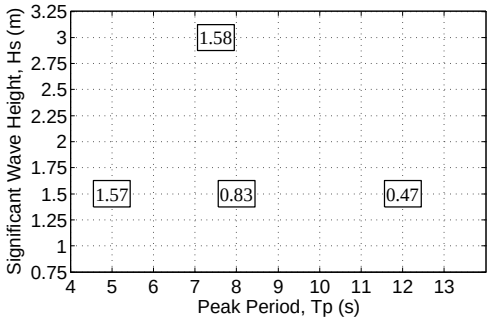

(b) RMS of Vertical Acceleration at the Forward Perpendicular

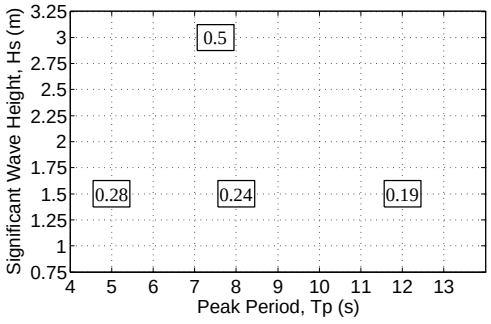

(c) RMS of Vertical Acceleration at the COG

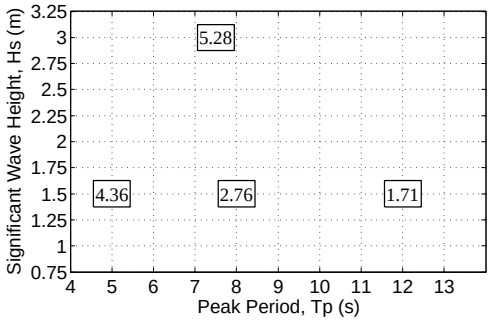

(d) RMS of Pitch Angle at the COG

Figure 5.37: MII and RMS Analysis of the Standard Wide Hulled Catamaran with a Raised Heaveplate

By altering the mass properties of the design to accommodate a heaveplate raised out of the water thus changing the ships draught and natural periods Figure 5.38 shows the results for the curved hulled catamaran with a heaveplate raised. The model is set up to be in transit mode as the heaveplate is raised. The MII is 0 for all cases tested. The RMS of vertical acceleration at the forward perpendicular passes for all sea states except for the following steep waves 1.5m Hs and a 5s Tp, 2m Hs and 6s Tp, 3s Hs and 7s and 8s Tp. However, as this is not a scenario where the WFSV is considering docking with the monopile higher limits apply [36] which are passed. The RMS of vertical acceleration at the COG is below the recommended limits for all cases and the RMS of pitch angle at the COG fails for the 3m sea state with a 7s Tp and a 2m Hs sea state with a 6s Tp.

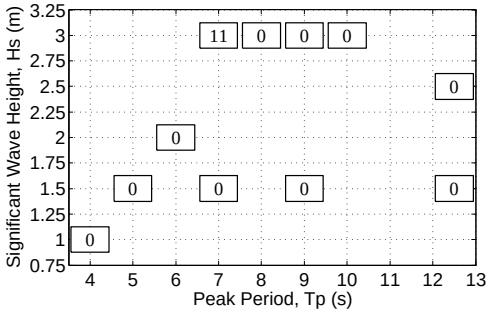

(a) MII of Pitch and Heave Accelerations at the Forward Perpendicular

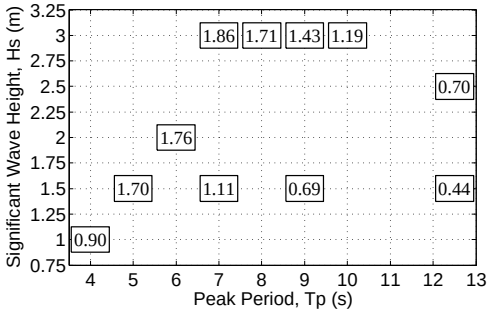

(b) RMS of Vertical Acceleration at the Forward Perpendicular

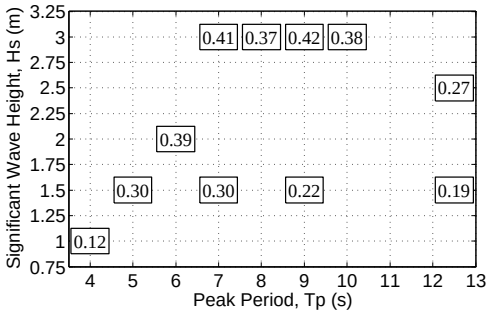

(c) RMS of Vertical Acceleration at the COG

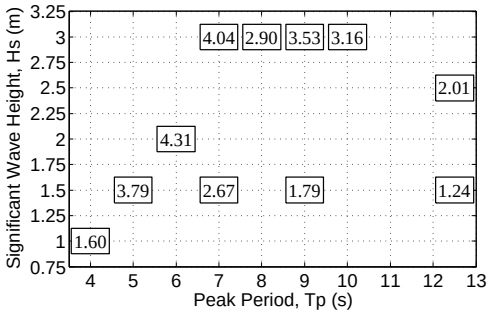

(d) RMS of Pitch Angle at the COG

Figure 5.38: MII and RMS Analysis of the Curved Hulled Catamaran with a Raised Heaveplate

5.8 Comparison with Published Data

The concept hull designs analysed in this chapter are different from those considered in other studies, hence a direct assessment cannot be made. To compare the RAO for ships of different lengths it is useful to nondimensionalise the variables being graphed. Frequency is nondimensionalised using length and the acceleration due to gravity, $\omega_0\sqrt{L/g}$. Pitch RAO is nondimensionalised with the wavenumber, $\xi_5/k\zeta_a$. Heave is already nondimensional as ξ_3/ζ_a is m/m.

Three designs were compared to the current craft; a monohull and two catamarans. The three craft were a 25.9m (85-foot) hardchine monohull [162], a 43.5m catamaran passenger ferry [163], and a V-1 scale model catamaran [164, 165]. The zero forward speed nondimensional RAOs for the 25.9m monohull, the 43.5m catamaran and a V-1 catamaran are presented in Figure 5.39 in comparison with the standard catamaran and the GDC presented in § 5.6 and the relevant RMS values for the 25.9m monohull are presented in Table 5.5.

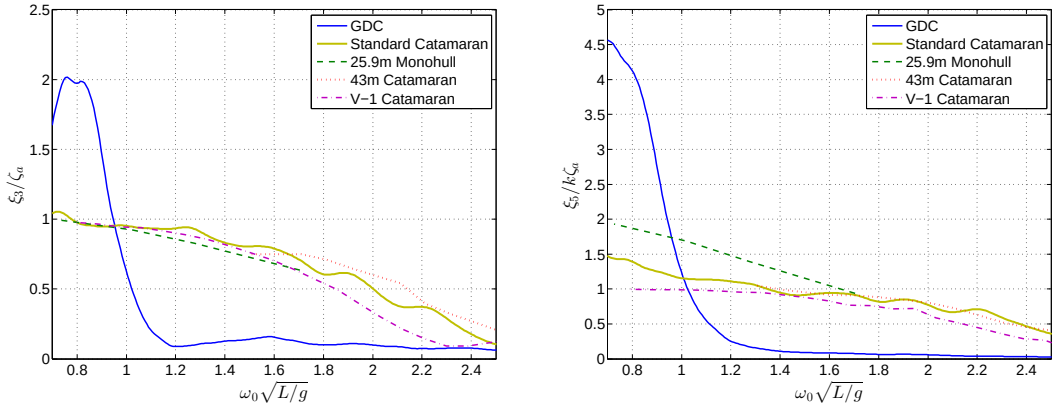

(a) Heave Comparison with Published Data (b) Pitch Comparison with Published Data

Figure 5.39: Heave and Pitch Nondimensional Amplitudes of the GDC and Standard Catamaran Compared with Published Data [162, 163, 164, 165]

When comparing the standard catamaran modelled it is clear that it has a similar response to the literature. The best WFSV concept of the physical model investigation (the GDC) when presented next the published data it is unmistakable that there is a large difference between them. The GDC has a large RAO in

long waves but a much smaller RAO in short waves. This is due to the vessels large natural periods and from its ability to damp motion for short waves, for the nondimensional frequency below 1.0, the benefits of heave and pitch damping begin to disappear.

Comparing the RMS responses of the 25.9m hardchine monohull with the standard catamaran model, tested in this work it can be seen when comparing Table 5.5 with those presented in Figure 5.22 earlier, that the Pitch RMS is comparable. The RMS of acceleration at the centre of gravity and the forward perpendicular are much greater for the catamaran, this could potentially be due to the simple hull design or possibly the frequency of interest, however, the heave RAO is very similar when comparing Figure 5.13 and the 25.9m hardchine monohull in Figure 5.39.

Table 5.5: RMS Responses of a 25.9m (85-foot) Hardchine Monohull [162]

Hs (m)	Tp (s)	Pitch RMS (deg)	RMS of Vert. Acc. at C.O.G. ($m\,s^{-2}$)	RMS of Vert. Acc. at F.P. ($m\,s^{-2}$)
1.8	6	2.6	0.010	0.036
1.8	8	2.2	0.009	0.020
1.8	10	1.7	0.008	0.020
1.8	14	1.0	0.005	0.007

5.9 Discussion

The zero forward speed physical model testing of WFSVs were analysed in this chapter, identifying a number of relationships between hull shapes. The experimental results were compared with previously published results, demonstrating the improvements in dynamic stability made.

It can be seen in Figure 5.39 and Table 5.5 that the standard catamaran is reasonably representative of those in the literature, though the RMS of acceleration at the centre of gravity and the forward perpendicular are much greater for the catamaran than the 25.9m monohull presented.

The tubular multihull designs showed that the spacing between tubes did not have a clear relationship with the RAO. In heave an increase in spacing resulted in an increased RAO, and in pitch the increased spacing improved the RAO. When the heaveplate was attached, increasing the spacing resulted in a reduction in heave and pitch RAO, however as the spacing increased so did the draught and the depth of the heaveplate. The difference between a standard catamaran and the tubular multihull was marginal. Ballasting some of the lower tubes could provide benefit but this quickly becomes a semisubmersible; an interesting study could be to model flexible tubes as per the bamboo ones on the replica ship built for the China Voyage.

Analysis of the catamaran models with heaveplates shows that a heaveplate does not function well on a conventional style catamaran, primarily due to the shallow draught coupled with large heave damping resulting in hull slamming. However, by narrowing the hulls and increasing the draught, the performance improves substantially. As a vessel intended for use solely at the wind farm it provided an excellent option for accessing the wind turbines above a 3m Hs. The curved hulled catamaran design was able to raise the heaveplate and hence travel from port to wind farm, though it did not perform quite as well as the standard catamaran in the transfer operation.

Analysing the different heaveplates attached to the curved hulled design it was found that the larger the heaveplate the greater the reduction in RAO, however the longitudinal span of the heaveplate was reduced and that appeared to make the model unsteady, and change the natural period. Increasing the depth of the heaveplate resulted in a general decrease in heave and pitch RAO. The models with a 6 and 9m draught faired relatively well in the MII, and RMS metrics, showing that the difference in heaveplate depth between 6, 9, and 12m may

not be as significant as postulated.

The study of dual heaveplates showed that the size of the heaveplate produced greater motion reduction than the angle of the heaveplate and that the change of angle altered the response and natural period of the larger heaveplates motion the most. The best angle of a heaveplate to reduce heave RAO was 0°, and the best angle to reduce pitch RAO was 22.5°. All the relationships between RAO and heaveplate type were hampered by changes in natural period of the model, making RAO comparisons difficult. Generally, the natural period in pitch and heave decreased as the inclination of the heaveplates increased.

Comparing the curved hulled catamaran with dual heaveplates totalling 112m^2 set horizontally in Figure 5.20a & 5.20b with the curved hulled catamaran with a singular 115.5m^2 heaveplate in Figure 5.18a & 5.18b it can be seen that the former performs much better in pitch, and heave. Thus, if the area of the heaveplate is not sufficiently spread from the COG then the damping for pitch motion was small, and as the heave is damped the pitch response was large. Hence, it can be inferred from the results presented that heaveplates should be sufficiently large and sufficiently spread from the COG in X and Z to produce optimal results.

The GDC showed how changing details of a hull can alter the natural period and the RAO. Though in essence the same design as the narrow hulled catamaran with a heaveplate, model alterations in buoyancy to allow for engines and access, and a change in mass layout, resulted in a substantially different RAO, particularly in pitch. The GDC performs exceptionally well, passing the proposed limits for all sea states tested. This is comparable to the narrow hulled catamaran with a heaveplate which performed similarly as expected, as the GDC's design was based on the narrow hulled catamaran. It can also be noted that the curved hulled catamaran model with a 178.5m^2 heaveplate at a 12m depth shown in Figure 5.27 does not perform as well as the GDC.

MII is a good indicator of acute instances of coupled accelerations that affect a persons safety and ability to carry out a task on board a vessel. As an example Lloyd's Register incudes MII as an assessment parameter for the "safety of em-

barked persons" [166]. In addition, MII is another tool that gives designers an indication of a vessels performance [167, 168, 169]. That is the subject of recent research for maritime applications [170]. In the presented work MII events correlate with severe motions as expected, thus it can be concluded that MII is of interest to the issue as presented to determine if it is safe to be on deck at the time of transfer.

The following vessel motion limits were applied to the zero forward speed motion of a WFSV in this research are summarised in Table 5.4. For MII a limit rate of 0.1–0.5 tips per minute is proposed to be acceptable for vessels considering docking with a monopile [103]. It should be noted however that the MII limit rate could potentially be restricted to 0.1 tips per minute, as in most cases where it is higher the RMS of pitch and/or other limits are exceeded. However, some vessels might find this restrictive if the other metrics of motion are below the proposed thresholds. Applying the following accelerational RMS limits of 0.15g at the forward perpendicular [97] was found to be useful in comparing the standard catamaran with other models in this study. The metrics of 0.05g at the COG and a pitch RMS of 4° as previously suggested for WFSVs [88] proved to also be useful in comparing the standard catamaran with other models in this study. When compared to the RAO curves it is observed that MII has moderate correlation with the RAOs. These limits are less than the limit motions for ships in transit as when the WFSV approaches the monopile, manoeuvrability is critical, and in the case where the WFSV must manoeuvre away from the monopile at short notice there may be crew or technicians on the foredeck.

The confidence limits of the physical model testing are subject to the accuracy and precision of numerous components including but not limited to; wave probes, repeatability of waves, repeatability of tests, motion sensing camera system. In § 5.3 sample wave calibration time traces showing the radiated wave effect, and wave spectra are outlined, in addition to sample wave spectra created. The waves were calibrated without the model in the tank prior to testing, the reflection coefficient was recorded for the waves generated, calculated with

the Funke and Mansard method [155]. The waves remained reasonably stable when the model was in the tank. The % error in wave height and periods was noted with an aim to keep the error within 5% of the intended value. When adding these together and comparing with the discussion in § 5.8 it can be seen that the level of error in this testing is within the usual tolerances for tank testing. A recent publication of validation of numerical tests shows that this is an area of ongoing interest [171]; best practice currently tends to assume that the physical model is correct barring scaling issues, however this is overly simplistic. The ITTC have written about the need to look at uncertainty in physical model testing and have produced a guidance document [172] on the expression of uncertainty in experimental hydrodynamics. Overall, the experimental work presented in this section was completed to a high level of accuracy from the model build, to instrumentation setup, wave calibration, and data acquisition.

Chapter 6

Numerical and Physical Modelling Comparison

6.1 Introduction

This section compares the numerical models created in CFD and BEM simulations (in ANSYS CFX and AQWA) outlined in Chapter 4 with physical models tested in the wave basin discussed Chapter 5. Numerical and physical model comparisons were carried out to determine how valid the numerical analysis was in predicting the model's behaviour.

Numerical and physical models each have their own advantages and disadvantages. The principal disadvantages of numerical modelling relate to either that the numerical models are built on assumptions such as potential flow theory or they are too large to compute for long enough or to compute a sufficiently large domain in 6 degrees of freedom, as can be the case with CFD. By validating numerical models with physical ones, they can be used in conjunction to expedite the optimal design of floating structures [173, 154].

As the tubular multihull design is based on the premise of a large amount of viscous forces on the horizontal tubes of the model a CFD program was utilised. BEM model analysis was utilised for the standard catamaran and for the catamarans with heaveplates as they were well represented by that numerical method.

All models were tested physically at 1:25 scale as discussed in Chapter 5. The numerical simulation and scaled physical model testing will be compared in the following sections through the RAO curves generated:

§ 6.2 Standard Catamaran

§ 6.3 Tubular Multihull

§ 6.4 Catamarans with Single Heaveplates

§ 6.5 Heaveplate Depth and Area Comparison

§ 6.6 Curved Hulled Catamaran with Dual Heaveplates

§ 6.7 Catamarans with a Raised Heaveplate

6.2 Standard Catamaran

In Figure 6.1 it can be seen that close similarity is shown in heave and that the numerical model over predicts the pitch RAO of the catamaran at resonance.

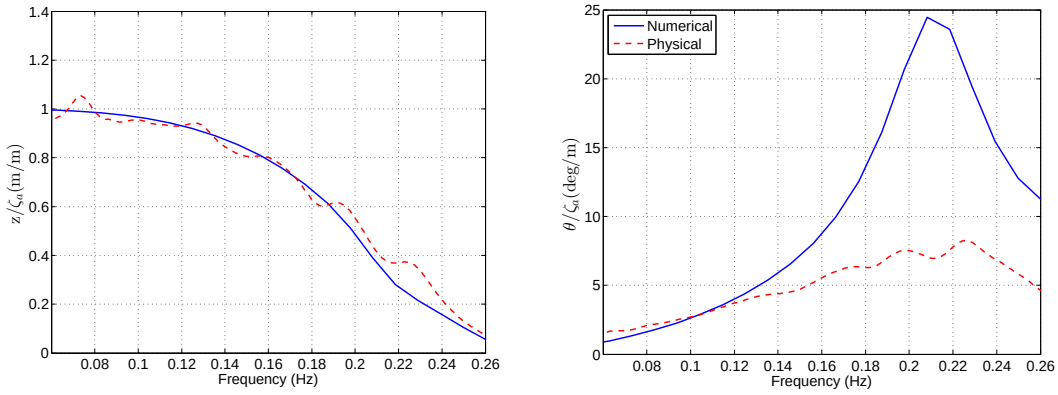

(a) Heave

(b) Pitch

Figure 6.1: Numerical and Physical Modelling RAO for a Standard Catamaran

6.3 Tubular Multihull

Figure 6.2 shows the RAO output from the CFD testing alongside the regular RAO results from the tank testing of the tubular multihull model T1000. Close similarity is displayed, particularly at the lower frequency ranges, showing evidence that viscous damping forces are accounted for.

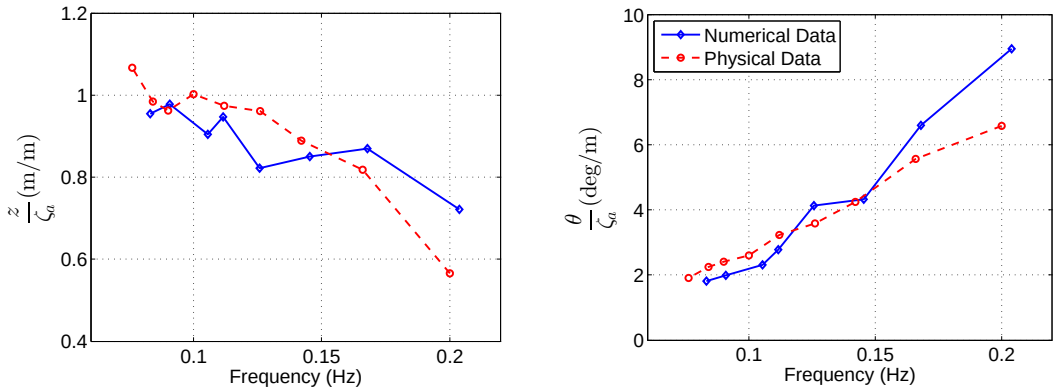

(a) Heave

(b) Pitch

Figure 6.2: Numerical and Physical Modelling RAO for the Tubular Multihull, T1000

6.4 Catamarans with Single Heaveplates

In Figures 6.3 & 6.4 the narrow and wide hulled catamaran with a 12m deep heaveplate are presented. The heave RAO for the narrow hulled catamaran shows good agreement aside from around resonance. The numerical pitch RAO is generally smaller than the physical for most frequencies except at resonance.

Examining the wide hulled catamaran in Figure 6.4, the heave RAO in the numerical model is not reprehensive of the physical model, this is likely due to the slamming induced on the hull that occurs due to a shallow draught and large heave resistance. This was not predicted in the numerical model as the heave RAO is not very small apart from wave frequencies above 0.2Hz. Surprisingly, this issue does not seem to have influenced the pitch RAO, with good agreement

being demonstrated.

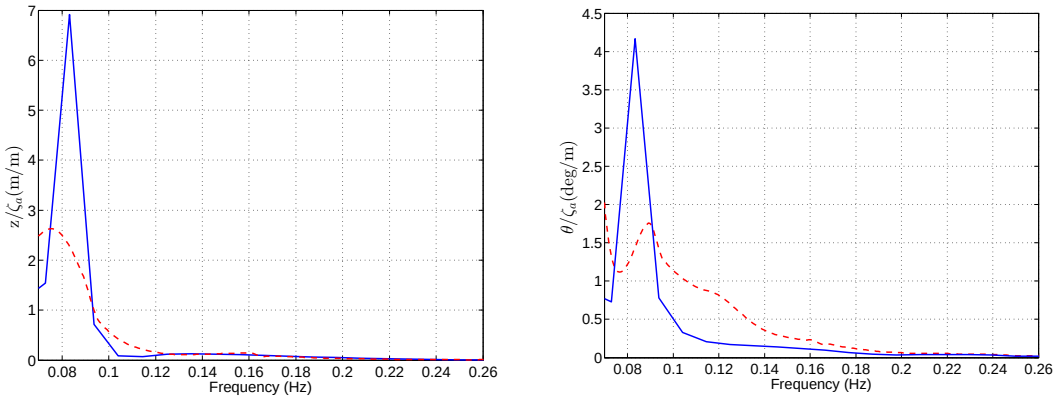

(a) Heave (b) Pitch

Figure 6.3: Numerical and Physical Modelling RAO Curves for the Narrow Hulled Catamarans with a Heaveplate at 12m Draught

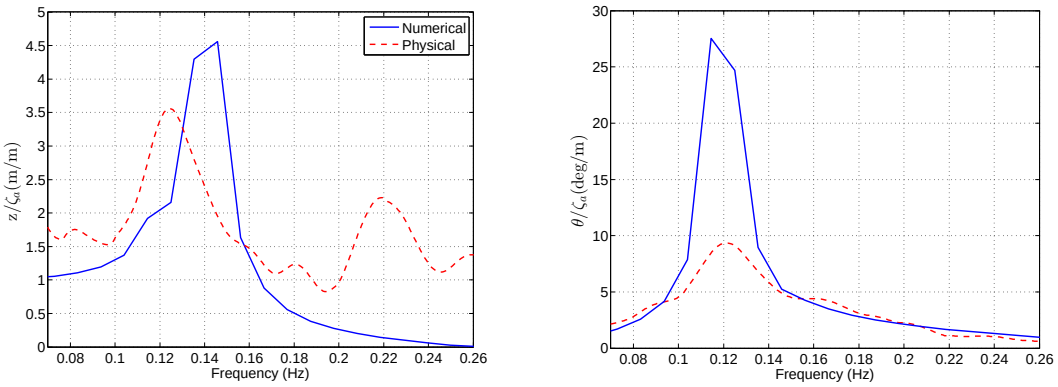

(a) Heave (b) Pitch

Figure 6.4: Numerical and Physical Modelling RAO Curves of the Wide Hulled Catamarans with a Heaveplate at 12m Draught

In Figure 6.5 it can be observed that in heave the curved hulled catamarans motions are overestimated at the natural period and underestimated at frequencies above it. In pitch, the numerical modelling more closely represents the physical modelling aside from frequencies close to resonance.

Comparing the numerical and physical modelling of the GDC it is clear that there is a good correlation between the models. In both the heave and pitch

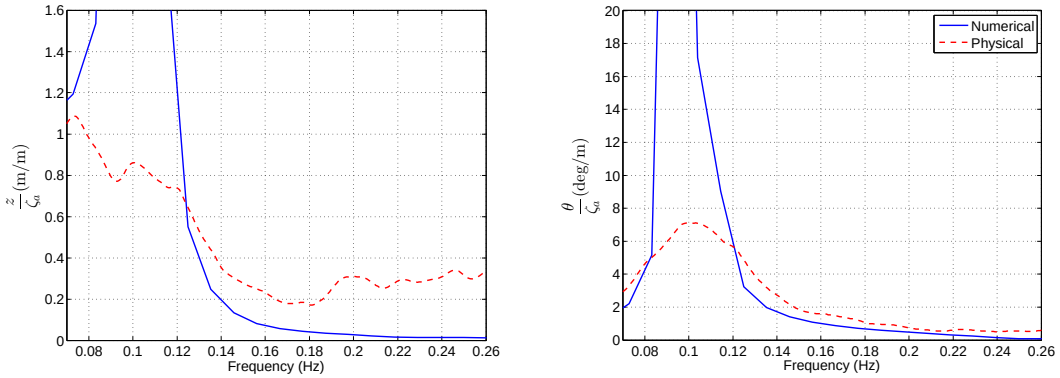

(a) Heave (b) Pitch

Figure 6.5: Numerical and Physical Modelling RAO for the Curved Hulled Catamaran with a Heaveplate at 12m Draught

graphs displayed in Figure 6.6 the natural period is at the same location in heave and pitch. The amplitude of the numerical RAO is less than the physical model around 0.1Hz and tends to get closer to the physical model as the frequency increases.

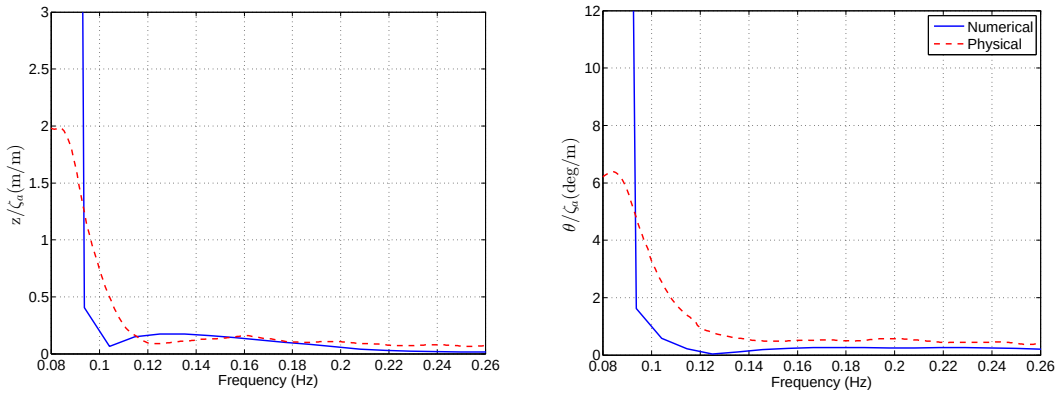

(a) Heave (b) Pitch

Figure 6.6: Numerical and Physical Modelling RAO for the GDC with a Heaveplate at 12m Draught

6.5 Heaveplate Depth and Area Comparison

In Figure 6.7 the numerical and physical modelling of a catamaran with a 178.5m^2 heaveplate at three depths is considered. In heave, the natural period is between 0.1-0.15Hz for all depths. In pitch, the natural period closely relates between the numerical and physical RAO plots in addition to the off peak RAO amplitude values.

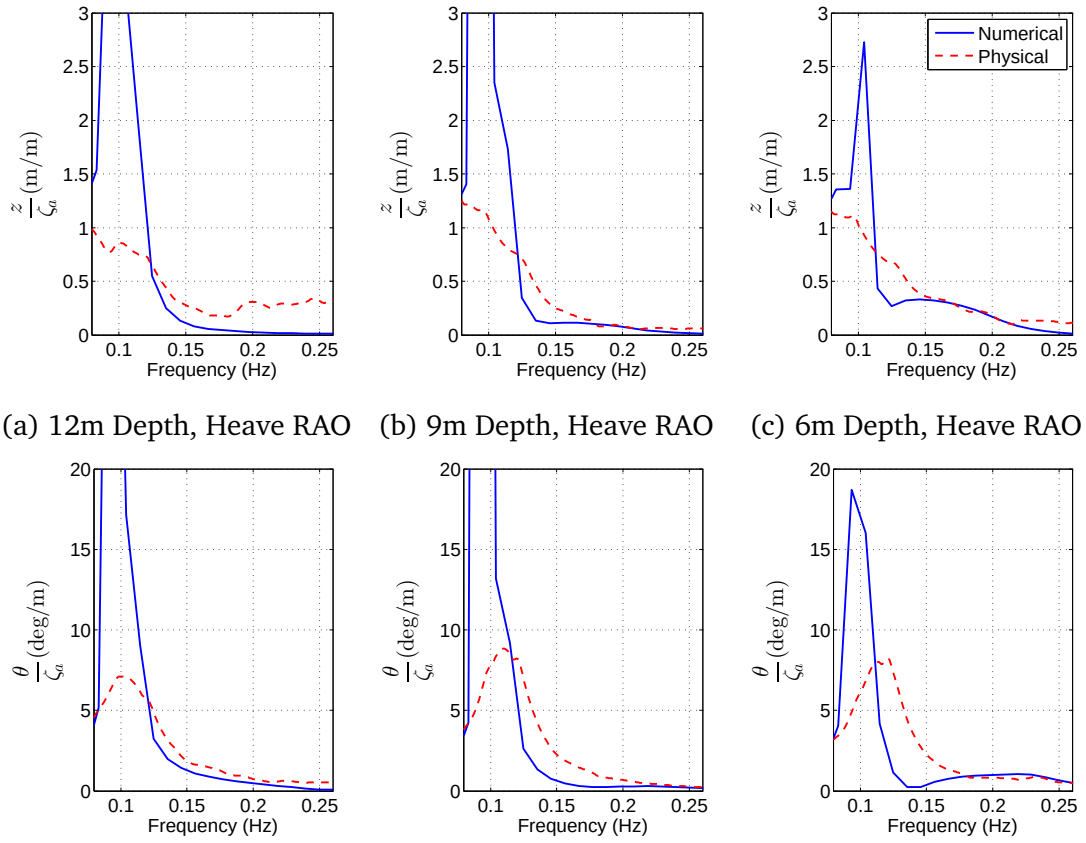

(a) 12m Depth, Heave RAO (b) 9m Depth, Heave RAO (c) 6m Depth, Heave RAO

(d) 12m Depth, Pitch RAO (e) 9m Depth, Pitch RAO (f) 6m Depth, Pitch RAO

Figure 6.7: Numerical and Physical Modelling of the 178.5m^2 Heaveplate on the Curved Hulled Catamaran at Varying Depths

In general, it can be said that the heave and pitch models were not predicted well by the BEM. The RAO at the natural period is much larger for the numerical model than the physical model due to there being no additional damping terms added to the numerical model. This accounts for the overall slightly lower phys-

ical model RAO. In Figure 6.7a there is a large discrepancy between the heave RAO magnitude between 0.15 and 0.26Hz. This effect is also seen with other heaveplates at that depth as can be seen in Figure 6.8a , 6.8b, & 6.8c The BEM model has greater accuracy in predicting the pitch motions.

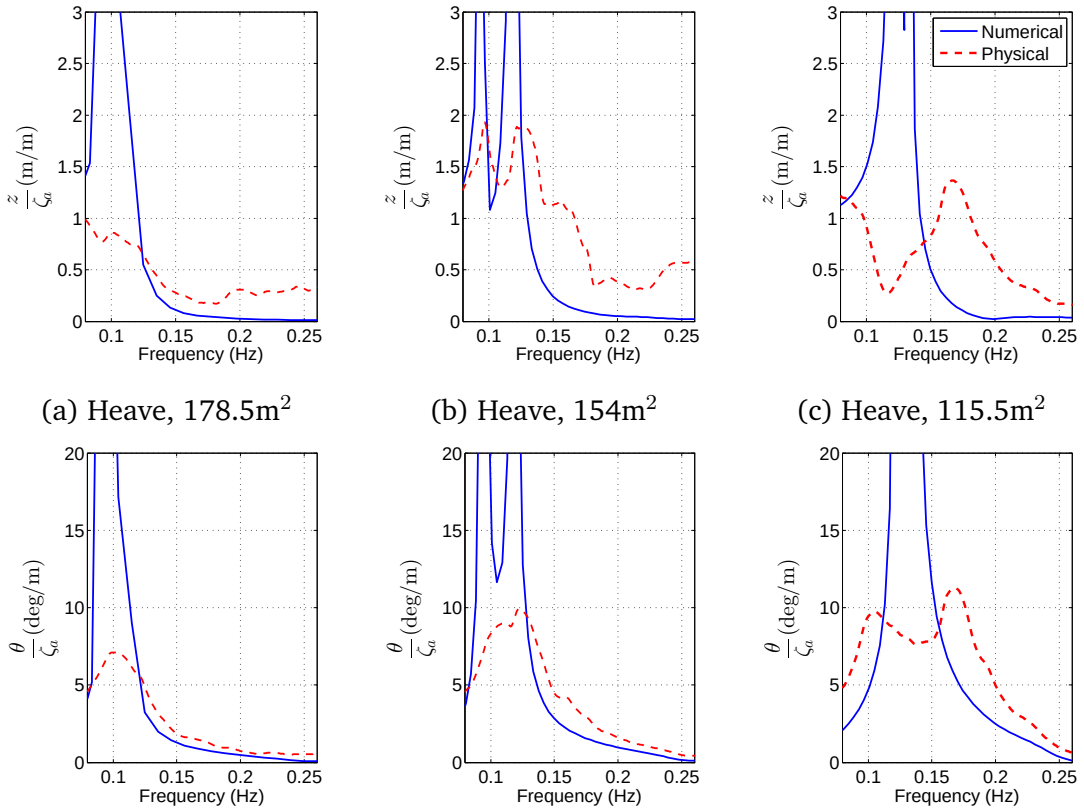

(a) Heave, 178.5m^2 (b) Heave, 154m^2 (c) Heave, 115.5m^2

(d) Pitch, 178.5m^2 (e) Pitch, 154m^2 (f) Pitch, 115.5m^2

Figure 6.8: Numerical and Physical Modelling RAO Curves Comparing Variation of Heaveplate Areas at 12m Depth on the Curved Hulled Catamaran

From the comparison of the numerical modelling with the physical modelling it was previously stated that there was good agreement in some areas and poor agreement in other areas. The significance of this is that as was previously acknowledged BEM models require estimated damping terms to provide accurate results, particularly at the natural period. The numerical and physical modelling of three heaveplates of varying area on the curved hulled catamaran in Figure 6.8 showed some interesting results. In heave the 178.5m^2 heaveplate

at 12m draught numerical model is larger at the natural period as expected and much smaller for high frequencies. The 154m^2 heaveplate has a double peak in both the numerical and physical model in heave. The 115.5m^2 heaveplate has a natural period offset in heave between the numerical and physical model. In general, all the models graphed in heave have numerical RAOs that are less than the physical ones for the higher frequencies. In pitch, the peaks are all at a slightly higher frequency and the magnitude of the RAO spectrum is underestimated for low frequencies. At frequencies higher than the natural period, the numerical model values for 154m^2 and 115.5m^2 are higher than the physical model and slightly smaller for the 178.5m^2 heaveplate.

6.6 Curved Hulled Catamaran with Dual Heaveplates

Figure 6.9 shows the heave and pitch RAOs for the 56m^2 dual heaveplate model. The modelling of the dual heaveplate designs had some discrepancies between the numerical and physical model. The heave for 0° and 22.5° of heaveplate inclination are both over predicted, the heave RAO for 45° is much more similar by comparison. The pitch RAO is very similar for each angle setting and the numerical model over predicts the magnitude at resonance for each case as expected. There is also coupling between heave and pitch as has been seen also seen in Figure 6.9. Examining Figure 6.10 it is discernible that the general trend of magnitude for the heave RAO for the numerical and physical model is similar, except at resonance as expected. In pitch, there is some agreement both in magnitude and peak frequency of the RAO.

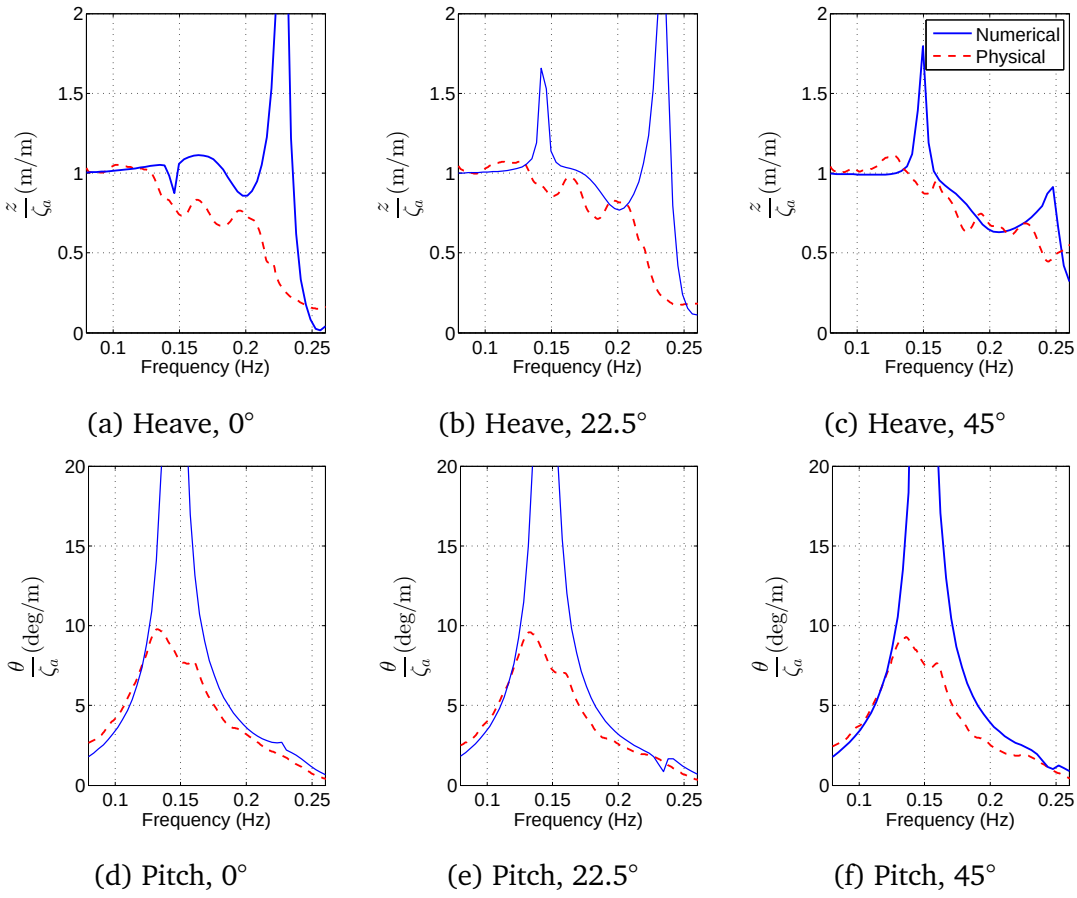

(a) Heave, 0° (b) Heave, 22.5° (c) Heave, 45°

(d) Pitch, 0° (e) Pitch, 22.5° (f) Pitch, 45°

Figure 6.9: RAOs for Dual Heaveplates of an Area of 56m^2 at a 12m Draught

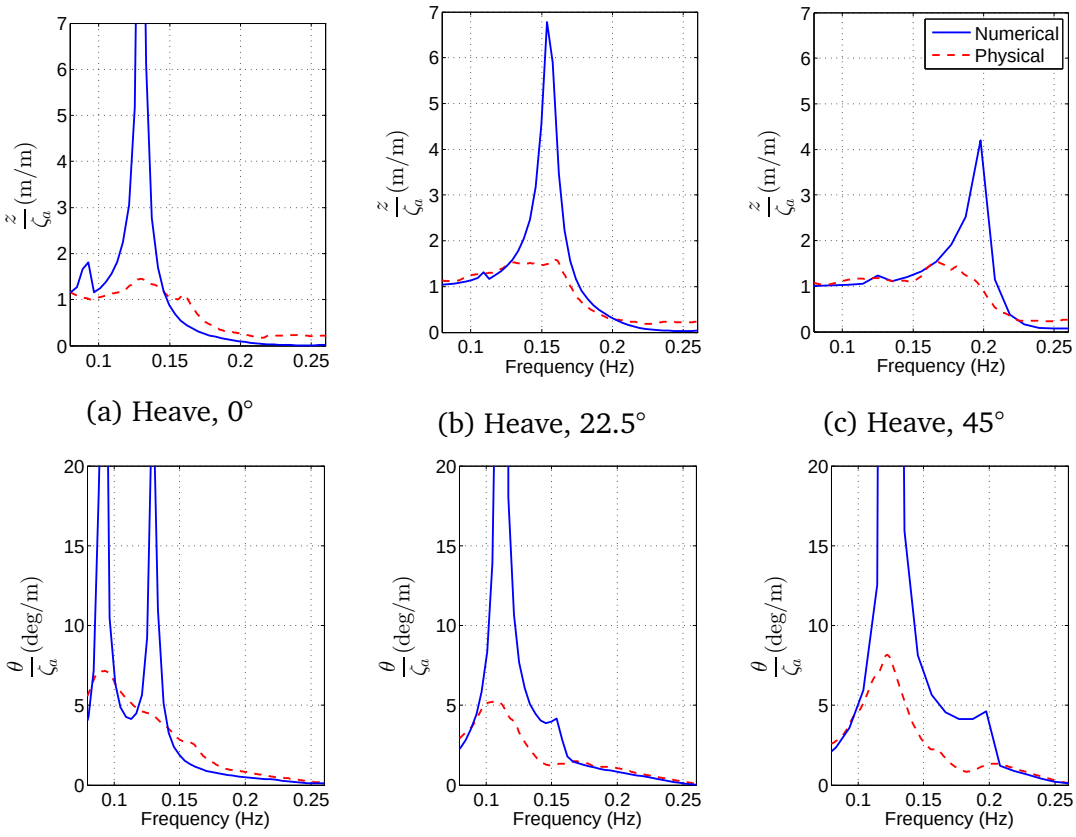

(a) Heave, 0° (b) Heave, 22.5° (c) Heave, 45°

(d) Pitch, 0° Dual Heaveplate (e) Pitch, 22.5° (f) Pitch, 45°

Figure 6.10: Numerical and Physical Modelling RAO Curves for the Dual Heaveplates of an Area of 112m^2 at a 12m Draught

6.7 Catamarans with a Raised Heaveplate

Figure 6.11 graphs the curved hulled catamaran and the wide hulled catamaran with the heaveplate raised out of the water. For these models there appears to be a very good relationship between the magnitude of the numerical and physical RAO. In heave the numerical model produces larger results at low frequencies and lower results for high frequencies for the curved hulled catamaran and the opposite for the wide hulled catamaran. At the natural period of pitch, the curved hulled catamaran the physical model is smaller than the numerical model as expected.

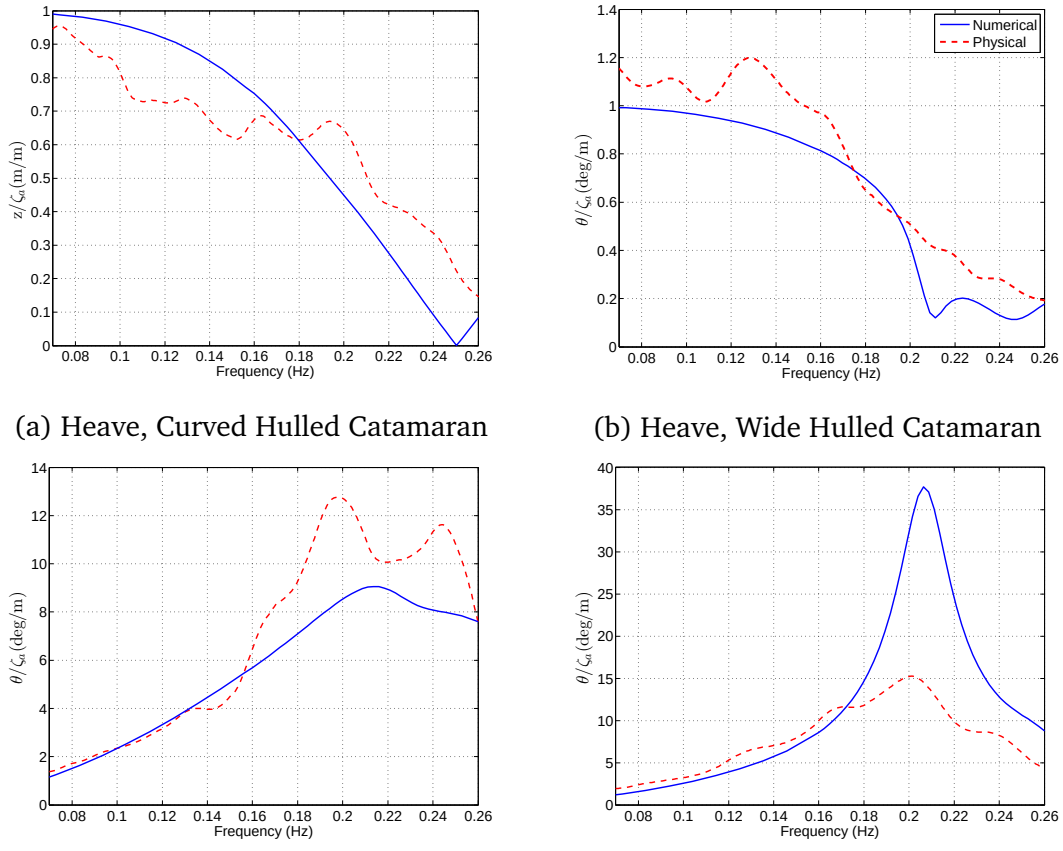

(a) Heave, Curved Hulled Catamaran

(b) Heave, Wide Hulled Catamaran

(c) Pitch, Curved Hulled Catamaran

(d) Pitch, Wide Hulled Catamaran

Figure 6.11: Numerical and Physical Modelling RAO Curves for the Wide Hulled Catamaran and the Curved Hulled Catamaran with Heaveplates Raised

6.8 Discussion

This chapter compares the numerical simulations with the scaled physical modelling carried out for the zero forward speed RAOs. Depending on the nature of the model both CFD and BEM codes were used in the simulation of the designs in this thesis. Though the numerical models presented provide indicators of a model's characteristics they did not describe them accurately enough to solely rely on numerical modelling techniques when investigating novel floating designs. It could be concluded than an iterative approach to design is required.

The modelling in ANSYS CFX show good correlation with the physical model for the case presented, however the time and computational power required to run the simulations prevented a larger number of cases from being computed.

The modelling in ANSYS AQWA show the general shape and magnitude of the heave and pitch RAOs. The AQWA models were more accurate in predicting the RAO magnitudes when linearised viscous damping was applied to the numerical model.

By examining the overall comparison between the numerical and physical modelling it can be seen that there is variation between the outputs. For the CFD numerical modelling there is not sufficient work carried out to provide a relevant assessment. In relation to the BEM numerical modelling and the comparative physical modelling conducted, there are some differences, these are largest around the natural frequency, but outside of this region there is close correlation between the results. For a discussion on the confidence limits of the physical modelling see § 5.9, and for numerical modelling see § 4.6. As both methods have weaknesses, predominantly due to scale issues and numerical damping methods, it would be recommended that larger scale physical modelling or full scale data collection be carried out. In addition, the numerical modelling could be improved particularly in the setup of the CFD model, and by the addition of frequency dependent numerical damping in the BEM models.

Chapter 7

WFSV Interaction with a Monopile

7.1 Introduction

This section details the physical modelling of the interactions of a WFSV with a monopile. The results for physical model tests carried out in the wave tank are presented for the general low frequency motions of a ship 0.08–0.25Hz (4–12.5s) at full scale [156]. Vessel response in the wake of a monopile is investigated as well as when a bollard pull is simulated with a constant force. The limits for carrying out a transfer published in the literature are revisited and compared with a standard catamaran model 24m long with 2m demihulls.

From the previous series of testing a number of promising designs are tested to understand their performance while interacting with the monopile. The hull geometry and heaveplate influence on performance metrics is examined concerning the number of horizontal disconnects, lateral and vertical slips and as well as maximal and RMS of linear movement, accelerations and angular motion.

To understand the effect of wave heading on transfer operations a directional study was carried out on the GDC model and compared with the standard catamaran model tested under similar conditions in order to produce 360° performance plots (P-Plots) that can compare different WFSVs. 360° performance plots are a version of operability diagrams similar to the ones used in seakeeping

analysis to illustrate the operability limits in seas of differing headings. In this chapter polar plots limit sea states which transfers may be made to a turbine for different vessels are detailed. Performance plots are outlined in greater detail in 2.7.

7.2 Modelling Overview

Monopile foundation piles have diameters ranging from 2.3–7.5m [174, 175, 176, 177]. The monopile used in this study was a constant diameter of 6.25m. It was created by an unplasticised polyvinyl chloride pipe that was bolted to an internal steel box section, that was itself supported on a large diameter galvanised steel frame. This was then weighed down with lead and the top of the monopile was braced to the bridge to prevent any motion. Figures 7.1 & 7.2 show the setup and testing of the narrow hulled catamaran with the monopile, (larger pitch motion than anticipated, required that the monopile be build up to prevent the model's bow hitting the monopile.)

The coefficient of friction between the fender of a WFSV and the monopile landing point is quite variable as it depends on the fender material, compression of the fender, the amount of marine growth on the monopile, and wetness. Previous studies of WFSVs interacting with monopile used a range of coefficients of friction from, μ_s = 0.7–1.2 [8, 69, 89, 134]. As it is possible to vary the coefficient of friction by increasing the normal force a coefficient of friction on the lower end of this range was used. The material chosen for the interaction was closed cell polyethylene foam for the fender and an unplasticised polyvinyl chloride for the monopile, which in combination have a static coefficient of friction between, μ_s = 0.45–0.75 [178, 179, 180].

The physical modelling of a WFSV interacting with a monopile included two mooring setups, firstly the model was slack moored behind the monopile and in the second method the model was moored to the monopile by means of a constant force. In the first instance the aim was to determine the difference in

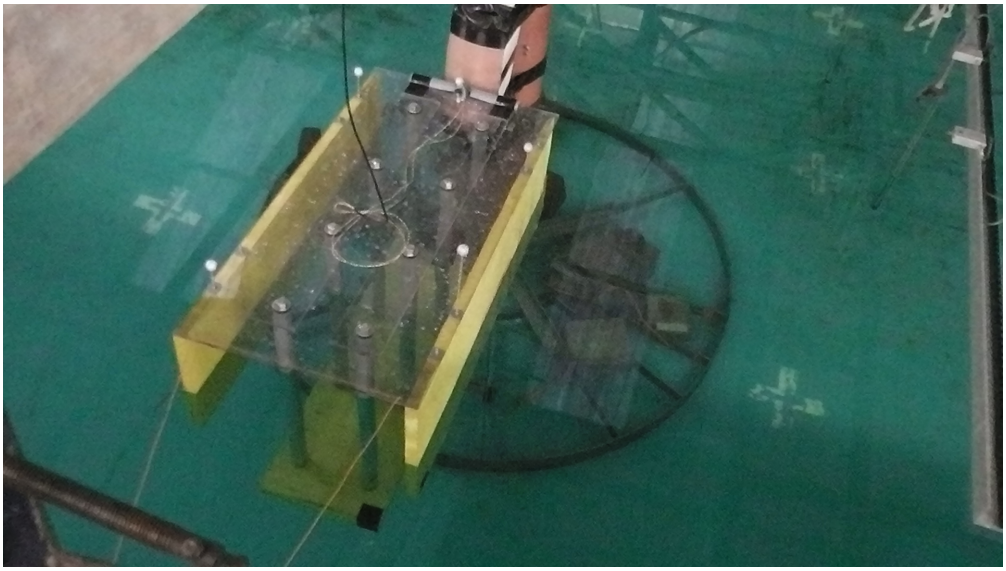

Figure 7.1: Model Setup for the Narrow Hulled Catamaran Experimental Testing of the Vessel with the Monopile

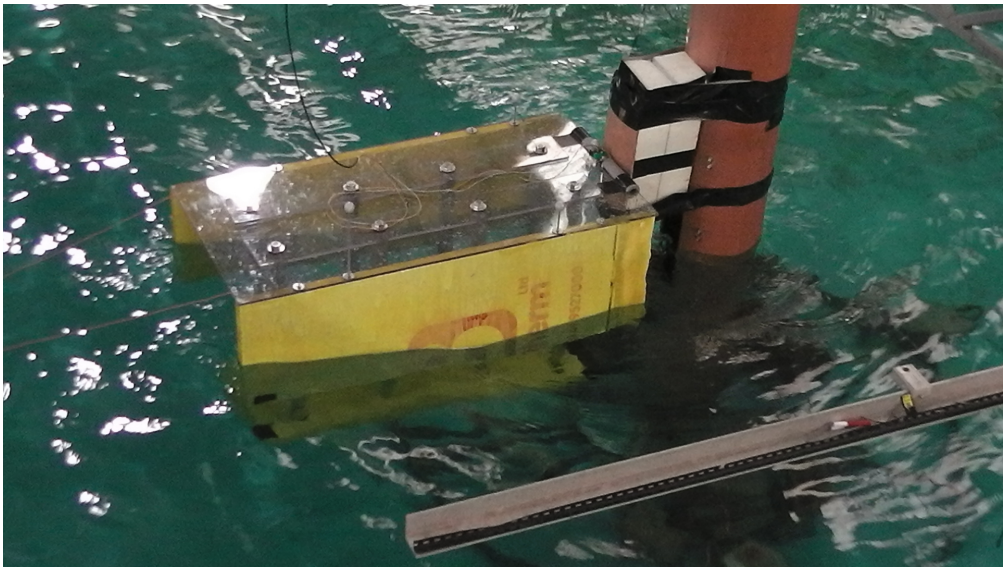

Figure 7.2: Experimental Testing of the Narrow Hulled Catamaran with the Monopile Interacting with Waves

vessel RAO behind a monopile compared to being in the open seaway. In the second case the significance of bollard pull was studied.

To create the bollard pull, a small section of the monopile was cut out to allow a line to be run from the model to a pulley in the monopile. A known lead weight was then placed at the end of the line in such a way that it would not be immersed in water. At the stern the model was slack moored to prevent excessive yawing. A strain gauge was placed on the line between the first pulley and the model to record the perceived bollard pull of the model and an accelerometer was placed at the bow of the model alongside the Qualisys marker, as can be viewed in Figure 7.3.

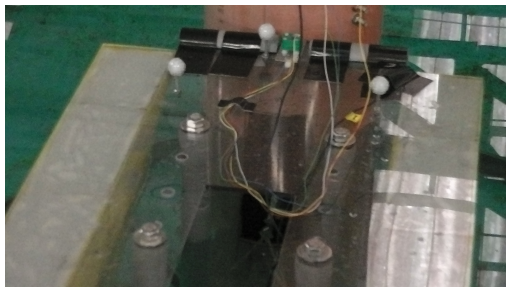

Figure 7.3: Instrumentation at the Bow

Both the WFSV fender and the monopile must be designed against the large forces both planned and accidental due to the docking of WFSVs for transfer operations [181]. The loads on an offshore wind turbine vary from 50kN to 5 MN, in addition it is noted in the design that supply vessels may grow in size over the operational life of the wind farm and that special purpose vessels should be handled by specific case-by-case safety assessments [87, 134, 181, 182, 183]. These are dependent on the loads considered from planned daily loads to rare accidental loads involving rapid deceleration.

The investigation of other wave directions aside from head waves are also of importance, as such heading angle was incorporated in the testing for the GDC model and the standard catamaran model was used for comparison. The angles studied were from 0° head seas to 180° following seas in 45° steps. Using the data from these tests the limits that make a transfer difficult were then examined and performance plots were created, performance plots are outlined further in 2.7.

As discussed in § 5.4 the data analysed removed high frequency scale effects, and the corresponding parameters of interest were extracted from the Qualisys

6 DOF data. The sea states analysed were the same as per the RAO tests summarised in Appendix E.

7.3 Limits for Carrying out a Transfer

The required limits of key parameters for a safe transfer are presented and discussed in § 2.7 & § 2.10 of the Literature Review, and are limited to the number of vertical slips and maximum roll angle. The general limits of motion that safe operations can be carried out on deck in a seaway were discussed in § 5.7 and summarised in Table 5.4. These related to MII forward perpendicular, RMS of Vertical Acceleration at the forward perpendicular and COG, as well as RMS of Pitch Angle at the COG. To quantify the limit motions for a transfer from WFSV to a monopile, the following parameters were examined during the experimental study;

- number of horizontal X disconnects, and lateral Y and vertical Z slips from the point of contact
- the maximal and RMS values of the linear movement
- the maximal and RMS values of, roll and pitch motion
- the maximal and RMS values of accelerations of the forward perpendicular, in X, Y, Z and resultant directions

When establishing the limits for transfer to a turbine, it should be noted that the sum of different motions affects a person greater than one directional motion [170]. The frequency range used to calculate RMS values was set between 0.06Hz–1Hz, a bandwidth slightly larger than presented for the RAOs [184]. There are a number of charts explaining the frequency and magnitude of acceleration at which varying degrees of discomfort are felt, nonetheless, in regards to MII the frequency is generally lower and the magnitude of acceleration is higher [170, 185, 186].

It has been postulated that provided the ship is able to maintain contact then the limit to safe transfers are the rate of vertical slips and the RMS of roll angle [88]. In relation to the confidence limits for these vertical slips 95% has been suggested as desirable, notwithstanding this it is noted that from experience of current industry practice this is much lower and sometimes as low as 70%, a confidence limit of 75% then presented [88], and this is the reference limit considered in the current study. Wave period is an issue when calculating confidence limits, as for longer period waves there tend to be less but more severe slips, in this study a number of slips allowed in the test period were defined and applied to all wave conditions.

An RMS limit of 3° applies to roll and it was found that the accelerations of 0.04g horizontally and 0.05g vertically in the technician saloon to be representative of the ships limit for carrying out transfers [88] incidentally these accelerations are the same limits given for transit passengers [97]. It can also be noted in relation to a maximum motion limit [42] set a limit of 0.5m for all x, y, and z motion to carry out transfers. The limits used in this analysis are tabulated in Table 7.1 and explained in the subsequent paragraph for clarity.

Table 7.1: WFSV Monopile Access Limits

Metric	Limit
Vertical and Lateral Slips	75% (53 slips in test duration)
Horizontal Disconnects	75% (53 disconnects in test duration)
RMS of Linear Movement	0.5m
Maximum Linear movement	1.5m
RMS of Roll	3°
RMS of Pitch	3°
RMS of Lateral Acceleration	0.04g
RMS of Vertical Acceleration	0.05g

Applying these limits to the tests carried out it can be determined that the no slip limit using an average period of 6s and a confidence level of 75% the number of allowable slips a test duration was 53. The roll limit RMS was 3° as given and a pitch limit of 3° is also applied as it is also a rotation about the contact point on a horizontal axis. The limit of heave acceleration at the forward perpendicular is taken to be 0.04g horizontally and 0.05g vertically. The maximum positional movement in x, y, and z should be less than 0.5m. However, from examining the motions of a generic style standard catamaran WFSV in the scaled physical model testing in § 7.5.2 & 7.6.2 the RMS of x, y, and z movement is set at 0.5m and the maximum x, y, and z movement is increased to 1.5m.

7.4 Vessel Response in the Wake of a Monopile

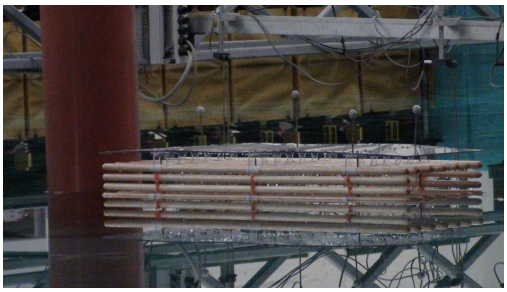

Figure 7.4: Model in the Wake of the Monopile

By placing the tubular multihull behind a scale model of a wind turbine foundation the influence that will have on the vessels motion can be determined. Figure 7.4 shows the setup of the tubular multihull slack moored in the wake of the monopile. The response of this case was investigated to see if the wave climate in the monopiles wake had a noticeable outcome on the WFSVs motions. The response function was calculated with long crested wave spectra without the monopile present so as compare the response for a variety of spectra with and without a monopile present.

The relationship between wavelength and monopile is defined such that if $D/L < 0.2$ the pile is classed a slender body and does not significantly alter the wave [128]. Where D is the diameter of the monopile and L is the wavelength. In the case of a monopile with a diameter of 6.25m the pile is classed as slender for

waves with a wavelength greater than 31.25m, which corresponds to a wave period of about 4.55s, for deep water. For wave periods below 4.55s the monopile should have a greater influence on the wave climate and potentially reduce the WFSVs motions due to it being a slender body. As is marked in Figure 7.5 the opposite occurs in practice, though only by a small amount. Overall though the RAO for a vessel in open waters to those in the wake of a monopile are very simmilar and the small differences shown in Figure 7.5 could be attributed to experimental error.

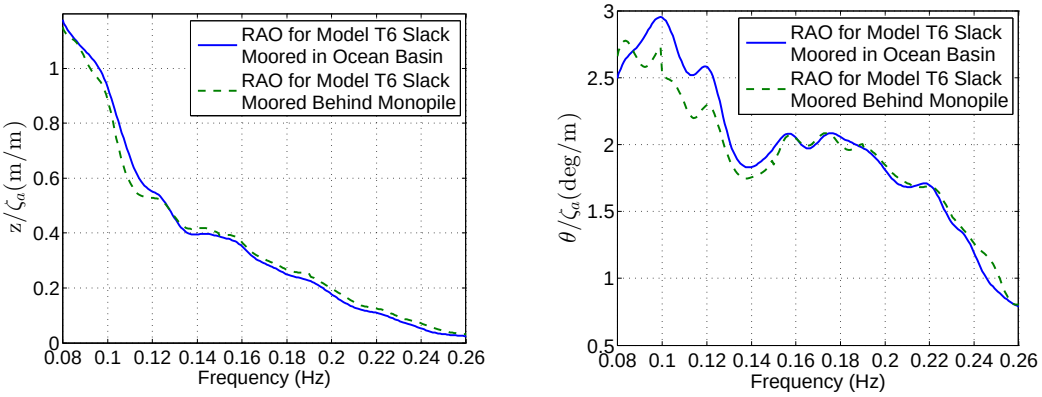

(a) T6 Heave monopile RAO

(b) T6 Pitch monopile RAO

Figure 7.5: Comparison of Performance in the Wake of the Monopile to the RAO Without a Monopile Present

7.5 WFSV Interacting with a Monopile in Head Seas

7.5.1 Overview

This section focuses on WFSVs interacting with a monopile in head seas. Figure 7.6 shows the curved hulled catamaran maintaining contact with the monopile in head seas. In the subsequent subsections the horizontal x disconnects, maximum z motion, and the number of slips in the z direction are presented for each of the following cases:

§ 7.5.2 presents the performance of a standard catamaran

§ 7.5.3 compares the effect of variation in depth of heaveplate

§ 7.5.4 the narrow hulled catamaran with a heaveplate

§ 7.5.5 examines the influence of bollard pull

§ 7.5.6 discusses the performance of dual heaveplates

7.5.2 Standard Catamaran

With regard to number of vertical slips for a basic standard catamaran design docked at the monopile it can be observed in Table 7.2 that the number of z slips exceed 53, the limit for the test duration, for all sea states above 1.5m Hs. Some very extreme peak values of z motion are recorded for the 3m sea states, up to 6.91m for the 7s Tp at m Hs sea state. This is due to the fact that once the frictional force is overcome the vessel tended to follow the wave motion until static frictional contact was regained. Table 7.2 also shows the x disconnects which occur for sea states above 1.5m Hs.

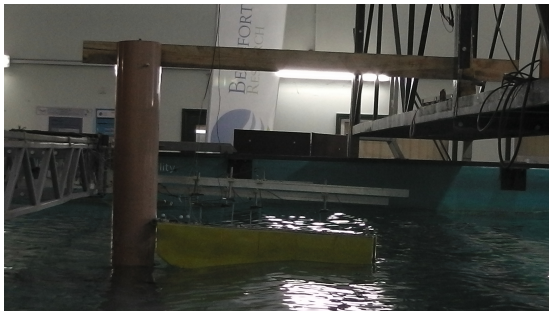

Figure 7.6: Curved Hulled Catamaran with a Heaveplate Interacting with the Monopile in Head Seas

Table 7.2: Properties of the Standard Catamaran when Docked at the Monopile with a 45t Bollard Pull

Wave Condition		Metric Considered		
Hs (m)	Tp (s)	No. z Slips	Maximum z motion (m)	No. x disconnects
1	4	0	0.02	0
1.5	5	7	0.66	0
1.5	7	21	2.84	0
1.5	9	16	1.59	0
1.5	12.5	28	0.79	0
2	6	82	2.52	1
2.5	12.5	79	3.05	0
3	7	142	6.91	6
3	8	112	4.71	2
3	9	96	4.75	2
3	10	105	3.23	1

7.5.3 Depth of Heaveplate

In Table 7.3 the number of times the vertical movement exceeds 0.25m is detailed for the curved hulled catamaran with a the heaveplate area of 178.5m^2 set at 12, 9, and 6m draught respectively. From 6m to 9m there is a reduction of 48% for the wave conditions tested and further reduction of 33% when reducing the heaveplate to a 12m depth. With a 66% decrease noted between 6m to 12m depth. Though the number of times the model with 6m of draught experiences a vertical slip is excessive it does not exceed the threshold of 53 for the test duration for any sea state. The fail mode for these models comes from maximum vertical motions.

Table 7.4 shows the relationship between heaveplate depth and maximum vertical movement, for the curved hulled catamaran with the heaveplate set at 12, 9, and 6m draught respectively. For the larger waves it was advantageous to have a deep heaveplate, though for smaller wave heights this was not always

Table 7.3: Vertical Slips Related to Depth of Heaveplate

Wave Condition		Heaveplate Depth (m)		
Hs (m)	Tp (s)	12	9	6
1	4	0	0	0
1.5	5	0	0	0
1.5	7	0	0	1
1.5	9	0	0	0
1.5	12.5	0	0	0
2	6	5	0	5
2.5	12.5	0	0	5
3	7	11	9	29
3	8	9	20	37
3	9	9	22	27
3	10	6	12	12
	Σ	40	63	116

the case, for example the wave series 2m Hs with a 6s Tp and 1.5m Hs with a 9s Tp. Indicating that other factors besides the heaveplate were affecting the heave motion for these cases. Higher friction could be employed in reducing the vertical motions, therefore potentially reducing the required bollard pull.

In Table 7.5 the difference in horizontal disconnections, where the bow is moved away from the monopile, were compared with heaveplate depth for the curved hulled catamaran are shown, the heaveplate area was kept constant at 178.5m^2 for depths of 12,9, and 6m. The disconnections occurred due to a large wave load on the bow of the vessel, which was greater than the current bollard pull. The extra drag from the deep hull draught, heaveplate and jacks whilst reducing the heave and pitch motion considerably from the standard catamaran tested with the heaveplate resulted in the requirement for larger bollard pulls to maintain contact than that with the catamaran, 35t was found to be optimal. Table 7.5 shows how decreasing the depth of the heaveplate has very little influence on the loss of contact incidences.

As was previously shown in Tables 7.3,7.4, & 7.5 the depth of heaveplate

Table 7.4: Maximum Vertical Movement (m) Related to Depth of Heaveplate

Wave Condition		Heaveplate Depth (m)		
Hs (m)	Tp (s)	12	9	6
1	4	0.01	0.01	0.01
1.5	5	0.02	0.04	0.04
1.5	7	0.06	0.1	0.34
1.5	9	0.1	0.11	0.1
1.5	12.5	0.15	0.13	0.12
2	6	0.45	0.2	0.78
2.5	12.5	0.21	0.23	0.69
3	7	1.22	3.15	4.69
3	8	1	1.41	2.85
3	9	0.98	1.56	1.95
3	10	0.77	1.15	1.56

Table 7.5: X Direction Disconnects, where the Bow is Moved away from the Monopile in the X direction, Related to Depth of Heaveplate

Wave Condition		Heaveplate Depth (m)		
Hs (m)	Tp (s)	12	9	6
1	4	0	0	0
1.5	5	0	0	0
1.5	7	0	0	0
1.5	9	0	0	0
1.5	12.5	0	0	0
2	6	0	0	0
2.5	12.5	0	0	0
3	7	5	6	5
3	8	3	3	3
3	9	1	0	1
3	10	0	0	0
	Σ	9	9	9

influences the performance at the monopile. In Figure 7.7 the significance of heaveplate depth is displayed in terms of the number of pass and fails at 0° heading and 35t bollard pull, with a heaveplate of an area of 178.5m^2. All depths passed for the cases tested up to 2.5m Hs. The tests with a 3m Hs showed that as the heaveplate depth increased the number of passes increased, from 0 at 6m depth, 2 at 9m depth and all four at a depth of 12m. These results correspond with the vertical motion data tabulated in Tables 7.4 but not with the vertical slips and horizontal disconnects in Table 7.3 & 7.5, which is accurate as the limits in Table 7.3 & 7.5 are not exceeded but those in Table 7.4 are exceeded.

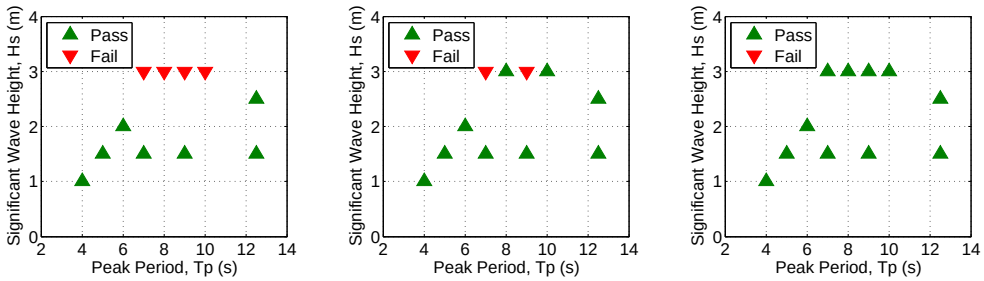

(a) 6m (b) 9m (c) 12m

Figure 7.7: Heaveplate Depth Performance while Interacting with the Monopile for the 178.5m^2 Heaveplate, at a Constant Bollard Pull of 35t

7.5.4 Narrow Hulled Catamaran with a Heaveplate

The narrow hulled catamaran with a heaveplate was tested for head waves while docked at the monopile. A bollard pull of 25t was used, this was found to maintain sufficient contact for sea states with a 3m Hs. Figure 7.6 shows the values for number of vertical slips, maximum vertical movement and number of horizontal disconnects. Although the values recorded are not exceptionally better than those recorded for similar heaveplate properties on the curved hulled catamaran the bollard pull required was much less, 25t over the 35t required for the curved hulled catamaran. When taking into consideration the promising properties of the zero forward speed RAO, MII, acceleration and pitch metrics discussed

in § 5.6.4 & § 5.7.3 it was concluded that the design should be further worked upon to fulfil naval architect requirements and create the design known as the GDC.

Table 7.6: Properties of the Narrow Hulled Catamaran when Docked at the Monopile with a 25t Bollard Pull

Wave Condition		Metric Considered		
Hs (m)	Tp (s)	No. z Slips	Maximum z motion (m)	No. x disconnects
1.5	5	0	0.08	0
1.5	8	1	0.25	0
1.5	12	6	0.29	0
3	9	9	0.59	4

7.5.5 Bollard Pull

Figures 7.8 & 7.9 show the relationship between bollard pull and heaveplate depth for sea states with a 7s and 8s Tp. Generally, as heaveplate depth and bollard pull are increased the responses decreases, though there are a number of cases where this is not so. These show that the breakdown of the z motion changes, for example sometimes the RMS increases even though the maximum reduces, see Figure 7.8 c & f.

Table 7.7 & 7.8 show the variation in vertical motion at the bow of the curved hulled catamaran with a heaveplate at a 12m draught related to bollard pull force. Increasing the bollard pull from 35–45t reduced the number of vertical slips by 70%.

Examining the curved hulled catamaran for the influence of bollard pull in Table 7.9 it can be seen that the largest readings were for the 3m waves, reducing from 5, 3, 1 @ 35t for 7, 8, 9s respectively to 4, 1 0 at 40t and 3, 0, 0 at 45t. Increasing the bollard pull from 35–45t reduced the number of horizontal

disconnects by 44%. This shows a very strong correlation between bollard pull and number of horizontal loss of contact incidences. This correlates with DNV-GL design guidelines with regards to bollard pull and wave load [66].

It can be seen that bollard pull, and heave damping are critical factors in reducing movement of the bow at the monopile, particularly for larger waves. Furthermore, it is clear that after 45/50t there is no net improvement.

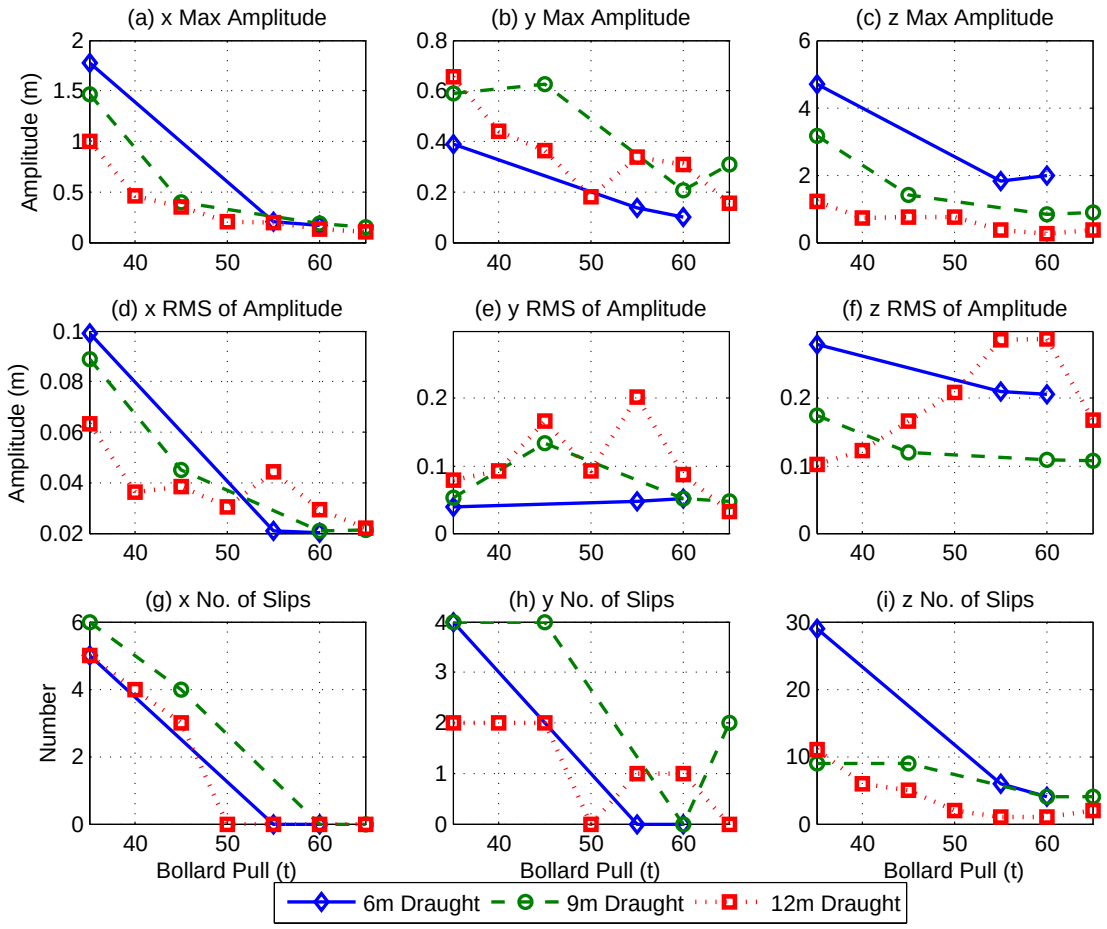

Figure 7.8: X, Y, and Z Motion of the Curved Hulled Catamaran with a 178.5m^2 Heaveplate at a 3m Hs and 7s Tp at 0° Heading

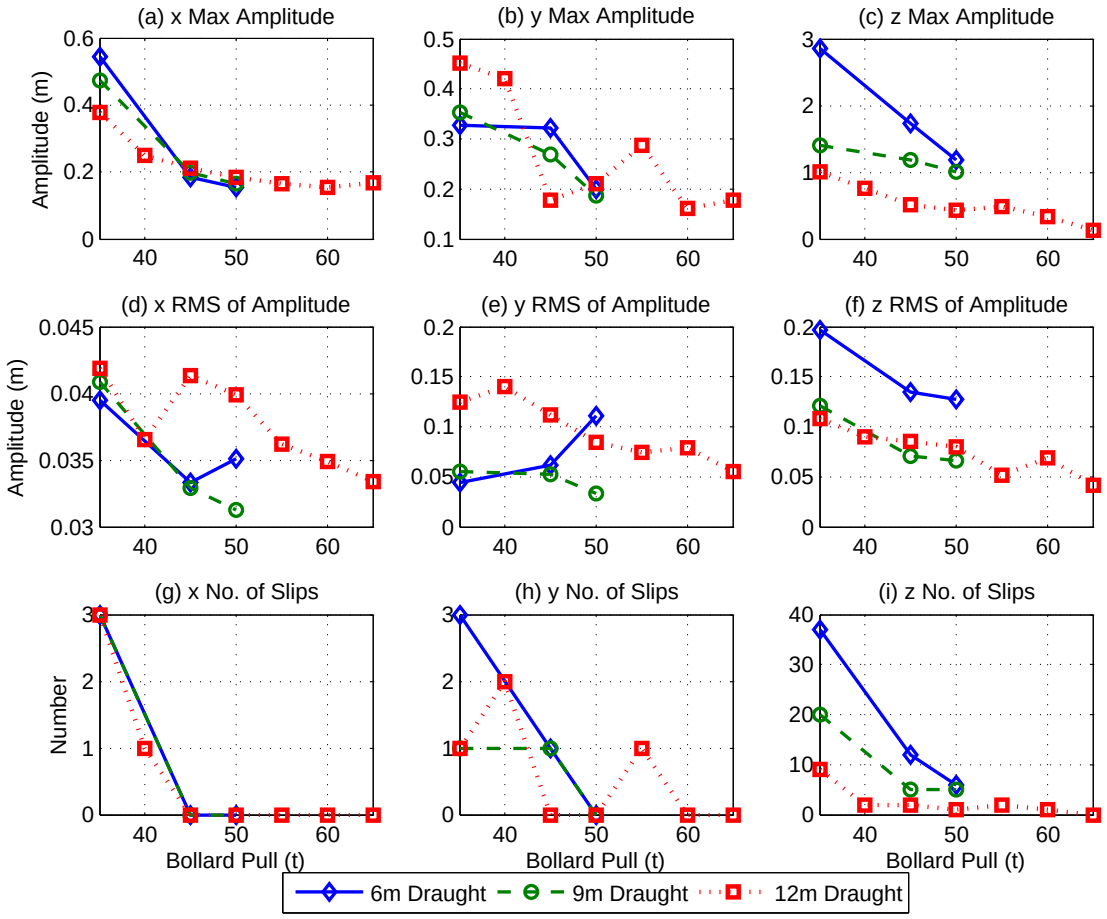

Figure 7.9: X, Y, and Z Motion of the Curved Hulled Catamaran with a 178.5m^2 Heaveplate at a 3m Hs and 8s Tp at 0° Heading

Table 7.7: Vertical Slips Related to Bollard Pull

Wave Condition		Bollard Pull (tonnes)						
Hs (m)	Tp (s)	35	40	45	50	55	60	65
1	4	0	0	0	0	0	0	0
1.5	5	0	0	0	0	0	0	0
1.5	7	0	3	0	0	0	0	0
1.5	9	0	0	0	0	0	0	0
1.5	12.5	0	0	0	0	0	0	0
2	6	5	3	4	0	3	0	0
2.5	12.5	0	0	0	0	0	0	0
3	7	11	6	5	2	1	1	2
3	8	9	2	2	1	2	1	0
3	9	9	3	1	1	1	0	0
3	10	6	4	0	0	0	0	1
	Σ	40	21	12	4	7	2	3

Table 7.8: Maximum Vertical Movement (m) Related to Change of Bollard Pull

Wave Condition		Bollard Pull (tonnes)						
Hs (m)	Tp (s)	35	40	45	50	55	60	65
1	4	0.01	0.08	0.01	0.03	0.02	0.02	0.05
1.5	5	0.02	0.05	0.02	0.04	0.04	0.03	0.04
1.5	7	0.06	0.53	0.05	0.06	0.06	0.05	0.08
1.5	9	0.1	0.09	0.09	0.1	0.09	0.1	0.1
1.5	12.5	0.15	0.16	0.14	0.15	0.15	0.14	0.14
2	6	0.45	0.45	0.47	0.23	0.33	0.04	0.25
2.5	12.5	0.21	0.22	0.19	0.22	0.22	0.2	0.2
3	7	1.22	0.71	0.75	0.76	0.36	0.26	0.36
3	8	1	0.76	0.51	0.44	0.49	0.34	0.13
3	9	0.98	0.62	0.28	0.31	0.27	0.16	0.15
3	10	0.77	0.45	0.2	0.17	0.23	0.2	0.26

Table 7.9: X Direction Disconnects Related to Bollard Pull for the Curved Hulled Catamaran with a 178.5m^2 Heaveplate at 12m Draught

Wave Condition		Bollard Pull (tonnes)						
Hs (m)	Tp (s)	35	40	45	50	55	60	65
1	4	0	0	0	0	0	0	0
1.5	5	0	0	0	0	0	0	0
1.5	7	0	0	0	0	0	0	0
1.5	9	0	0	0	0	0	0	0
1.5	12.5	0	0	0	0	0	0	0
2	6	0	0	0	0	0	0	0
2.5	12.5	0	0	0	0	0	0	0
3	7	5	4	3	0	0	0	0
3	8	3	1	0	0	0	0	0
3	9	1	0	0	0	0	0	0
3	10	0	0	0	0	0	0	0
	Σ	9	5	3	0	0	0	0

7.5.6 Curved Hulled Catamaran with Dual Heaveplates

The dual heaveplate models analysed in this section are of a total area of 112m^2 at 0°, 22.5°, and 45° as they performed much better than the smaller ones in earlier testing Figure 7.10 shows the dual heaveplate model with horizontal heaveplates.

Table 7.10 shows similar results to Table 7.11 showing that the 22.5° model performs best. The reduction in heave damping and increase in surge load when the heaveplates are angled at 45° cause it to behave poorly compared to 22.5°.

Table 7.11 shows the maximum z motion of the dual heaveplate models set at varying angles; 0°, 22.5°, & 45°. The models performed similarly in terms of maximum motion with the 22.5° and 45° model generally performing better than the horizontal one. Examining the percentage of sea states that are accessible based on the limit of 1.5m presented in § 7.3 for maximum vertical movement, the 22.5° model performs best with 64% followed by the 45° model at 55% and

finally the horizontal mode with 36%.

Table 7.12 shows the relationship between the angle of the dual heaveplate setups and number of loss of contacts. As can be seen there is a slight reduction when moving to 22.5° but a large increase when moving to 45°. This can be attributed to the increase in wave load area when increasing to 45°.

Examining the pass or fail plot for the curved hulled catamaran with two heaveplates each set at 0, 22.5, and 45° in Figure 7.11 it discernible that the angle has a substantial influence on the overall performance of the WFSV. These tests were for 0° heading and a bollard pull of 35t. The curved hulled catamaran with dual heaveplates set at 22.5° passes for all the waves tested up to 2.5m Hs, and for an angle of 45°, while it passes the 2.5m Hs sea state at a 12.5s Tp at fails on the 2m Hs at a 6s Tp, a much steeper sea state.

Figure 7.10: Curved Hulled Catamaran with Dual Heaveplates 112m^2 0° at 12m Draught

Table 7.10: Vertical Slips Related to Angle of Heaveplate

Wave Condition		Angle		
Hs (m)	Tp (s)	0 deg	22.5 deg	45 deg
1	4	0	0	0
1.5	5	0	0	8
1.5	7	35	8	21
1.5	9	24	4	5
1.5	12.5	3	0	0
2	6	34	43	90
2.5	12.5	54	12	15
3	7	124	84	103
3	8	117	85	93
3	9	122	59	80
3	10	105	50	62
	Σ	618	345	477

Table 7.11: Maximum Vertical Movement Related to Angle of Heaveplate

Wave Condition		Angle		
Hs (m)	Tp (s)	0 deg	22.5 deg	45 deg
1	4	0.01	0.01	0.02
1.5	5	0.13	0.16	0.56
1.5	7	2.83	1.29	1.41
1.5	9	1.26	0.72	0.6
1.5	12.5	0.5	0.13	0.1
2	6	2.24	1.21	1.6
2.5	12.5	2.09	1.12	0.75
3	7	5.88	5.28	5.48
3	8	5.03	2.36	4
3	9	3.85	2.42	2.26
3	10	3.38	2.2	2.37

Table 7.12: X Direction Disconnects Related to Angle of Heaveplate

Wave Condition		Angle		
Hs (m)	Tp (s)	0 deg	22.5 deg	45 deg
1	4	0	0	0
1.5	5	0	0	0
1.5	7	0	0	1
1.5	9	0	0	0
1.5	12.5	0	0	0
2	6	5	0	5
2.5	12.5	0	0	5
3	7	11	9	29
3	8	9	20	37
3	9	9	22	27
3	10	6	12	12
	Σ	40	63	116

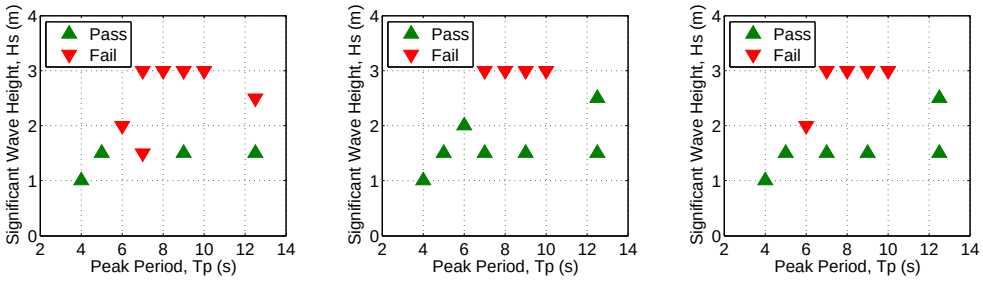

(a) 0° (b) 22.5° (c) 45°

Figure 7.11: Curved Hulled Catamaran with Dual Heaveplates of 112m^2 Performance while Interacting with the Monopile

7.6 Motions of a Catamaran WFSV Interacting with a Monopile at Varying Wave Headings

7.6.1 Introduction

In this section a directional study of the catamaran model used in these experiments was carried out to understand the catamarans performance and compare with the current literature allowing limits to be ratified for the experimental setup and allowing additional models to be compared with like for like experiments. In addition, the results in this section are aggregated in the development of polar performance plots in § 7.7. Operability diagrams are used in seakeeping analysis to show vessel limits in seas of differing conditions e.g. directional RAOs, the incidence of slamming events, the limit speeds the vessel may travel, or the accuracy with which station keeping may be maintained for a vessel using dynamic positioning (DP), these are often carried out using polar diagrams. In the following sections polar performance plots are used to represent the limit sea states with which transfers may be made to a turbine. These are discussed in greater detail in 2.7.

7.6.2 RMS and Maximum Motions Recorded

A standard 24m long catamaran with 2m wide demihulls was tested with different bollard pulls and directions to determine what the limitations were for a standard catamaran. In addition, these experiments provided a baseline for which to compare other models as the testing setup is similar.

Examining the case of the catamaran with varying angles with a 45t bollard pull it can be observed in Figure 7.14 that the catamaran is regularly exceeding 0.5m. As a 1.5m Hs is standard operating condition for a catamaran it was concluded that the dynamic friction between the fender and the monopile was too small. Setting the limit to 1.5m allowed 72.5% of the waves to pass the limit metric. The RMS of z motion was then set nominally at 0.5m. These limits were

additionally applied to the x and y motions.

The number disconnects in the X direction, and slips in the Y and Z directions were recorded. The minimum movement for a slip/disconnect was set at 0.01m model scale or 0.25m at full scale. The rational being that the marker that recorded motion of the vessel was slightly offset from the bow, hence there was always a residual motion from pitch motion. (The motion of the marker, point was analysed rather than the exact point of contact, as the model was rotating about the point of contact most of the time and when a disconnect occurred the model rotated about an unknown point determined by the mooring and the centre of gravity.)

Horizontal x motion and number of slips are graphed in Figure 7.12. The maximum x motion set at 1.5m is not exceeded. The RMS of x motion set at 0.5m is not surpassed. In Figure 7.13 the limits for y motion are not exceeded at all ad only of any significance for short beam and stern quartering sea states. In Figure 7.14 the z motion limit for maximum z motion is exceeded 72.5% as specified earlier the RMS of linear motion is not exceeded. The RMS of the x, y, and z motion follow a similar trend to the maximum motion or number of slips, and hence could be a predictor of loss of contact. A limit in the range of 0.15–0.25m may be more accurate than 0.5m but to accurately predict this more data would be required.

The angular motions were considered, examining Figure 7.16 it can be seen that the maximum roll and pitch motion is loosely linked to the x, y, and z motions. The RMS of angular motion as shown in Figure 7.15 these correlate well with maximal angular motions, the roll limit is far from exceeded and the pitch limit is exceeded on two occasions. In some instances, a large z motion is correlated with a large pitch angle.

Accelerations in the X, Y, Z, and resultant, (R) directions are displayed in Figures 7.18 & 7.17. These are very small and much less than suggested in the seaway at the forward perpendicular. This is due in part from the fact that the bow is maintaining position when docked at the monopile. the vertical move-

ments may be large but the acceleration is damped by the friction force. The results are similar to the positional results and showed the highest accelerations for Z and directions, slightly smaller for X directions and much smaller for Y directions. Again it can be seen that for larger accelerations both maximum and RMS values roughly correlate with large vertical slips. Installing accelometers on the bow of a vessel recording and presenting RMS and maximal acceleration to the bridge of the WFSV could provide useful information to making decisions whether or not a transfer should take place. Thus, it could be suggested to reduce these limits to reflect that, accelerations are inherently small but when they do happen they tend to correlate with other unwanted motions. Such as a large number of x disconnects, y or z slips, or a large linear motion.

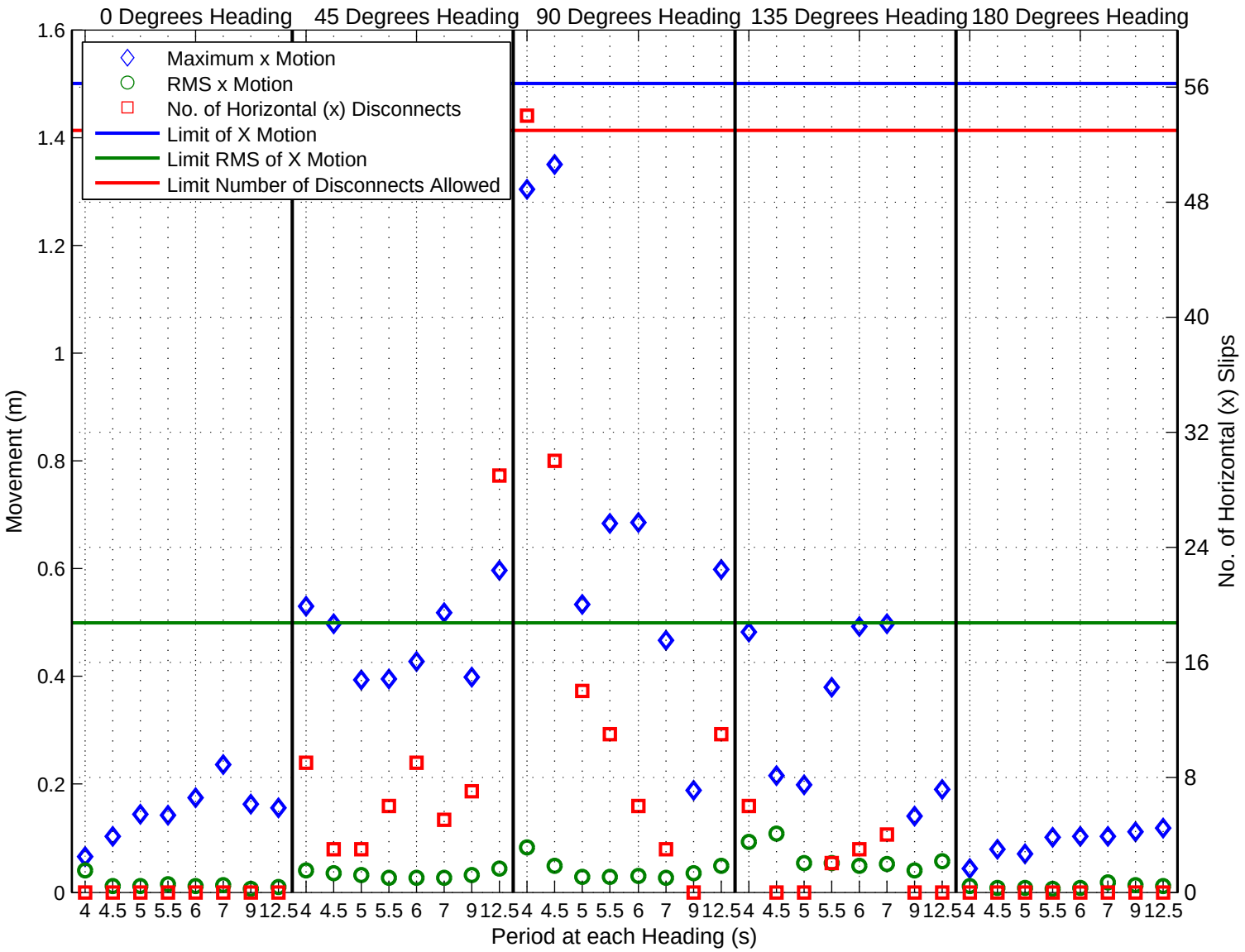

Figure 7.12: Catamaran XYZ Motion at the Monopile: X Directional Motion

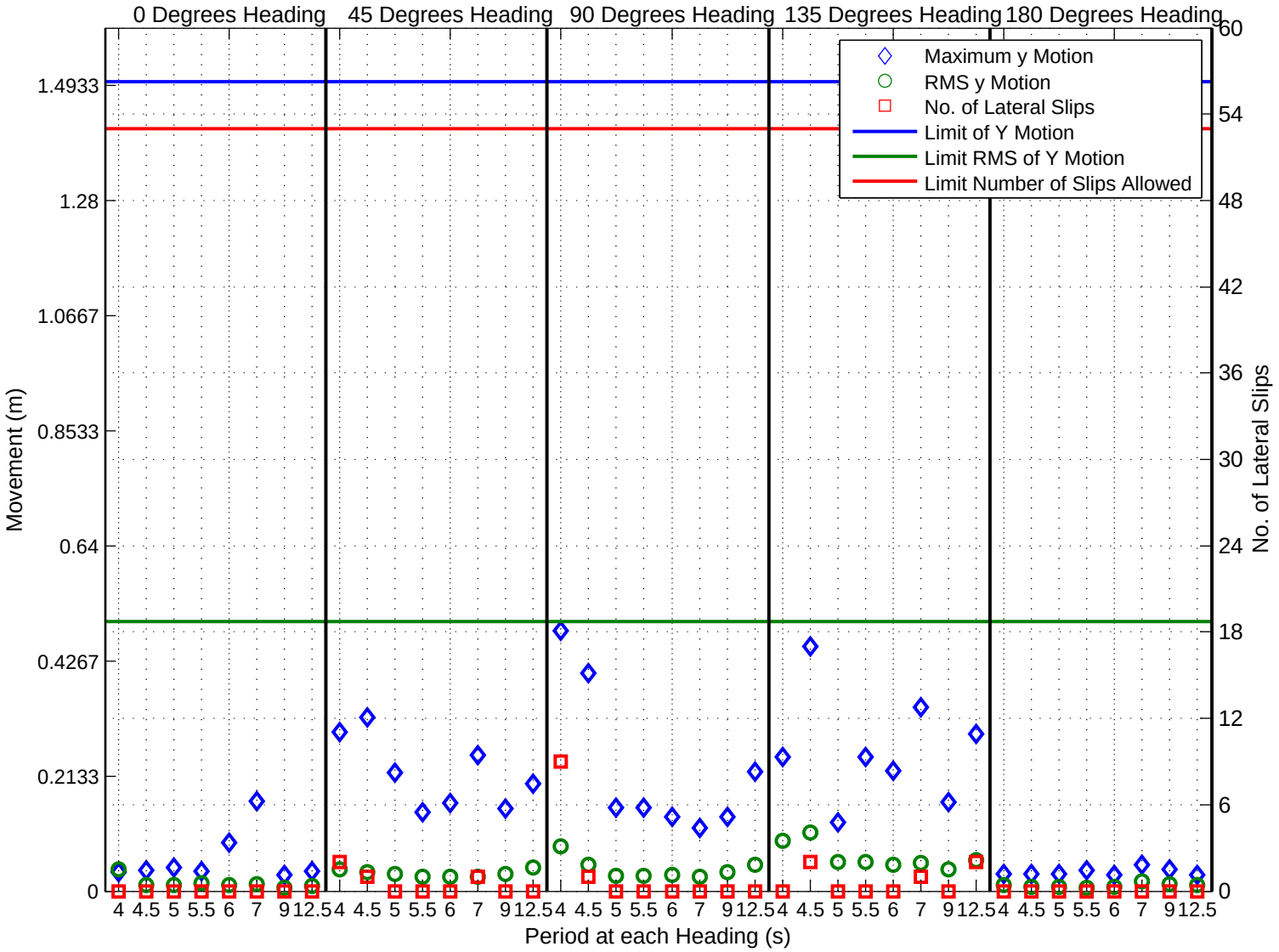

Figure 7.13: Catamaran XYZ Motion at the Monopile: Y Directional Motion

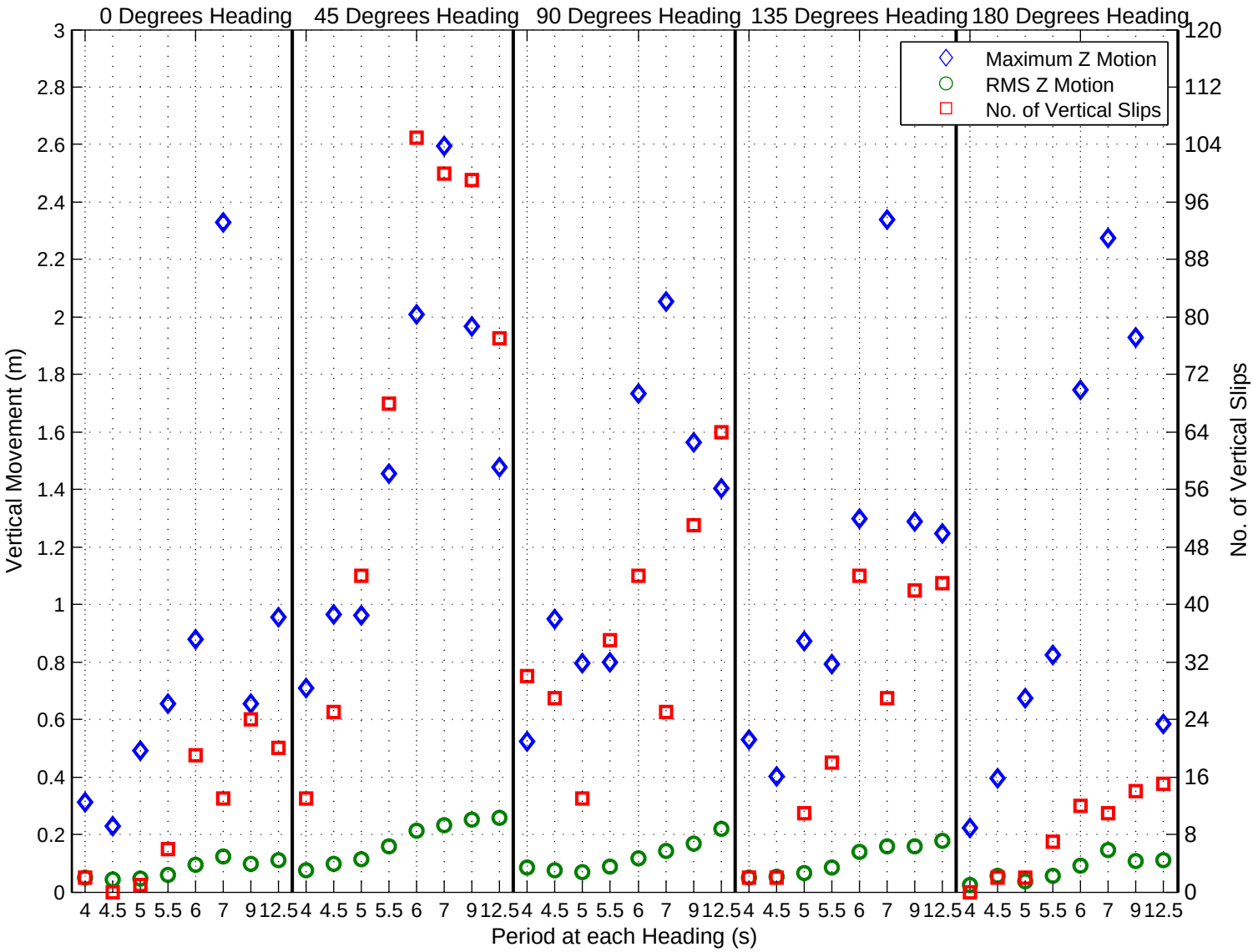

Figure 7.14: Catamaran XYZ Motion at the Monopile: Z Directional Motion

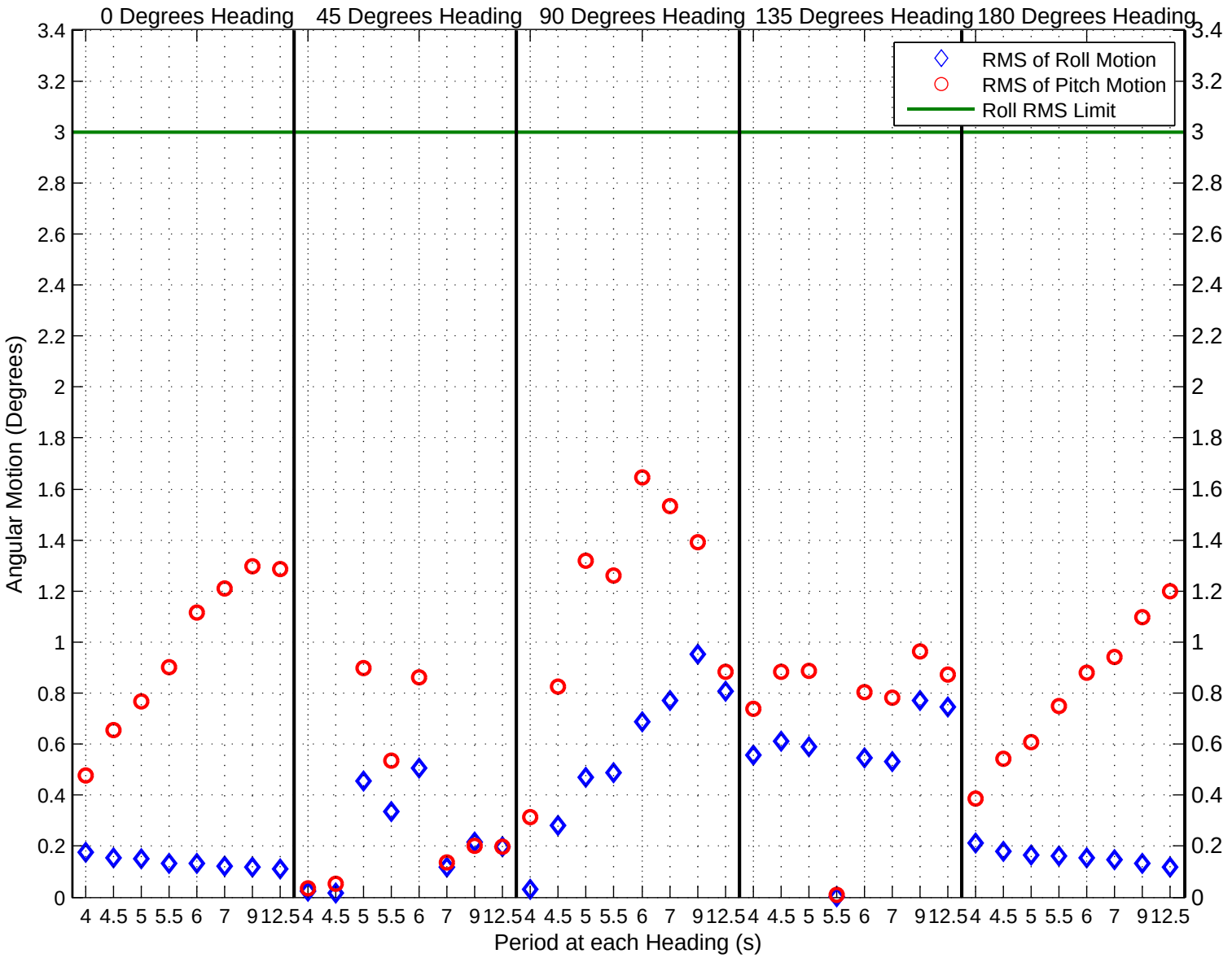

Figure 7.15: Catamaran Motion at the Monopile: RMS Angular Motion

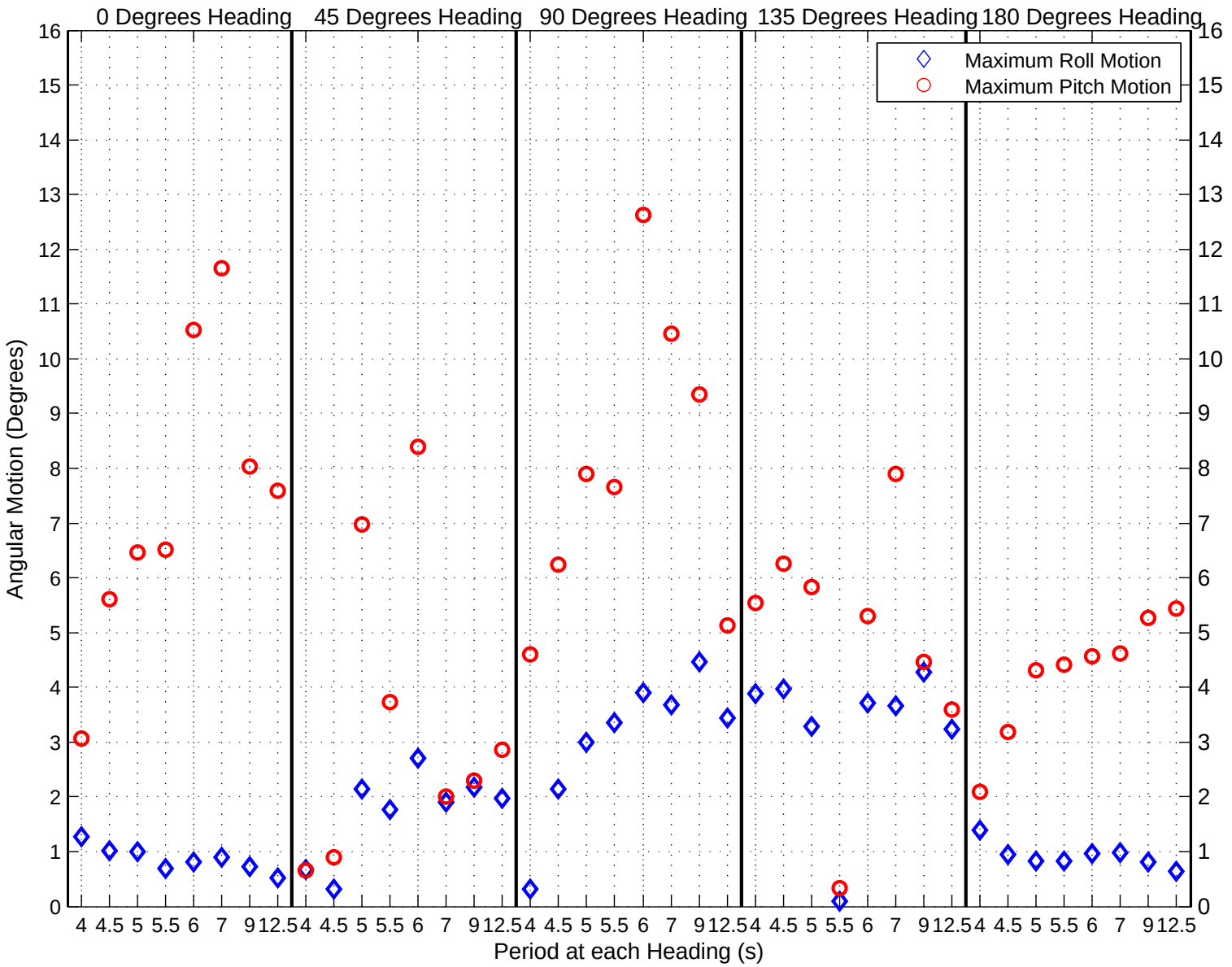

Figure 7.16: Catamaran XYZ Motion at the Monopile: Maximum Angular Motion

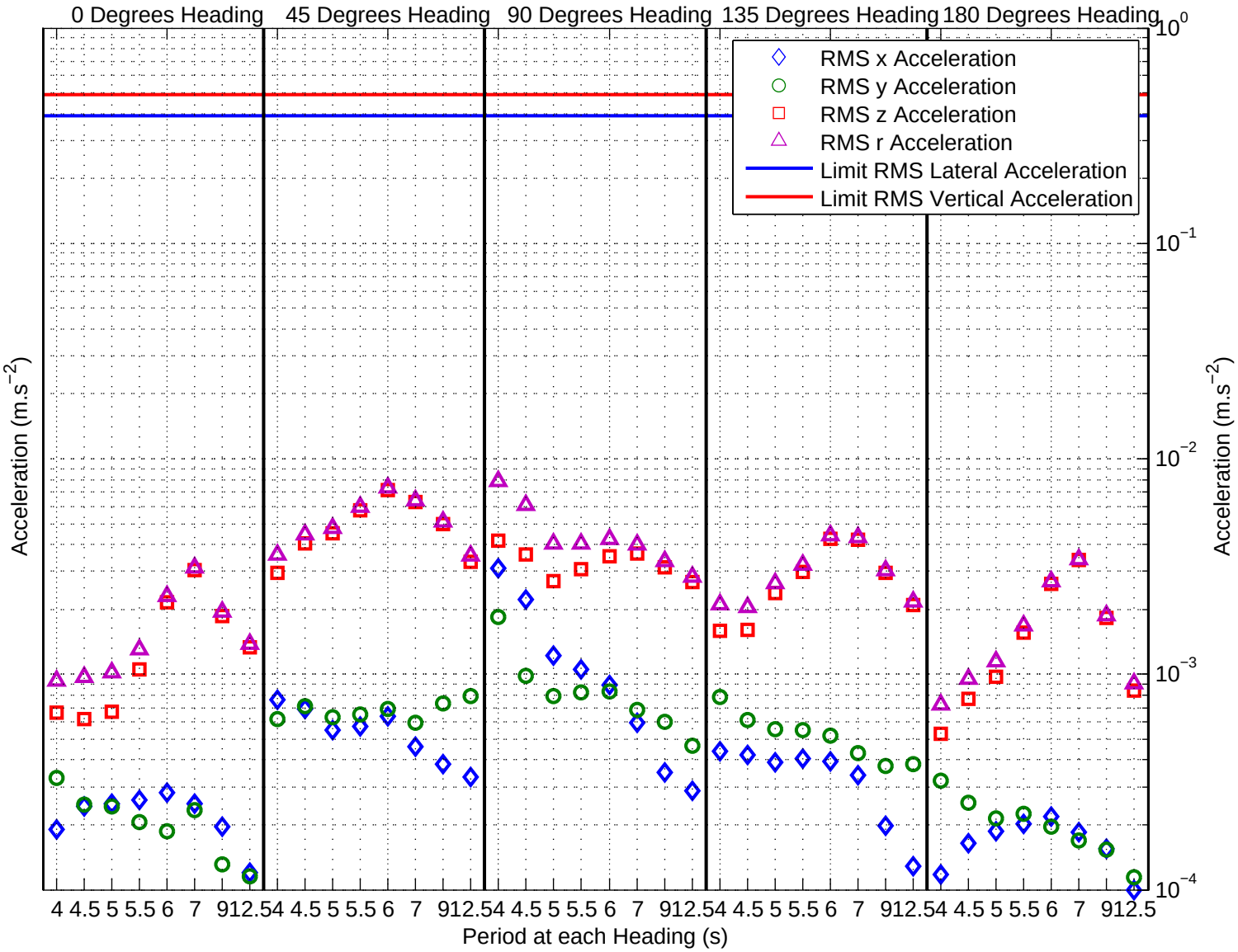

Figure 7.17: Catamaran XYZ Motion at the Monopile: RMS Acceleration

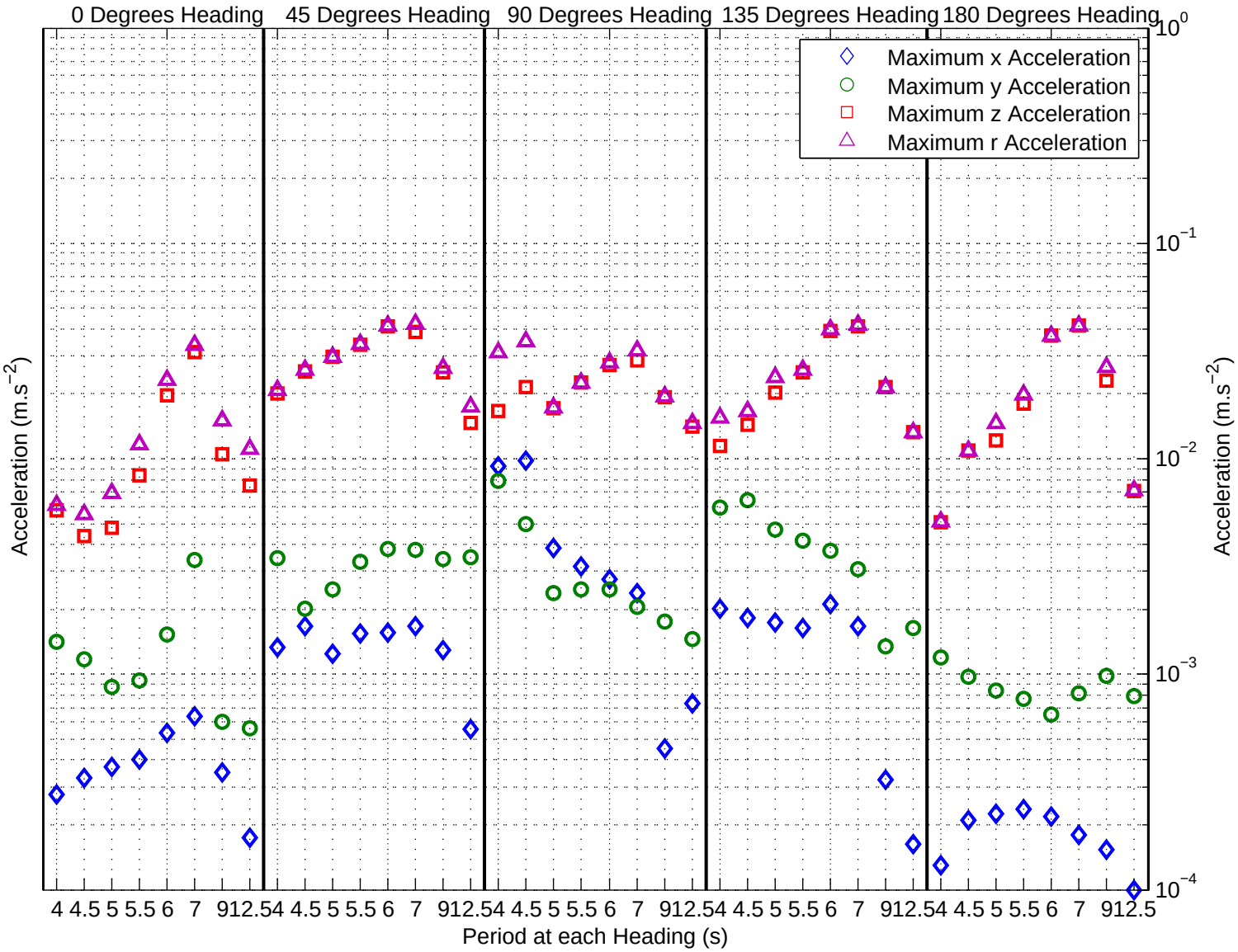

Figure 7.18: Catamaran XYZ Motion at the Monopile: Maximum Acceleration

7.6.3 Pass/Fail Graphs for a Standard Wide Hulled Catamaran WFSV with Varying Limits

By applying the limits estimated in the previous sections it is noticeable that the thresholds of limit motion have a large effect on the resulting accessibility, particularly with maximum linear movement and vertical slips, hence the limits were varied to check the effect on the resulting motion. The definitions of median, strict, and relaxed are given in the table 7.13

Table 7.13: WFSV Monopile Access Limits Sensitivity Analysis

Metric	Median Limits	Strict Limits	Relaxed Limits
Vertical and Lateral Slips	75%	80%	70%
Horizontal Disconnects	75%	80%	70%
RMS Linear movement	0.5m	0.4m	0.6m
Maximum Linear movement	1.5m	1m	2m
RMS Roll Limit	3°	3°	3°
RMS Lateral Acceleration	0.04g	0.04g	0.04g
RMS Vertical Acceleration	0.05g	0.05g	0.05g

Figures 7.20–7.23 represent the results of applying these limits to the standard catamaran tested. The bollard pull is significantly higher than standard, this is because it is one of the critical components determining the maximum sea state that a WFSV can operate in, hence it is a simple solution to increasing a catamarans performance [187]. In addition, the designs tested later in this section required a high bollard pull to successfully operate, therefore a high bollard pull was examined, so that the comparison between designs focused on hull design and not bollard pull.

Figure 7.20 shows how with this model setup at 0° the catamaran was able to carry out transfers in 50% of the wave series tested at 1.5m Hs with a 35t bollard pull. As the bollard pull was increased to 45t the steep 2m Hs wave passed. At

50t the long 2.5m Hs wave passed the required limits, though at 55t it fails by a small margin. Finally, with a 65t bollard pull the 3m Hs waves began passing.

The impact wave direction has on accessibility with a bollard pull of 45t, and the median limits shown in Figure 7.21 the following can be seen; In all cases the steep one metre wave passed. The periods of each of the 1.5m Hs was kept consistent allowing each heading to be compared accurately, the number of passes out of 8 for each heading for the set limits starting at 0° were, 7, 3, 3, 7, and 5 respectively. This shows that the heading angles of 45° and 90° are the most challenging for carrying out transfers, however given the nature of the mooring set up, it might be useful to compare with a self-propelled and steered model, as it has been previously demonstrated that a catamaran in quartering and beam waves performed much better than head or stern waves when interacting with a monopile, particularly for long period waves [88].

Varying the motion limits gives a clearer picture of the error range, this sensitivity analysis of was carried out for five different wave headings from 0 to 180°. Figures 7.22 & 7.23 show the results of using strict and relaxed limits as per Table 7.13. When comparing the pass/fail plots for the baseline median limits in Figure 7.21 against the strict and relaxed limits in Figures 7.22 & 7.23 it can be seen that increasing and decreasing the limit motions that may be sustained is reflected in the amount of sea states that a WFSV can access a monopile. This demonstrates the consequence limits have on the accessibility of a monopile. Thus, further full scale studies are required to determine which motions are actually safe/unsafe.

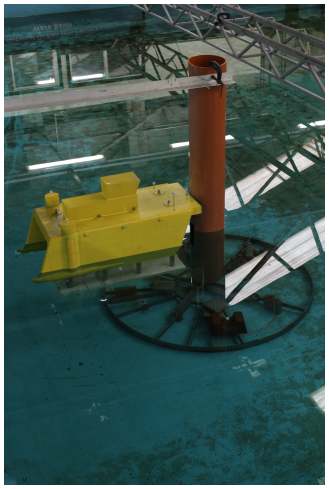

Figure 7.19: GDC Model Docked with the Monopile, Still Water

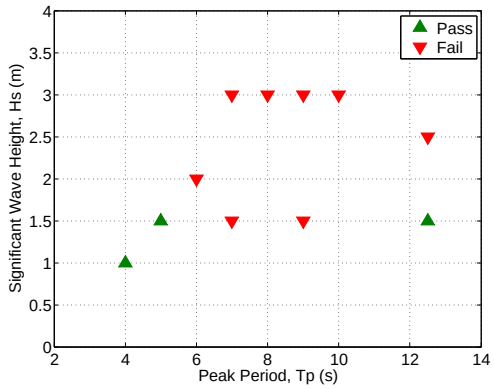

(a) 35t Bollard Pull

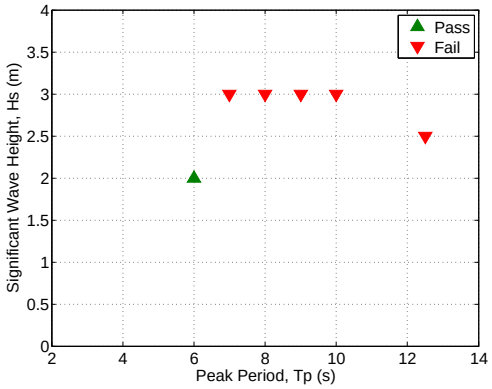

(b) 45t Bollard Pull

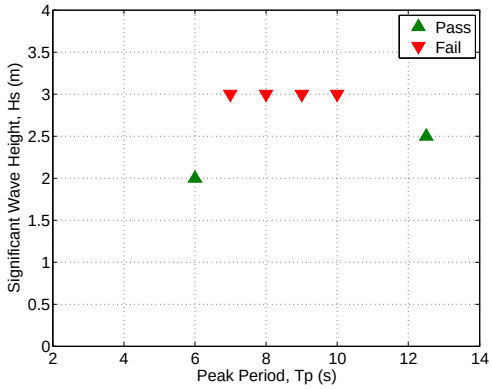

(c) 50t Bollard Pull

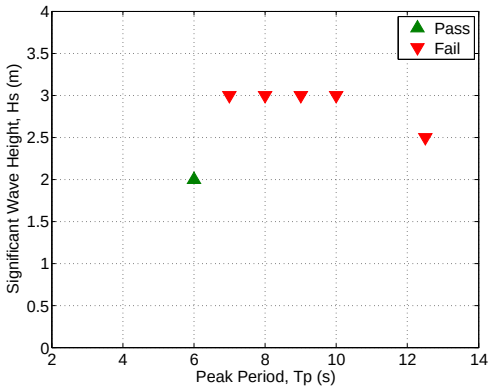

(d) 55t Bollard Pull

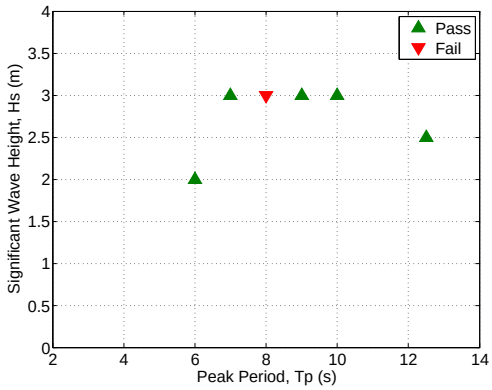

(e) 65t Bollard Pull

Figure 7.20: Bollard Pull Influence on a Standard Catamaran Performance while Interacting with the Monopile (Median Limits)

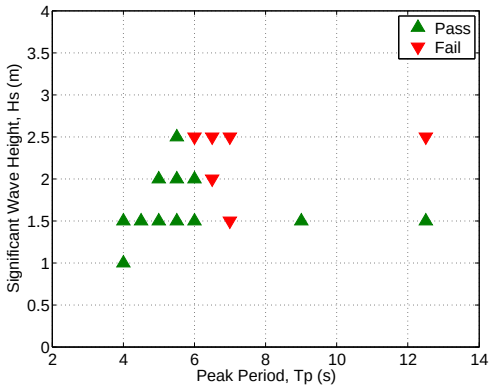

(a) 0° Heading to Monopile

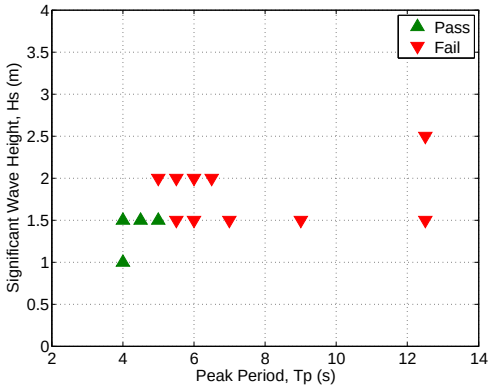

(b) 45° Heading to Monopile

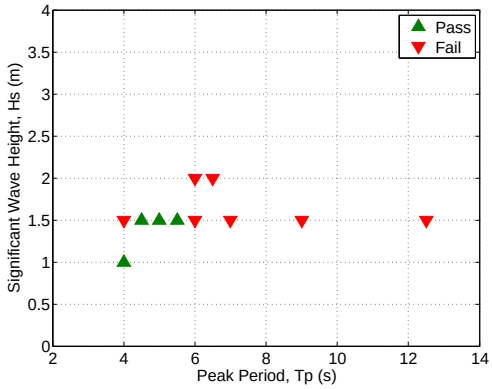

(c) 90° Heading to Monopile

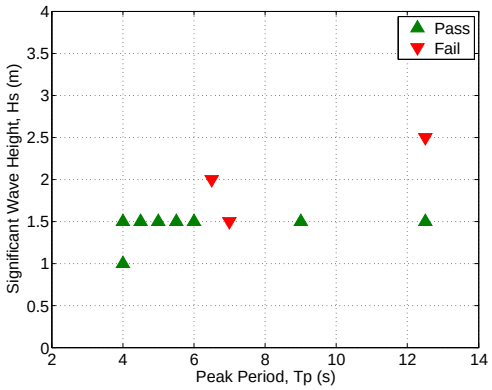

(d) 135° Heading to Monopile

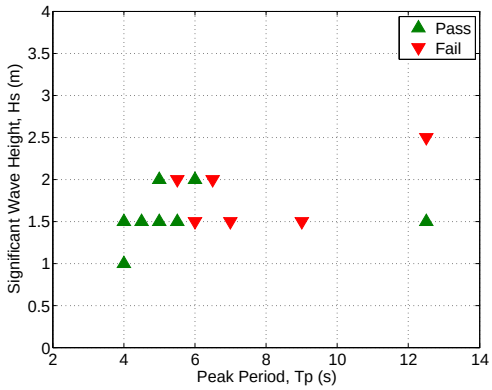

(e) 180° Heading to Monopile

Figure 7.21: Standard Catamaran Performance while Interacting with the Monopile with a 45t Bollard Pull with Median Limits

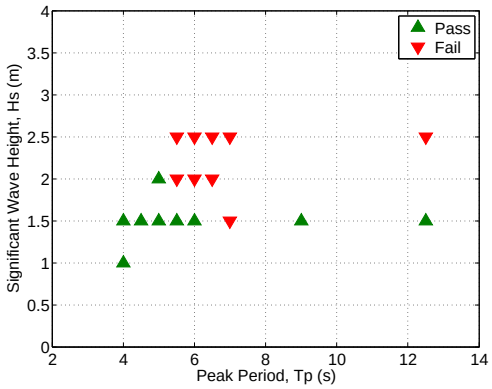

(a) 0° Heading to Monopile

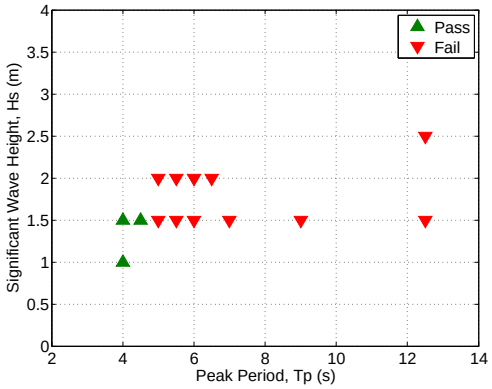

(b) 45° Heading to Monopile

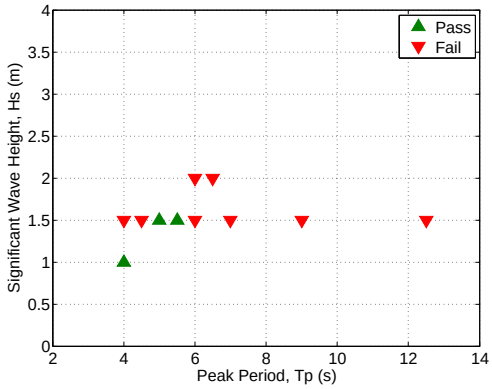

(c) 90° Heading to Monopile

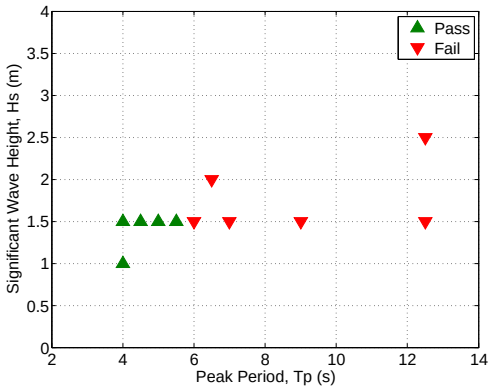

(d) 135° Heading to Monopile

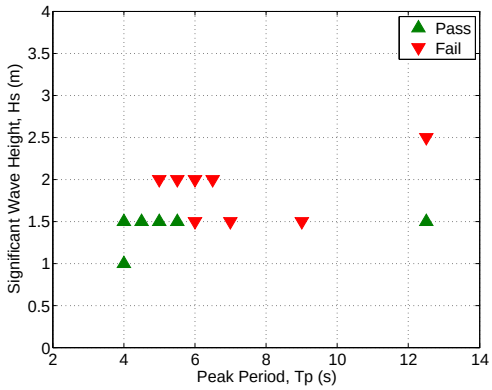

(e) 180° Heading to Monopile

Figure 7.22: Standard Catamaran Performance while Interacting with the Monopile with a 45t Bollard Pull with Strict Limits

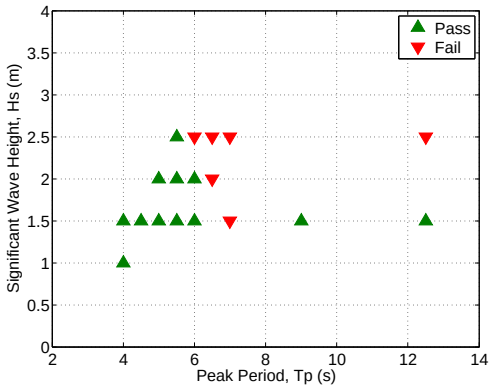

(a) 0° Heading to Monopile

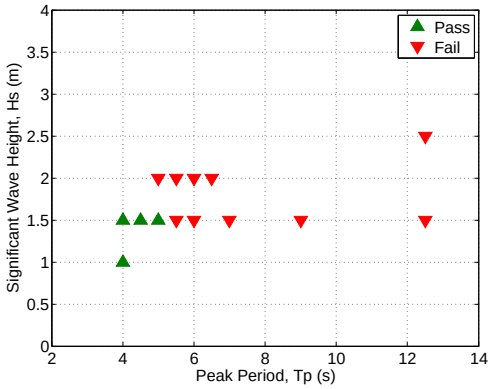

(b) 45° Heading to Monopile

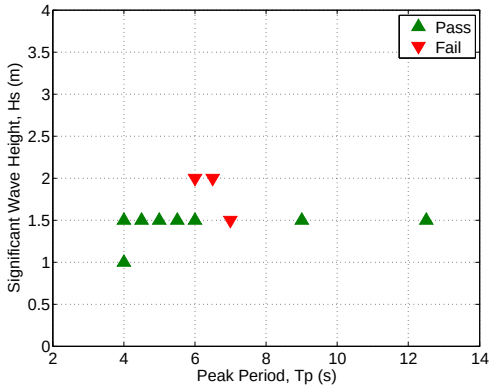

(c) 90° Heading to Monopile

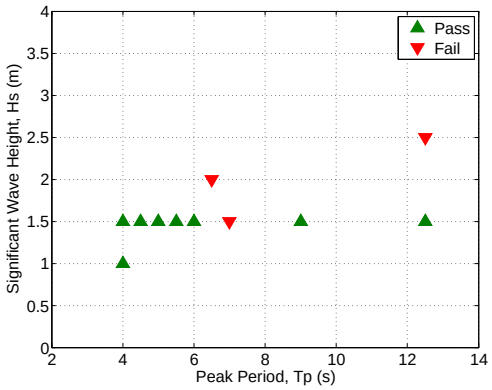

(d) 135° Heading to Monopile

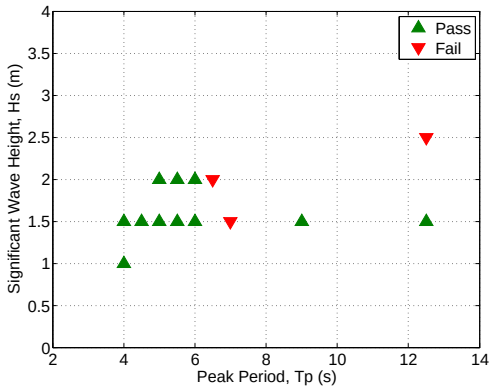

(e) 180° Heading to Monopile

Figure 7.23: Standard Catamaran Performance while Interacting with the Monopile with a 45t Bollard Pull with Relaxed Limits

7.7 Development of Polar Performance Plots

In this section the GDC model is used to compare a novel WFSV with that of a catamaran WFSV performance while docked at a monopile. To compare WFSV performance it has been proposed [20, 86, 87, 88, 89] that performance plots be used as discussed in § 2.7 earlier. Operability diagrams are often used in seakeeping analysis to represent the variability of operational limits in seas of differing headings, these are often carried out using polar plots. These plots are used to represent a wide variety of seakeeping parameters such as directional RAOs, the incidence of slamming events, the limit speeds the vessel may travel, or the accuracy with which station keeping may be maintained for a vessel using dynamic positioning (DP). In this instance polar plots are used to represent the limit sea states with which transfers may be made to a turbine.

In Figure 7.24 the performance plots for the GDC and catamaran are presented, showing the significant wave height at varying angles that they can transfer personnel safety. The motions of the GDC at headings from 0 to 180° in 45° steps (each tested in a similar setup to Figures 7.19, 7.25 in the wave basin.) are represented in Figures 7.26 & 7.27 for 35 and 45t bollard pulls.

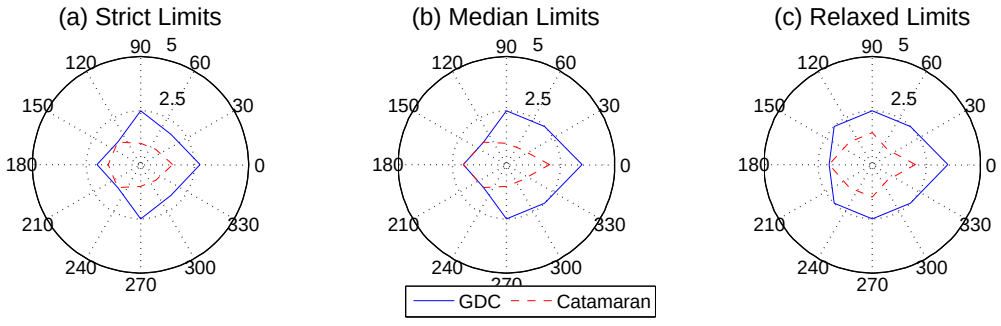

Figure 7.24: Performance Plot, Showing Hs (m) Plotted Against Heading angle, (°)

The performance plots were created by aggregating the outputs for 35t and 45t bollard pull from Figures 7.26–7.31, by representing a 50% pass rate for the wave conditions tested. Both the GDC and catamaran had a similar setup, with

the same bollard pull and fender material. The sensitivity analysis data is also represented in Figure 7.24.

From Figure 7.24 it can be observed that the catamaran performs well in head seas and struggles with beam and quartering seas. Examining Figures 7.28–7.31 it is evident how varying the threshold of limit motion that the vessel can operate effects the resulting limit access Hs for each direction, similar to § 7.13. It can be observed that with the current limits the results are very similar, except for bow quartering seas which seem to reduce with increased bollard pull, and beam and stern quartering seas which increase with increased bollard pull. The performance limits that the GDC can provide a safe access is dependent on wave heading, ranging from 1.5m Hs to 3.5m Hs. The GDC performance excels in seas with a heading from 0–90 degrees. Though its performance is limited in stern and stern quartering seas.

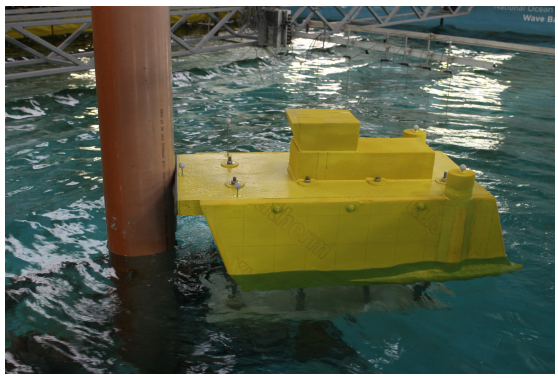

(a) Quartering Seas

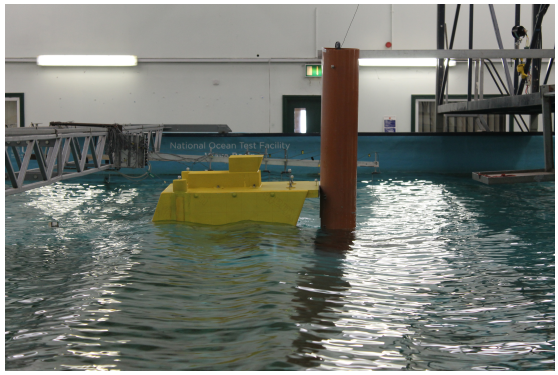

(b) Stern Seas

Figure 7.25: GDC Model Docked with the Monopile

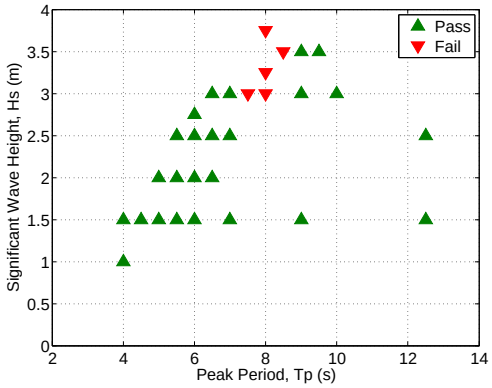

(a) 0° Heading to Monopile 35t Bollard Pull

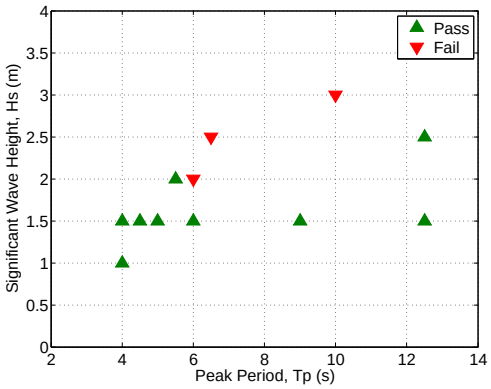

(b) 45° Heading to Monopile 35t Bollard Pull

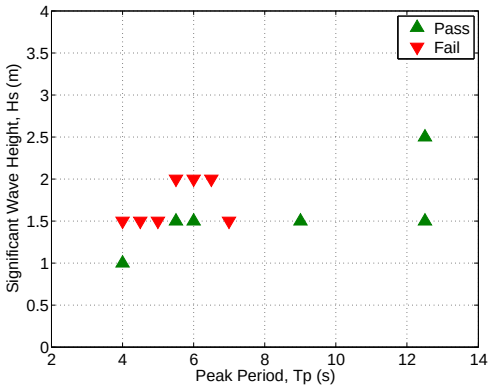

(c) 90° Heading to Monopile 35t Bollard Pull

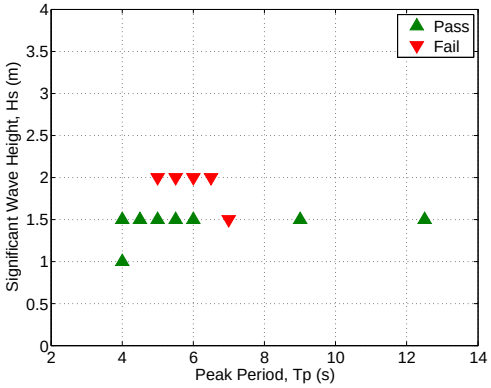

(d) 135° Heading to Monopile 35t Bollard Pull

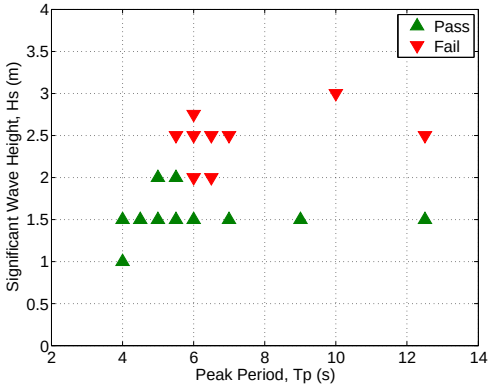

(e) 180° Heading to Monopile 35t Bollard Pull

Figure 7.26: GDC Performance while Interacting with the Monopile 35t Bollard Pull with Median Limits

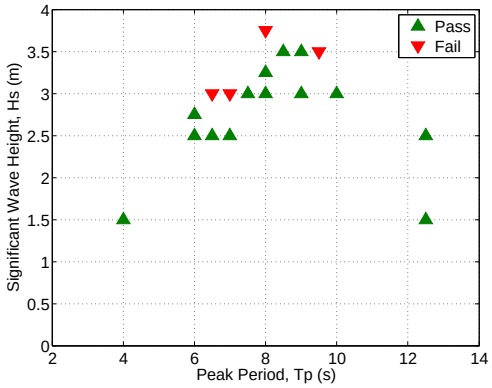

(a) 0° Heading to Monopile 45t Bollard Pull

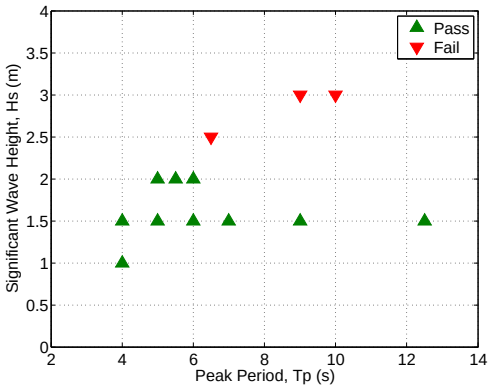

(b) 45° Heading to Monopile 45t Bollard Pull

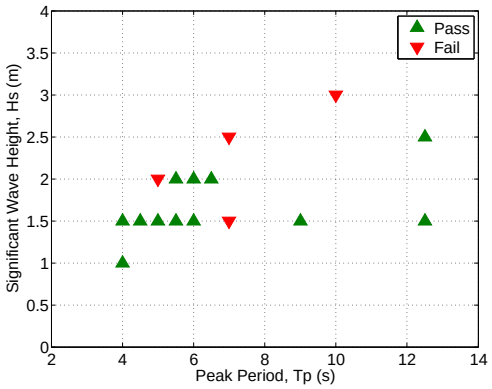

(c) 90° Heading to Monopile 45t Bollard Pull

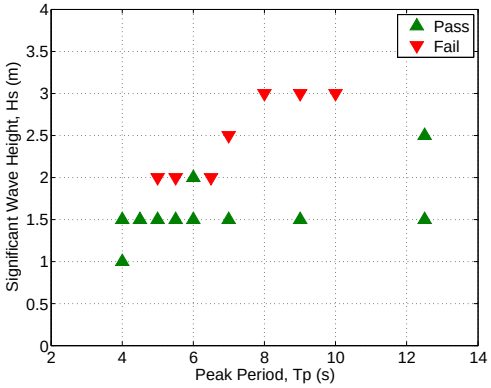

(d) 135° Heading to Monopile 45t Bollard Pull

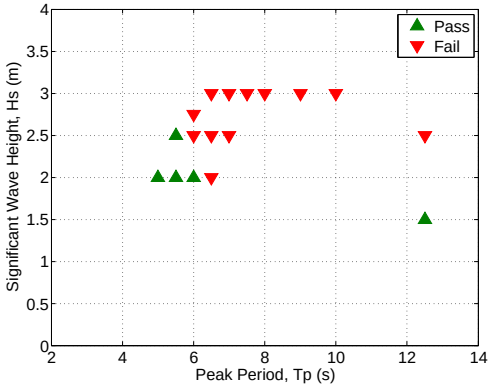

(e) 180° Heading to Monopile 45t Bollard Pull

Figure 7.27: GDC Performance while Interacting with the Monopile 45t Bollard Pull with Median Limits

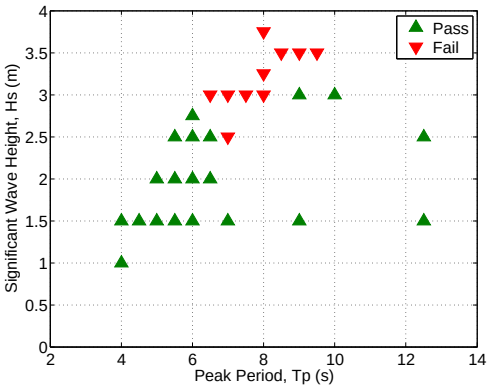

(a) 0° Heading to Monopile

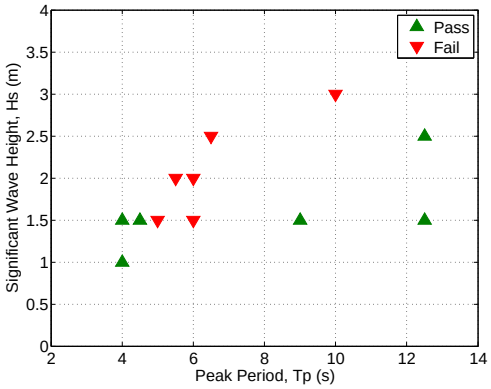

(b) 45° Heading to Monopile

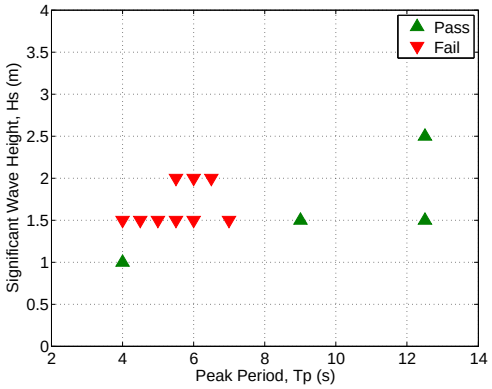

(c) 90° Heading to Monopile

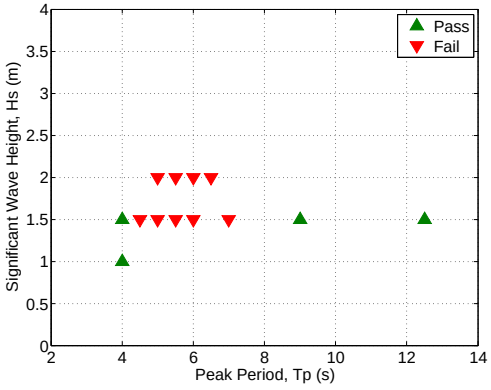

(d) 135° Heading to Monopile

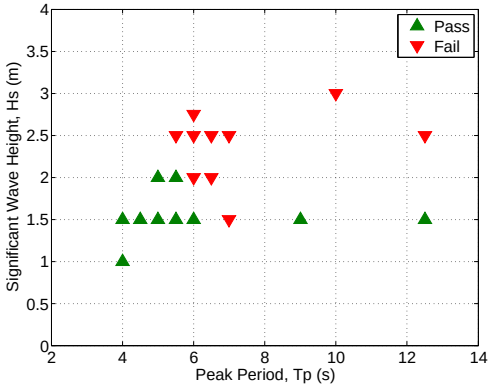

(e) 180° Heading to Monopile

Figure 7.28: GDC Performance while Interacting with the Monopile 35t Bollard Pull with Strict Limits

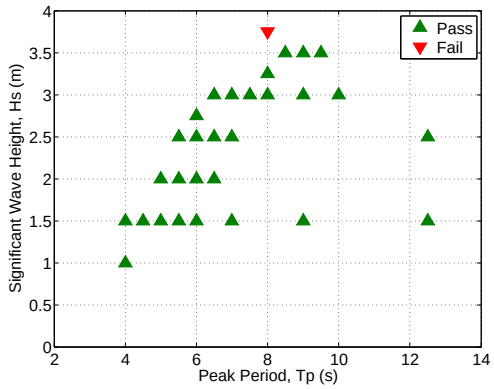

(a) 0° Heading to Monopile

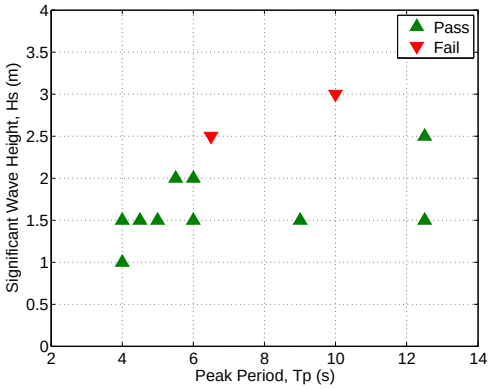

(b) 45° Heading to Monopile

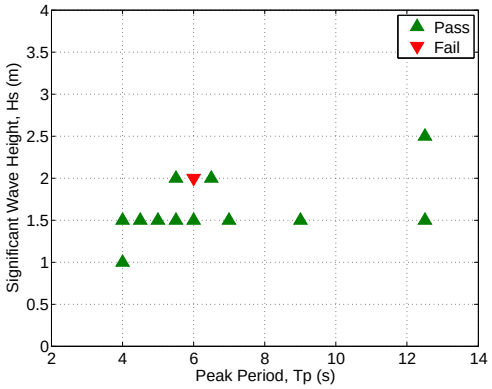

(c) 90° Heading to Monopile

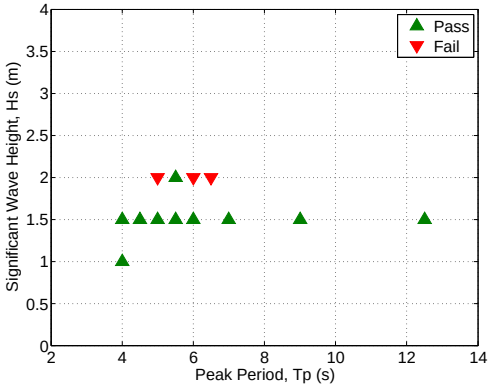

(d) 135° Heading to Monopile

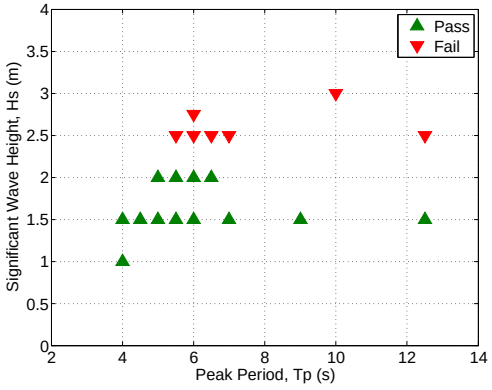

(e) 180° Heading to Monopile

Figure 7.29: GDC Performance while Interacting with the Monopile 35t Bollard Pull with Relaxed Limits

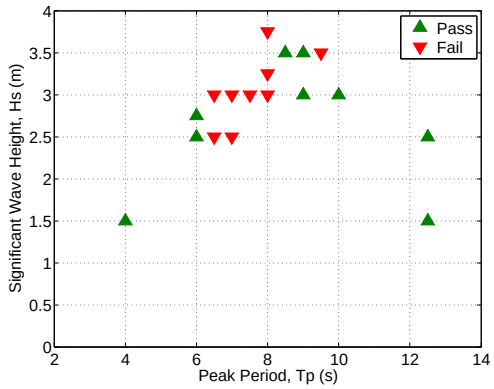

(a) 0° Heading to Monopile

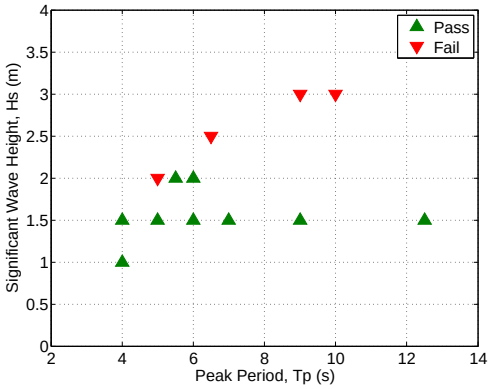

(b) 45° Heading to Monopile

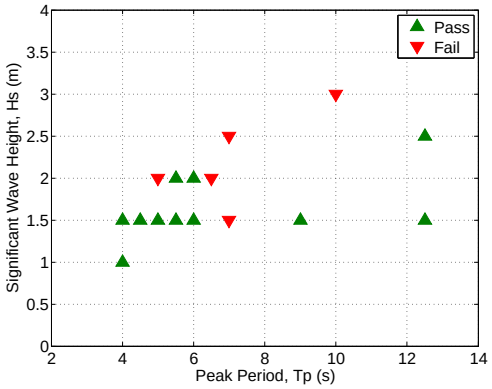

(c) 90° Heading to Monopile

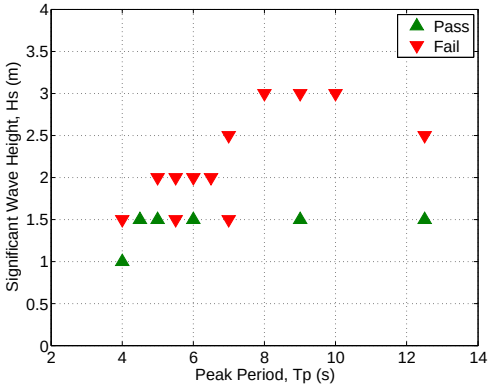

(d) 135° Heading to Monopile

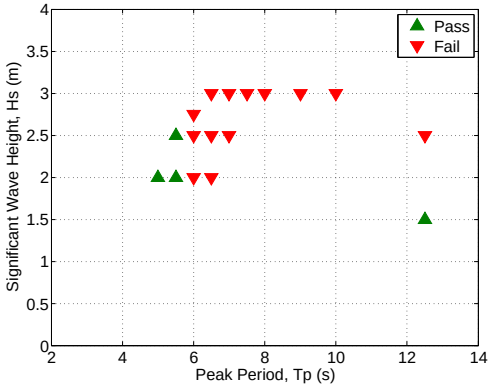

(e) 180° Heading to Monopile

Figure 7.30: GDC Performance while Interacting with the Monopile 45t Bollard Pull with Strict Limits

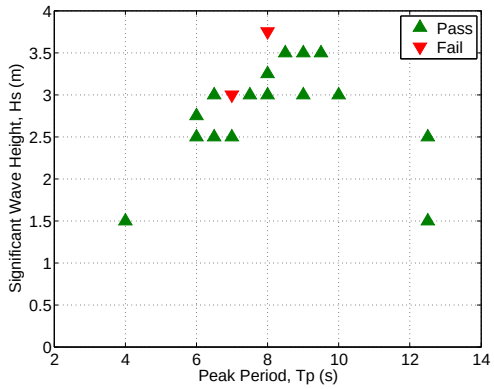

(a) 0° Heading to Monopile

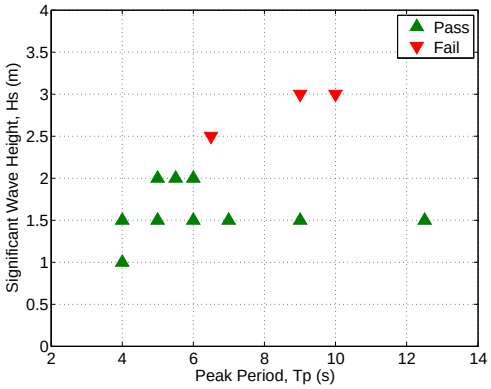

(b) 45° Heading to Monopile

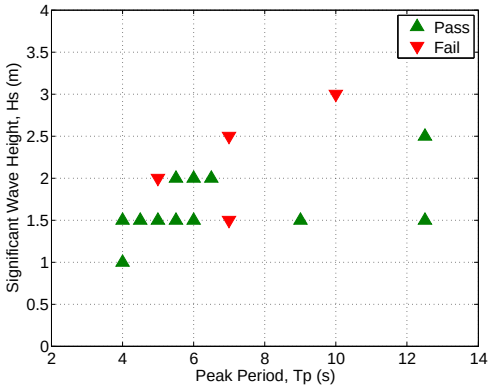

(c) 90° Heading to Monopile

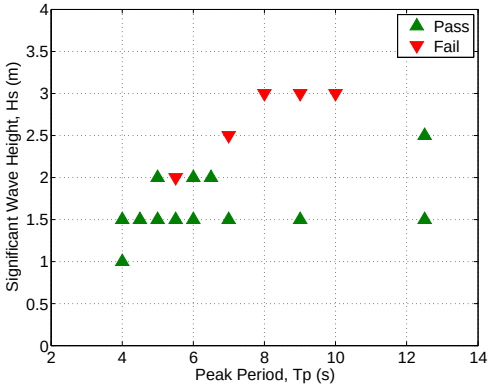

(d) 135° Heading to Monopile

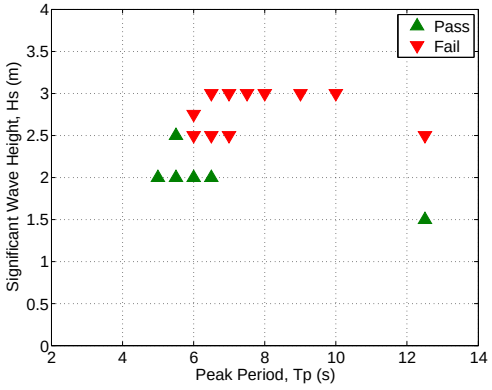

(e) 180° Heading to Monopile

Figure 7.31: GDC Performance while Interacting with the Monopile 45t Bollard Pull with Relaxed Limits

7.8 Estimation of Operational Limits from RAO Data

This section aims to compare the zero forward speed motion of a WFSV with that of the WFSVs interaction with the monopile, in order to have an estimation of the possibility of a transfer based on the WFSVs behaviour prior to making contact with the monopile.

By comparing the limits presented in Table 5.4 of § 5.7 with the figures in the same section it can be seen that the MII limits are rarely exceeded and that the acceleration and pitch limits are regularly exceeded. Comparing these cases to the pass or fail analysis at the monopile it can then be examined if these are useful metrics with which to estimate the possibility of a transfer. When the limits in Table 7.1 are compared with the tables and figures in this chapter in particular the pass/fail charts for head seas a number of conclusions can be made. In particular with reference to the estimation of the possibility of a transfer based on the zero forward speed motion of the vessel the following can be seen:

For the standard catamaran at 0° as seen in Figures 7.20,7.21a, 7.22a & 7.23a when compared with Figure 5.22 it can be seen that the MII at the forward perpendicular and RMS of vertical and horizontal acceleration at the COG are poor indicators of a transfer outcome as they all pass up to a 3m Hs, however the RMS of pitch angle fails for a 2m Hs with a 6s Tp and at a 3m Hs it also fails for 7, 8, & 9s Tp. For the pass fail charts in Figures 7.20,7.21a, 7.22a & 7.23a it can be seen that a 2m Hs with a 6s Tp at 0° fails for a 35t bollard pull at 0° and passes for higher bollard pulls. When examining other directions, the 2m Hs with a 6s Tp is the cut off point for performance with it failing at 45, 90 and 135° headings with median limits in Figure 7.21a. For stricter limits it fails for all headings and passes for more headings for relaxed limits failing for 45 & 90°. The waves at 3m Hs and a 7, 8, & 9s Tp all either failed or were not tested when interacting with the monopile as smaller waves had failed, the only case some of them passed was with a 65t bollard pull. The sea state 2.5m Hs at a 12.5s Tp passed the RMS of pitch requirement whilst at zero forward speed however on

passed the interaction with the monopile limits at 0° and the high bollard pulls of 50 & 65t. In addition, a number of waves at a 1.5m Hs waves failed the limits for interaction with the monopile. From this comparison it can be concluded that the zero forward speed motion of a catamaran WFSV gives an estimation of whether a transfer may take place but is not accurate for all cases.

The zero forward speed motion metrics and the interaction with the monopile of the curved hulled catamaran with a 178.5m^2 heaveplate at depths of 6, 9, and 12m is shown in Figures 5.27, 5.28, & 5.29 and Figure 7.7 respectively. The fail cases with zero forward speed motion were 3m Hs at 8, 9, & 10s Tp and 2.5m Hs at a 12.5s Tp. However, when interacting with the monopile at 0° with a 35t bollard pull it can be seen that the 2.5m Hs at a 12.5s Tp sea state passes for all heaveplate depths. The performance at a 3m Hs fails for all cases at a 6m depth and the performance improves as the heaveplate depth increases, this is not reflected in the zero forward speed motion metrics. Similar to the catamaran performance at the monopile is not accurately predicted by the zero forward speed motion characteristics.

The zero forward speed motion metrics and the interaction with the monopile of the curved hulled catamaran with dual heaveplates of 112m^2 at 0° heading are presented in Figures 5.34, 5.35, & 5.36 and 7.11a, 7.11b, & 7.11c respectively. For the 0° case the fail cases at 3m and 2.5m Hs were predicted by the zero forward speed characteristics, however the fail cases at 2m Hs at 6s Tp and 1.5m Hs at 7s Tp were not predicted. For the 22.5° heaveplate inclination the fail cases at 3m Hs were predicted by the zero forward speed characteristics, though the 2m Hs at 6s Tp and 1.5m Hs at 12.5s Tp failed for the RMS of acceleration at the COG they passed when interacting with the monopile. For the final case of the dual heaveplate inclined at 45° all the fail cases at the monopile are predicted by the zero forward speed motion characteristics.

The zero forward speed motion metrics is shown in Figure 5.30 and the interaction with the monopile of the GDC is illustrated in Figures 7.26–7.31. The GDC performs very well in the zero forward speed scenario failing for RMS of

pitch for a 3.5m Hs at 9.5s Tp. For similar sea states when applying a thrust on the monopile it can be seen that the GDC performs well with a 0° heading, failing for a small number of the higher sea states. Similar to the previous cases it can be seen that zero forward speed motion of the WFSV is indicative of performance at the monopile but not an accurate estimation of its performance.

7.9 Discussion

This chapter examined the interaction of a WFSV with a monopile. The results were for the general low frequency motions of a ship were considered. The limits for a safe step across transfer, vessel response in the wake of a monopile, aspects of a WFSV interacting with a monopile in head seas, as well as a directional study that lead to the development of performance plots were presented in this chapter.

The vessel response in the wake of a monopile was investigated in § 7.4 using the amplitude data for the waves recorded without a monopile present. Overall, the response for a vessel in open waters to those in the wake of a monopile are for all intents and purposes the same as the small differences could be attributed to experimental error. Given that for most wave conditions tested, the monopile could be classed as a slender body this was expected. Hence, wave climate in the wake of a monopile was found to not have a meaningful result on the motion of the tubular multihull tested. However, this does not negate the difficulties in manoeuvring due to the slightly more erratic, and turbulent sea found in the wake of the monopile.

The limits for carrying out a transfer published in the literature were examined. The maximum x, y and z limits were found to be in disagreement with the model tests carried out at a 1.5m Hs, the industry standard, possibly due to low fender friction. New limits were estimated and implemented accordingly, so that the different model tests in this thesis could be compared with like for like experiments. Sensitivity analysis was carried out on these limits, allowing a

maximum movement of 1, 1.5, and 2m respectively. The confidence limit that vertical slips and horizontal disconnects would not occur were also varied from 70–80%. A maximum allowable movement of 1.5m and a confidence limit of 75% for vertical slips and horizontal disconnects was found to be comparable to the literature for the standard catamaran design tested.

The hull geometry influence on performance metrics was examined with vertical slips and horizontal disconnects and maximum movement in those directions. An increase in heaveplate depth had a positive effect on vertical motion, reducing the number of vertical slips, but a negative effect on horizontal motion, increasing the number of horizontal disconnects occurring.

For the case with dual heaveplates set at angles of 0°, 22.5°, and 45° respectively it can be observed that in general the 22.5° angle performs best when reducing the number of loss of contact instances and maximum vertical movement.

Investigating the two variables of heaveplate depth and bollard pull concurrently it can be seen that though an increase in bollard pull, or an increase in the depth of the heaveplate generally provides an increase in performance, this is not always the case. There appears to be a point for each configuration after which any additional increase in bollard pull or depth is not advantageous and in quite a few cases actually became worse. Highlighting diminishing returns of increasing improvements beyond a set point.

A directional study was carried out on the GDC model and compared with the standard catamaran model tested under similar conditions. Variation of threshold limits to transfer was carried out strict, median, and relaxed limits were examined graphically showing pass or fail output for the wave conditions tested. Two bollard pull conditions were examined 35t and 45t. The GDC is best utilised with a bollard pull of 45t and a 360 Performance Plot comparing it to the catamaran shows this in Figure 7.24. The lines plotted are for a 50% or greater pass rate for the sea states tested at that heading. This provides a quantitative method of comparing WFSV interaction with a monopile. Increasing the number

of wave conditions and heading angles tested would improve the accuracy of the comparison.

Finally, an attempt at estimating the WFSV to monopile transfer operation limits from the RAO data was carried out by comparing metrics of the zero forward speed motion of a WFSV with the pass and fail cases when interacting with the monopile. However, the data presented here showed to be inconclusive to determine a clear relationship. In some cases, the fail cases were predicted and in others they were not.

Chapter 8

Conclusions and Suggestions for Further Research

8.1 Introduction

The offshore wind industry is at a time of rapid expansion, increasing the need to have a clearer understanding of the hydrodynamics of the interaction of a WFSV with an offshore wind farm monopile foundation. As wind farms move into deeper, stormier, further offshore locations the availability of weather windows below 1.5m Hs will reduce, and the requirement for vessels that exceed this limit will increase. This thesis improved this understanding, allowing vessels to safely access wind turbines in higher sea states, through the numerical and physical modelling of WFSVs.

The motions of a WFSV at zero forward speed were investigated, and the limiting metrics for deck operations were determined in relation to a WFSV. The nature of a WFSV interaction with a monopile was studied and the limiting metrics for a step across transfer were examined. A generic WFSV design was considered as well as a number of vessels with innovative hull designs to increase the Hs in which transfers can take place. The importance of vessel shape and the addition of heaveplates on improving the performance of WFSVs were analysed. The magnitude of each design's motion was quantified and compared.

8.2 Interaction of a WFSV with a Monopile

The interaction of a WFSV with a monopile was examined in detail in this thesis, in particular, the following aspects were examined; the vessel response in the wake of a monopile, the limits on a safe step across transfer, the importance of hull shape, bollard pull, heaveplate arrangement, and wave direction. The following items were concluded from these experiments:

1. The WFSV response in the wake of a monopile was not found to be significantly different to that in the open seaway. Though this does not negate the difficulties in manoeuvring due to the slightly more erratic, and turbulent sea found in the wake of the monopile.
2. Adding heave damping with heaveplates provides benefits for a WFSVs docking operation, however increasing heave damping changes the principal fail condition from vertical slips to horizontal disconnects. For example, increasing the bollard pull from 35 to 45t reduced the number of vertical slips by 70%, and the number of horizontal axial disconnects by 44% for the Curved Hulled Catamaran with a 178.5m^2 Heaveplate at 12m Draught. In addition, for the Curved Hulled Catamaran when increasing the heaveplate depth from 6m to 12m there is a 66% reduction of vertical slips.

8.3 WFSV Operational Limits

Quantifying the operational limits of a WFSV can give better prediction of weather windows, enabling more efficient use of resources, in addition safer operations can be achieved. This research focused on the limits of zero forward speed motion of the WFSV to simulate a WFSV considering docking with a monopile, and the limits at time of transfer when docked. For the designs tested in this thesis, the following conclusions were drawn;

1. The most relevant metrics for zero forward speed motion were a MII and RMS of vertical acceleration at the forward perpendicular, RMS of vertical

acceleration at the COG, and RMS of pitch angle. These limits are less than the limit motions for ships in transit because when the WFSV approaches the monopile manoeuvrability is critical, and in the case where the WFSV must manoeuvre away from the monopile at short notice there may be crew or technicians on the foredeck. The following vessel motion limits applied to WFSVs studied in this research:

(a) MII limit: 0.1–0.5 tips per minute.

(b) RMS of vertical acceleration at the forward perpendicular: 0.15g.

(c) RMS vertical acceleration at the COG: 0.05g.

(d) RMS of pitch: 4°.

2. The limits used for the interaction with the monopile proved to be difficult to quantify. A confidence level of 75% for the number of allowable vertical slips was found to be accurate with the literature. Other metrics investigated were lateral slips and horizontal disconnections as well as RMS and maximal values for; linear movements, angles of roll and pitch, and acceleration. However, these require further data to accurately recommended limits.

8.4 Innovative Hull Design

While investigating the tubular multihull and different catamarans with heaveplates, a number of relationships between hull shapes, zero forward speed vessel motion, and interaction with the monopile were identified as follows;

1. The tubular multihull designs tested showed little improvement on a catamaran design. The addition of a heaveplate significantly improved the RAOs as was seen in Figure 5.14 in § 5.6.3.

2. The best angle of the dual heaveplates to reduce heave RAO was 0°, and the best angle to reduce pitch RAO was 22.5°. The models that could

operate in the most conditions according to the MII and RMS limits were the same for all angles with two 28m^2 heaveplates and for 0° for two 56m^2 heaveplates. When docked with the monopile the model with two 56m^2 heaveplates at 0° performed best.

3. To safely access wind turbines with bow transfers at sea states at and above a 3m Hs the 24m GDC presents an option. It achieves this through the use of a large deep ballasted heaveplate, deep narrow demihulls, and a high bollard pull. In the experimental work carried out the bow contact was sufficient for transfers in head seas of 3.75m Hs at 8s Tp.
4. To carry out transfers up to a 3m Hs, and to transit technicians from port to the wind farm the 30m curved hulled catamaran is a possible option. It achieves this by being wider at the transit waterline, thus providing sufficient stability for the operation. In the experimental work carried out the bow contact was sufficient for transfers in head seas of 3m Hs between 7-10s Tp.

8.5 Concluding Remarks

In this thesis the issue of increasing access for the “step over” method of bow transfers has been discussed. The interaction of WFSVs with the monopile were examined, and the limits of acceptable motion were reviewed. Furthermore, innovative hull designs were considered, with an emphasis on heaveplates. Carrying out transfers at and above a 3m Hs with this method is very challenging when the possible Hmax values are considered. Thus, as has been determined, substantial heave damping and bollard pull forces are required, for which a design cost would be associated. However, carrying out these bow transfers do offer advantages over solely using Service Operations Vessels (SOVs), notably the turnover time between transfers, and manoeuvrability advantages. Therefore, it can be concluded that smaller craft have a place in servicing far shore wind farms in high sea states, and the designs analysed in this thesis may be

suitable. Areas of interest for further research are presented in the next section.

The confidence limits pertaining to both the physical and numerical modelling in this work underpin the conclusions reached. The confidence limits of the physical model testing are subject to the accuracy and precision of numerous components including but not limited to, wave probes, repeatability of waves, repeatability of tests, and motion sensing camera system. In § 5.3 sample wave time traces showing the radiated wave effect, and wave spectra were outlined, it can be seen that the level of error in this testing is within the usual tolerances for tank testing. The numerical modelling carried out in this thesis laid the groundwork for the physical modelling that these conclusions are drawn from, improvement in the numerical damping methods would improve future work. Overall, the experimental work presented in this thesis was completed to a high level of accuracy from the model build, to instrumentation setup, wave calibration, and data acquisition.

8.6 Further Research

The research presented in this thesis used CFD, and BEM numerical models, as well as scaled physical models to develop an understanding of the influence of hull geometry, and heaveplates on the performance of a WFSV operating close to a wind turbine while transferring personnel between the wind turbine and the WFSV. A number of facets of this subject may be of interest for further examination, including but not limited to;

1. A detailed study of the performance of various WFSVs between 1 and 1.5m Hs for all headings, to determine a baseline of WFSV transfer performance, as there appears to be a large variation in the literature.
2. Friction analysis at the fender. The coefficient of friction between the rubberised fender and the tower is generally unknown. There are a large number of different fender designs on the market, with varying performance. In addition, marine growth on the monopile affects friction.

3. Some fail cases correlated with angular and acceleration measurements, a warning system based on these measurements may be useful. In addition, methods of measuring and/or predicting the very short term wave conditions could be useful, as large linear motions at the bow when docked at the monopile can occur when the number of slips and RMS of linear motion is low.

4. As the GDC had impressive performance, further research is warranted to study the seakeeping in greater detail. Moreover, a steered self-propelled model with an improved fender design could be tested interacting with a monopile. Thus, it would be recommended that larger scale physical modelling be carried out to reduce scale effects in the testing.

References

[1] P. Villiers. Access systems: The access challenge. http://www.offshorewind.biz/2013/06/18/access-systems-the-access-challenge/, 2013. [Date accessed: 20/08/2015].

[2] M. Bilgili, A. Yasar, and E Simsek. Offshore wind power development in europe and its comparison with onshore counterpart. *Renewable and Sustainable Energy Reviews*, 15(2):905–915, 2011.

[3] C. Birch and C. Gormsen. Recent developments in offshore foundation design. In *EWEC-Conference*, pages 365–368, 1999.

[4] 4coffshore. Vindeby offshore wind farm. http://www.4coffshore.com/windfarms/vindeby-denmark-dk06.html, 2016. [Date accessed: 06/12/2016].

[5] A. Ho, A. Mbistrova, and G. Corbetta. The European offshore wind industry - key trends and statistics 2015. http://www.ewea.org/fileadmin/files/library/publications/statistics/EWEA-European-Offshore-Statistics-2015.pdf, 2015. [Date accessed: 21/03/2016].

[6] A. Ho and A. Mbistrova. The European offshore wind industry - key trends and statistics 1st half 2016. https://windeurope.org/wp-content/uploads/files/about-wind/statistics/WindEurope-mid-year-offshore-statistics-2016.pdf, 2016. [Date accessed: 23/09/2016].

[7] Sustainable Energy Authority of Ireland. Wind energy roadmap.

http://www.seai.ie/Publications/Statistics_Publications/SEAI_2050_Energy_Roadmaps/Wind_Energy_Roadmap.pdf, 2011. [Date accessed: 17/08/2015].

[8] M. Martini, A. Jurado, R. Guanche, and I. Losada. Probabilistic assessment of floating wind turbine access by catamaran vessel. *Energy Procedia*, 94:249–260, 2016.

[9] Forewind. Dogger bank overview. http://www.forewind.co.uk/dogger-bank/overview.html, 2015. [Date accessed: 20/08/2015].

[10] GL Garrad Hassan. Operations and maintenance opportunities in scotland - an insight into opportunities for scottish ports and the o&m supply chain. https://www.scottish-enterprise.com/~/media/se/resources/documents/mno/offshore%20wind%20operations%20and%20maintenance%20opps.pdf, 2013. [Date accessed: 18/12/2016].

[11] International Marine Contractors Association. Transfer of personnel to and from offshore vessels and structures. London, United Kingdom, 2014. International Marine Contractors Association.

[12] RenewableUK. Offshore wind and marine energy health and safety guidelines volume 2. London, United Kingdom, 2014. RenewableUK.

[13] UK Maritime & Coastguard Agency. Safety during transfers of persons to and from ships. Southampton, United Kingdom, 2016. K Maritime & Coastguard Agency.

[14] National Workboat Association. Good practice guide for offshore energy service vessels. United Kingdom, 2015. National Workboat Association.

[15] GL Garrad Hassan. A guide to uk offshore wind operations and maintenance. http://www.4-power.eu/media/3109/offshore-wind-guide-june-2013.pdf, 2013. [Date accessed: 19/08/2015].

[16] 4C Offshore. Wind farm service vessels. http://www.4coffshore.com/windfarms/vessel-category-wind-farm-service-vcid2.html, 2015. [Date accessed: 17/12/2016].

[17] Esvagt. Esvagt faraday, howpublished = "http://www.esvagt.com/fleet/wind-service-operations-vessels/esvagt-faraday/", note = [Date accessed: 23/03/2016], 2016.

[18] J.C. Kalis and D. de Koningh. On the functional design of an offshore wind maintenance support vessel. In *Design and Operation of Wind Farm Support Vessels*, pages 165–172, London, United Kingdom, 2014. Damen Shipyards, The Royal Institution of Naval Architects.

[19] A. Benoist. Mother-ship concept: The answer to the challenge of uk round 3? In *Design and Operation of Wind Farm Support Vessels*, pages 123–127, London, United Kingdom, 2014. STX France, The Royal Institution of Naval Architects.

[20] Carbon Trust. Offshore wind accelerator media briefing. https://www.carbontrust.com/media/314182/carbon-trust-owa-media_briefing-21-may-2013.pdf, 2013. [Date accessed: 13/08/2015].

[21] L.W.M.M. Rademakers and H. Bramm. O&M aspects of the 500 MW offshore wind farm at NL7. https://www.ecn.nl/fileadmin/ecn/units/wind/docs/dowec/10080_002.pdf, 2002. [Date accessed: 16/10/2015].

[22] S. Livaniou, S. Iordanis, P. Anaxagorou, B. Mocanu, R. Sykes, J. Goormachtigh, J.M. Christensen, J.T. Kristensen, and M. Antrobus. Key design parameters and criteria related to installation and maintenance vessels design; their layouts, crane operations and access systems D.3.2. http://www.leanwind.eu/wp-content/uploads/GA_614020_LEANWIND_D3.2.pdf, 2015. [Date accessed: 04/08/2015].

[23] D. Bailey. *The NPL High Speed Round Bilge Displacement Hull Series: Resistance, Propulsion, Manoevring and Seakeeping Data*. Royal Institution of Naval Architects, 1976.

[24] G. Marsh. Deep offshore O&M: Accessing all areas. *Renewable Energy Focus*, 14(1):25–30, 2013.

[25] G. Marsh. WFSV: Hull form focus. *Renewable Energy Focus*, 14(1):32–36, 2013.

[26] *Offshore Wind Vessel Directory 2016*. Navingo BV, 2016.

[27] Windcat Workboats. http://www.windcatworkboats.com/wp-content/uploads/2014/09/Windgrip_11.jpg, 2014. [Date accessed: 21/03/2016].

[28] A2Sea. Wind supporter technical specifications. http://www.a2sea.com/wp-content/uploads/2013/04/Techsheet_WIND+SUPPORTER.pdf, 2013. [Date accessed: 21/03/2016].

[29] Bard. The first special vessel for personnel transfer in offshore wind farms. http://www.bard-offshore.de, 2014. [Date accessed: 20/10/2015].

[30] J. Kecsmar, J.W. McFann, and D. Low. The swath ctv - finally coming of age. In *Design and Construction of Wind Farm Support Vessels*, pages 55–66, London, United Kingdom, 2017. Ad Hoc Marine Designs Ltd, The Royal Institution of Naval Architects.

[31] S. Smid, O. Mala, and M. Rannala. Cost-benefit analysis on crew transfer vessels to minimize downtime of future wind parks. In *Design and Operation of Wind Farm Support Vessels*, pages 83–89, London, United Kingdom, 2014. Tallinn University of Technology Estonia, The Royal Institution of Naval Architects.

[32] Austal. Austal wind express tri swath 27. http://www.austal.com/sites/default/files/data-sheet/Austal%20Wind%20Express%20TRI%20SWATH%2027%20Cable%20Bay.pdf, 2013. [Date accessed: 23/03/2016].

[33] Mobimar. Offshore wind farm service and crew transfer. http://www.mobimar.com/workboats-offshore_wind_farm_service_and_crew_transfer, 2015. [Date accessed: 20/10/2015].

[34] Fjellstrand. Windserver30 offshore wind farm service craft. http://renews.biz/68575/fisher-champions-canadian-vision/, 2013. [Date accessed: 25/09/2016.

[35] Umoe Mandal. Wavecraft. http://www.um.no/web/um200.nsf/pages/WaveCraft, 2013. [Date accessed: 25/09/2016].

[36] O.M. Faltinsen. *Hydrodynamics of High-Speed Marine Vehicles*. Cambridge University Press, 2005.

[37] M. Jupp, R. Sime, and E. Dudson. XSS - a next generation windfarm support vessel. In *Design and Operation of Wind Farm Support Vessels*, pages 43–51, London, United Kingdom, 2014. The Royal Institution of Naval Architects.

[38] Wind Power Support. Floating hotels. `http://www.windpowersupport.com/floating-hotels/`, 2015. [Date accessed: 22/10/2015].

[39] Wind Power Support. Wind power support - wind solution. `http://www.windpowersupport.com/floating-hotels/`, 2016. [Date accessed: 23/03/2016].

[40] DBB Jack-Up Services A/S. J/U wind server. `http://dbbjackup.dk/wp-content/uploads/WIND-SERVER_Technical-Specifications.pdf`, 2015. [Date accessed: 22/10/2015].

[41] A.A. van der Bles. Tuning hull optimization and transfer system in design of w2w vessel for best habitability and workability above 3m significant wave height. In *Design and Construction of Wind Farm Support Vessels*, pages 33–37, London, United Kingdom, 2016. Conoship International BV, The Royal Institution of Naval Architects.

[42] D.J.C. Salzmann. *Ampelmann Development of the Access System for Offshore Wind Turbines*. PhD thesis, 2010.

[43] A. Attari, G.O. Okuyemi, J. Goormachtigh, J.M. Christensen, J.T. Kristensen, J.K. Nielsen, J.M.F. Hernando, M.F. Beghi, M. Antrobus, M. Layng, N. Valverde, P. Perrocheau, R. Sykes, V. de Laleu, and Y. Rolland. WP framework/industry challenges report construction, deployment and installation work package 3 deliverable 3.1. `http://www.leanwind.eu/wp-content/uploads/LEANWIND_D3-1_Executive-Summary.pdf`, 2014. [Date accessed: 04/08/2015].

[44] Zbridge. Zbridge, access concept for far & large offshore wind farms. `http://www.tki-windopzee.nl/files/2015-02/06.Zbridge.`

Reinout%20Prins.pdf, 2016. [Date accessed: 11/04/2016].

[45] We@Sea. Ampelmann; a motion-compensating platform for accessing wind turbines. http://www.we-at-sea.org/wp-content/uploads/2013/01/1512004-012_summary.pdf, 2013. [Date accessed: 19/10/2015].

[46] UPTIME. Increase uptime through safe access. http://www.uptime.no/wp-content/uploads/brochure.pdf, 2016. [Date accessed: 11/04/2016].

[47] Osbut Power. MaXccess. http://www.windenergynetwork.co.uk/wp-content/uploads/2013/12/OPP-13-004-MaXccess-T12-T18.pdf, 2013. [Date accessed: 17/12/2016].

[48] Autobrow. Innovative autobrow system. http://www.autobrow.com/www.autobrow.com/Autobrow.html, 2015. [Date accessed: 16/10/2015].

[49] Houlder and BMT Nigel Gee. Houlder TAS heralds step change in transfer safety and operability for offshore wind. http://www.bmt.org/news/2012/10/houlder-tas-heralds-step-change-in-transfer-safety-and/operability-for-offshore-wind/, 2002. [Date accessed: 16/10/2015].

[50] Momac. Momac offshore access systems MOTS 500 and MOTS G / GA / 1000. http://www.momac-robotics.de/db/docs/momac-offshore-access-systems-MOTS--500-MOTS-1000EXT-and-MOTS/G-v.2012-11-01.pdf, 2015. [Date accessed: 16/10/2015].

[51] Offshore Ship Designers. IMT972 wind farm service vessel. http://www.offshoreshipdesigners.com/assets/Uploads/IMT972-WFV-Data-Sheet-no-GA.pdf, 2015. [Date accessed: 25/09/2016].

[52] S. McCartan, B. Verheijden, M. Ltzhft, and D. Boote. Design-driven innovation: Mothership concepts for accessing the far shore wind farms. In *Design and Operation of Wind Farm Support Vessels*, pages 91–110, London, United Kingdom, 2014. EBDIG-IRC Coventry University UK, Chalmers

University of Technology Sweeden, DITEN University of Genoa Italy, The Royal Institution of Naval Architects.

[53] D. Knox. Submersible hull catamaran: The future of offshore support vessels. In *Design and Operation of Wind Farm Support Vessels*, pages 53–70, London, United Kingdom, 2014. OSSeas Cocsulting, The Royal Institution of Naval Architects.

[54] Offshore Ship Designers. Transpar: A craft with a radically different approach. http://www.andrewsafer.com/MRL034.pdf, 2016. [Date accessed: 25/09/2016.

[55] Offshore Ship Designers. Fisher champions canadian vision deal with extreme ocean to promote transpar access vessel. http://renews.biz/68575/fisher-champions-canadian-vision/, 2014. [Date accessed: 25/09/2016.

[56] Nauti-Craft. Ship & boat international july/august 2016 - nauti by nature. http://www.nauti-craft.com/news.html, 2016. [Date accessed: 25/09/2016.

[57] M.J. Longman. Developments in computer modeling of attitude and ride control systems for a suspended multi-hulled windfarm vessel. In *Design and Operation of Wind Farm Support Vessels*, pages 147–154, London, United Kingdom, 2014. Nauti-Craft Pty Ltd, The Royal Institution of Naval Architects.

[58] North Sea Logistics. North sea logistics pivoting deck vessel. http://www.northsealogistics.co.uk/, 2011. [Date accessed: 25/09/2016.

[59] D. James and M. Collu. A novel design for an offshore wind farm vessel: application of the aerodynamically alleviated marine vechicle (aamv). In *Design and Operation of Wind Farm Support Vessels*, pages 99–110, London, United Kingdom, 2015. Cranfield University, The Royal Institution of Naval Architects.

[60] Maurizio Collu, Minoo H Patel, and Florent Trarieux. High speed marine vehicles with aerodynamic surfaces: Development of a dynamic model for

a novel configuration. 2008.

[61] Adair GW Williams. Aerodynamic forces on high speed multi-hulled marine vehicles. 2008.

[62] T. Grafton M. Schei-Nilsson. Development of rules for classification of wind farms service craft. In *Design and Operation of Wind Farm Support Vessels*, pages 1–7, London, United Kingdom, 2014. The Royal Institution of Naval Architects.

[63] Lloyd's Register. Guidance notes for the classification of wind farm service vessels. London, United Kingdom, 2012. Lloyd's Register.

[64] D.J. Cantello and A.B. Wilde. Fatigue and safety - manning levels, competence & qualifications. In *Design and Operation of Wind Farm Support Vessels*, pages 9–14, London, United Kingdom, 2014. TV SD PMSS, The Royal Institution of Naval Architects.

[65] T. Brand T. Dobbins, J. Hill. Human systems integration requirements for wind farm support vessel design and operation. In *Design and Operation of Wind Farm Support Vessels*, pages 15–19, London, United Kingdom, 2014. STResearch Ltd, Trident Marine Ltd, StrongWake, The Royal Institution of Naval Architects.

[66] DNV-GL. Service on windfarms and other offshore installations. DNV-GL, 2013.

[67] Z. Gao, Lin L. Wilson G. A., Y. Zhao, C. Li, and T. Moan. Numerical simulation of marine operations and prediction of operability using response-based criteria with an application to installation of offshore wind turbine support structures. 2016.

[68] W.G. Acero, L. Li, Z. Gao, and T. Moan. Methodology for assessment of the operational limits and operability of marine operations. *Ocean Engineering*, 125:308–327, 2016.

[69] M.K. Wu. Numerical analysis of docking operation between service vessels and offshore wind turbines. *Ocean Engineering*, 91:379–388, 2014.

[70] Lloyd's Register. Rules and regulations for the classification of special

service craft. London, United Kingdom, 2016. Lloyd's Register.

[71] International Maritime Pilots Association. Guidance for naval architects and shipyards on the provision of pilot boarding arrangements. 2012.

[72] British Ports Association, the UK Major Ports Group (UKMPG), and the Technical & Training Committee of the United Kingdom Maritime Pilots Association (UKMPA). The embarkation and disembarkation of pilots code of safe practice. 2007.

[73] International Association of Classification Societies Ltd. Boat transfers safe practice. International Association of Classification Societies Ltd., 2014.

[74] G+ Offshore wind health and safety association. G+ offshore wind health and safety association 2013 annual incident data report. G+ Offshore wind health and safety association, 2014.

[75] G+ Offshore wind health and safety association. G+ offshore wind health and safety association 2014 annual incident data report. G+ Offshore wind health and safety association, 2015.

[76] G+ Offshore wind health and safety association. G+ offshore wind health and safety association 2015 annual incident data report. G+ Offshore wind health and safety association, 2016.

[77] G+ Offshore wind health and safety association. Uk offshore wind hse statistics 2014 report. G+ Offshore wind health and safety association, 2015.

[78] G+ Offshore wind health and safety association. Uk offshore wind hse statistics 2015 report. G+ Offshore wind health and safety association, 2016.

[79] International Marine Contractors Association. Imca safety flash 19/15. http://www.imca-int.com/media/221272/imcasf19-15.pdf, 2015. [Date accessed: 11/12/2016].

[80] International Marine Contractors Association. Imca safety flash 06/15. , 2015. [Date accessed: 11/12/2016].

[81] International Marine Contractors Association. Imca safety flash 03/16. http://www.imca-int.com/media/231635/imcasf03-16.pdf, 2015. [Date accessed: 11/12/2016].

[82] Caithness Windfarm Information Forum. Wind turbine accident compilation. http://www.caithnesswindfarms.co.uk/fullaccidents.pdf, 2015. [Date accessed: 13/08/2015].

[83] Marine Accident Investigation Branch. Crush incident during transfer from bottom dump barge to tug willem-b with loss of 1 life. https://assets.digital.cabinet-office.gov.uk/media/547c717fed915d4c1000010d/willem_b.pdf, 2015. [Date accessed: 26/10/2015].

[84] International Association of Oil & Gas Producers. Water transport accident statistics. report no. 434-10. http://www.ogp.org.uk/pubs/434-10.pdf, 2010. [Date accessed: 11/12/2016].

[85] J. Spouge, P. Strong, and R. Proctor. Risks of marine transfer of personnel offshore. 2014.

[86] Carbon Trust. Page 2 issue 10 february 2015 offshore wind accelerator newsletter. http://www.carbontrust.com/media/640008/owa-newsletter-2015-02-february.pdf, 2015. [Date accessed: 13/08/2015].

[87] S. Phillips, I.B. Shin, C. Armstrong, and D. Kyle-Spearman. Performance evaluation of wind farm support vessels. In *Design and Operation of Wind Farm Support Vessels*, pages 141–145, London, United Kingdom, 2014. Seaspeed Marine Consulting Ltd, The Royal Institution of Naval Architects.

[88] S. Phillips, I.B. Shin, and C. Armstrong. Crew transfer vessel performance evaluation. In *Design and Operation of Wind Farm Support Vessels*, pages 29–33, London, United Kingdom, 2015. Seaspeed Marine Consulting Ltd, The Royal Institution of Naval Architects.

[89] H. Maclean, C. Armstrong, I. Shin, and S. Phillips. Fast crew transfer ves-

sels - transit and transfer performance research. In *Design and Construction of Wind Farm Support Vessels*, pages 19–24, London, United Kingdom, 2016. Seaspeed Marine Consulting Ltd, The Royal Institution of Naval Architects.

[90] D.E. Hasselmann, M. Dunckel, and J.A. Ewing. Directional wave spectra observed during jonswap 1973. *Journal of physical oceanography*, 10(8):1264–1280, 1980.

[91] Guttorm Grytoyr and Oddrun Steinkjer. Uncertainty of long term fatigue load of subsea well heads. In *ASME 2012 31st International Conference on Ocean, Offshore and Arctic Engineering*, pages 639–646. American Society of Mechanical Engineers, 2012.

[92] L.W.M.M. Rademakers. Installation, operations and maintenance. `http://www.we-at-sea.org/wp-content/uploads/2013/01/We@Sea-RL5-report.pdf`, 2010. [Date accessed: 19/08/2015].

[93] D.J.C. Salzmann, J.V.D. Tempel, F.W.B. Gerner, A.J. Gbel, and J.M.L. Koch. Ampelmann demonstrator developing a motion compensating platform for offshore access. In *European Wind Energy Conference*, Milan, Spain, 2007. Delft University of Technology.

[94] T.A. Santos, E. Carichas, N. Fonseca, J. Pessoa, F. Duarte, J.V. Abreu, L. Baptista, J. Cruz, and M. Leal. Development of an integrated system for personnel and equipment transfer to offshore wind turbines. In *1st International Conference on Maritime Technology and Engineering*, 2011.

[95] M. O'Connor, T. Lewis, and G. Dalton. Weather window analysis of Irish west coast wave data with relevance to operations & maintenance of marine renewables. *Renewable energy*, 52:57–66, 2013.

[96] Marine Institute. Irish weather buoy network. `http://www.marine.ie/Home/site-area/data-services/real-time-observations/irish-weather-buoy-network?language=en`, 2015. [Date accessed: 16/10/2015].

[97] NordForsk. Seakeeping performance of ships, in assessment of a ship

performance in a seaway, trondheim, Norway. 1987.

[98] M.G. Parsons S.C. Stephens. Effects of motion at sea on crew performance: A survey. *Marine Technology*, 39(1):29–47, 2002.

[99] G.C. Soares, N. Fonseca, and R. Centeno. Seakeeping performance of fishing vessels in the portuguese economic zone. In *Intl Conf on Seakeeping and Weather*, London, United Kingdom., 1995. RINA.

[100] A.C. Bittner and J.C. Guignard. Human factors engineering principles for minimizing adverse ship motion effects: Theory and practice. *Naval Engineers Journal*, 97(4):205–213, 1985.

[101] J.L. Colwell. Nato performance assessment questionnaire (paq): Problem severity and correlation for ship motions, fatigue, seasickness and task performance. 2000.

[102] J.H. Erikson. Common procedures for seakeeping in the ship design process. *STANAG*, 4154:2000, 2000.

[103] R. Graham. Motion-induced interruptions as ship operability criteria. *Naval Engineers Journal*, 102(2):65–71, 1990.

[104] P. Crossland and K.J.N.C. Rich. Validating a model of the effects of ship motion on postural stability. In *International Conference of Environmental Ergonomics*, volume 77, pages 385–388, 1998.

[105] E. Nocerino. *Human postural stability onboard ship as seakeeping criterion. Stance control model and procedure for validating it: a proposal*. PhD thesis, 2010.

[106] A.R.J.M. Lloyd. Seakeeping: ship behaviour in rough weather. 1989.

[107] R. Graham, A.E. Baitis, and W.G. Meyers. On the development of seakeeping criteria. *Naval Engineers Journal*, 104(3):259–275, 1992.

[108] L.W. Hanyok. Methods for calculating motion induced interruptions as applied to a space capsule after splashdown, 2012.

[109] MARIN. Coordinate systems, year = 2016, howpublished = "`https://wiki.marin.nl/index.php/Coordinate_systems`", note = [Date accessed: 28/07/2016].

[110] Per Martin Martinussen. Parametric roll resonance of a fishing vessel as function of forward speed and sea state. 2011.

[111] R. Bhattacharyya. *Dynamics of Marine Vehicles*. John Wiley & Sons, 1972.

[112] S.K. Chakrabarti. *Hydrodynamics of Offshore Structures*. WIT Press, 1987.

[113] V. Jaksic, C.S. Wright, J. Murphy, C. Afeef, S.F. Ali, D.P. Mandic, and V. Pakrashi. Dynamic response mitigation of floating wind turbine platforms using tuned liquid column dampers. *Philosophical Transactions of the Royal Society of London A: Mathematical, Physical and Engineering Sciences*, 373(2035):20140079, 2015.

[114] V. Jaksic, C. Wright, C. Afeef, S.F. Ali, J. Murphy, and V. Pakrashi. Performance of a single liquid column damper for the control of dynamic responses of a tension leg platform. In *Journal of Physics: Conference Series*, volume 628, page 012058. IOP Publishing, 2015.

[115] C.A. Garrido Mendoza. *Hydrodynamic forces on heave plates for offshore systems oscillating close to the seabed or the free surface*. PhD thesis, Navales, 2015.

[116] B. Molin. Hydrodynamic modeling of perforated structures. *Applied Ocean Research*, 33(1):1–11, 2011.

[117] C. López Pavón. *Selected topics in the Hydrodynamics of floating offshore wind turbines: heave damping and second order surge motions*. PhD thesis, Navales, 2015.

[118] D. Roddier and C. Cermelli. Floating wind turbine platform with ballast control and mooring system, July 17 2014. US Patent App. 14/218,805.

[119] D. Roddier, C. Cermelli, A. Aubault, and A. Weinstein. Windfloat: A floating foundation for offshore wind turbines. *Journal of Renewable and Sustainable Energy*, 2(3):033104, 2010.

[120] M. Lake, H. He, A.W. Troesch, M. Perlin, and K.P. Thiagarajan. Hydrodynamic coefficient estimation for tlp and spar structures. *Journal of Offshore Mechanics and Arctic Engineering*, 122(2):118–124, 2000.

[121] S. Sudhakar and S. Nallayarasu. Influence of heave plate on hydrody-

namic response of spar hull. In *30th Ocean Offshore and Arctic Engineering Conference (OMAE 2011)*, 2011.

[122] L. Tao and D. Dray. Hydrodynamic performance of solid and porous heave plates. *Ocean Engineering*, 35(10):1006–1014, 2008.

[123] C.A. Garrido-Mendoza, K.P. Thiagarajan, A. Souto-Iglesias, A. Colagrossi, and B. Bouscasse. Computation of flow features and hydrodynamic coefficients around heave plates oscillating near a seabed. *Journal of Fluids and Structures*, 59:406–431, 2015.

[124] K.H. Vu, B. Chenu, and K.P. Thiagarajan. Hydrodynamic damping due to porous plates. In *Proceedings of the WSEAS International Conference on Fluid Mechanics, Corfu*, pages 17–19, 2004.

[125] B. Molin, F. Remy, and T. Rippol. Experimental study of the heave added mass and damping of solid and perforated disks close to the free surface. In *Proceedings of the IMAM Conference, Varna*, 2007.

[126] J. Li, S. Liu, M. Zhao, and B. Teng. Experimental investigation of the hydrodynamic characteristics of heave plates using forced oscillation. *Ocean Engineering*, 66:82–91, 2013.

[127] O.M. Faltinsen. *Sea loads on ships and offshore structures*, volume 1. Cambridge university press, 1993.

[128] J.R. Morison, J.W. Johnson, S.A. Schaaf, et al. The force exerted by surface waves on piles. *Journal of Petroleum Technology*, 2(05):149–154, 1950.

[129] J.N. Newman. *Marine Hydrodynamics*. The MIT press, 1977.

[130] J. Falnes. *Ocean Waves and Oscillating Systems*. Cambridge University Press, 2002.

[131] L.H. Holthuijsen. *Waves in Oceanic and Coastal Waters*. Cambridge University Press, 2007.

[132] William Finnegan and Jamie Goggins. Linear irregular wave generation in a numerical wave tank. *Applied Ocean Research*, 52:188–200, 2015.

[133] P Schmitt, K Doherty, D Clabby, and T Whittaker. The opportunities and

limitations of using cfd in the development of wave energy converters. In *RINA Marine and Offshore Energy Conference*, 2012.

[134] T. Josse, A. Billet, and 2011 Leen, S.B. Prediction of supply vessel motion during transfer to a fixed structure. In *ASME 2011 30th International Conference on Ocean, Offshore and Arctic Engineering*. American Society of Mechanical Engineers, 2011.

[135] E. Berg. Calculation of relative motion between offshore wind turbine and a service vessel, 2012.

[136] D.F. González, M. Lemmerhirt, M. Abdel-Maksoud, M. König, and A. Düster. Numerical and experimental investigation regarding the landing manoeuvre of a catamaran vessel at an offshore wind turbine in waves. In *ASME 2015 34th International Conference on Ocean, Offshore and Arctic Engineering*. American Society of Mechanical Engineers, 2015.

[137] M. König, A. Düster, D.F. González, and M. Abdel-Maksoud. Simulation of safety-relevant situations regarding the interaction of service ships with offshore wind turbine plants. In *ASME 2015 34th International Conference on Ocean, Offshore and Arctic Engineering*, pages V007T06A044–V007T06A044. American Society of Mechanical Engineers, 2015.

[138] M. König, D. F. González, M. Abdel-Maksoud, and A. Düster. Numerical investigation of the landing maneuver of a crew transfer vessel to an offshore wind turbine.

[139] Michele Martini, Alfonso Jurado, Raúl Guanche, and I.J. Losada. Evaluation of walk-to-work accessibility for a floating wind turbine. In *ASME 2016 35th International Conference on Ocean, Offshore and Arctic Engineering*, pages V006T09A038–V006T09A038. American Society of Mechanical Engineers, 2016.

[140] R. Guanche, M. Martini, A. Jurado, and I.J. Losada. Walk-to-work accessibility assessment for floating offshore wind turbines. *Ocean Engineering*, 116:216–225, 2016.

[141] J.H. Evans. Basic design concepts. *Journal of the American Society for*

Naval Engineers, 71(4):671–678, 1959.

[142] D.J. Singer, N. Doerry, and M.E. Buckley. What is set-based design? *Naval Engineers Journal*, 121(4):31–43, 2009.

[143] A. Hargadon and R.I. Sutton. Building an innovation factory. *Harvard business review*, 78(3):157–66, 1999.

[144] J. Shore. Continuous design. *IEEE Software*, 21(1):20–22, 2004.

[145] M.A. Rosenman. An exploration into evolutionary models for non-routine design. *Artificial Intelligence in Engineering*, 11(3):287–293, 1997.

[146] John S Gero. Creativity, emergence and evolution in design. *Knowledge-Based Systems*, 9(7):435–448, 1996.

[147] T. Severin. *The China Voyage*. Little, Brown and Company, 1994.

[148] DNV Det Norske Veritas. Hull structural design - ships with length less than 100 metres. 2015.

[149] DNV-GL. Rules for classification and construction, i ship technology, 1 seagoing ships, 1 hull structures. DNV-GL, 2016.

[150] R.K. Sykes. *The Hydrodynamics of an Oscillating Water Column An Investigation Using Numerical and Physical Modelling*. PhD thesis, 2011.

[151] R.K. Sykes, A.W. Lewis, and G.P. Thomas. A hydrodynamic study of a floating circular owc. In *Proceedings of the 8th European Wave and Tidal Energy Conference, Uppsala, Sweden*, 2009.

[152] R.K. Sykes, A.W. Lewis, and G. Thomas. A numerical and physical comparison of a geometrically simple fixed and floating oscillating water column. In *ASME 2008 27th International Conference on Offshore Mechanics and Arctic Engineering*, pages 659–668. American Society of Mechanical Engineers, 2008.

[153] USACE. Coastal engineering manual, em 1110-2-1100, chapter 1 water wave mechanics. ii-1-132. *Engineer Manual 1110-2-1100, US Army Corps of Engineers*, 2002.

[154] Majid A Bhinder, Aurélien Babarit, Lionel Gentaz, and Pierre Ferrant. Potential time domain model with viscous correction and cfd analysis of a

generic surging floating wave energy converter. *International Journal of Marine Energy*, 10:70–96, 2015.

[155] E.P.D. Mansard and E.R. Funke. The measurement of incident and reflected spectra using a least squares method. *Coastal Engineering Proceedings*, 1(17), 1980.

[156] G. Payne. Guidance for the experimental tank testing of wave energy converters. `http://www.supergen-marine.org.uk/sites/supergen-marine.org.uk/files/publications/WEC_tank_testing.pdf`, 2008. [Date accessed: 14/12/2015].

[157] DNV-GL. Rules for classification of ships / high speed, light craft and naval surface craft, part 6, chapter 11, hull monitoring systems. DNV-GL, 2011.

[158] A. Savitzky and M.J.E. Golay. Smoothing and differentiation of data by simplified least squares procedures. *Analytical chemistry*, 36(8):1627–1639, 1964.

[159] S. Butterworth. On the theory of filter amplifiers. *Wireless Engineer*, 7(6):536–541, 1930.

[160] G.D. Bergland. A guided tour of the fast fourier transform. *IEEE spectrum*, 6(7):41–52, 1969.

[161] A. Nazarov, P. Suebyiw, and A. Piamalung. Experimental assessment of impact loads on catamaran structures. In *Design and Operation of Wind Farm Support Vessels*, pages 75–83, London, United Kingdom, 2015. Albatros Marine Design Co. Ltd., The Royal Institution of Naval Architects.

[162] A.E. Baitis, W.G. Meyers, D.A. Woolaver, and C.M. Lee. A seakeeping comparison between three monohulls, two swaths, and a column-stabilised catamaran designed for the same mission. Technical report, DTIC Document, 1975.

[163] G.C. Soares and M. Maron. Model tests of the motions of a catamaran hull in waves. 1999.

[164] C.C. Fang, H.S. Chan, and A. Incecik. Investigation of motions of catamarans in regular wavesi. *Ocean engineering*, 23(1):89–105, 1996.

[165] C.C. Fang, H.S. Chan, and A. Incecik. Investigation of motions of catamarans in regular wavesii. *Ocean engineering*, 24(10):949–966, 1997.

[166] Lloyd's Register. Rules and regulations for the classification of naval ships, publisher = Lloyd's Register, address = London, United Kingdom. 2017.

[167] M Hossein Ghaemi and Henryk Olszewski. Total ship operability–review, concept and criteria. *Polish Maritime Research*, 24(s1):74–81, 2017.

[168] S Gaglione, V Piscopo, and A Scamardella. The overall motion induced interruptions as operability criterion for fishing vessels. *Journal of Marine Science and Technology*, 21(3):517–532, 2016.

[169] Jakub Montewka, Floris Goerlandt, Gemma Innes-Jones, Douglas Owen, Yasmine Hifi, and Romanas Puisa. Enhancing human performance in ship operations by modifying global design factors at the design stage. *Reliability Engineering & System Safety*, 159:283–300, 2017.

[170] Gregory E Gehl. *Assessing motion induced interruptions using a motion platform*. PhD thesis, Monterey, California: Naval Postgraduate School, 2013.

[171] Erik Verboom and F van Walree. Validation of time domain panel codes for prediction of large amplitude motions of ships. In *Proceedings of the 12th Int. Conf. on Stability of Ships and Ocean Vehicles (STAB 2015). Glasgow, UK*, 2015.

[172] International Towing Tank Conference. Recommended procedures; guide to the expression of uncertainty in experimental hydrodynamics. ITTC, 2014.

[173] C.L. Siow, J. Koto, H. Abyn, and N.M. Khairuddin. Linearized morison drag for improvement semi-submersible heave response prediction by diffraction potential. *Science and Engineering*, 6, 2014.

[174] V. Martínez-Chaluisant. Static and dynamic response of monopiles for offshore wind turbines. Master's thesis, University of Wisconsin-Madison, 2011.

[175] A.C.V. da Fonseca. Diameter effects of large scale monopiles-a theoretical

and numerical investigation of the soil-pile interaction response. 2015.

[176] 4C Offshore. Monopiles support structure. http://www.4coffshore.com/windfarms/monopiles-support-structures-aid4.html, 2015. [Date accessed: 13/12/2016].

[177] A.H. Tricklebank, P.H. Halberstadt, B.J. Magee, and A. Bromage. Concrete towers for onshore and offshore wind farms. http://www.windfarmbop.com/wp-content/uploads/2012/07/Concrete-Towers-for-Onshore-and-Offshore-Wind-Farms.pdf, 2012. [Date accessed: 17/12/2016].

[178] KV Shooter and D Tabor. The frictional properties of plastics. *Proceedings of the Physical Society. Section B*, 65(9):661, 1952.

[179] M.F. Ashby. *Materials selection in mechanical design 2^{n}d Edition*. Butterworth-Heinemann, 1999.

[180] A.J. Peacock. *Handbook of Polyethylene - Structures, Properties, and Applications*. Marcel Dekker, Inc., 2000.

[181] DNV. Dnv-os-j101 design of offshore wind turbine structures. DNV, 2014.

[182] DNV-GL. Dnvgl-st-0126 edition support structures for wind turbines. DNV-GL, 2016.

[183] IEC. Iec 61400-3:2009 wind turbines - part 3: Design requirements for offshore wind turbines. IEC, 2009.

[184] C. Gasparotti and E. Rusu. Seakeeping numerical analysis in irregular waves of a containership. *Mechanical Testing & Diagnosis*, 1(3), 2013.

[185] P. Matsangas and M.E. McCauley. Motion-induced interruptions and postural equilibrium in linear lateral accelerations. http://calhoun.nps.edu/bitstream/handle/10945/37012/NPS-OR-13-005.pdf?sequence=4&isAllowed=y, 2013. [Date accessed: 14/12/2015].

[186] Y.C.V. da Costa and T.D. de Araújo. Evaluation of dynamic behavior of waffle slab to gym center. *Latin American Journal of Solids and Structures*, 11(7):1114–1131, 2014.

[187] DNV Det Norske Veritas. Tentitive rules for service craft carrying up to 12

passengers. 2012.

[188] ANSYS AQWA. Aqwa theory manual. ANSYS, Inc., 2015.

[189] N.D.P. Barltrop. Floating structures: a guide for design and analysis. vols. 1 and 2. 1998.

[190] ANSYS CFX. User reference material. ANSYS, Inc., 2010.

[191] R.G. Dean and R.A. Dalrymple. *Water Wave Mechanics for Engineers and Scientists*. Prentice-Hall Inc., 1984.

[192] A. Lal and M. Elangovan. CFD simulation and validation of flap type wave-maker. *World Academy of Science, Engineering and Technology*, 46:76–82, 2008.

[193] M.C. Silvia, M.A. Vitola, W.T. Pinto, and C.A. Levi. Numerical simulation of monochromatic wave generated in laboratory: Validation of a cfd code. In *23 Congresso Nacional de Transport Aquaviario Construcao Naval Offshore*, pages 1–12, 2010.

[194] W. Finnegan and J. Goggins. Numerical simulation of linear water waves and wave-structure interaction. *Ocean Engineering*, 43:23–31, 2012.

[195] L. Tao, B. Molin, Y.M. Solin, and K. Thiagarajan. Spacing effects on hydrodynamics of heave plates on offshore structures. *Journal of Fluids and structures*, 23(8):1119–1136, 2007.

Appendices

Appendix A

Example WFSVs

Table A.1: Catamaran WFSV Examples

Company	Name	Length [m]	Service Speed [knots]	No. of Passengers
A2 Sea	Wind Supporter	24	18.6	12
A2 Sea	Wind Transfer	21	20	12
Windcat Workboats	WindCat MK 1 Series	15	25	12
Windcat Workboats	WindCat MK 2 Series	18	25	12
Windcat Workboats	WindCat MK 3 Series	18	26	12
Windcat Workboats	WindCat MK 4 Series	27	26	45
MPI Workboats	MPI Dorothea	17.5	22	12
MPI Workboats	MPI Don Quixote	20.6	23	12
MPI Workboats	MPI Rosinante	16	25	12
MPI Workboats	MPI Napoleon	22	23	12
South Boats	16m WFSV	16	20	12
South Boats	17m WFSV	17.47	22	12
South Boats	19m WFSV	19.5	21	12
South Boats	21m WFSV	21.01	25	12
South Boats	22m WFSV	22.8	23	12
South Boats	24m WFSV	25.14	23	12
South Boats	26m WFSV	26.77	23	12
BMT	24m WFSV	24	26	12
BMT	20m WFSV	20.4	24	12
BMT	17m WFSV	17.4	25	12
Island Shipping	Island Panther	17	20	12
Sure Wind	Sure Star	26	22	12
Alicat	Dalby Wharfe	21	24	12

Table A.2: Monohull WFSV Examples

Company	Name	Length [m]	Service Speed [knots]	No. of Passengers
A2 Sea	Wind Supporter	24	18.6	12
A2 Sea	Wind Transporter	25.1	24	12
A2 Sea	ANHOLT WIND	25.1	24	12
A2 Sea	DJURS WIND	25.1	24	12
A2 Sea	WIND SUPPLIER	32.2	25	24

Table A.3: SWATH WFSV Examples

Company	Name	Length [m]	Service Speed [knots]	No. of Passengers
Wind MW	Natalia Bekker	26.4	18	12
A2 Sea	SEA BREEZE	24.76	18	24
A2 Sea	SEA GALE	24.76	18	24
A2 Sea	SEA HURRICANE	24.76	18	24
A2 Sea	SEA STORM	24.76	18	24
CTruk	CWhisper	20	20	12
Danish Yachts	SWATH 25M	25	25	24

Table A.4: TriSWACH and SemiSWATH WFSV Examples

Company	Name	Length [m]	Service Speed [knots]	No. of Passengers
BMT Nigel Gee	XSS Cymyran Bay	25.4	25	12
Austal	Wind Espress TriSWATH	27.2	23	12
Mobimar	Mobimar 23 Wind	22.5	25	12
Mobimar	Mobimar 18 Wind	22.5	20	12

Appendix B

ANSYS AQWA and CFX

B.1 ANSYS AQWA

The following is a summary of the relevant details as applied to the numerical modelling carried out in this thesis from the 2015 ANSYS AQWA theory manual [188].

ANSYS AQWA is a BEM solver using linear potential flow theory to describe the motion of the floating structure. As this theory is based on the assumption that the flow is irrotional and non-viscous it is suitable for situations where the floating body is wallsided and the influence of viscous forces is relatively small.

ANSYS AQWA calculates the hydrodynamic loading on a marine structure caused by the kinematics of water particles in waves, motions of the structure as well as the interactions between waves and the structure. AQWA solves for three categories of hydrodynamic loading on marine structures: drag load, wave exciting load, and inertia load, as is recommended in "Floating Structures: a guide for design and analysis, Vol. 1 [189]." AQWA uses potential flow theories for solving the wave inertia load and wave exciting load. AQWA uses three dimensional panel methods to analyse the hydrodynamic behaviour of a large-volume structure in waves. AQWA simulates the linearized hydrodynamic fluid wave loading on floating bodies which is carried out using three-dimensional radiation/diffraction theory, if required Morison's equation can be specified for the relevant bodies. The analysis is carried out on regular waves in the frequency domain. AQWA solves the incident wave, hydrodynamic diffraction, and Radiation wave potential for a floating body as per Equation B.1 where Φ_I is the incident potential, Φ_D is the diffracted potential and Φ_R is the radiated potential.

$$\Phi\left(x,y,z,t\right) = \Phi_I\left(x,y,z,t\right) + \Phi_D\left(x,y,z,t\right) + \Phi_R\left(x,y,z,t\right) \tag{B.1}$$

AQWA then solves the Laplace equation B.2 using the inputted boundary conditions. The real-time motion of a floating body or bodies while operating in regular or irregular waves can be simulated, in which:

$$\nabla^2\Phi = \frac{\partial^2\Phi}{\partial x^2} + \frac{\partial^2\Phi}{\partial y^2} + \frac{\partial^2\Phi}{\partial z^2} = 0 \tag{B.2}$$

The main theoretical assumptions and limitations of linear potential theory which are employed in AQWA are listed below:

- The body or bodies have zero or very small forward speed.
- The fluid is inviscid and incompressible, and the fluid flow is irrotational.
- The incident regular wave train is of small amplitude compared to its length (small slope).
- The motions are to the first order and hence must be of small amplitude. All body motions are harmonic. The linearized drag damping on the Morison elements or any additional user-defined viscous damping can be optionally included in the equation of motion.

The linearized drag due to Morison elements (tube, disc), wind and dynamic cables can also be simulated in AQWA if explicitly specified.

Additionally, the motion of a floating body can be simulated in the time domain, using the output of the frequency domain analysis. AQWA estimates the nonlinear Froude-Krylov and hydrostatic forces under an instantaneous incident wave surface [188].

B.2 ANSYS CFX

The following is a summary of the relevant details as applied to the numerical modelling carried out in this thesis from the 2010 ANSYS CFX user reference material [190].

Computational fluid Dynamics (CFD) computes the full Navier-Stokes equations. The fluid modelling software ANSYS CFX solves the unsteady three-dimensional Reynolds Averaged Navier-Stokes (RANS) Equation for simulating a 3-D Numerical Wave Tank (NWT) and floating object. This sofware was used for modelling a design that rellied heavily on visocus forces for damping its motion.

CFX is a general-purpose RANS solver, which is based on the Finite Volume Method (FVM). The amount and size of these volumes are defined by a mesh specified by the user, with the accuracy and simulation time directly proportional to the mesh resolution. Mesh types that may be used are triangular, quadrilateral, tetrahedral, hexahedral, pyramid, and prism (wedge) volumes. Multiphase simulations for the free surface deformation are computed using the Volume of Fraction (VOF) method. Furthermore, CFX has a rigid body solver incorporated that computes the movement of a floating structure. The partial differential Navier-Stokes equations are the fundamental equations of fluid flow and heat transfer, solved by the CFX solver:

$$\frac{\partial \mathbf{u}}{\partial t} + \left(\mathbf{u} \cdot \overline{V}\right)\mathbf{u} = -\frac{1}{\rho}\overline{V}p + \gamma\overline{V}^2\mathbf{u} + \frac{1}{\rho}\mathbf{F} \tag{B.3}$$

Where, $\mathbf{u}$ is the velocity component, $\overline{V}$ is the displaced volume, ρ is the density of the fluid, p is pressure, γ is the dynamic viscosity and $\mathbf{F}$ is the force component.

The fundamental equations that CFX uses in the presented research are detailed here. The governing transport equations for mass, momentum and energy conservations are reproduced [190]. The Continuity Equation is:

$$\frac{\partial \rho}{\partial t} + \overline{V} \cdot (\rho \mathbf{U}) = 0 \tag{B.4}$$

The momentum Equations are:

$$\frac{\partial (\rho \mathbf{U})}{\partial t} + \overline{V} \cdot (\rho \mathbf{U} \bigotimes \mathbf{U}) = -\overline{V}p + \overline{V} \cdot \tau + S_M \tag{B.5}$$

Where, t is time, $\mathbf{U}$ vector of velocity $U_{x,y,z}$, p is the static pressure, S_M represents external momentum sources and τ is the stress tensor, related to the strain by:

$$\tau = \mu\Big[\overline{V}\mathbf{U} + \left(\overline{V} \cdot \mathbf{U}\right)^T - \frac{2}{3}\delta\, \overline{V} \cdot \mathbf{U}\Big] \tag{B.6}$$

Where, μ is the molecular viscosity, and T is the temperature.

The Total Energy equation in CFX is:

$$\frac{\partial(\rho h_{tot})}{\partial t} - \frac{\partial p}{\partial t} + \overline{V} \cdot (\rho \mathbf{U} h_{tot}) = \overline{V} \cdot \left(\lambda \overline{V} T\right) + \overline{V} \cdot (\mathbf{U} \cdot \tau) + \mathbf{U} \cdot S_M + S_E \quad \text{(B.7)}$$

Where S_E represents external energy sources, and h_{tot} is the total enthalpy, related to the static enthalpy h(T,p) by:

$$h_{tot} = h + \frac{1}{2}\mathbf{U}^2 \quad \text{(B.8)}$$

The term $\overline{V} \cdot (\mathbf{U} \cdot \tau)$ represents the work due to viscous stresses and is called the viscous work term.

The term $(\mathbf{U} \cdot S_M)$ represents the work due to external momentum sources and is currently neglected by CFX.

Multiphase simulations for free surface deformation were computed using Volume of Fraction (VOF) method. The movement of the vessel was computed using the rigid body solver incorporated in CFX. The VOF Method that CFX uses is the Volume fraction of the q^{th} fluid, α_q the appropriate variable and properties are assigned to each cell within the domain. Tracking of the interfaces is done through the solution of the continuity equation for the volume fraction of the phases. For the q^{th} phase:

$$\frac{d}{dt}\alpha q + \mathbf{u}.\overline{V}\alpha q = 0 \quad \text{(B.9)}$$

$$\sum_{q=1}^{n} \alpha q = 1 \quad \text{(B.10)}$$

A single momentum equation is solved throughout the domain, and the resulting velocity field is shared among the phases. The momentum equation depends on the volume fraction of all phases through the fluid properties, which is determined by the presence in each control volume.

$$\rho = \sum_{q=1}^{n} \alpha q.\rho q \quad \text{(B.11)}$$

Appendix C

Model Properties

Table C.1: Main Particulars of the Tubular Multihull Models (All designs 24m long at waterline)

Model	Displacement (t)	Vertical Centre of Gravity (m)	Heaveplate Area (m^2)	I_{xx} ($kg\,m^2$)	I_{yy} ($kg\,m^2$)	I_{zz} ($kg\,m^2$)
T1000	65	2.8	N/A	$4.9x10^5$	$3.0x10^6$	$3.3x10^6$
T2000	74	2.5	192	$5.1x10^5$	$3.8x10^6$	$3.6x10^6$
T3000	65	2.6	N/A	$8.0x10^5$	$3.1x10^6$	$3.0x10^6$
T4000	88	2.7	192	$8.3x10^5$	$4.2x10^6$	$4.0x10^6$
T5000	74	2.8	N/A	$7.8x10^5$	$3.6x10^6$	$3.3x10^6$
T6000	102	4.0	192	$2.4x10^6$	$5.3x10^6$	$4.4x10^6$
T7000	65	3.7	N/A	$2.4x10^5$	$3.0x10^6$	$1.5x10^6$
T8000	72	3.2	192	$5.1x10^5$	$3.5x10^6$	$3.3x10^6$
T9000	65	3.5	N/A	$1.7x10^5$	$3.0x10^6$	$3.2x10^6$
T10000	67	2.7	192	$1.0x10^4$	$3.0x10^6$	$3.2x10^6$

Table C.2: Catamaran Model Properties (All designs 24m long at waterline)

Model	Displacement (t)	Vertical Centre of Gravity (m)	Heaveplate Area (m^2)	I_{xx} ($kg\,m^2$)	I_{yy} ($kg\,m^2$)	I_{zz} ($kg\,m^2$)
Standard Catamaran	68.1	5.7	N/A	$2.90x10^6$	$4.87x10^6$	$4.35x10^6$
Wide Hulled Catamaran With a heaveplate	282.9	7.7	154	$2.29x10^7$	$3.16x10^7$	$1.38x10^7$
Wide Hulled Catamaran With a heaveplate Raised	181.0	7.5	N/A	$8.85x10^6$	$1.59x10^7$	$1.12x10^7$
Narrow Hulled Catamaran	282.6	7.9	154	$2.33x10^7$	$3.21x10^7$	$1.38x10^7$
GDC	368	7.5	176	$2.00x10^7$	$3.60x10^7$	$1.50x10^7$

Table C.3: Curved Hulled Catamaran Model Properties (All designs 30m long at waterline)

Model	Displacement (t)	Vertical Centre of Gravity (m)	Heaveplate Area (m^2)	I_{xx} ($kg\,m^2$)	I_{yy} ($kg\,m^2$)	I_{zz} ($kg\,m^2$)
178.5m^2 Heaveplate at 12m draught	292.8	8.2	178.5	2.14x10^7	4.21x10^7	2.62x10^7
178.5m^2 Heaveplate at 9m draught	291.3	7.1	178.5	1.23x10^7	3.30x10^7	2.60x10^7
178.5m^2 Heaveplate at 6m draught	289.9	2.9	178.5	1.02x10^7	3.07x10^7	2.59x10^7
154m^2 Heaveplate at 12m draught	329.6	8.4	154	2.13x10^7	3.56x10^7	2.00x10^7
115.5m^2 Heaveplate at 12m draught	272.3	9.1	115.5	1.68x10^7	2.63x10^7	1.48x10^7
28m^2 Dual Heaveplates at 0° inclination	273.1	9	56	1.57x10^7	4.10x10^7	3.05x10^7
28m^2 Dual Heaveplates at 22.5° inclination	273.5	9	56	1.74x10^7	4.30x10^7	3.08x10^7
28m^2 Dual Heaveplates at 45° inclination	273.2	9	56	1.67x10^7	4.29x10^7	3.14x10^7
56m^2 Dual Heaveplates at 0° inclination	273.4	8.9	112	1.59x10^7	3.63x10^7	2.57x10^7
56m^2 Dual Heaveplates at 22.5° inclination	273.4	8.8	112	1.60x10^7	3.68x10^7	2.61x10^7
56m^2 Dual Heaveplates at 45° inclination	272.8	9	112	1.47x10^7	3.72x10^7	2.77x10^7
Heaveplate Raised	226.7	9.1	N/A	1.84x10^7	3.01x10^7	1.68x10^7

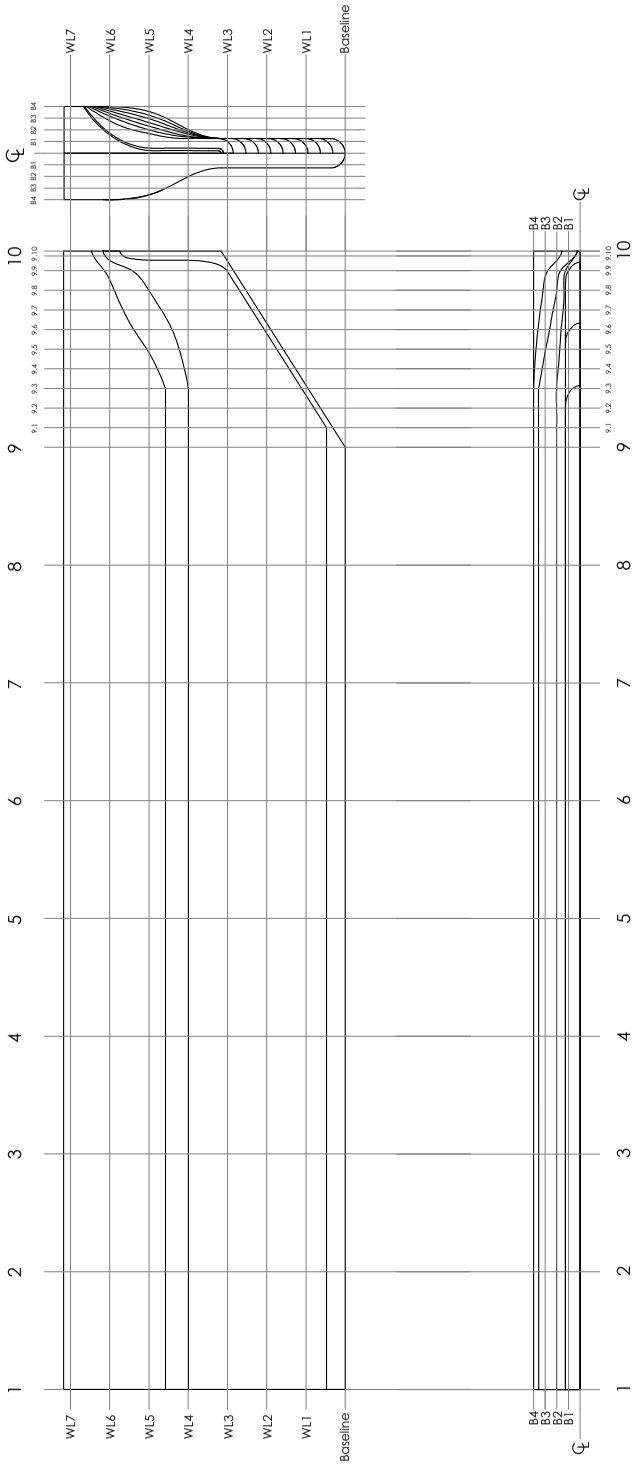

Figure C.1: Curved Hulled Catamaran Lines Plan

Appendix D

CFD Numerical Modelling

D.1 Setup of a NWT

The NWT created for the presented research followed the general geometric layout of a physical wave tank, containing a wavemaker, area for the model to be placed and a beach as is depicted in Figure D.1. The waves generated at the wavemaker travel along the domain interact with the rigid body located at a central point in the NWT and are dissipated on the parabolic beach.

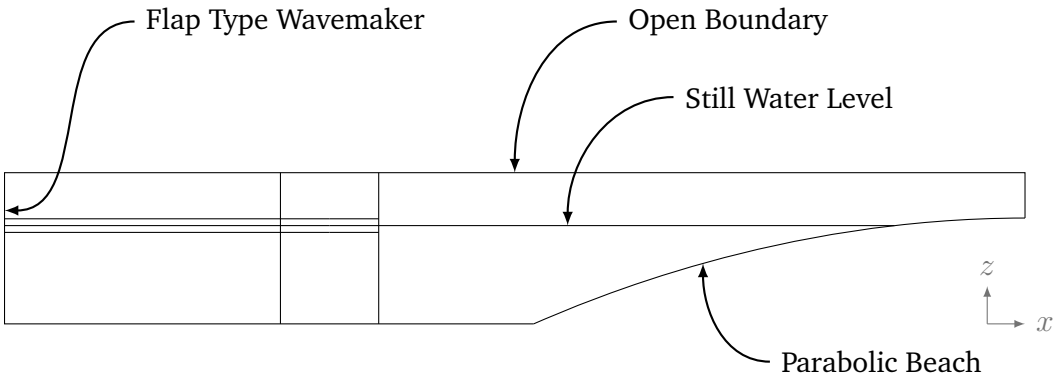

Figure D.1: CFD Layout

To setup a simulation the geometry of the wavetank is first specified and then the physics governing the fluid flow in the domain are defined. A mesh is created that specifies the finite volumes that CFX will solve for the domain simulate. A sensitivity analysis may be carried out, as the accuracy and simulation time is directly proportional to the mesh resolution. The simulation is then run without a model to calibrate the waves produced. Following this, a rigid body is then inserted in the domain and defined accordingly. (A rigid body defines a free floating body in the analysis domain in CFX.) When the same wave conditions are produced again the reactionary motions of the rigid body may be extracted and compared to the wave motion. The computational power required for such a simulation is high and thus in this study the waves were limited to regular waves.

To simulate a NWT in CFX a number of physical models and settings were implemented. To simulate the two fluids water and air a multiphase homo-

geneous model with the standard free surface model was utilised. To ensure interaction between the fluids the heat transfer model was isothermal, though the amount of actual heat transfer was minimal. To account for turbulence the shear stress transport model was selected, this accounts for the transport of the turbulent shear stress and predicts the onset and magnitude of flow separation under pressure gradients. To describe the buoyancy effects in the domain a fluid buoyancy model based on density difference was included. The interface compression level which controls the interface sharpness for free surface flows, was set to 2 which implements an aggressive compression and produces a sharp interface between the two fluids. The two fluids air and water have a density of 1.185kg m^{-3} and 1025kg m^{-3} respectively. The thickness of the entire domain is 1/14 of the modelled vessel width. This translates to a half cylinder and half the spacing between cylinders, with an overall domain thickness of 0.5 x Sh = 629.5mm. The input physics of the model are summarised in Table D.1.

Figure D.1 which showed the domain configuration for a full scale simulation has a domain size 500m long, 75m high and a 50m water depth. The NWT allows 150m for the waves to fully form, and allow for the transient standing wave to sufficiently decay, there is then a 50m section to place the model. There is a flap type wave-maker on the left, defined as a no slip wall, that generates waves according to Equation D.1 [191].

$$\frac{H}{S_0} = \frac{4\ sinh\ kh}{sinh\ 2kh + 2kh}\Big[sinh\ kh + \frac{1 - cosh\ kh}{kh}\Big] \tag{D.1}$$

Where:

- S_0 in the stroke length of the wavemaker (m)
- H is the wavemaker displacement at height z_{swl} (m)
- h is the depth of water (m)
- $k = \frac{2\pi}{\lambda}$
- λ is the wavelength (m)

Table D.1: CFX Input Physics

Parameter	Setting
Fluid Model	Multiphase Homogeneous Model
Heat Transfer Model	Isothermal
Turbulence Model	Shear Stress Transport Model
Fluid Buoyancy Model	Density Difference
Free Surface	Standard Free Surface Model
Interface Compression Level	2 (Aggressive Compression)
Air Density	1.185kg m^{-3}
Water Density	1025kg m^{-3}
NWT Length	500m
NWT Height	75m
NWT Water Depth	50m
NWT Thickness	0.6295m

The following equation D.2 was used to control the mesh motion at the flap type wave-maker [192].

$$X_{disp} = \frac{z_{swl} + h}{D} A_f.sin(\omega t) \tag{D.2}$$

Where:

- X_{disp} is the wavemaker displacement (m)
- z_{swl} is the distance from still water level (m)
- h is the depth of water (m)
- D is the CFX Domain Height (m)
- A_f is the wavemaker stroke length at top of domain (m)
- t is time

At the top of the domain in Figure D.1 there is a boundary, defined as an opening, which allows air to enter and exit as required when the waves oscillate. This boundary has a stationary mesh with the mass and momentum physics defined by pressure and direction. The relative pressure is zero and the flow direction is normal to the boundary with a medium intensity turbulence model of 5%. The two vertical lines shown inside the domain are fluid to fluid interface boundaries which are set at 150m and 200m from the wavemaker respectively. They are specified in the model as a method of extracting wave height. The volume fraction of fluid on the surface is recorded to determine the wave height. The mesh motion, mass and momentum definition and turbulence model at this location is based on a conservative interface flux. At the end of the wave tank there is a parabolic beach defined as no slip smooth walls to dissipate the wave energy by means of wave breaking. Additionally, the NWT's base, and end wall are defined as no slip, smooth walls. In addition, the symmetry boundary condition was utilised in the model to maintain the mesh size to a minimum for a three dimensional simulation. Table D.2 summarises these domain configurations.

Table D.2: CFX Domain Configuration

Location	Boundary Setting	Principal Physics Setting
flap type wave maker	no slip wall	$X_{disp} = \frac{z_{swl}+h}{D}\ A_f.sin(\omega t)$
Top Boundary	Opening	Pressure and Direction
Wave Measurement Lines	Fluid to Fluid Interface	Conservative Interface flux
Front and Rear Face of Domain	Symmetry	Zero Normal Gradient
Beach	no slip wall	Stationary

The mesh used in the model is refined at the water surface, to prevent what is known as “numerical damping” where the wave height diminishes as it propagates. This numerical damping is further influenced by the time step and it is recommended that the time step be 1/100 of the wave period [193]. In the simulations performed, a time step of 0.05s was used, as the minimum wave period was 5s. A high resolution advection scheme was used to create a robust spatial gradient in the simulation. The second order backwards Euler transient scheme was used to account for rotation momentum. The turbulence numerics were first order, reducing simulation time. The coefficient loop is set to a minimum of 1 to a maximum of 10, with the convergence criteria for the residual type RMS to have a target of 1E04.

D.2 Simulation of Regular Waves in a NWT

In order to determine the accuracy of wave propagation throughout the NWT, a series of simulations were run without a rigid body in the domain. A transient analysis was run with a 90s duration with a time step of 0.05s. Eight regular waves were tested as outlined in Table D.3 and graphed in Figure D.2. There is a greater increase in wave height than expected and the period is close to the input values. This is an issue relating to the physics of the simulation or the method ANSYS CFX employs to calculate the flow between each individual volume. It has been reported [192, 194] that there is a reduction in wave height throughout the domain due to numerical damping in the solver, and this was observed in initial set-up, hence the mesh size was increased substantially in this model. Though, this seems to have uncovered another issue in the numerical solver, as can be seen in Table D.3, the output wave readings were very large compared to the expected input waves. A detailed convergence study could be carried out to investigate this, nonetheless in this study the output wave height and period was simply recorded as the waves acting on the floating body in the NWT.

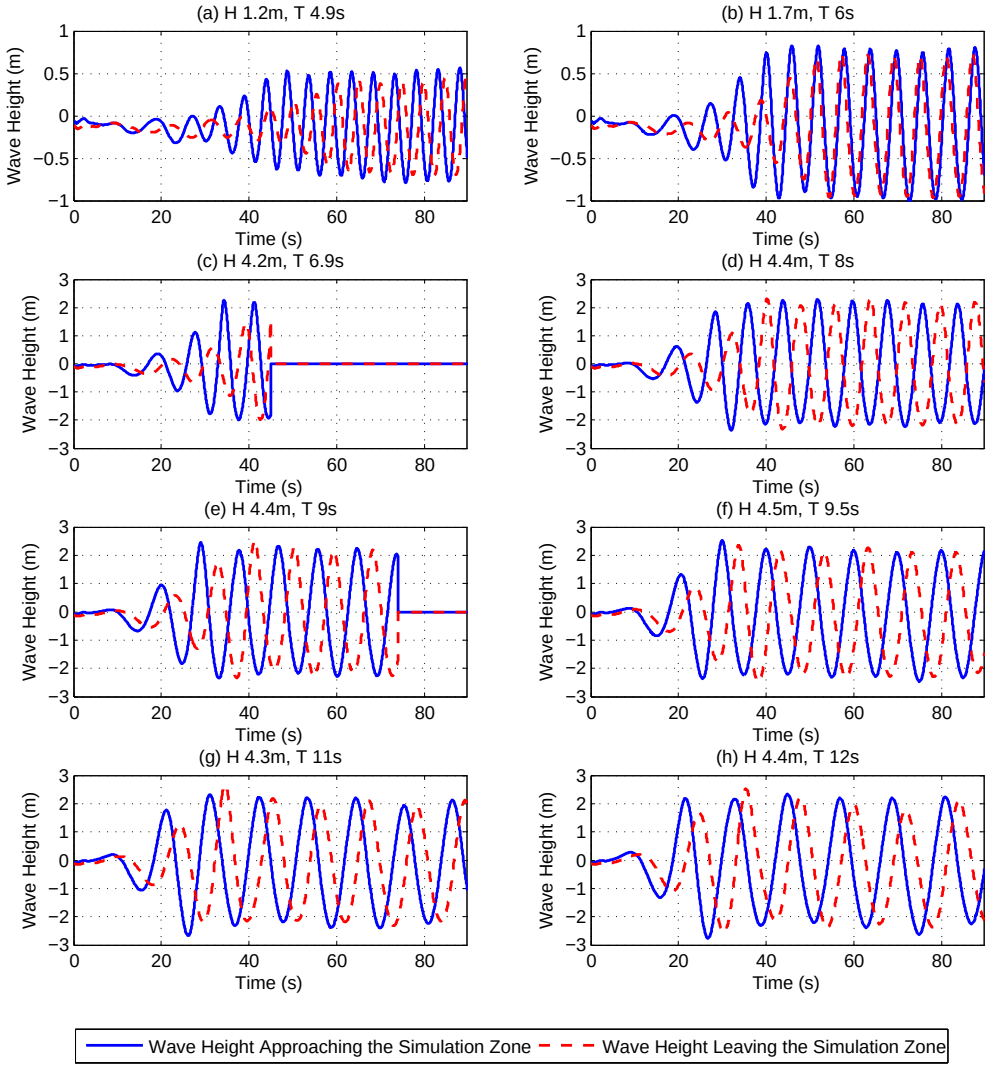

Figure D.2: Wave Height Approaching and Leaving the Simulation Zone without a Model in Place

D.3 Tubular Multihull Numerical Modelling

Following on from the previous section where a NWT was calibrated the tubular multihull modelled as a rigid body is described in the domain. The motions of the rigid body are computed and compared to the wave motion determined in the wave generation tests in § D.2.

Table D.3: Regular Waves Analysed in CFX

Input Wave Parameters		Output Wave Readings	
Wave height (m)	Wave Period (s)	Wave Height (m)	Wave Period (s)
1.0	5.0	1.2	4.9
1.5	6.0	1.7	6.0
3.0	7.0	4.2	6.9
3.0	8.0	4.4	8.0
3.0	9.0	4.4	9.0
3.0	10.0	4.5	9.5
3.0	11.0	4.3	11.0
3.0	12.0	4.4	12.0

Figure D.3 shows the domain configuration, which differs from the initial wave generation model by including the rigid body which is situated inside the circular area referred to as the rigid body domain. The circle and other lines shown inside the domain are fluid to fluid boundaries which aid mesh optimisation [194, 192]. The rigid body in the system adds an extra degree of complexity therefore the solver now has to solve for the NWT domain as well as simultaneously solving for the rigid body. The rigid body solver coupling control updated its solution every coefficient loop up to a maximum of 40 iterations to achieve convergence. The Simo Wong integration method was used for the angular momentum equation control.

The rigid body had a mass of 4643kg and a mass moment of inertia of 2.49x10^{5}kg m^2 in I_{yy}. It had translational degrees of freedom in the X and Z axes and rotational degrees of freedom about the Y axes. Figures D.4 & D.5 display the mesh used in the CFD simulation which has 2,028,443 elements, where the mesh is refined at the water surface, and around the rigid body.

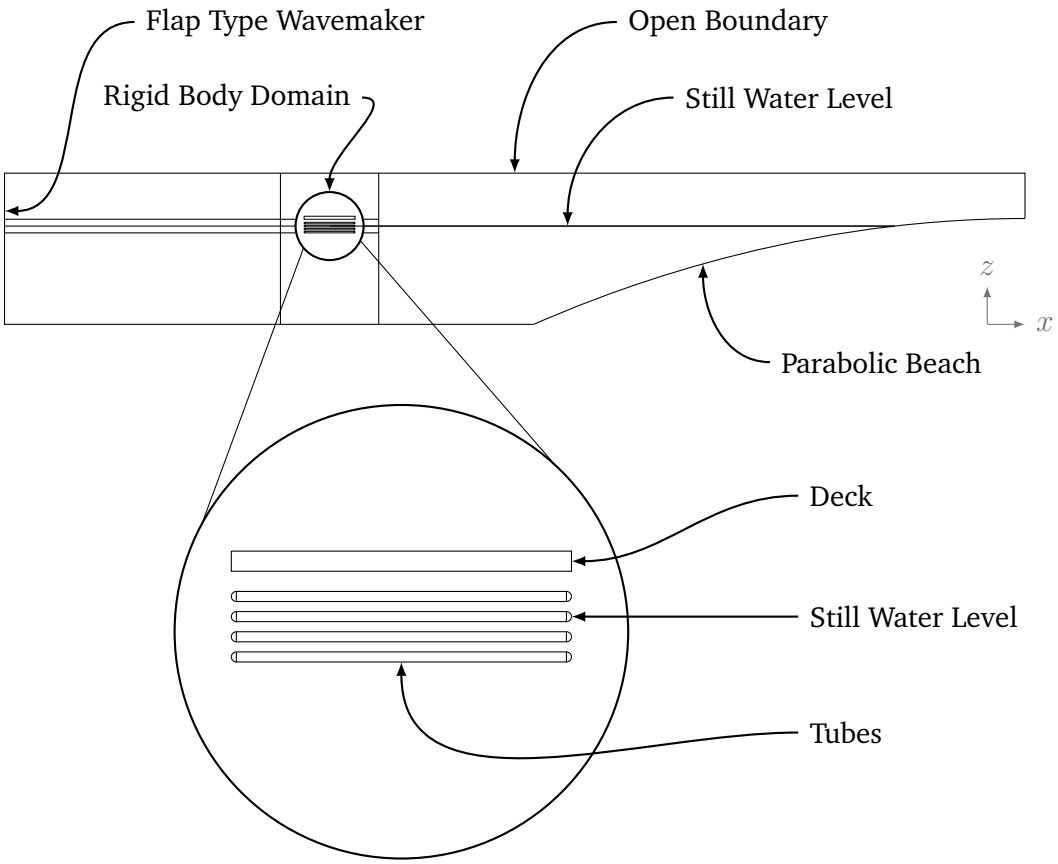

Figure D.3: CFD Layout with the Rigid Body Geometry Inserted

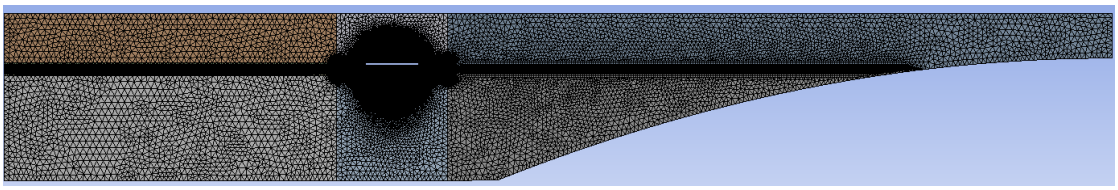

Figure D.4: Mesh Density of the CFX Domain

A small time step coupled with a large number of mesh elements will accrue a long simulation time, it is for this reason that CFX models are time-consuming operations, all the same the output is very detailed. For example, on an Intel Xeon, 16 processor @ 2.27GHz with 96 GB of RAM on a 64-bit operating system, a computation time of 1.7 hours per second of simulation was required for the simulation presented. As was outlined in § D.1 symmetry was utilised in the model to maintain the mesh size to a minimum for a three dimensional simu-

lation, resulting in a thickness of 629.5mm. This comprised of the thickness of half a tube and half the spacing between the tubes. As a result of symmetry only three degrees of freedom were modelled, surge, heave, and pitch.

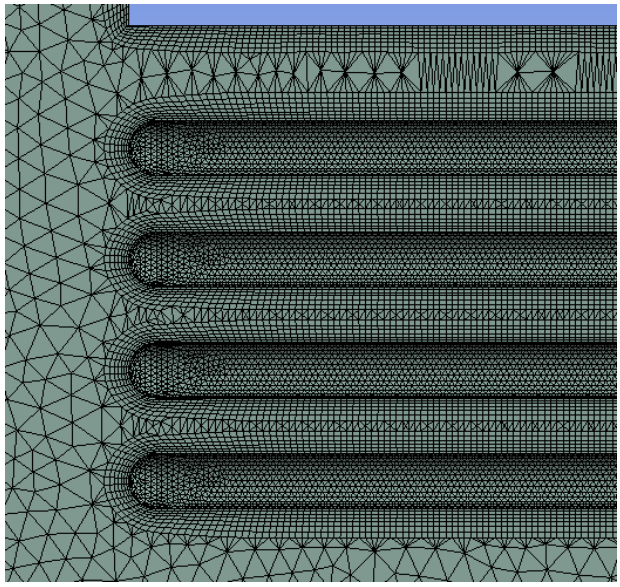

Figure D.5: Detailed View of Mesh Around Tubes

Due to the nature of the flow around the tubes, and the forces induced on them the coupling between the rigid body solver and the fluid solution was enhanced to achieve a convergent solution. In addition, relaxation of the mesh near a boundary allowed greater mesh motion where necessary.

Table D.4: Rigid Body Numerical Model Properties

Parameter	Setting
Mass	4643kg
Iyy	2.49E05kg m^2
Translational Degrees of Freedom	X and Z Axes
Rotational Degrees of Freedom	Y Axes
Mesh Elements	2,028,443
Domain Thickness	0.6295m

D.4 Results of the Tubular Multihull Numerical Modelling

The results explored in this section are for the output from the rigid body simulation. Figure D.6 shows a series of images that track the vessels movements as it encounters a wave. with an incident wave height of 3.67m and a period of 6.1s. The vessel is following the wave profile in this situation and the motion is unsatisfactory as the pitch and heave response is quite large relative to the wave.

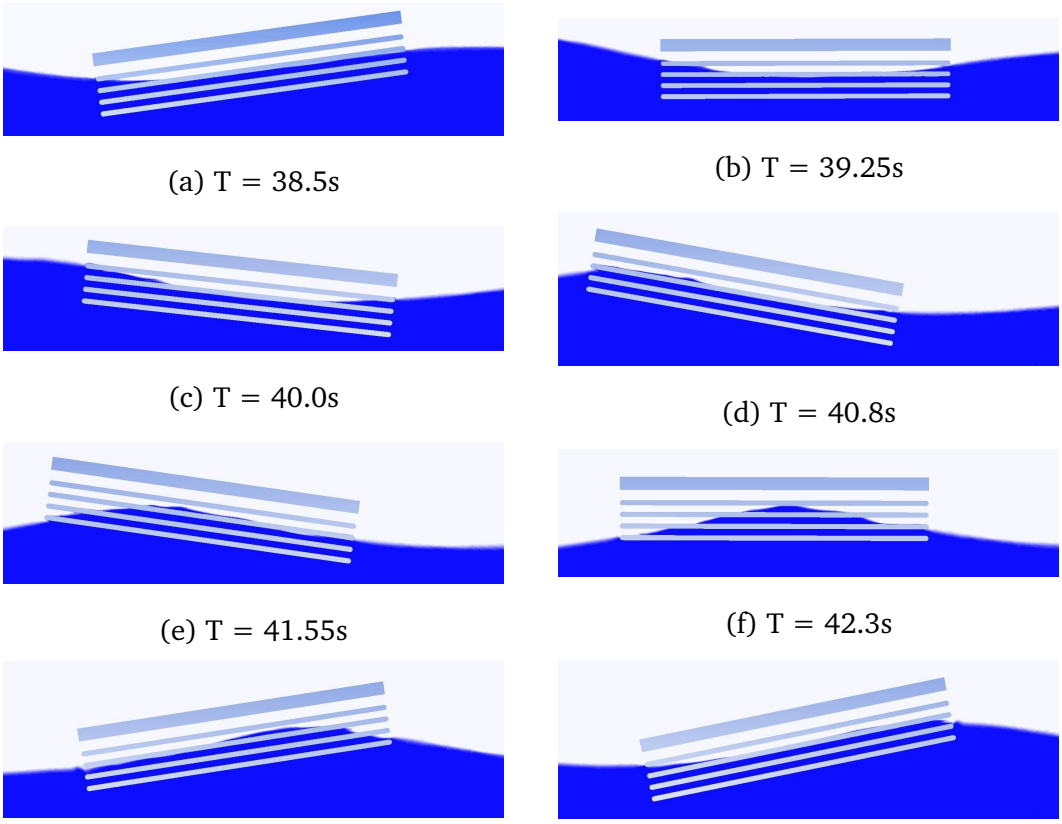

(a) T = 38.5s

(b) T = 39.25s

(c) T = 40.0s

(d) T = 40.8s

(e) T = 41.55s

(f) T = 42.3s

(g) T = 43.05s

(h) T = 43.7s

Figure D.6: Vessel Motion Throughout a Wave, H 3.67m, T 6.1s

Figure D.7 shows the heave time series for each of the eight wave conditions. Depending on the wave condition the simulation takes about 20–50s to achieve a steady state condition, the same time as for the waves to fully form. There is a substantial amount of heave motion being experienced by the rigid body and generally increases for longer periods.

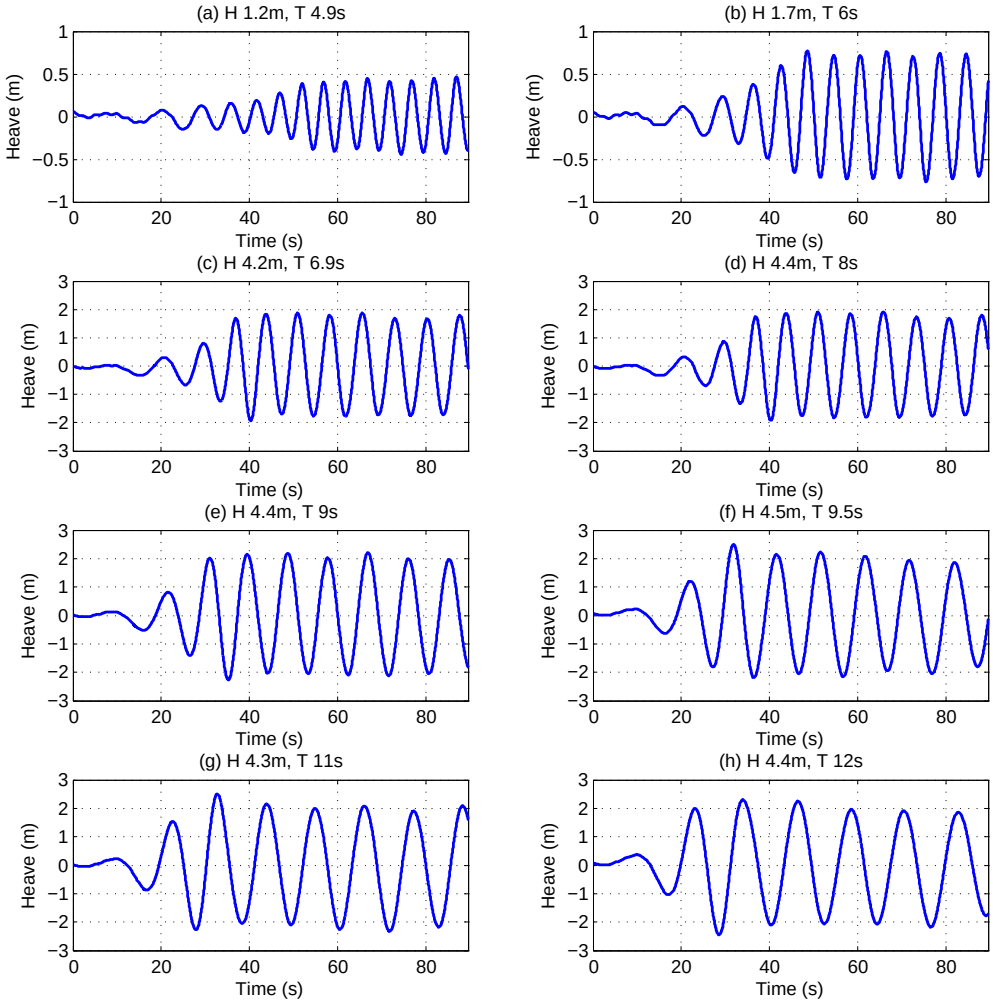

Figure D.7: Numerical Heave Time Series CFX

The pitch time series for each wave condition is plotted in Figure D.8. Similar to the heave time series the pitch time series shows that once the wave height has fully developed in the domain the pitch reaches a steady state situation. In the case of Figures D.8c– D.8h there appears to be a large pitch motion prior to reaching a steady state, this is not the case for shorter waves. Maximum

pitch amplitude occurs for the waves with a period of 6.9 and 8s, the amplitude of pitch motion then reduces as the period increases. Though the wave height for the 4.9 and 6s waves is lower the pitch amplitude does not decrease much, indicating that the natural period of pitch is in that region.

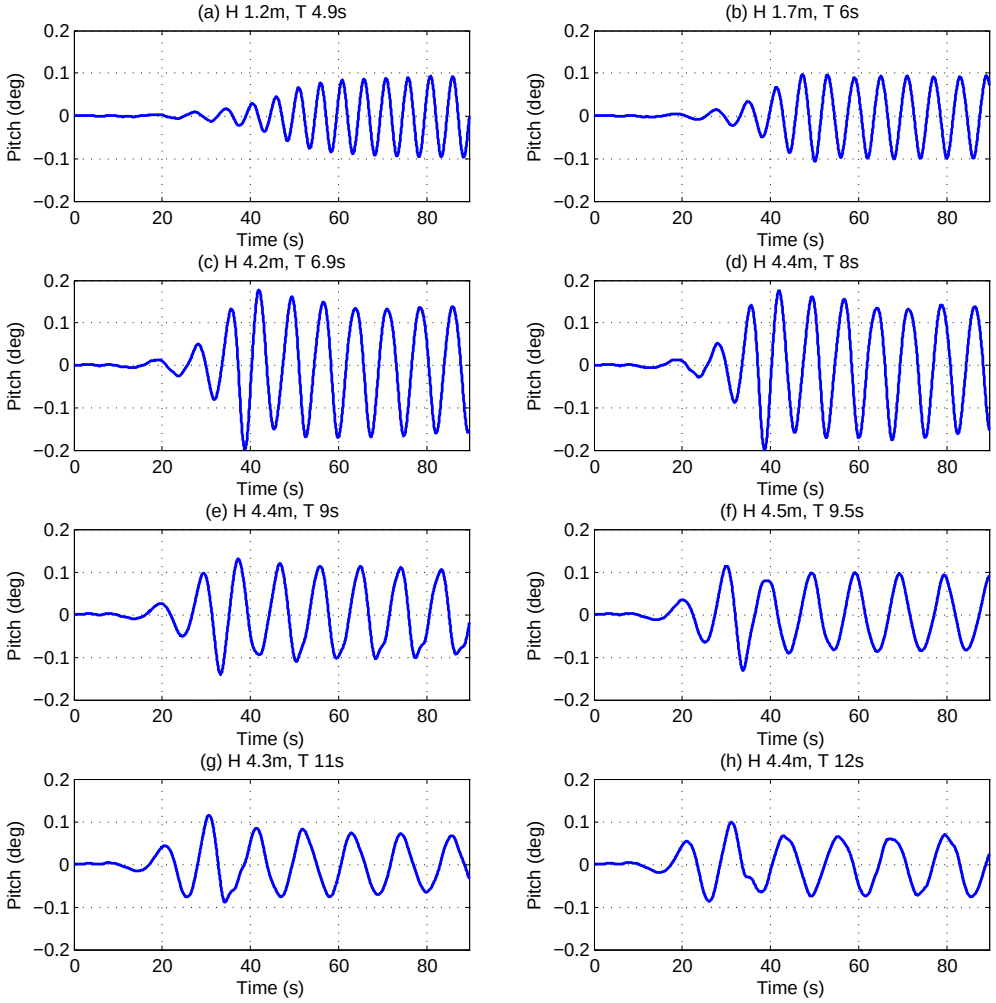

Figure D.8: Numerical Pitch Time Series CFX

Figure D.9 graphs the heave and pitch RAO for the tubular multihull based on the information from the time series plots. The RAO for heave tends to 1 for low frequency waves and the pitch RAO appears to be approaching the natural frequency for higher frequency waves. The shape and amplitude do not appear to be much different than for a monohull of a similar length [162].

In Figure D.10 it is demonstrated that the wave height in the simulation,

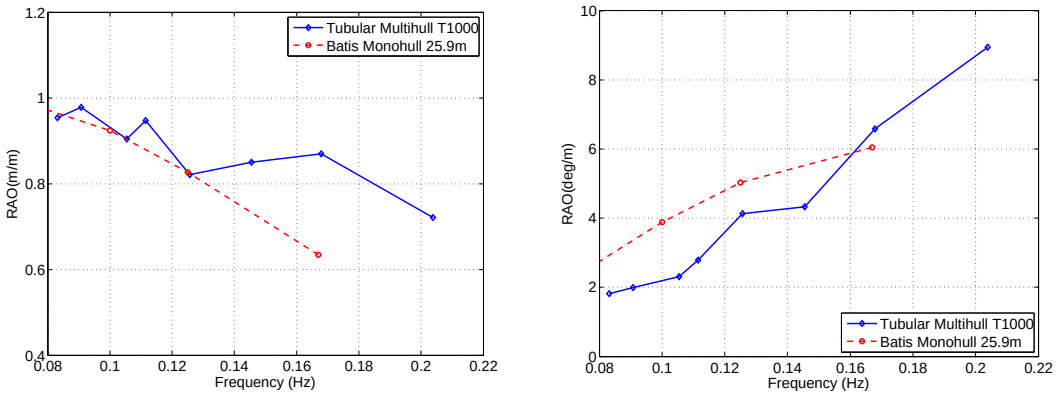

(a) Heave

(b) Pitch

Figure D.9: Model T1000 Regular RAO from Numerical Model Testing with ANSYS CFX Compared with a 25.9m Monohull from the Literature [162]

which includes the rigid body, is higher than that without. This is possibly due to the model taking up a substantial amount of the domain width, which is half a tube and half the spacing between tubes. To determine the extent of radiated waves a longer simulation with more locations recording wave height is required and the rigid body should be placed further from the wavemaker to take sufficient readings to measure this.

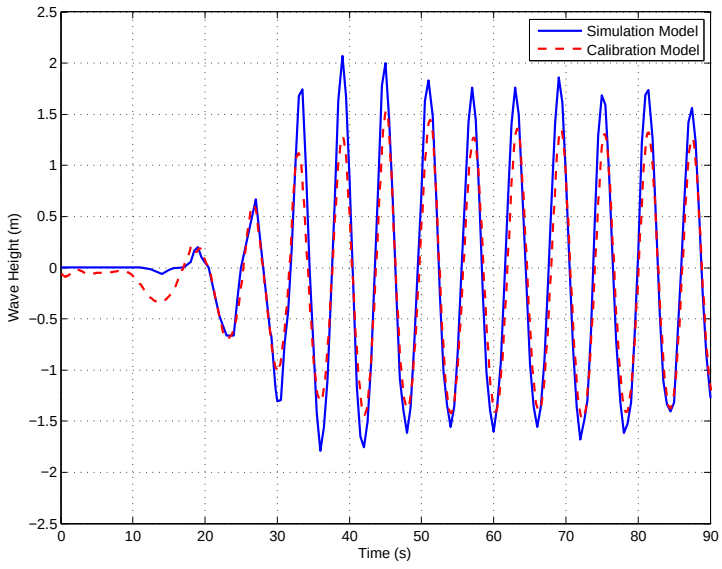

Figure D.10: Wave Height Difference in Simulation

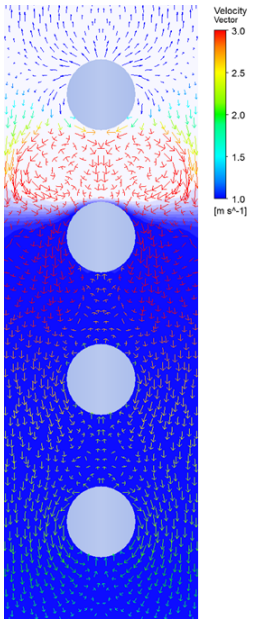

Figure D.11: Velocity Vector of Flow

Figure D.11 shows a sample section through the model at 41.55s at a location of 4.251m in the negative X direction from the centre of gravity of the vessel for a simulation with a 3.67m H and a 6.1s T. The image shown has been mirrored once to give a clearer picture of the flow around the tubes. The velocity of the water is quite high reaching $3\,\mathrm{m\,s^{-1}}$ and naturally decreases with depth. There are small areas above and below the tubes with velocity normal to the tubes, that represent an eddy moving with the same velocity as the tube at the same location. The velocity of the air is quite high near the free surface, as is expected as the water moves with a similar velocity at that location, but air is compressible and hence reduces rapidly. Moreover, it has negligible impact on the vessels motion as air has low density and hence minimal momentum.

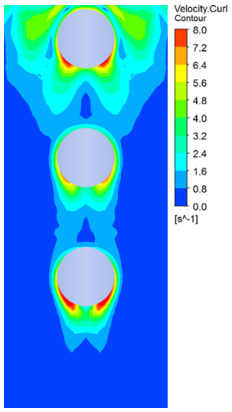

Figure D.12: Velocity Curl Contour Map around Submerged Tubes

Figure D.12 shows the instantaneous water vorticity at 41.55s at a location of 4.251m in the negative X direction from the centre of gravity of the vessel for a simulation with a 3.67m H and a 6.1s T. Vorticity is a measure of the amount of rotation in a fluid and is computed as the curl of the velocity field and hence referred to as the velocity curl in Figure D.12. The graph of vorticity enables the visualisation of the vortex shedding pattern. In order to maximise the heave and pitch damping then vortex shedding must be optimised [125, 195]. This may be investigated by adding sharp edges to the tubes [115]

Appendix E

Experimental Test Outline

Table E.1: Test Schedule for the Tubular Multihull: Regular Waves

Test No	H (m)	T (s)	f (Hz)	Test No	H (m)	T (s)	f (Hz)
1	1.5	4	0.25	14	3	7	0.14
2	1.5	6	0.17	15	3	8	0.13
3	1.5	8	0.13	16	3	9	0.11
4	1.5	10	0.1	17	3	10	0.1
5	1.5	12	0.08	18	3	11	0.09
6	2.25	4	0.25	19	3	12	0.08
7	2.25	6	0.17	20	3	13	0.08
8	2.25	8	0.13	21	3	14	0.07
9	2.25	10	0.1	22	4	6	0.17
10	2.25	12	0.08	23	4	8	0.13
11	3	4	0.25	24	4	10	0.1
12	3	5	0.2	25	4	12	0.08
13	3	6.1	0.16				

Table E.2: Test Schedule for the Tubular Multihull: Irregular Sea States

(a) JONSWAP Sea States

Test No	Hs (m)	Tp (s)	fp (Hz)
26	1.5	5	0.20
27	1.5	8	0.13
28	1.5	12	0.08
29	3	7.5	0.13

(b) Bretschnider Sea States

Test No	Hs (m)	Tp (s)	fp (Hz)
30	1.5	5	0.20
31	1.5	8	0.13
32	1.5	12	0.08
33	3	9	0.11

Table E.3: Test Schedule for the Narrow and Wide Hulled Catamarans: Regular Waves

Test No	H (m)	T (s)	f (Hz)	Test No	H (m)	T (s)	f (Hz)
1	1.5	4	0.25	12	3	6	0.17
2	1.5	6	0.17	13	3	7	0.14
3	1.5	8	0.13	14	3	8	0.13
4	1.5	10	0.1	15	3	9	0.11
5	1.5	12	0.08	16	3	10	0.1
6	2.25	4	0.25	17	3	11	0.09
7	2.25	6	0.17	18	3	12	0.08
8	2.25	8	0.13	19	3	13	0.08
9	2.25	10	0.1	20	4	6	0.17
10	2.25	12	0.08	21	4	8	0.13
11	3	5	0.2	22	4	10	0.1

Table E.4: Test Schedule for the Narrow and Wide Hulled Catamarans: Irregular Sea States

(a) JONSWAP Sea States

Test No	Hs (m)	Tp (s)	fp (Hz)
23	1.5	5	0.2
24	1.5	8	0.13
25	1.5	12	0.08
26	3	7.5	0.13

(b) Bretschnider Sea States

Test No	Hs (m)	Tp (s)	fp (Hz)
27	1.5	5	0.20
28	1.5	8	0.13
29	1.5	12	0.08
30	3	9	0.11

Table E.5: Test Schedule for the Curved Hulled Catamaran

(a) Regular Waves

Test No	H (m)	T (s)	f (Hz)
1	3	5	0.20
2	3	6	0.17
3	3	7	0.14
4	3	8	0.13
5	3	9	0.11
6	3	10	0.10
7	3	11	0.09
8	3	12	0.08
9	3	13	0.08
10	2.25	4	0.25

(b) JONSWAP Sea States

Test No	Hs (m)	Tp (s)	fp (Hz)
11	1	4	0.25
12	1.5	5	0.20
13	2	6	0.17
14	3	7	0.14
15	3	8	0.13
16	3	9	0.11
17	3	10	0.10
18	2.5	12.5	0.08
19	1.5	7	0.14
20	1.5	9	0.11
21	1.5	12.5	0.08

Table E.6: Test Schedule for the GDC: JONSWAP Sea States

Test No	Hs (m)	Tp (s)	fp (Hz)	Test No	Hs (m)	Tp (s)	fp (Hz)
1	1	4	0.25	16	2.5	6.5	0.15
2	1.5	4	0.25	17	2.5	7	0.14
3	1.5	4.5	0.22	18	2.5	12.5	0.08
4	1.5	5	0.2	19	2.75	6	0.17
5	1.5	5.5	0.18	20	3	6.5	0.15
6	1.5	6	0.17	21	3	7	0.14
7	1.5	7	0.14	22	3	7.5	0.13
8	1.5	9	0.11	23	3	8	0.13
9	1.5	12.5	0.08	24	3	9	0.11
10	2	5	0.2	25	3	10	0.1
11	2	5.5	0.18	26	3.25	8	0.13
12	2	6	0.17	27	3.5	8.5	0.12
13	2	6.5	0.15	28	3.5	9	0.11
14	2.5	5.5	0.18	29	3.5	9.5	0.11
15	2.5	6	0.17	30	3.75	8	0.13